This is to certify that the

dissertation entitled
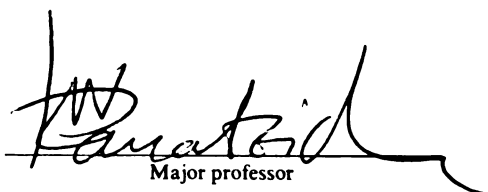
Synthesis of Electrically Conductive Polymer/
Inorganic Composites ∿ In-Situ Oxidative Polymerization/
Intercalation of Conducting Polymers in Layered Hosts

presented by

Chun-Guey Wu

has been accepted towards fulfillment
of the requirements for

_____Ph.D._____ degree in _Chemistry_

_____
Major professor

Date __May 11, 1992__

PLACE IN RETURN BOX to remove this checkout from your record.
TO AVOID FINES return on or before date due.

DATE DUE	DATE DUE	DATE DUE
1 1 1 8 0 9 JAN 0 7 2001		
MAY 2 5 2003 1 2 0 - 7		

MSU Is An Affirmative Action/Equal Opportunity Institution
c:\circ\datedue.pm3-p.1

SYNTHESIS OF ELECTRICALLY CONDUCTIVE POLYMER/INORGANIC COMPOSITES~ *IN-SITU* OXIDATIVE POLYMERIZATION/ INTERCALATION OF CONDUCTING POLYMERS IN LAYERED HOSTS.

By

Chun-Guey Wu

A DISSERTATION

Submitted to
Michigan State University
in partial fulfillment of the requirements
for the degree of

DOCTOR OF PHILOSOPHY

Department of Chemistry

1992

ABSTRACT

SYNTHESIS OF ELECTRICALLY CONDUCTIVE POLYMER/INORGANIC COMPOSITES~ *IN-SITU* OXIDATIVE POLYMERIZATION/ INTERCALATION OF CONDUCTING POLYMERS IN LAYERED HOSTS.

By

Chun-Guey Wu

The redox intercalation of polyaniline, polypyrrole and polythiophene in V_2O_5 xerogel is a topotactic reaction which was achieved by reacting aniline, pyrrole and 2,2'-bithiophene with V_2O_5 xerogel. Upon intercalation, the interlayer spacings expanded from 11.55Å to 13.94Å, 15.20Å and 14.70Å for polyaniline/V_2O_5 polypyrrole/V_2O_5 and polythiophene/V_2O_5 respectively. These data are consistent with containing alternating monolayers of conducting polymers and V_2O_5 xerogel. The room temperature conductivity of polymer/V_2O_5 composites is in the range of $10^{-4} \sim 10^0 \ \Omega^{-1}cm^{-1}$ and decreases with decreasing temperature. The charge transport properties of these composites vary significantly from each other. They can be semiconductors or metal-like, with n-type or p-type conductivity depending on the reaction media, polymer/V_2O_5 ratio and polymer molecular weight. Upon standing in air, the magnetic moment of all polymer/V_2O_5 composites decreases. This is due to reoxidation of some of V^{4+} centers to V^{5+} by oxygen. Another effect

oxygen has on $(PANI)_x V_2O_5 nH_2O$ is to cause the intercalated polyaniline chains to oxidatively polymerize further to form longer chains. This increases the conductivity.

$(PANI)_x FeOCl$ was obtained by reacting FeOCl with excess aniline in acetonitrile at room temperature. The resulting products have interlayer spacing equal to 13.96Å which is also consistent with containing alternating monolayers of FeOCl and polyaniline. X-ray and electron diffraction studies of single crystal $(PANI)_x FeOCl$ show a superlattice phenomenon suggesting a regular arrangement of polyaniline chains in FeOCl layers. The room temperature conductivity of $(PANI)_x FeOCl$ is around 10^{-3} to 10^{-1} $\Omega^{-1}cm^{-1}$ and the thermoelectric power of all samples shows p-type semiconductor behavior. Upon sitting in air (aging), two separate processes occurred: the FeOCl is hydrolyzed to β-FeOOH, and polyaniline chains continue to oxidatively polymerize forming longer chains of polymer.

Intercalation of polyfuran was achieved by taking advantage of the lower oxidation potentials of terfuran and quaterfuran. Two different products were isolated depending on the reaction conditions. In refluxing MeOH or CH_3CN, the resulting product r-$(PFu)_x FeOCl$, is a topotactic intercalation. However, the products isolated from methanothermal synthesis, m-$(PFu)_x FeOCl_y(OMe)_{1-y}$ in which the Cl atoms in FeOCl were partially replaced by MeO groups. Although the physicochemical properties of both phases are similar, r-$(PFu)_x FeOCl$ has higher conductivity than m-$(PFu)_x FeOCl_y(OMe)_{1-y}$. Variable temperature thermopower data of both products show typical p-type semiconductor behavior similar to $(PANI)_x FeOCl$.

TO MY FAMILY

ACKNOWLEDGEMENT

The project would not have been successful without the help of so many sincere persons. First and foremost thanks to my advisor Mercouri G. Kanatzidis whose scientific ingenuity, wise guidance and financial support contribute to my completion of the degree requirements. Throughout this journey, he made himself available to me whenever I needed help and advice.

I would like to express my great appreciation to Professor C. R. Kannewurf and his students, D. DeGroot, H. Marcy and J. Schinler for performing all the charge transport measurements, Professor E. LeGoff and M. Benz for providing the terfuran and quaterfuran monomers, Professor H. Eick for help with X-ray powder diffraction, Professor K. Klemparens and S. Flegler for good discussions for Electron Microscope experiment, Professor T. J. Pinnavaia, Professor J. L. Dye and Professor J. E. Jackson for serving in guidance committee.

I would also like to thank all in the Kanatzidis group and my friend Hai-Yen whose friendship and kindness made my graduate career smooth and very pleasant. I give special thanks to Sandeep Dhingra who has helped me through all my difficult times in the past four years.

Finally, thanks to my parents who support me in every endeavor I choose.

TABLE OF CONTENTS

CHAPTER 4. Synthesis and Characterization of Conducting Polythiophene/V$_2$O$_5$ Bronze ~ *In-situ* Intercalation of Polythiophene in V$_2$O$_5$ Xerogel

ix

LIST OF TABLES

xi

LIST OF FIGURES

LIST OF SCHEMES

ABBREVIATIONS

DSC: Differential Scanning Calorimetry.

EPR: Electron Paramagnetic Resonance.

GPC: Gel Permeation Chromatography.

PANI: Polyaniline.

PFu: Polyfuran.

Ppy: Polypyrrole.

Pth: Polythiophene.

SAED: Selected Area Electron Diffraction.

SEM: Scanning Electron Microscopy.

TEM: Transmission Electron Microscopy.

TGA: Thermogravimetric Analysis.

CHAPTER 1

INTRODUCTION

The field of "Low Dimensional Conductors" has attracted considerable attention recently. Both chemists and physicists are actively investigating the synthesis and properties of this class of materials. The activity was initially stimulated by the hypothesis that a one-dimensional organic compound can be designed that would exhibit room temperature superconductivity [1]. The magnitude of conductivity in these materials is dictated at least in part by structural constraints [2]. Organic metals beautifully illustrate this point. Various systems which have successfully produced low dimensional conductors include the following several categories [3]

1. Linear chain of transition metals complexes, such as $K_2Pt(CN)_4Br_{0.3}.3.0H_2O$.

2. Stack of donors and acceptors molecules, (TTF-TCNQ).

3. Intercalated graphites, (C_8K).

4. Intercalated 2-D chalcogenides, (M_xTaS_2).

5. Langmuir-Blodgett (LB) multilayers.

6. Linear conjugated polymers, such as polyacetylene, polypyrrole and polythiophene.

Especially intriguing among these classes of materials are the linear conjugated organic conductive polymers. Since the first electrically conductive polymer, polyacetylene, was discovered by H. Shirakawa and coworkers 15 years ago [4], conducting polymers

have become a new class of materials under rapid expansion [5]. Several prototype conductive polymers, such as polythiophene (Pth) and its derivatives, poly-p-phenylene (PPP), polyfuran (PFu), polypyrrole (Ppy) and polyaniline (PANI), have attracted attention because of their interesting electronic properties. Rapid progress has demonstrated that the potential exists for the discovery of new concepts and phenomena as well as the development of new technology. The wide-spread fascination is clearly motivated by their perceived technological potential. In fact, electrically conducting or semiconducting applications are the last great challenge for polymeric materials.

These polymers are usually composed of highly conjugated linear chains and their electronic structure is based upon the overlap of the p-orbitals of the backbone carbon atoms [6]. They can be oxidized or reduced more easily and reversibly than traditional non-conjugated polymers. Except for polyacetylene, almost all conducting polymers can be prepared by either electrochemical or chemical oxidative polymerization of the corresponding monomers as shown below:

Electrochemical polymerization [7]:
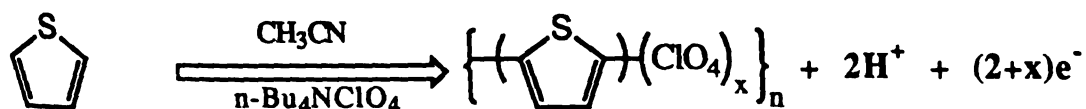
$$\text{[thiophene]} \quad \xrightarrow[\text{n-Bu}_4\text{NClO}_4]{\text{CH}_3\text{CN}} \quad \left\{ \left[\text{[thiophene]} \right] (\text{ClO}_4)_x \right\}_n + 2\text{H}^+ + (2+x)\text{e}^-$$

Chemical polymerization [8]:

$$2 \, x \left\langle \bigcirc \right\rangle - NH_2 \xrightarrow[HCl_{(aq)}]{(NH_4)_2S_2O_8} \left(\left\langle \bigcirc \right\rangle - \overset{+}{N} = \left\langle \bigcirc \right\rangle = \overset{+}{N} \right)_x + 2SO_4^{2-} + NH_4^+ + 2H^+$$
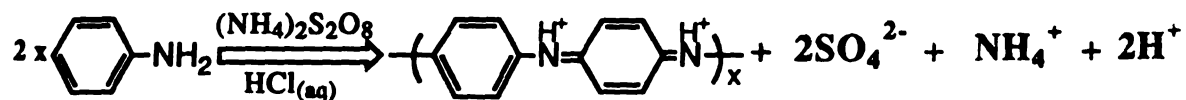
In the neutral state, these conjugated polymers are either insulators or semiconductors. Upon doping (partial oxidation or reduction), they become electrically conducting and display nearly metal-like behavior. At the same time, the color and physicochemical properties also change. This doping-undoping process is reversible. The doping of these conjugated polymers induces charge transfer along the chains which leads to significant local relaxations. Therefore, the equilibrium geometry in the ionized state is different from that in the ground state. This means that the electronic structure is affected by the localized electronic states in the band gap which modify the π system.

The electrical properties of any materials are determined by their electronic structure. The theory that most reasonably explains the electronic structure of materials is band theory [9]. Conductive polymers are peculiar in that their electrical conductivity cannot be explained by simple band theory. For example, simple band theory cannot explain why the charge carriers in polyacetylene and polythiophene are spinless. Extensive studies of these polymers with various spectroscopic methods such as EPR [10] and optical [11] absorption as well as theoretical works [12] point to the formation of polarons (single charge paramagnetic state) and bipolarons (doubly

charged spinless bound states of two holes). Therefore, conduction by polarons and bipolarons is now thought to be the dominant mechanism of charge transport in polymers with non-degenerate (non equivalent resonance form) ground states. The degenerate ground state always refer to two geometric structures corresponding to the same total energy. The evolution of the band structure of polythiophene on doping [13] is shown in Figure 1.1. The band formation of polypyrrole upon doping is similar to that of polythiophene [5,12]. In the neutral state, the band gap of polythiophene is equal to 2.2 eV which is a semiconductor. At a doping level of less than 1%, the formation of polarons is evident. As the doping level is increased to a few percent, polarons start to bind in pairs to form diamagnetic bipolaron states. When the doping level becomes heavy (up to 30%), the bipolaron states overlap to form two bands in the gap. Consequently, the band gap decreases and becomes as small as 0.14 eV and the polymer shows high conductivity.

The oxidation state of the polymers will affect their electrical, optical and mechanical properties as well as thermal stability. For example, the charge transport properties are especially sensitive to the synthesis conditions and degree of reduction or oxidation. Polyaniline also shows sensitivity to the degree of protonation. The wide diversity of electrical, electrochromic and optical properties make conducting polymers attractive for several technological applications. These include rechargeable batteries [14], electronic devices [15], electrochromic display devices [16], sensors (pH, gas) [17], gas transport [18], anticorrosion protection of electrochemical

2.2 eV

]0.71 eV

}0.61 eV

neutral   < 1% doping   5% doping   heavy doping

(a)   (b)   (c)   (d)
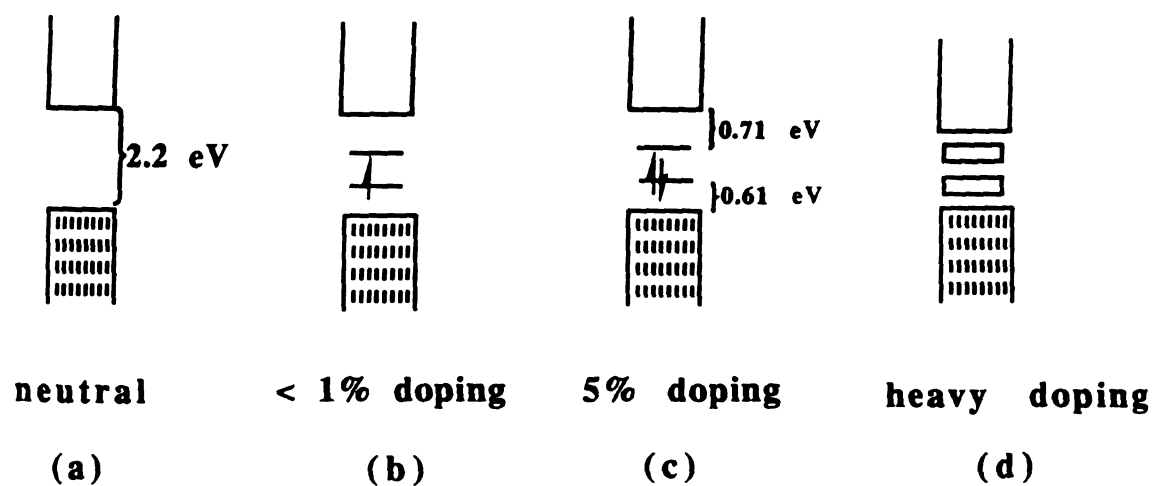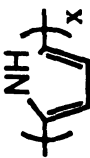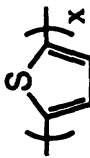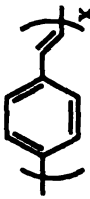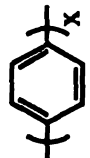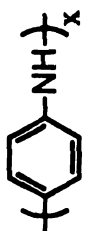
Figure 1.1. The band structure of polythiophene upon doping. (a) Neutral state (b) Less than 1 % doping (c) Few percent doping (d) Heavy doping.

photovoltaic devices [19] and photoelectrolysis cells [18], information storage [22] and electromagnetic shielding materials [21]. Recently, biomedical applications have also been mentioned [23]. Table 1.1 lists some prototype conductive polymers and the highest conductivity achieved to date. The room temperature conductivity of these polymers falls in a very wide range from 200 to 10^5 $\Omega^{-1}cm^{-1}$. The conductivity of iodine-doped polyacetylene [24] is comparable to that of copper metal. In order to get a better idea of the magnitude of conductivity, Figure 1.2 shows the conductivities of some well known materials.

Conducting polymers could potentially combine, in one material, the performance and processing advantages of organic polymers and the electrical properties' of semiconductors and metals. However, the intense effort to understand the chemistry and physics of these polymers has been hampered by their amorphous nature and the insolubility in common organic solvents. Therefore, structure/property relationships are not totally understood. One principal goal of this field is to achieve a fundamental understanding of the relationship between chemical structure and electronic properties of the conjugated polymers. For example, it has been known that the orientation of conductive polymers will affect the conductivity [25]. Conductivity is the product of two important factors: the number of carriers and carrier mobility. The mobility of the carriers in conducting polymers will be determined by several effects, including chain perfection and crystallinity, both of which are a function of chain alignment. Furthermore, regardless of electrochemical or chemical syntheses, these polymers always

Table 1.1. The Conductivities of Some Prototype Conductive Polymers.

Polymer	Structure	Conductivity (S/cm)
Polyacetylene	$(CH)x$	10^5, highly oriented
Polypyrrole		~ 500-7500, highly oriented
Polythiophene		~1000, highly oriented
Polyphenylvinylene		~10000, highly oriented
Poly-p-phenylene		~1000, highly oriented
Polyaniline		~200, highly oriented

$$\begin{array}{ll}
10^{6} & \text{Copper} \\
 & \text{Platinum} \\
10^{4} & \text{Bismuth} \\
 & \text{Graphite} \\
10^{2} & \\
10^{0} & \\
10^{-2} & \text{Germanium} \\
10^{-4} & \\
 & \text{Silicon} \\
10^{-6} & \\
10^{-8} & \\
 & \text{Polyethylene} \\
10^{-10} & \\
10^{-12} & \\
10^{-14} & \text{Diamond} \\
10^{-16} & \\
10^{-18} & \text{Quartz}
\end{array}$$

Highly oriented polyacetylene

Conducting Polymers
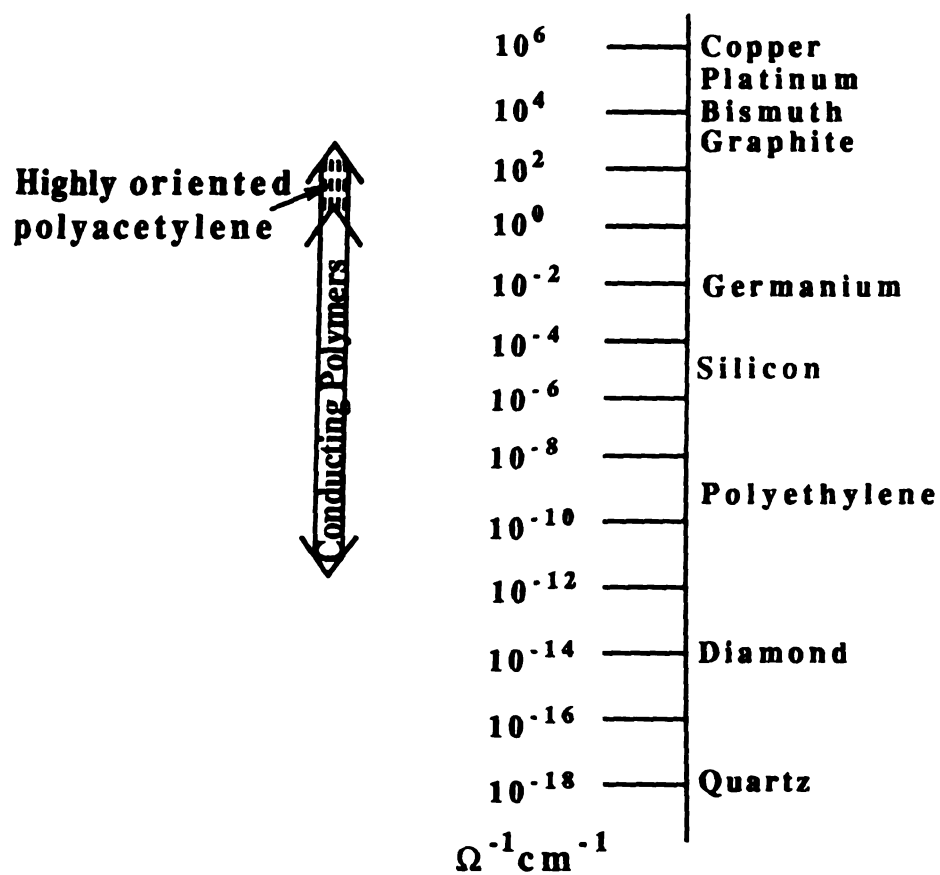
$\Omega^{-1} \text{cm}^{-1}$

* Note: Vertical scale shows room temperature conductivity in $\Omega^{-1}\text{cm}^{-1}$

Figure 1.2. The conductivity of conjugated polymers relative to some well known materials.

contain some structural defects such as double bond hydrogenation, crosslinking etc. The variation of conductivity with preparation methods also suggests that the low conductivities of conductive polymers are not an intrinsic property. They may result from the higher degree of structural defects and low crystallinity, which decrease the mobility of the carriers. The future of this field of research relies on creative synthesis of new systems with completely aligned chains containing fewer structural defects which would achieve higher conductivity and facilitate structure characterization.

Several methods have been used to align the polymer chains and thus achieve higher conductivity. Shirakawa and coworkers [26] have demonstrated that polymerization of polyacetylene on specific substrates produces highly oriented film with conductivities of 10^4 $\Omega^{-1}cm^{-1}$ after doping. Aldissi et al. [27] have produced highly conducting ($\sim 10^4$ $\Omega^{-1}cm^{-1}$) water soluble polythiophene film by passing a solution of polythiophene through a magnetic field while simultaneously removing the solvent. Several groups have prepared well oriented polymers by stretching polymer films or fibers [28].

One particular way to prepare more oriented conductive polymers may be by *intercalating* these polymers in structurally restricted hosts. By using layered materials, the intercalated polymers can, in principle, be forced to orient themselves within the host structure. Intercalation chemistry may prove to be a new route to prepare well oriented polymers. The resulting products would also represent a new class of organic/inorganic hybrid materials with interesting electrical properties.

Intercalation/Insertion Chemistry:

Intercalation can be viewed as the reversible insertion of a species into a matrix with the identity of both the guest and host being preserved. However, the term is usually used loosely even for irreversible insertion reactions. Intercalation compounds are of interest not only as catalytic materials [29] but also as low-dimensional conductors [30]. The intercalated guests can be inorganic or organic molecules, neutral or ionic species. The hosts can be two or three dimensional compounds. Most generally, intercalation refers to insertion of guest species in a layered structure followed by expansion of one crystallographic axis. Intercalation chemistry can be regarded basically as the result of competition between the cost in strain energy needed to open the van der Waals gap of a two dimensional structure and the gain in electronic energy after intercalation. There are three most common driving forces for intercalation reactions.

1. Ion-Exchange:
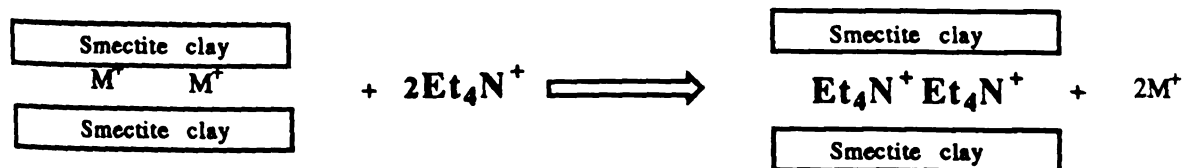
Smectite clay
$M^+ \quad\quad M^+$
Smectite clay

$+ \; 2Et_4N^+ \Longrightarrow$

Smectite clay
$Et_4N^+ \; Et_4N^+$
Smectite clay

$+ \quad 2M^+$

The Et_4N^+ ion can be intercalated inside the smectite clay layers by ion-exchange. In this case, Et_4N^+ is a guest and the smectite clay is a host [31].

2. Acid/Base or Coordination Interaction:
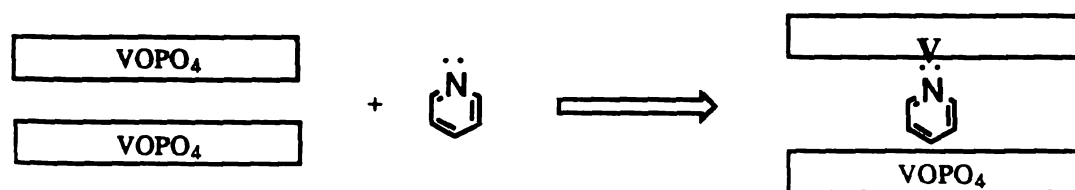
The vanadium atoms in $VOPO_4$ have empty coordination (or Lewis acid) sites. Some good bases such as pyridine can be intercalated inside $VOPO_4$ host by acid/base (or coordination) interaction [32].

3. Redox Reaction:
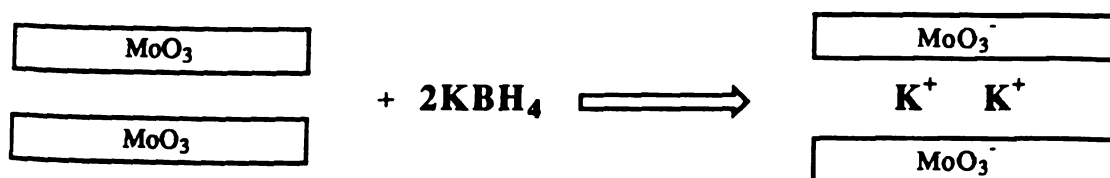
A class of layered compounds which have reducible metal centers. Upon reacting with reducing agents like BH_4^-, the host layers are reduced and cations insert inside the host to balance the resultant negative charge [33]. In the example listed above the K^+ ion is able

to be inserted in MoO_3 host by redox reaction. In another type of redox intercalation, the guest species itself acts as the reducing agent. The intercalation involves charge transfer between the guest molecules and the layered host, as observed in TTF intercalated FeOCl [34]. Mössbauer studies of intercalated FeOCl show a reduction of Fe^{3+} to Fe^{2+} in agreement with the charge transfer from guest to host. In such a delocalized system the extent of intercalation depends on three factors: the stability of Fe^{3+} oxidation state, the ionization potential of guest, and the rigidity of the host lattice.

Large molecular weight polymers can not be easily intercalated inside the hosts because of slow kinetics and insolubility in common organic solvents. However, the fact that conducting polymers are prepared by oxidative polymerization of the corresponding monomers, leads to the intriguing idea of using monomer instead of polymer. Thus by choosing the right hosts (good oxidants), and the right guest monomers (good polymerizable reductant) the polymer may be formed and at the same time inserted in the host via redox intercalation. Here the host acts as an oxidant to oxidize the monomer to polymer and further partially oxidize the polymer. The host itself is reduced and therefore can be regarded as a dopant. This idea was first proved by Kanatzidis and coworkers in 1987 by *in-situ oxidative polymerization/ intercalation* of polypyrrole and polythiophene in layered FeOCl [35]. The resulting conductive organic polymer/inorganic nanocomposites showed high electrical conductivity.

In order to extend this field of research, we sought other host materials, such as V_2O_5 xerogel. Layered V_2O_5 xerogel has been

known for more than a century. It is a semiconducting material with diverse intercalation chemistry. Furthermore, it is a good oxidant and the intercalation of conducting polymers in this host can be achieved by *in-situ* oxidative polymerization/ intercalation of respective monomers. We have proved that some well known conductive polymers such as **polypyrrole, polythiophene, polyaniline** were able to intercalate in V_2O_5 xerogel by redox intercalation. The resulting products can be viewed as conducting polymers-derived molecular scale nanocomposites with interesting charge transport properties.

To extend the intercalation chemistry of conducting polymers in **FeOCl**, two other polymers, **polyaniline and polyfuran**, were chosen. The mechanism of charge transport in polyaniline is different from that in polypyrrole and polythiophene [36] and the detailed structural knowledge in this polymer is highly desirable. We decided to examine the polyaniline/FeOCl system in the hope of obtaining crystalline samples of intercalated polyaniline. This work also contradicts the previous report [37] which claimed that aniline does not intercalate in FeOCl.

Polyfuran is a known but not well studied conducting polymer. The furan ring is relatively unstable compared to other heterocyclic conducting polymers such as polypyrrole and polythiophene. Polyfuran prepared from furan and its derivatives always contains a high number of structural defects and shows low electrical conductivity. We investigated polyfuran/FeOCl system hoping that the polyfuran formed in the layers of crystalline host would have fewer structural defects and a well defined structure.

Work centered on the idea of polymer inclusion in fixed inorganic hosts is rare and the little that has been reported has been recent after the Kanatzidis et al report [35]. Soma and coworkers first reported the polymerization of benzene [38] and thiophene [39] in the interlayers of clays by reacting benzene, thiophene and their derivatives with Cu^{2+}-montmorillonite and Fe^{3+}-montmorillonite. The formation of polymer cations was proved by resonance Raman spectroscopy. However, there is no firm evidence showing that the polymers were formed inside the clay layers.

Hiroshi, Inoue and coworkers have prepared polyaniline chains inside montmorillonite clay by absorbing aniline molecules into a clay modify electrode followed by electrochemical oxidative polymerization [40]. This is the first report of electrochemical polymerization of intercalated organic molecules. The oxidation process is very slow and the interlayer spacing of aniline/montmorillonite is changed from 15.6Å to 13.0Å after polymerization. It is therefore, suggested that before polymerization, the aniline molecules are incorporated in clay with their phenyl groups perpendicular to the clay layers. Upon polymerization the arrangement changed into a planar one in the clay sheets. However, there are no complete structural spectroscopic or charge transport data on this material.

Thomas Bein [41] and coworkers first inserted aniline in proton exchanged zeolites which they subsequently oxidatively polymerized by an external oxidant, such as $(NH_4)_2S_2O_8$. At the same time, they also used Cu^{2+} and Fe^{3+} ion exchanged zeolites as hosts, and *in-situ* oxidatively polymerized polypyrrole and polythiophene inside the

zeolites [41]. These intrazeolite Cu^{2+} and Fe^{3+} ions serve as oxidants for the oxidative polymerization reaction of pyrrole and thiophene. The formation of polymers was demonstrated by FTIR, EPR and electronic absorption data. The reaction rate of this system is slow and the resulting products are essentially insulators since the hosts themselves are electrically insulating materials.

Giannelis and coworkers used Cu^{2+} exchanged layered mica-type silicates as hosts and achieved *in-situ* oxidative polymerization/intercalation of polyaniline in clay layers [42]. The polyaniline formed inside the clay is the emeraldine base form which can be protonated by exposing to HCl vapor. The "as prepared" polyaniline intercalated clay shows excellent thermal stability up to 700°C. The room temperature conductivity of HCl exposed samples is 0.05 $\Omega^{-1}cm^{-1}$, an increase by five orders of magnitude with respect to Cu^{2+} exchanged host. The conductivity measurements perpendicular to the clay layers affirm the highly anisotropic nature of the intercalated materials.

Diaz, Galleja and coworkers have succeeded in intercalating polypyrrole in $[(Me_3Sn)_3Fe^{3+}(CN)_6]_x$ by reacting the latter with pyrrole at room temperature [43]. The resulting black product is a diamagnetic material with room temperature conductivity equal to 7.0×10^{-5} $\Omega^{-1}cm^{-1}$ which is 10^5 times higher than the alkali metal ion intercalated compound, $[Li_{0.3}(Me_3Sn)_3Fe^{3+}(CN)_6]_x$.

Recently, Caspar and coworkers at E. I. du Pont Inc. were able to introduce thiophene oligomers (n<10) in zeolites by reacting short chain thiophene oligomers (n= 2, 3, 4, 6) with thermally activated NaZSM-5 and Na-β zeolites [44]. These zeolites were used as

1. C

1. p

supporting matrices in which short chain oligomers of polythiophene can be prepared, doped to the conducting state, stabilized and spectroscopically characterized. The electronic absorption band energies of these materials were found to be a linear function of inverse chain length. These results can be used to predict the position of the electronic transition of bulk polythiophene. An interesting discovery in this study is that the radicals of thiophene oligomers (stable up to one month in the zeolite channels) couple gradually to form longer chains of oligomers upon heating (40~140°C) or standing for a longer time. All of the above work involved insulating materials as hosts and the resulting products, except (PANI)Cu-clay [42], have very low conductivity. Actually, in most cases no charge transport data were reported.

I. Guest Molecules ~ Conducting Polymers:

1. Polyaniline.

Polyaniline has been known for more than a century [45] as "aniline-black" and recently has attracted renewed interest [46]. The term "polyaniline" refers to a class of polymers consisting of up to 1000 or more (ring-N-) repeat units. Polyaniline is unique among conducting polymers by virtue of its electrical properties which can be reversibly controlled both by changing of its oxidation state and degree of protonation [47]. The substantial differences between polyaniline and other heterocyclic conducting polymers in the

physical phenomena are based on the key role of the ring torsion angle as well as the overlap of alternating nitrogen atoms and C_6 rings [48]. There are four different types [49] of polyaniline as showed in Scheme 1.1. Only the emeraldine salt is conducting.

Polyaniline exhibits excellent environmental stability and good conductivity [50]. It can be used in organic batteries [51], electrochromic displays [52], microelectronic devices and sensors [53], as corrosion inhibitor [54], nonlinear optical active media [55] and acid/base indicators [56]. Polyaniline is usually prepared by electrochemical [7,57] or chemical oxidation of aniline [58]. Its structure and charge transport properties depend on the synthetic conditions [59], such as oxidation potential, pH value of reaction medium and reaction temperature. There has been extensive investigation of its chemical structure by IR and Raman spectroscopies [60], ^{13}C and ^{15}N NMR spectroscopies [61], TG/DTA [62], X-ray photoelectron spectroscopy (XPS) [63], X-ray powder diffraction [64] and the study of model compounds [65]. However, our understanding of the structure is still fragmentary due to the amorphous or poor crystalline nature and the insolubility in common organic solvents, as well as complicated structural problems associated with single chains and their macromolecular aggregation. Therefore, the systematic control and modification of its physical, structural, and electronic properties is an active area of research [66].

One of the goals in this line of research is to optimize the charge transport properties and understand the relationship between electronic and lattice structure. This has been approached by preparing oriented or crystalline polymers. Progress in this area has
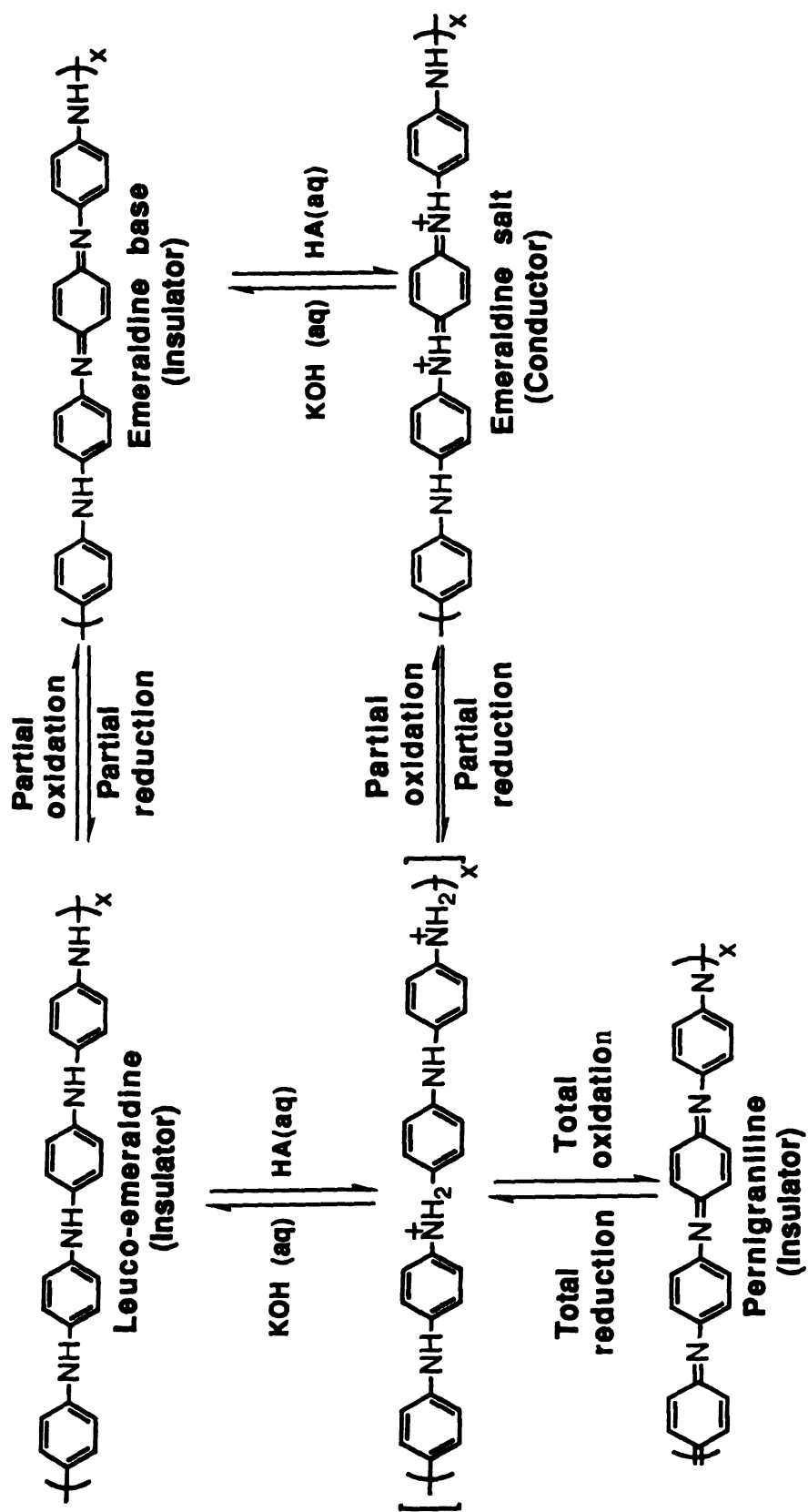
Scheme 1.1. Four different phases of polyaniline.

be

sou

str

un

pi

in

con

exi

wit

ma

res

2 P

by

bar

pro

sub

NMR

69,

mech

70,

been

condi

reacti

been made recently by MacDiarmid, Epstein [64] and coworkers who studied a microcrystalline form of polyaniline and proposed a crystal structure similar to polyethylene-sulfide based on X-ray powder diffraction data. The X-ray coherence length of polycrystalline polyaniline is still small (~ 50Å perpendicular to the chain and 150Å in the chain direction) and larger crystallites are not available.

Aniline is a cheap starting material and under certain conditions polyaniline can be fabricated into thin films [67] A moderately high electrical conductivity can be achieved by doping with non-oxidizing Bronsted acid. These desirable properties have made it the most extensively studied conductive polymer. In the past 5 years, more than a thousand papers have been published.

2. Polypyrrole.

Pyrrole is known to polymerize to a black powder referred as "pyrrole black" [68]. Polypyrrole is one of the most widely studied heteroaromatic conducting polymers because of its highly conducting properties and, in its doped state, it has better chemical and thermal stability than polyacetylene. Polymerization has been shown by ^{13}C NMR and IR techniques to occur mainly by α-carbon substitution [69]. However, the detail mechanism is still unclear. Two possible mechanisms have been proposed: via σ-radicals [7] and via π-radicals [70] as shown in Scheme 1.2. The charge transport mechanism has been rationalized by the polaron and bipolaron model [12d]. The conductivity of this polymer depends on the reaction solvent, reaction time and concentration of oxidant [71].
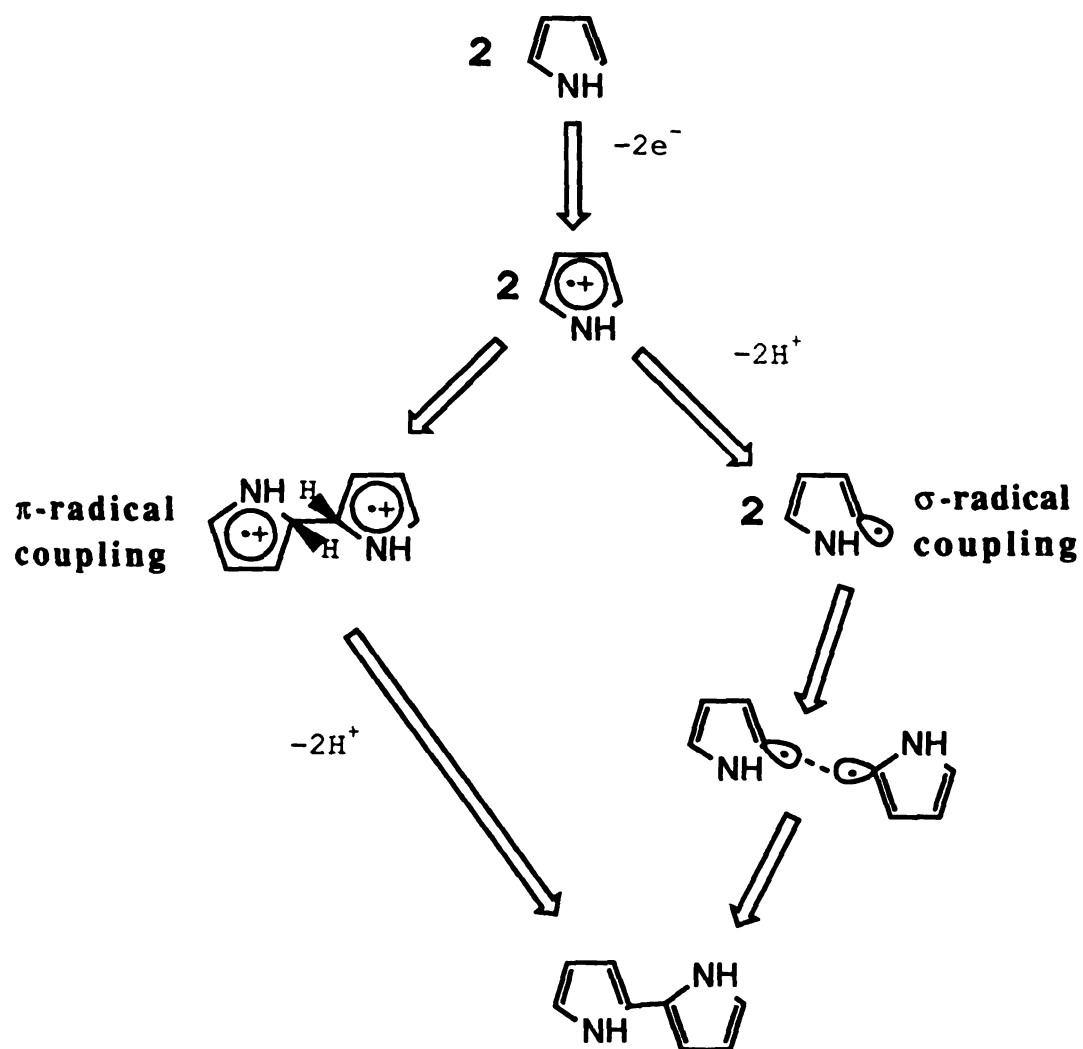
Scheme 1.2. Polymerization of pyrrole via σ-and π-radical coupling [70].

When the polymerization takes place in solvents possessing OH groups, high conductivity products can be obtained. Furthermore, the physical and charge transport properties of polypyrrole largely depend on the counter anions [72]. For instance, the mechanical properties are significantly improved by the incorporation of toluene sulfonate as an anion [72a]. The polymerization of polypyrrole can take place electrochemically [73] as well as chemically [74]. However, chemically prepared films are of poor quality; in some cases they are not even conducting [71]. Thus a chemical preparation of polypyrrole films remains a desirable goal. Intercalation of polypyrrole in layered hosts offers a good opportunity to prepare better oriented polymer through chemical polymerization as well as to study its intercalation with novel dopants such as electrically active metal oxides.

3. Polythiophene.

Polythiophene is also one of the prototype conducting polymers with good environmental stability. In fact, polythiophene and its derivatives are the first examples of conducting polymers that are stable toward oxygen and moisture both in their doped and undoped states. It can be prepared by either electrochemical [7,75] or chemical [76] polymerization of thiophene or 2,2'-bithiophene respectively. A chemically synthesized polymer, from the catalytic coupling of the Grignard reagent of 2,5-dibromothiophene by nickel salt, is produced in its undoped semiconducting state and can be

doped chemically to its conducting state [77]. The electrochemically synthesized polymer is obtained in the oxidized (doped) conducting state which can be chemically "compensated" or electrochemically undoped to its semi-conducting state [78]. Neutral polythiophene is a semiconductor with band gap (Eg) = 2.2 eV and is red colored. Upon doping, the electrical conductivity of the polymer film can be varied over 10 orders of magnitude and the color becomes black. The charge transport properties change from semiconducting to metal-like. The conductivity of polythiophene is not determined by the overall chain length, but by the abundance of long conjugated segments [79]. In other words, extension of the monomer's planarity will positively affect the conductivity [80]. Although detailed structural data on polythiophene are not yet available, the excellent optical and electrical properties would seem to imply a face-to-face interchain stacking. This face to face arrangement facilitates interchain electron transfer leading to extensive delocalization. It has been known that chemically polymerized polythiophene always contains some impurities and structural defects, such as cross-linkage, reticulation and β-carbon coupling [78,81]. However, a highly regular polymer backbone can be obtained by varying the nature of dopant and the structure of monomer [78]. In these respects, polythiophene appears to be a good model for the study of the parameters which control its physicochemical and electrical properties.

4. Polyfuran.

Polyfuran is a known but not well studied conductive polymer [82]. In the literature, up to hexafuran has been reported. The oligomers are prepared in low yield from the couping of shorter chain oligomers or monomer and involve very complicated organic synthesis [82]. Similar to polypyrrole and polythiophene, bulk polyfuran has been reported to be formed from furan by either electrochemical [83] or chemical [84] polymerization. However, due to the lower aromaticity of furan, as compared to pyrrole and thiophene, the conjugation of polyfuran is easily destroyed during or after polymerization [85]. The resulting polymer sometimes shows brown color with several structure defects, such as hydrogenation and ring opening [86]. Therefore, polyfuran is the most unstable and the least studied amongst the heterocycle ring-based conducting polymers. There are no detailed studies of the structure and physicochemical properties of this polymer. In fact there is no hard evidence that the reported material is actually polyfuran. Its electrical conductivity is very low. We have synthesized polyfuran from furan oligomers, such as terfuran and quaterfuran in which ring opening seems to be minimized [86]. The lower oxidation potential and better structural regularity of trimer and tetramer, compared to the furan monomer, may enable us to prepare polyfuran with better and more stable structure.

1

va
isl
ra
su
po
pr
by
co
by
ad
sen
pre
and
eva
con
thin
like
such

ray
micr
190

II. Layered Hosts:

1. $V_2O_5 1.6H_2O$ Xerogel.

One of the most versatile hosts for intercalation chemistry is vanadium pentoxide xerogel, $V_2O_5 1.6H_2O$. V_2O_5 gel has been known for more than one hundred years [87]. It received renewed attention recently by Livage and coworkers who have shown that these gels exhibit semiconducting properties [88]. V_2O_5 gel can be prepared by pouring molten crystalline V_2O_5 into cold water [89], by polycondensation of metavanadic acid [90] in water, by thermal hydrolysis of aqueous solution of $VOCl_3$ [91], by hydrolysis and condensation of vanadium alkoxides, $VO(OR)_3$ [92], or even hydrothermal method [93]. During preparation, some V^{5+} sites are reduced to V^{4+} to form a mixed valence compound. The semiconducting properties, which depend on the method of preparation, arise from the hopping of small polarons between V^{4+} and V^{5+} centers. Upon standing in air, the water in the gel gradually evaporates and finally a dry gel is obtained with certain water content, called a xerogel. The gel also can be easily fabricated into thin films and coatings by simply pouring it on different substrates like glass or plastics. Some potential applications have been proposed such as electrochromic [94] and switching devices [95].

The structure of V_2O_5 xerogel has been widely studied by X-ray [93,96], electron [97] and neutron [98] diffraction, electron microscopy [99], extended X-ray absorption fine structure (EXAFS) [100] and small angle X-ray scattering (SAXS) [101]. It has been

proposed that it is composed of corrugated rigid ribbons with average planar dimensions of the order of 1000Å x 100Å. The ribbons are formed by connecting several fibrils in the zig-zag fashion by sharing H_2O molecules [102]. The periodic structure of fibrils have repeat dimensions of 27Å x 3.6Å as shown in Scheme 1.3 [98] . The corrugation of the ribbon layers is equal to 2.8Å with one layer of H_2O inside the layer gallery. The interlayer spacing is 11.55Å. The intraribbon structure is thought to be closely related to crystalline orthorhombic V_2O_5 as shown in Figure 1.3   The vanadium atoms in the V_2O_5 slab are 5 coordinate with a square pyramidal geometry. Four V-O single bonds are in the equatorial position and one V=O double bond points out of the plane as shown in Figure 1.3b. V_2O_5 xerogel can be regarded as a hydrous oxide or composite of trapped H_2O and oxide networks. It contains three types of water [93]: free water (about 1 mole per mole of V_2O_5) which is reversibly adsorbed between the V_2O_5 layers and accounts for most of the H_2O content; a more strongly bonded H_2O (around 0.5 mole per mole of V_2O_5) and a very small amount of H_2O chemically bonded to vanadium atoms.

V_2O_5 xerogel is a porous and very reactive material. It has a turbostratic structure, in which the interlayer distances are the same but the flat ribbons stack at random orientation. It shows n-type semiconducting properties with room temperature conductivity around 10^{-5} $\Omega^{-1}cm^{-1}$ [104]. The conductivity arises from the hopping of small polarons [105] which are localized but mobile electrons. V_2O_5 xerogel can be dissolved in HCl or alkali and ammonium hydroxide. The intercalation reactions may involve cation-exchange
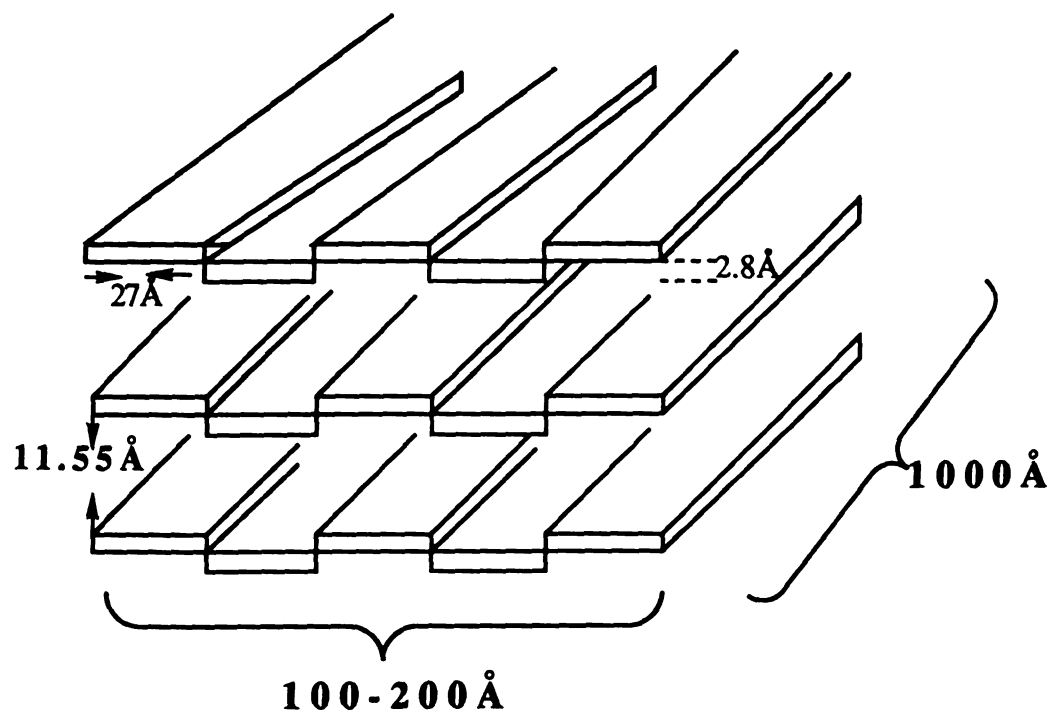
Scheme 1.3. Schematic representation of V₂O₅ layers. Proposed by Livage et al. [99].
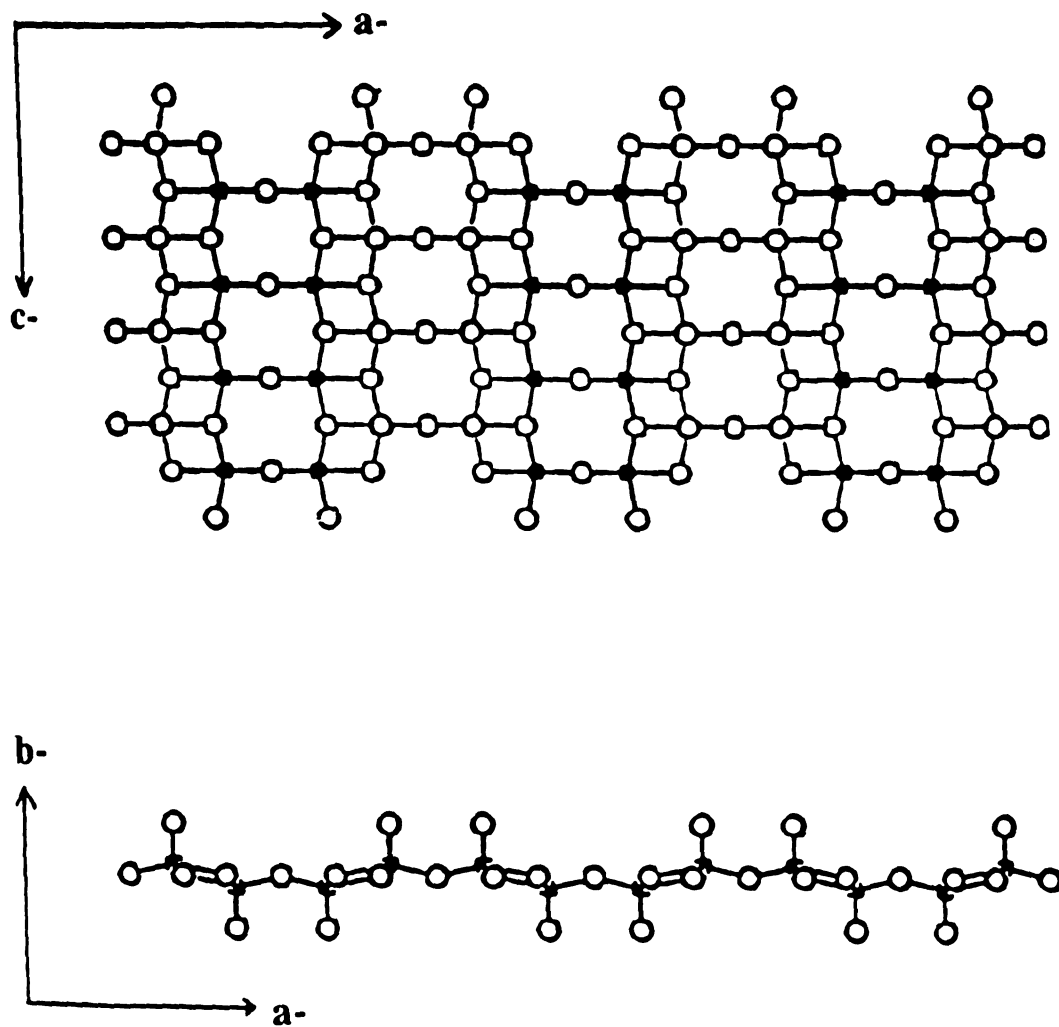
Figure 1.3. The structure of crystalline V_2O_5 (A) ac plane (B) ab plane.

[106], acid-base interaction [107] and redox reaction [108]. Several organic solvents [109], alkylammonium ions [109], ammonia and pyridine [107] have been reported to intercalate into V_2O_5 xerogel. Most interestingly, the xerogel is a strong oxidizing reagent. For example, it can be reduced by KBr at room temperature. Some molecules such as tetrathiafulvalene, benzidine [108] and ferrocene [110] have been known to intercalate in V_2O_5 xerogel via redox reaction. The resulting intercalates, called "molecular bronzes", show interesting electrical properties.

2. FeOCl.

FeOCl is a well defined crystalline material. It is a layered compound belonging to the orthorhombic space group Pmnm with two formulas per unit cell [111]. The unit cell parameters are a = 3.8Å, b = 7.92Å and c = 3.3Å. The layers consist of double sheets of cis-$FeCl_2O_4$ octahedra linked by sharing edges within the ac plane, which are held together by van der Waals interactions between the chlorine planes. The coordination of Fe is a distorted octahedron with four Fe-O bonds in the layer plane and two Fe-Cl bonds lining the van der Waals gap between the layers as shown in Figure 1.4. The interlayer spacing is 7.92Å and the interlayer Cl-Cl distance is 3.68Å. The b-axis is perpendicular to the layers. Figure 1.5 shows the arrangement of the ac-plane by looking down the b-axis.

FeOCl is a quasi-one-dimensional antiferromagnetic system with interesting but not well understood magnetic properties [112].
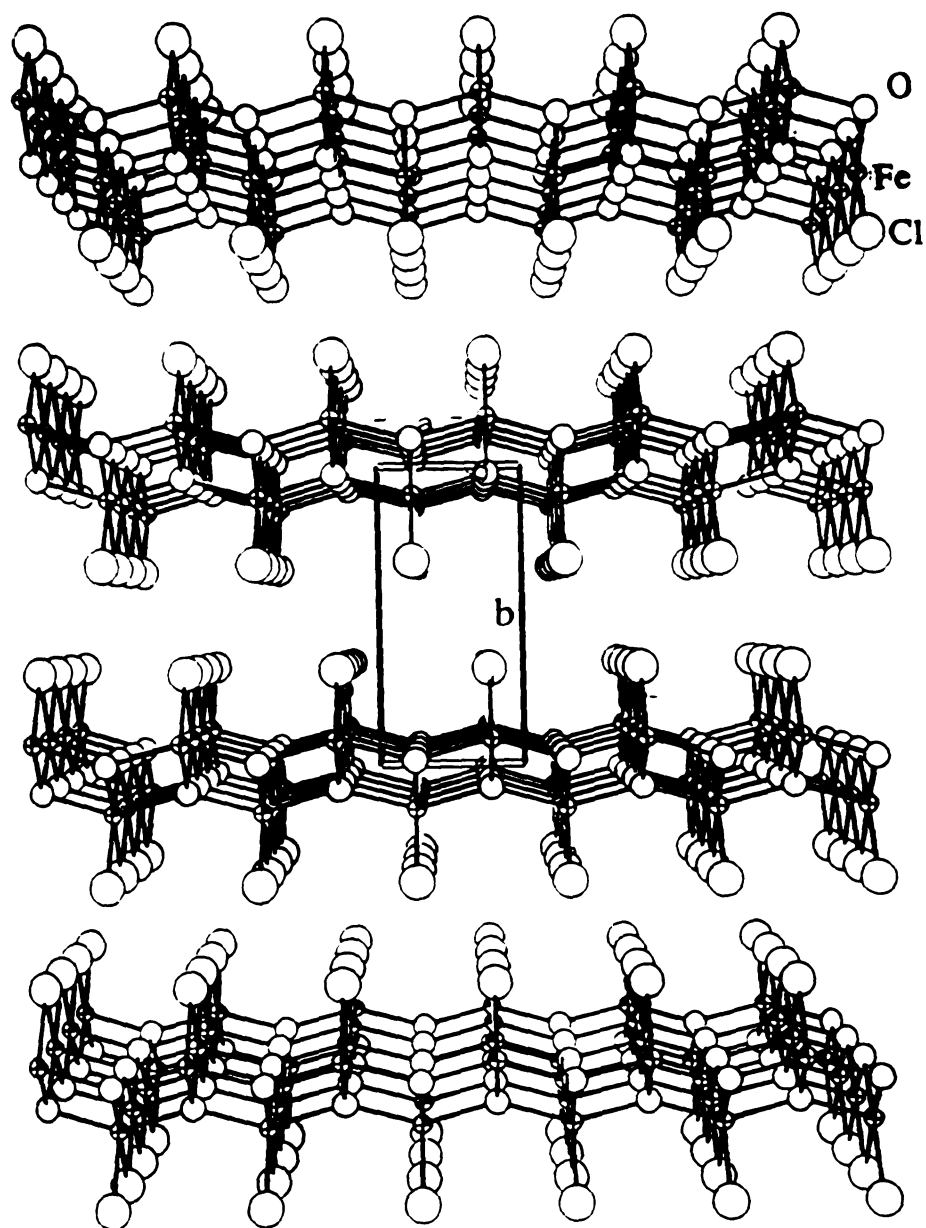
Figure 1.4. The crystal structure of FeOCl.
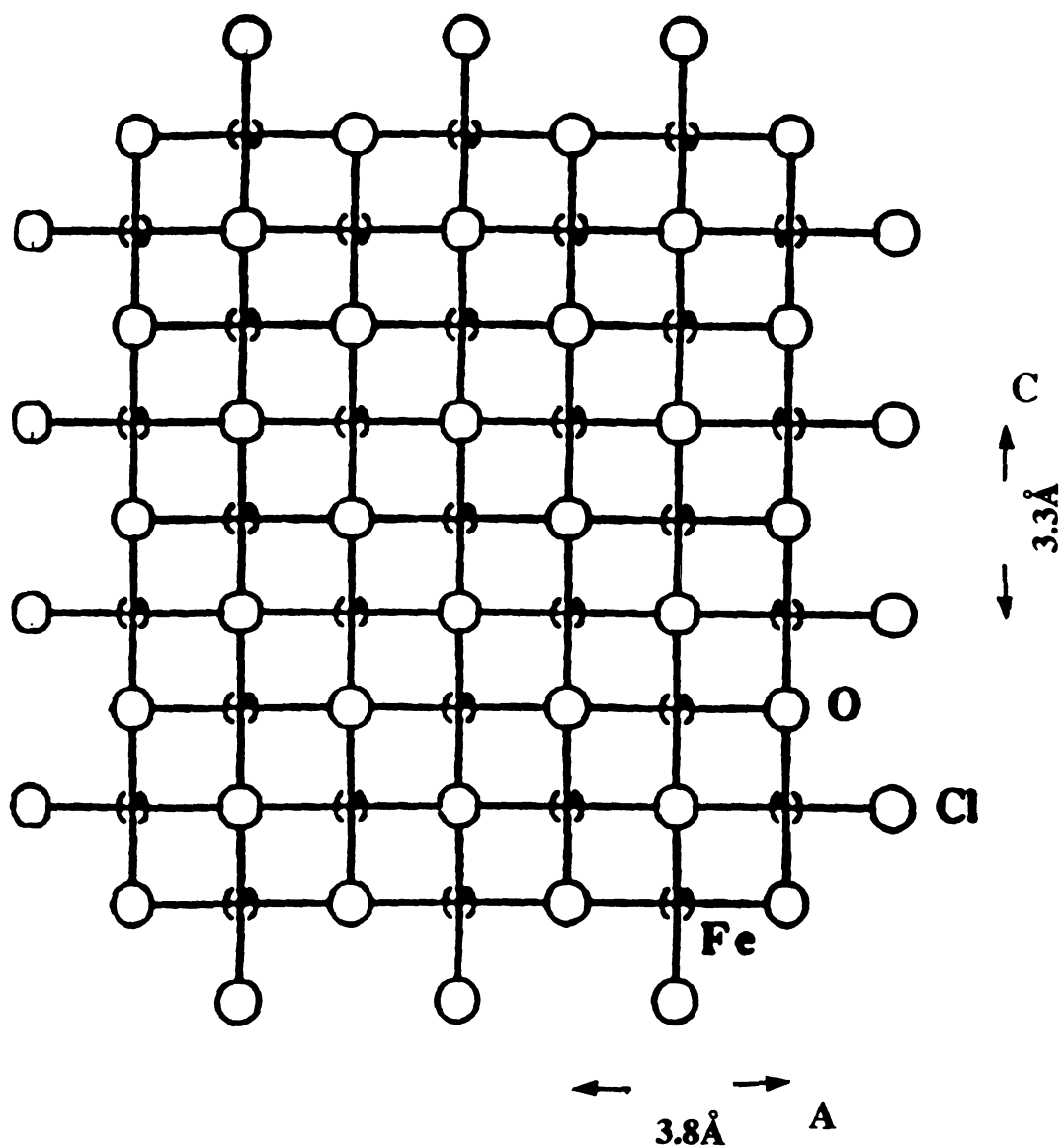
Figure 1.5. Projection of one slab of FeOCl in ac plane (looking down b axis).

In order to understand the magnetic behavior, several physicochemical studies, such as magnetic susceptibility [113], Mössbauer spectroscopy [114], powder neutron diffraction [115] and X-ray diffraction [116], have been employed. The potential application of FeOCl as a cathode material for a primary lithium batteries has been investigated [117].

The redox intercalation chemistry of FeOCl has been known since the early seventies [118]. Being a Fe^{3+} compound, its oxidation potential is significant. During intercalation, the guest species is oxidized and the FeOCl framework is reduced and the interlayer distance expands to accommodate the guest molecules. The intercalation reactions of FeOCl with a variety of organic compounds such as amine [119], pyridine [120], organometallic compounds [121], tetraselenafulvalene [122] and tetrathiofulvalene [123] are also well known. Non reducing cations also can be introduced by reduction with their BH_4^- [33] or I^- salts [124]. The good oxidizing properties of Fe^{3+} and the weak interaction (van der Waals force) between the layers make FeOCl a good candidate for redox intercalation.

LIST OF REFERENCES

LIST OF REFERENCES

1. (a) Little, W. A. *Phys. Rev.* **1964**, 134A, 1416-1424. (b) Greene, R. L.; Street, G. B. *Science* **1984**, 226, 651-656. (c) Ueno, H.; Shimizu, Y.; Mishima, T.; Shioya, J.; Yasuda, N. *Synth. Met.* **1991**, 41-43, 2703-2706. (d) Schmeisser, D.; Jimenez-Gonzales, A.; Schutz, J. U.; Jaborski, J.; Wustenhagen, U.; Umbach, Z.; Gopel, W. *Synth. Met.* **1991**, 41-43, 1809-1816.

2. (a) Melby, L. R. *Can. J. Chem.* **1965**, 43, 1448-1459. (b) Ferraris, J.; Cowan, D. O.; Walatka, V.; Perlstein, J. H. *J. Am. Chem. Soc.* **1973**, 95, 948-949. (c) Bechgaard, K.; Andersen, J. R. in *"The Physics and Chemistry of Low Dimensional Solids"* Alcacer, L. Ed. D. Reidel Publishing Co. **1980**, P247-263. (d) Wudl, F. in *"The Physics and Chemistry of Low Dimensional Solids"* Alcacer, L. Ed. D. Reidel Publishing Co. **1980**, P265-279. (e) Khidekel, M. L.; Zhilyaeva, E. I. *Synth. Met.* **1981**, 4, 1-34. (f) Hoffman, B. M.; Ibers, J. A. *Acc. Chem. Res.* **1983**, 16, 15-21. (g) Parkin, S. S. P.; Engler, E. M.; Schumaker, R. R.; Lagier, R.; Lee, V. Y.; Scott, J. C.; Greene, K. L. *Phys. Rev. Lett.* **1983**, 50, 270-273. (h) Urayama, H.; Yamochi, H.; Saito, G.; Nozawa, K.; Sugano, T.; Kinoshita, M.; Sato, S.; Oshima, K.; Kawamoto, A.; Tanaka, J. *Chem. Lett.* **1988**, 55-58.

3. "Lower Dimensional Systems and Molecular Electronics" NATO Advanced Study Institute Ed. R. M. Metzger et al Plenum Press N. Y. **1991**, 659-667.

4. (a) Shirakawa, H.; Louis, E. J.; MacDiarmid, A. G.; Chiang, C. K.; Heeger, A. J. *J Chem. Soc. Chem. Commun.* **1977**, 578-580. (b) Chiang, C. K.; Fincher, C. R.; Park, Y. W.; Heeger, A. J.; Shirakawa, H.; Louis, E. J.; Gau, S. C.; MacDiarmid, A. G. *Phys. Rev. Lett.* **1977**, 39, 1098-1101.

5. Kanatzidis, M. G. *Chemical&Engineering News* **1990**, 68, 36-54.

6. "Proceedings of the International Conference on Synthetic Metals" Santa Fe, NM, June 1988. (*Synth. Met.* **1988-1989**, 27, 28, 29.

7. Genies, E. M.; Bidan, G.; Diaz, A. F. *J. Electroanal. Chem.* **1983**, 149, 101-113.

8. (a) MacDiarmid, A. G.; Chiang, J. C.; Richter, A. J.; Somasir, N. L. D.; Epstein, A. J. In "Conducting Polymers" Alcacer, L. Ed; Reidel Dordreck Holland **1987**. (b) Genies, E. M.; Tsintaris, C.; Syed, A. A. *Mol. Cryst. Liq. Cryst.* **1985**, 121, 181-185. (c) Hand, R. L.; Nelson, R. F. *J. Am. Chem. Soc.* **1974**, 96, 850-860. (d) Somasir, N. L. D.; Epstein, A. J. in "Conducting Polymers" Alcacer, L. Ed. Reidel Dordrect Holland **1987**.

9. (a) Hoffmann, R. *Angew. Chem. Int. Ed. Engl.* **1987**, 26, 846-878. (b) Coman, D. O.; Wlygul, F. M. *Chemical&Engineering News* **1986**, 64, 28-45.

10. Tanaka, K.; Shichiri, T.; Yoshizawa, K.; Yamabe, T.; Hotta, S.; Shimotsuma, W.; Yamanchi, J.; Deguchi, Y. *Solid State Commu.* **1984**, 51, 565-567.

11. (a) Bredas, J. L.; Yakushi, K.; Scott, J. C.; Street, G. B. *Phys. Rev. B* **1984**, 30, 1023-1025. (b) Bredas, J. L. *Mol. Cryst. Liq. Cryst.* **1985**, 118, 49-56. (c) Chung, T.-C.; Kaufman, J. H.; Heeger, A. J.; Wudl, F. *Mol. Cryst. Liq. Cryst.* **1985**, 118, 205-215. (d) Chung, T.-C.; Kaufman, J. H.; Heeger, A. J.; Wudl, F. *Phys. Rev. B* **1984**, 30, 702-710.

12. (a) Patil, A. O.; Heeger, A. J.; Wudl, F. *Chem. Rev.* **1988**, 88, 183-200. (b) Bredas, J. L.; Chance, R. R.; Silbery, R. *Mol. Cryst. Liq. Cryst.* **1981**, 77, 319-322. (c) Bredas, J. L.; Chance, R. R.; Silbery, R. *Phys. Rev. B* **1982**, 26, 5843-5854. (d) Bredas, J. L.; Themans, B.; Fripiat, J. G.; Andre, J. M.; Chance, R. R. *Phys. Rev. B* **1984**, 29, 6761-6773. (e) Bredas, J. L.; Street, G. B. *Acc. Chem. Res.* **1985**, 18, 309-315.

13. Bredas, J. L.; Themans, B.; Fripiat, J. G.; Andre, J. M.; Chance, R. R. *Synth. Met.* **1984, 9,** 265-274.

14. (a) Genies, E. M.; Hany, P.; Santier. C. *J. Appl. Electrochem.* **1988, 18,** 751-756. (b) Nakajima, T.; Kawogoe, T. *Synth. Met.* **1989, 28,** C647-C654. (c) MacDiarmid, A. G.; Mu, S.-L.; Spmasir, N.L.D.; Wu, W. *Mol. Cryst. Liq. Cryst.* **1985, 121,** 187-190. (d) Inganas, O.; Lundstrom, I. *Synth. Met.* **1987, 21,** 13-19.

15. (a) Burroughes J. H.; Jones, C. A.; Friend, R. H. *Nature* **1988, 335,** 137-141. (b) Yoshino, K.; Kaneto, K.; Tekeda, S. *Synth. Met.* **1987, 18,** 741-746.

16. Kobayashi, T.; Yoneyama, H.; Tamvra, H. *J. Electroanal. Chem.* **1984, 161,** 419-423.

17. (a) Berthet, G.; Blank, J. P.; Germain, J. P.; Larbi, A.; Maleysson, C.; Robert, H. *Synth. Met.* **1987, 18,** 715-720. (b) Bjorklund, R. B.; Lundstroem, I. *J. Electron Mat.* **1984, 13,** 211-230.

18. Liang, W.; Martin, C. R. *Chem. Mater.* **1991, 3,** 390-391.

19. (a) Simon, R. A.; Ricco, R. A.; Wrighton, M. S. *J. Am. Chem. Soc.* **1982, 104,** 2031-2034. (b) Frank, A. J.; Glenis, S.; Nelson, A. J. *J. Phys. Chem.* **1989, 93,** 3815-3825. (c) Horowitz, G.; Tourillon, G.; Garnier, F. *J. Electrochem. Soc.* **1984, 131,** 151-156.

20. (a) Frank, A. J.; Honda, K. *J Phys. Chem.* **1982, 86,** 1933-1935. (b) Honda, K.; Frank, A. J. *J. Phys. Chem.* **1984, 88,** 5577-5582. (c) Gningue, D.; Horowitz, G.; Garnier, F. *J. Electrochem. Soc.* **1988, 135,** 1965-1969.

21. Meyer, W. H.; Kiess, H.; Binggeli, B.; Meier, E.; Harbeke, G. *Synth. Met.* **1985, 10,** 255-259.

22. Lindsey, S. F.; Street, G. B. *Synth. Met.* **1984/1985, 10,** 67-69.

23. Alper, J. *Science* **1989**, 246, 208-210.

24. Tsukamoto, J.; Takahashi, A. *Synth. Met.* **1991**, 41-43, 7-12.

25. (a) Shirakawa, H.; Ikeda, S. *Synth. Met.* **1979/1980**, 1, 175-184. (b) Theophilou, N. *Solid State Ionics* **1989**, 32/33, 582-593. (c) Plocharsk, J.; Pukack, W.; Roth, S. *Synth. Met.* **1991**, 41-43, 131-136. (d) Cao, Y.; Smith, P.; Heeger, A. J. *Synth. Met.* **1991**, 41-43, 181-184. (e) Bryce, M. R.; Chissel, A. D.; Gopel, J.; Kathirganathan, P.; Parker, D. *Synth. Met.* **1991**, 39, 397-400.

26. (a) Soga, S.; Hotta, O.; Sonoda, N.; Shriakawa, H.; Akagi, K. *Jpn. Kokai Tokkyo Koho* JP 02,138314. (b) Araya, K.; Shriakawa, H.; Akagi, K. *Jpn. Kokai Tokkyo Koho* JP 02,119008.

27. Aldissi, M. US Pat. Appl. US 155,450.

28. (a) Shirakawa, H.; Ikeda, S. *Synth. Met.* **1979/1980**, 1, 175-184. (b) Ogasawara, M.; Funabashi, K. *Jpn. Kokai Tokkyo Koho* JP 01,280528. (c) Fischer, J. E.; Tang, X.; Scherr, E. M.; Cajipe, V. B.; MacDiarmid, A. G. *Synth. Met.* **1991**, 41/43 661-664. (d) Gustasson, G.; Inganas, O.; Stafatrom, S.; Osterholm, H.; Laakso, J. *Synth. Met.* **1991** 41/43 593-596. (e) Monkman, A. P.; Adams, P. *Synth. Met.* **1991**, 40, 87-96.

29. (a) *"Intercalation Chemistry"* Whittingham, M. S.; Jacobson, A. J. Eds. Academic, N. Y. **1982**. (b) Boersma, M. A. M. *Catal. Rev.* **1974**, 10, 243-280. (c) Ebert, L. E. *Perprints Div. Petr. Chem. Am. Chem. Soc.* **1977**, 22, 69. (d) Pinnavaia, T. J.; Farzanch, F. *Inorg. Chem.* **1983**, 22, 2216-2220. (e) Figueras, F. *Catal. Rev.* **1988**, 30, 457-499. (f) Wang, M. C. *Clays&Clay Minerals.* **1991**, 39, 202-210.

30. (a) Davidov, D.; Selig, H. Eds *"Graphite Intercalation Compounds"* *Synth. Met.* **1988**, 23. (b) Acrivos, J. V. *NATO ASI Ser.* **1983**, C130, 479-493. (c) Averill, B. A.; Kauzlarich, S. M. *Mol. Cryst. Liq. Cryst.* **1984**, 107, 55-64. (d) Roth, S. *Synth. Met.* **1989**, 34, 617-622. (e) Whittingham, M. S.; Ebere, L. B. in *"Intercalated*

Layered Materials" Levy, F. A. Ed Reidel publishing Co. Dodrecht Holland **1979**, P533-562. (f) Rouxel, J.; Meerschaut, A.; Gressier, P. *Synth. Met.* **1989**, <u>34</u>, 597-607.

31. Pinnavaia, T. J. *Science* **1983**, <u>220</u>, 365-371.

32. Johnson, J. W.; Jacobson, A. J.; Brody, J. F.; Rich, S. M. *Inorg. Chem.* **1982**, <u>21</u>, 3820-3825.

33. Kanatzidis, M. G.; Marks, T. J.; *Inorg. Chem.* **1987**, <u>26</u>, 783-784.

34. Antonio, M. R.; Averill, B. A. *J Chem. Soc. Chem. Commun.* **1981**, 382-383.

35. (a) Kanatzidis, M. G.; Tonge, C. R.; Marcy, H. O.; Marks, T. J.; Kannewurf, C. R. *J. Am. Chem. Soc.* **1987**, <u>109</u>, 3797-3799. (b) Kanatzidis, M. G.; Marcy, H. O.; McCarthy, W. J.; Marks, T. J.; Kannewurf, C. R. *Solid State Ionics* **1989**, <u>32/33</u>, 594-608.

36. Javadi, H. H. S.; Anglepoulos, M.; MacDiarmid, A. G.; Epstein, A. J. *Synth. Met.* **1988**, <u>26</u>, 1-8.

37. Maeda, Y.; Yamashita, M.; Ohshio, H.; Tsutsumi, N.; Takashima, K. *Bull. Chem. Soc. Jpn.* **1982**, <u>55</u>, 3138-3143.

38. (a) Soma, Y.; Soma, M.; Harada, I. *J. Phys. Chem.* **1984**, <u>88</u>, 3034-3038. (b) Soma, Y.; Soma, M.; Harada, I. *Chem. Phys. Lett.* **1983**, <u>99</u>, 153-156. (c) Soma, Y.; Soma, M.; Harada, I. *J. Phys. Chem.* **1985**, <u>89</u>, 738-742.

39. Soma, Y.; Soma, M.; Furukawa, Y.; Harada, I. *Clays & Clay Minerals.* **1987**, <u>35</u>, 53-59.

40. Inoue, H.; Yoneyama, H. *J. Electroanal. Chem.* **1987**, <u>233</u>, 291-294.

41. (a) Enzel, P. Bein, T. *J. Phys. Chem.* **1989**, 93, 6270-6272. (b) Bein, T.; Enzel, P. *Synth Met.* **1989**, 29, E163-E168. (c) Enzel, P.; Bein, T. *J. Chem. Soc. Chem. Commun.* **1989**, 1326-1327. (d) Bein, T.; Enzel, P. *Mol. Cryst. Liq. Cryst.* **1990**, 181, 315-324. (e) Bein, T.; Enzel, P.; Benueu, F.; Zuppiroli, L. *Adv. Chem.* **1990**, 226, 433-449.

42. Mehrotra, V.; Giannelis, E. P. *Mat. Res. Soc. Symp. Proc.* **1990**, 171, 39-44.

43. Brandt, P.; Fischer, R. D.; Martinez, E. S.; Calleja, R. D. *Angew. Chem. Int. Ed. Engl.* **1989**, 28, 1265-1266.

44. Caspar, J. V.; Ramamurthy, V.; Corbin, D. R. *J. Am. Chem. Soc.* **1991**, 113, 600-610.

45. Letherby, H. *J. Chem. Soc.* **1862**, 15, 161-163.

46. (a) MacDiarmid, A. G.; Epstein, A. J. *Faraday Discuss Chem. Soc.* **1989**, 88, 317-332. (b) Epstein, A. J.; Ginder, J. M.; Zuo, F.; Woo, H. S.; Tanner, B. D.; Richter, A. F.; Angelopoulos, M.; Huang, W. S.; MacDiarmid, A. G. *Synth. Met.* **1987**, 21, 63-70.

47. MacDiarmid, A. G.; Somasiri, N. L. D.; Salaneck, W. R.; Lundstroem, I.; Liedberg, B.; Hassan, M. A.; Erlandsson, R.; Konrasson, P. Springer series in solid state science V63 Springer, Berlin, **1985**, 218.

48. (a) Stafstrom, S.; Bredas, J. L.; Epstein, A. J.; Noo, H. S.; Tanner, D. B.; Huang, W. S.; MacDiarmid, A. G. *Phys. Rev. Lett.* **1987**, 59, 1464-1467. (b) Santos, M. C. dos; Bredas, J. L. *Phys. Rev. Lett.* **1989**, 62, 2499-2502.

49. MacDiarmid, A. G.; Chiang, J. C.; Halpern, M.; Mu, W. L.; Somasiri, N. L. D.; Wu W.; Yaniger, S. I. *Mol. Cryst. Liq. Cryst.* **1985**, 121, 173-180.

50. Angelopoulos, M.; Ray, A.; MacDiarmid, A. G.; Epstein, A. J. *Synth. Met.* **1987**, 21, 21-30.

51. Kitani, A.; Kaga, M.; Sasak, K. *J. Electrochem. Soc.* **1988**, 2491-2496.

52. (a) Kobayashi, T.; Yoneyama, H.; Tamura, H. *J. Electroanal. Chem. Interfacial Electrochem.* **1984**, 161, 419-423. (b) MacDiarmid, A. G.; Mu, S. L.; Somasiri, N. L. D.; Wu, W. *Mol. Cry. Liq. Cry.* **1986**, 121, 187-190.

53. (a) Paul, E. W.; Ricco, A. J.; Wrighton, M. S. *J. Phys. Chem.* **1985**, 89, 1441-1447. (b) Chao, S. Wrighton, M. S. *J. Am. Chem. Soc.* **1987**, 109, 6627-6631. (c) Timoeeva, O. N.; Lubentsov, B. Z.; Sudakova, Ye. Z.; Cheryshov, D. N.; Khidekel, M. L. *Synth. Met.* **1991**, 40, 111-116.

54. Mengoli, G.; Musiani, M. M.; Pelli, B.; Vecchi, E. *J. Appl. Polym. Sci.* **1983**, 28, 1125-1136. (b) Mengoli, G.; Munari, M. T.; Bianco, P.; Musiani, M. M. *J. Appli. Polym. Sci.* **1981**, 26, 4247-4257.

55. Ginder, J. M.; Epstein, A. J.; MacDiarmid, A. G. *Synth. Met..* **1989**, 29, E395-E400.

56. Syed, A. A.; Dinesan, M. K. *Synth. Met.* **1990**, 36, 209-215.

57. (a) Mohilner, D. M.; Adams, R. N.; Argersinger, Jr., W. J. *J Am Chem. Soc.* **1962**, 84, 3618-3622. (b) Genies, E. M.; Lapkowski, M. *J. Electroanal. Chem.* **1988**, 249, 97-107.

58. (a) Chiang, J.-C.; MacDiarmid, A. G. *Synth. Met.* **1986**, 13, 193-205. (b) MacDiarmid, A. G.; Chiang, J.-C.; Richter, A. F.; Somasiri, N. L. D.; Epstein, A. J. *"Conducting Polymers"* ed. L. Alcacer (Reidel publications, Dordrecht) **1987**, 105. (c) Pron, A.; Genoud, F.; Menardo, C.; Nechtschein, M. *Synth. Met.* **1988**, 24, 193-201. (d) Armes, S. P.; Miller, J. F. *Synth. Met.* **1988**, 22, 385-393.

59

60

61

62

63

64

65.

66.

59. Lapkowski, M. *Synth. Met.* **1990**, 35, 169-182.

60. Cao, Y.; Li, S.; Xue, Z.; Guo, D. *Synth. Met.* **1986**, 16, 305-315.

61. (a) Kaplan, S.; Conwell, E. M.; Richter, A. F.; MacDiarmid, A. G. *Synth. Met.* **1989**, 29, E235-E242. (b) Menardo, C.; Nechtschein, M.; Rousseau, A.; Travens, J. P.; Hang, P. *Synth. Met.* **1988**, 25, 311-322. (c) Richter, A. F.; Ray, A.; Ramanathan, K. V.; Manohar, S. K.; Furst, G. T.; Opella, S. J.; MacDiarmid, A. G.; Epstein, A. J. *Synth. Met.* **1989**, 29, E243-E249. (d) Kaplan, S.; Conwell, E. M.; Richter, A. F.; MacDiarmid, A. G. *J. Am. Chem. Soc.* **1988**, 110, 764-768.

62. Wang, S. L.; Wang, F. S.; Ge, X. H. *Synth. Met.* **1986**, 16, 99-104.

63. Tan, K. L.; Tan, B. T. G.; Kang, E. T.; Neoh, K. G. *Phys. Rev.* **1989**, 8070-8073.

64. (a) Jozefowicz, M. E.; Laversanne, R.; Javadi, H. H. S.; Epstein, A. J.; Pouget, J. P.; Tang, X.; MacDiarmid, A. G. *Phys. Rev. B* **1989**, 39, 12958-12961. (b) Jozefowicz, M. E.; Epstein, A. J.; Pouget, J. P.; Masters, J. G.; Sun, A. R. Y.; Tang, X.; MacDiarmid, A. G. *Proc. ICSM 1906* (Tubingen, Sept. 1990) *Synth. Met.* **1991**, 41-43, 723-726.

65. (a) Wudl, F.; Augus, Jr R. O.; Lu, F. L.; Allemand, P. H.; Vachon, D. J.; Nowak, M.; Liu, Z. X.; Heeger, A. J. *J. Am. Chem. Soc.* **1987**, 109, 3677-3684. (b) Baughman, R. H.; Wolf, J. F.; Eckhardt, H.; Lagerstedt, I. *Synth. Met.* **1988**, 25, 121-137. (c) Vachon, D.; Angus, R. O.; Lu, F. L.; Nowak, M.; Liu, Z. X.; Schaffer, H.; Wudl, F.; Heeger, A. J. *Synth. Met.* **1987**, 18, 297-302. (d) Lu, F.-L.; Wudl, F.; Nowak, M.; Heeger, A. J. *J. Am Chem. Soc.* **1986**, 108, 8311-8313.

66. (a) Tan, F. R.; Bard, A. J. *J. Electrochem. Soc.* **1986**, 133, 301-304. (b) Penner, R. M.; Martin, C. R. *J. Electrochem. Soc.* **1986**, 133, 310-315.

67. Genies, E. M.; Boyle, A.; Lapkowski, M.; Tsintavis, C. *Synth. Met.* **1990, 36,** 139-142.

68. Gardini, G. P. *Adv. Heterocycl. Chem.* **1973, 15,** 67-98.

69. Street, G. B.; Clarke, T. C.; Krounbi, M.; Kanazawa, K.; Lee, V.; Pfluger, P.; Scott, J. C.; Weiser, G. *Mol. Cryst. Liq. Cryst.* **1982, 83,** 253-264.

70. Tanaka, K.; Shichiri, T.; Toriumi, M.; Yamabe, T. *Synth. Met.* **1989, 30,** 271-281.

71. Machida, S.; Miyata, S.; Techagumpuch, A. *Synth. Met.* **1989, 31,** 311-318.

72. (a) Diaz, A. F.; Hall, B. *IBM J. Res. Dev.* **1983, 27,** 342-347. (b) Yamaura, M.; Sato, K.; Hagiwara, X *Synth. Met.* **1991, 39,** 43-60. (c) Zotti, G.; Schiavon, G.; Comisso, N. *Synth. Met.* **1991, 40,** 309-316.

73. (a) Dall'Olio, A.; Dascola, G.; Varacca, V.; Bocchi, V. *C. R. Acad. Sci. Paris Ser. C* **1968, 267,** 433-435. (b) Satoh, M.; Kaneto, K.; Yosho, K. *Synth. Met.* **1986, 14,** 289-296. (c) Kanazawa, K. K.; Diaz, A. F.; Gill, W. D.; Grant, P. M.; Street, G. B. *Synth. Met.* **1979/1980 1,** 329-336.

74. (a) Salmon, M.; Kanazawa, K. K.; Diaz, A. F.; Krounbi, M. *J. Polym. Sci. Polym. Lett. Ed.* **1982, 20,** 187-193.

75. (a) Hotta, S.; Hosaka, T.; Shinotsuma, W. *Synth. Met.* **1983, 6,** 317-318. (b) Kaneto, K.; Yoshino, K.; Inuishi, Y. *Jpn. J. Appl. Phys. Part 2* **1982, 21,** L567-L568.

76. Inoue, M. B.; Velaquez, E. F.; Inoue, M. *Synth. Met.* **1988, 24,** 223-228.

77. Yamamoto, T.; Sanechika, K.; Yamamoto, A. *J. Polym. Sci. Polym. Lett. Ed.* **1980**, 18, 9-12.

78. *"Handbook of Conducting Polymers"* Ed. T. A. Skotheim Marcel Dekker Inc. **1986** Vol. 1, 193-350.

79. (a) Akimoto, M.; Furukawa, Y.; Takeuch, H.; Harada, I.; Soma, Y.; Soma, M. *Synth. Met.* **1986**, 15, 353-360. (b) Cao, Y.; Guo, D.; Pang, M.; Qian, R. *Synth. Met.* **1987**, 18, 189-194.

80. Danill, R.; Taliani, C.; Zamboni, R.; Giro, G. *Synth. Met.* **1986**, 13, 325-328.

81. Kossmehl, G.; Chatzitheodorou, G. *Mol. Cryst. Liq. Cryst.* **1982**, 83, 291-296.

82. (a) Zotti, G.; Schiavon, G.; Comisso, N.; Berlin, A.; Pagani, G. *Synth. Met.* **1990**, 36, 337-351. (b) Tourillon, G.; Garnier, F. *J. Electroanal. Chem.* **1982**, 135, 173-178. (c) Oshawa, T.; Kaneto, K.; Yoshino, K. *Jpn. J. Appl. Phys.* **1984**, 23, L663-L665. (d) Salaneck, W. R.; Bredas, J. L.; Wu, C. K.; Nillsson, J. O. *Synth. Met.* **1987**, 21, 57-61. (e) Yamamoto, T.; Sanechika, K.; Yamamoto, A. *Chem. Lett.* **1981**, 1079-1082.

83. (a) Leung, W.-Y. Ph-D Dissertation, Michigan State University **1988**. (b) Kauffmann, T.; Lexy, H. *Chem. Ber.* **1981**, 114, 3667-3673. (c) El-Hajj, T.; Martin, J. C.; Descotes, G. *J. Heterocyclic. Chem.* **1983**, 20, 233-235.

84. Armour, M.; Davies, A. G.; Upadhyay, J. *J. Polym. Sci.* **1967**, 5, 1527-1538.

85. Gandini, A. *Adv. Polym. Sci.* **1977**, 25, 47-96.

86. Glenis, S.; Wu, C.-G.; Kanatzidis, M. G. work in progress.

87. Ditle, A. *Seances Acad. Sci.* **1885**, 101, 6987-6989.

88. (a) Bullot, J.; Gallais, O.; Ganthier, M.; Livage, *J. Appl. Phys. Lett.* **1980,** 36, 986   (b) Livage, J. *Chem. Mater.* **1991,** 3, 578-593.

89. (a) Mullier, E. *Z. Chem. Ind. Kolloide* **1911,** 8, 302-307.   (b) Mullier, E. *Z. Chem. Ind. Kolloide* **1904,** 8, 1098-1104.

90. Lemerle, J.; Nejam, L.; Lefebvre, J. *J. Inorg. Nucl. Chem.* **1980,** 42, 17-20.

91. Wegelin, G. *Z. Chem. Ind. Kolloide* **1912,** 11, 25-28.

92. Prandtl, W.; Hess, L. *Z. Anorg. Allgem. Chem.* **1913,** 82, 103-129.

93. (a) Aldebert, P.; Baffier, N.; Gharbi, N.; Livage, J. *Mater. Res. Bull.* **1981,** 16, 669.   (b) Shrivastava, O. P.; Komarneni, S.; Malla, P. *Mater. Res. bull.* **1991,** 26, 357-366.

94. (a) Anderson, A. M.; Granquvist, C. G.; Stevens, J. R. *Appl. Optics* **1989,** 28, 3295-3302.   (b) Talledo, A.; Anderson, A. M.; Granquvist, C. G. *J. Mater. Res.* **1990,** 5, 1253-1265.

95. (a) Bullot, J.; Gallais, O.; Gauthier, M.; Livage, J. *Phys. Status Solidi: A* **1982,** 71, K1-K4.   (b) Livage, J.; Lemerle, J. *Inn. Rev. Mater. Sci.* **1982,** 12, 103-122.

96. Legendre, J. J.; Aldebert, P.; Baffier, N.; Livage, J. *J. Coll. Interface Sci.* **1983,** 94, 84-89.

97. Legendre, J. J.; Livage, J. *J. Coll. Interface Sci.* **1983,** 94, 75-83.

98. Aldebert, P.; Hasslin, H. W.; Baffier, N.; Livage, J. *J. Coll. Interface Sci.* **1984,** 98, 478-483.

99. Livage, J.; Gharbi, N.; Leroy, N. C.; Michaud, M. *Mat. Res. Bull.* **1978,** 13, 1117-1124.

100. Stizza, S.; Mancini, G.; Benatto, M.; Matoli, C. R.; Garcia, J.; Bianconi, A. *Phys. Rev. B* **1989**, 40, 12229-12236.

101. Kamiyama, T.; Itoh, T.; Suzuki, K. *J. Non-cryst. Solid* **1988**, 100, 466-470.

102. Livage, J.; Barboux, P.; Badot, J. C.; Baffier, N. *Mat. Res. Soc. Symp. Proc.* "Better Ceramics Through Chemistry III" **1988**, 121, 167-177.

103. Barboux, P.; Baffier, N.; Morineau, M.; Livage, J. *Solid State Ionics* **1983**, 9/10, 1073-1080.

104. Bullot, J.; Gallais, O.; Ganthier, M.; Livage, J. *Appl. Phys. Lett.* **1980**, 36, 986-988.

105. (a) Baffier, N.; Znaidi, L.; Huber, M. *Mat. Res. Bull.* **1990**, 25, 705-713. (b) Bouhaouss, A.; Aldebert, P.; Baffier, N.; Livage, J. *Rev. Chim. Min.* **1985**, 22, 417-426. (c) Bouhaouss, A.; Aldebert, P. *Mat. Res. Bull.* **1983**, 18, 1247-1256.

106. Casal, B.; Ruiz-Hitzky, E.; Crespin, M.; Tinet, D.; Galvan, J. C. *J. Chem. Soc. Faraday Trans. 1* **1989**, 86, 4167-4177.

107. (a) Erre, R.; Masbah, H.; Crespin, M.; Van Damme, H.; Tinet, D. *Solid State Ionics* **1990**, 37, 239-251. (b) Masbah, H.; Tinet, D.; Crespin, M.; Erre, R.; Setton, R.; Van Damme, H. *J. Chem. Soc. Chem. Commun.* **1985**, 935-936. (c) Van Damme, H.; Letellier, M.; Tinet, D.; Kihal, B.; Erre, R. *Mat. Res. Bull.* **1984**, 19, 1635-1642.

108. Aldebert, P.; Baffier, N.; Gharbi, N.; Livage, J. *Mat. Res. Bull.* **1981**, 16, 949-955.

109. Clement, R. P.; Davies, W. B.; Ford, K. A.; Green, M. L. H.; Jacobson, J. J. *Inorg. Chem.* **1978**, 17, 2754-2758

110

111

112

113

114

115

116

117

118

119

120

121

110. Lind, M. D. *Acta. Cryst.* **1970,** B20, 1058-1062.

111. Bannwart, R. S.; Phillips, J. E.; Herber, R. H. *J. Solid State Chem.* **1987,** 71, 540-542.

112. (a) Bizette, H.; Adam, A. *C. R. Acad. Sci. Paris Ser.* **1972,** 275, 911-913. (b) Grant, R. *J. Appl. Phys.* **1971,** 42, 1619-1622.

113. (a) Herber, R. H.; Macda, Y. *Inorg. Chem.* **1980,** 19, 3411-3418. (b) Herber, R. H. *Acc. Chem. Res.* **1982,** 15, 216-224.

114. Adam, A.; Buisson, G. *Phys. Status. Solidi* **1975,** 30, 323-329.

115. Venien, J. P.; Palvadeau, P.; Calvaris, G. *C. R. Acad. Sci. Ser. 2* **1981,** 292, 1259-1262.

116. Takchara, Z.; Kanamura, K.; Imanishi, N.; Zhen, C. *Bull. Chem. Soc. Jpn.* **1989,** 62, 3609-3613.

117. Halbert, T. R.; Scanlon, J. *Mat. Res. Bull.* **1979,** 14, 415-421. (b) Kanawaru, F.; Shimada, M.; Koizumi, M.; Takano, M.; Takada, T. *J. Solid State Chem.* **1973,** 7, 297-299. (c) Kanawaru, F.; Koizumi, M. *Jpn. J. Appl. Phys.* **1974,** 13, 1319-1320. (d) Kikkawa, S.; Kanawaru, F.; Koizumi, M. *Bull. Chem. Soc. Jpn.* **1979,** 52, 963-966.

118. Weiss, A.; Sick, Z. *Naturforsch Teil.* **1978,** B33, 1087-1090.

119. Palvadeau, P.; Coic, L.; Rouxel, J.; Portier, J. *Mat. Res. Bull.* **1978,** 13, 221-227.

120. Schafer-Stahl, H.; Abele, R. *Mat. Res. Bull.* **1980,** 15, 1157-1165.

121. Bringley, J. F.; Averill, B. A. *Mol. Cryst. Liq. Cryst.* **1988,** 170, 215-222.

122. Antonio, M. R.; Averill, B. A. *J. Chem. Soc. Chem. Commun.* **1981**, 282-283.

123. Banewicz, J. J.; Maquire, J. A. *Mat. Res. Bull.* **1988**, <u>21</u>, 93-98.

CHAPTER 2

NOVEL LOW-DIMENSIONAL CONDUCTING POLYMER/METAL OXIDE COMPOSITES: *IN-SITU* OXIDATIVE POLYMERIZATION/ INTERCALATION OF ANILINE IN V₂O₅ XEROGEL

ty

Th

str

in

an

for

ac

low

no

oxi

fra

Cu

the

poly

ther

poly

air

the

anil

mol

phys

decr

ABSTRACT

Polyaniline can be intercalated in the layered $V_2O_5nH_2O$ xerogel by *in-situ* oxidative polymerization/ intercalation of aniline in air. The reaction is facile and topotactic in nature, in which the layer structure remains intact after intercalation. The observed 2.39Å net interlayer expansion corresponds to expulsion of one layer of water and insertion of a monolayer of polyaniline. The polyaniline is formed as the emeraldine salt. Evidence is presented that oxygen acts as an electron acceptor during the reaction. This explains the lower spin number of $(PANI)_xV_2O_5nH_2O$, calculated from magnetic moment, than expected assuming all the electrons obtained from the oxidative polymerization of aniline are transferred to the V_2O_5 framework. All $(PANI)_xV_2O_5nH_2O$ samples are paramagnetic with a Curie-Weiss and a temperature independent Van Vleck contribution.

The room temperature conductivity of $(PANI)_xV_2O_5nH_2O$ is in the range of 10^{-4} to $10^0 \, \Omega^{-1}cm^{-1}$ depending on the degree of polymerization of polyaniline inside the layers. Room temperature thermoelectric power is negative (-30~-300 $\mu V/K$) depending on the polymer content and the degree of polymerization. Upon standing in air (aging), two reactions occur independently: the reoxidization of the reduced V_2O_5 framework and further oxidative coupling of aniline oligomers inside the V_2O_5 layers lead to longer chain molecules. These observations are supported by several physicochemical data. The magnetic moment of $(PANI)_xV_2O_5nH_2O$ decreases gradually upon exposure to air but it does not change

when the sample is stored in vacuum. Gel permeation chromatography (GPC) analysis results show that, although both samples show a mutli-modal molecular weight distribution, the molecular weight of polyaniline extracted from aged $(PANI)_x V_2O_5 n H_2O$ is larger than that extracted from the fresh samples. The thermal stability of polyaniline extracted from aged $(PANI)_x V_2O_5 n H_2O$ is better than that extracted from fresh sample. The conductivity of aged samples increases 100 times. The Seebeck coefficient for freshly prepared samples is negative and independent of temperature whereas for aged samples it is relatively small, negative and increases with raising temperature, characteristic of a n-type conductor.

I. Introduction:

Currently the investigation of electrically conducting organic polymers is an active area of research [1]. Among them, polyaniline and its derivatives are probably the most rapidly growing class as can be seen from the publications of the last several years. Polyaniline has been known since the last century as aniline black [2] and it attracted renewed attention by the discovery of its promising electrical properties which can be reversibly controlled by its oxidation state and degree of protonation [3]. It is usually prepared by electrochemical [4,5] or chemical oxidation [6] of aniline. The resulting products are of poor crystallinity and insoluble in common organic solvents. There have been extensive studies of its chemical structure by various spectroscopic methods [7,8]. However, due to the lack of precise structure information on single chains as well as interchain organization, a good understanding of the conducting mechanisms and significant improvement in electrical properties have not yet been achieved.

Based on the rationale given in chapter 1, we describe the preparation of a novel material in which polyaniline chains are sandwiched (intercalated) between layers of V_2O_5 xerogel. The spectroscopic and physicochemical characterization of this material, along with its charge transport properties are described.

II

D

r

a

N

so

we

an

Kn

Fo

pre

pov

ins

as

pre

con

diff

200

spa

was

The

II. Experimental Section:

Reagents: NaOH, HCl, NaVO$_3$, 2,6 dimethyl-aniline, (NH$_4$)$_2$S$_2$O$_8$, Dimethyl sulfoxide (DMSO), N-methylformamide (NMF), 1,4-bis[2-(5-phenyloxazolyl)]benzene (POPOP), N,N'-bis(p-methybenzylidene)-α,α-bi-p-toluidine (BMBT) and HPLC graded N-methyl-pyrrolidinone (NMP), tetrahydrofuran (THF) were purchased from commercial sources and used without further purification. CH$_3$CN and C$_6$H$_5$NH$_2$ were dried under CaH$_2$ and were distilled under vacuum or in the atmosphere prior to use.

Physicochemical Methods.

Elemental analyses were done by Galbraith Laboratories, Knoxville, TN and Oneida Research Services, INC, Whitesboro, N.Y. Fourier Transform Infrared (FTIR) spectra were recorded from pressed KBr pellets using a Nicolet 740 FTIR spectrometer. X-ray powder diffraction studies were carried out with a Phillips XRG-3000 instrument using Ni-filtered Cu Kα radiation. The samples were run as either films or powders because pressed pellets show significant preferential orientation. The interlayer spacing was further confirmed by using a Rigaku rotating anode X-ray powder diffractometer, Rigaku-Denki/RW400F2 (Rotaflex), at 45KV and 100mA. Transmission-mode diffraction patterns and accurate d-spacings were obtained with this instrument. Oxygen consumption was detected by an YSI Model 53 oxygen monitor with a closed cell. The oxygen concentration measured at an empty cell is defined as 0

% and the oxygen concentration of distilled water saturated with oxygen at room temperature is defined as 100 %. The amount of oxygen consumed is the decrease of oxygen concentration after reaction of monomer with V_2O_5 xerogel for 20 minutes.

Gel Permeation Chromatography (GPC) results were obtained by using a Perkin Elmer 250 HPLC with binary LC pump and LC-235 diode array uv/vis detector. The column used was a PLgel 10 mm mixed B column which has a column efficiency of more than 35,000 plates per meter. In a typical procedure, 5 mg of emeraldine base was dissolved in 1.5 ml NMP. The mixture was then filtered through 4500Å pore size filter which was purchased from Phenomenex Inc., Torrance, CA. The column and detector were maintained at room temperature (18°C). The injection volume was 25 μl and the flow rate was 1 ml/min, using N-methyl-2-pyrrolidinone as an eluent. Monodispersed polystyrene standard (purchased from Polymer Laboratories Inc., Amherst, MA.) with molecular weight ranging from 580 to 7,100,000 was used for constructing the calibration curve shown in Figure 2.1. The molecular weight of polyaniline was obtained from a comparison of the retention times of the polymer with polystyrene standard at the same flow rate and eluent. Two model compounds: 1,4-bis[2-(5-phenyloxazolyl)]benzene (POPOP) and N,N'-bis(p-methybenzylidene)-α,α-bi-p-toluidine (BMBT) with structures more closely resembling that of aniline oligomers, were used to further correct the molecular weight obtained with the polystyrene calibration.

Thermogravimetric Analysis (TGA) and Differential Scanning Calorimetry (DSC) were performed with Shimadzu TGA-50 and DSC-
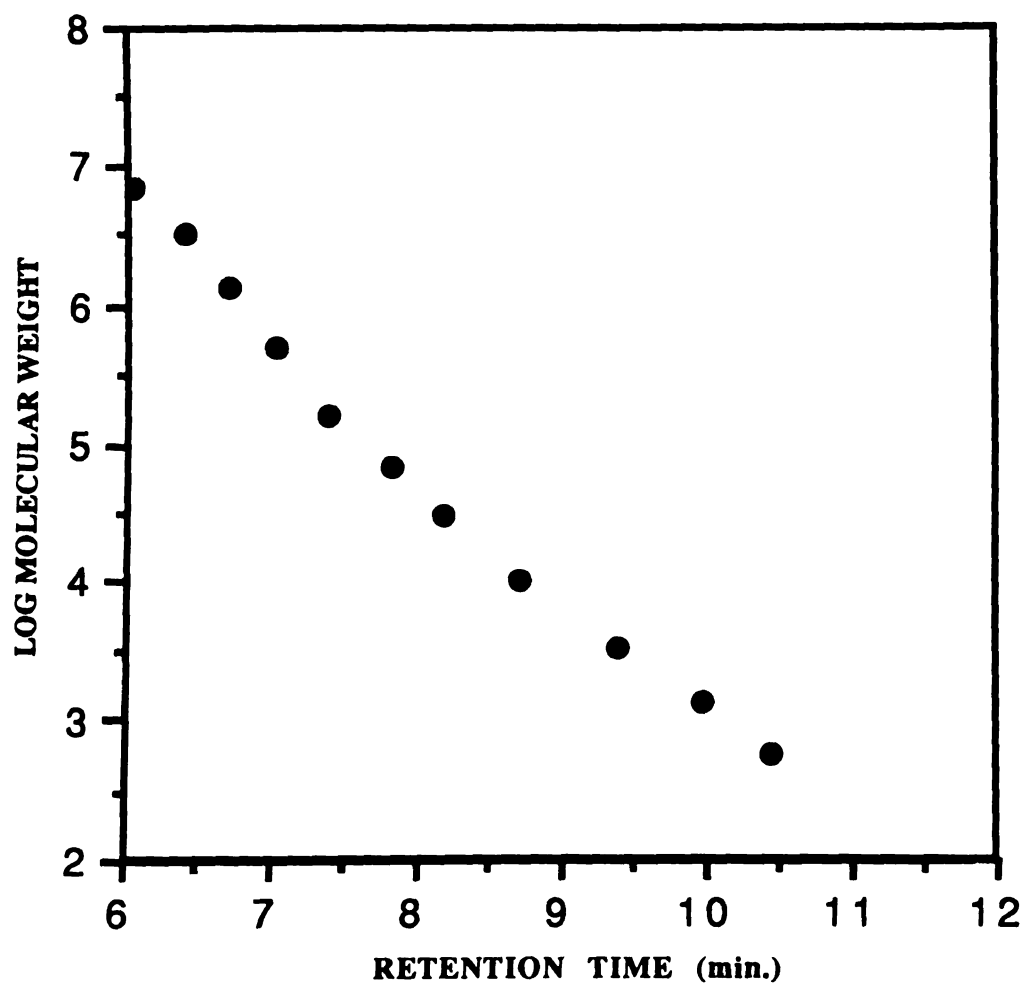
Figure 2.1. Calibration curve: Molecular weight versus retention time of polystyrene standard.

sp

ge

fr

of

se

ra

sp

ra

sc

wi

dip

M

Di

Th

dor

res

stu

ele

10

pre

dep

was

spa

furt

Pyr

Spe

50 thermal analysis system using dry oxygen or nitrogen as carrier gas at flow rate of 72 ml per minute. The TGA experiments were run from room temperature to 1000°C (or 800°C) at a linear heating rate of 10°C (or 5°C) per minute. DSC experiments were run at temperatures between 20°C to 500°C under nitrogen with heating rate of 5°C per minute. Electron Paramagnetic Resonance (EPR) spectra were recorded on a Varian E-4 EPR spectrometer at room temperature or liquid nitrogen temperature. The solid samples were scanned from 2900 to 3900 gauss at 8~32 gauss field modulation with 0.1 second time constant. The field was calibrated with 2,2-diphenyl-1-picrylhydrazyl (DPPH, $g = 2.0036$). Scanning Electron Microscopy (SEM) equipped with a TRACOR Northern Energy Dispersive Spectroscopy (EDS) and Transmission Electron Microscopy (TEM) with Selective Area Electron Diffraction (SAED) studies were done with JEOL-JSM 35CF at 20 KV and a JEOL-100 CX(II) at 100 KV respectively. The samples for SEM imaging were mounted on Al stubs with graphite paint without further coating. Samples for electron diffraction studies were dispersed in acetone, sonicated for 10 minutes then deposited in holey film-coated copper grids. For preparing V_2O_5 gel, a drop of very diluted V_2O_5 wet gel was deposited on the copper grid and dried in air. A thin layer of xerogel was formed on the grid which was used for SAED studies. The d-spacings calculated from diffraction patterns (Bragg rings) were further calibrated by aluminum standard after each measurement. Pyrolysis mass spectra were obtained with a JEOL JMS-AX505H Mass Spectrometer with temperature programming probe.

Variable temperature magnetic susceptibility data were collected on a Quantum Design SQUID system at various magnetic fields (500~1500 gauss). A known quantity of material was placed in a plastic bag and purged with Ar gas before closing. The resulting magnetic data were further corrected for the diamagnetic contribution of the container. Measurements were made with an ascending temperature ramp from 5K to 300K. Direct-current electrical conductivity and thermopower measurements were made on compactions of powder in pellet form, free standing films or single crystals. Conductivity measurements were performed in the usual four-probe geometry with 60mm and 25mm gold wires used for the current and voltage electrodes, respectively. Measurements of the pellet cross-sectional area and voltage probe separation were made with a calibrated binocular microscope. Conductivity data were obtained with the computer-automated system described elsewhere [9]. Thermoelectric power measurements were made by using a slow ac technique [10] with 60mm gold wires serving to support and conduct heat to the sample, as well as to measure the voltage across the sample resulting from the applied temperature gradient. In both measurements, the gold electrodes were held in place on the sample with a conductive gold paste.

All charge transport measurements were done by Carl R. Kannewurf and coworkers in Electrical Engineering Department, Northwestern University. The protocol for charge transport measurements has been reports by professor Kannewurf et al. [11,12].

Preparation of $V_2O_5nH_2O$ Xerogel.

A HVO_3 solution was obtained by dissolving 4.0 g (32.8 mmol) of $NaVO_3$ in 250 ml distilled H_2O, and passing the solution through a H^+ ion-exchange column packed with 30 g of Dowex-50X2-100 resin. Upon standing, the yellow $HVO_3(aq)$ polymerized within 24 to 96 hours to a V_2O_5 sol which thickens to become a V_2O_5 gel via a sol-gel transition. The gel was then poured on glass substrates and the excess water was allowed to evaporate upon standing in air. The dark red film formed on the surface of glass has the chemical formula $V_2O_5nH_2O$ (n~1.6 depending on ambient humidity). The dry film can be peeled off as a free standing film or it can be ground into powder for subsequent use.

Preparation of $(PANI)_{0.44}V_2O_50.7H_2O$ Film.

In a typical reaction, 2.0 g (21.5 mmol) of aniline was mixed with 30 ml distilled H_2O (the mixture is not necessarily a homogeneous solution). To this was added 0.5 g (2.37 mmol) of V_2O_5 xerogel film. The mixture was allowed to stand at room temperature for 24 hours in air. The black pieces of film were isolated by filtration, washed with acetone and dried in vacuum. Elemental analysis: Calcd. for $(C_6H_4NH)_{0.44}V_2O_50.7H_2O$: C, 13.51%; H, 1.58%; N, 2.63%; V, 43.47%. Found: C, 12.92%; H, 1.53%; N, 2.53%; V, 41.69%.

Preparation of $(PANI)_{0.19}V_2O_50.6H_2O$ Film.

0.1 g (1.1 mmol) of aniline was dissolved in 20 ml distilled H_2O, followed by addition of 0.6 g (2.84 mmol) of V_2O_5 xerogel film. The mixture was allowed to stand at room temperature for 5 hours in air. The product was isolated by filtration, washed with acetone and dried in vacuum. Elemental analysis: Calcd. for $(C_6H_4NH)_{0.19}V_2O_50.6H_2O$: C, 6.50%; H, 1.02%; N, 1.26%; V, 48.46%. Found: C, 6.37%; H, 1.16%; N, 1.33%; V, 47.08%.

Preparation of $(PANI)_{0.77}V_2O_50.26H_2O$ Powder.

0.5 g (2.38 mmol) of V_2O_5 xerogel (fine powder) was added in 85 ml 3.5 wt% of aniline aqueous solution. The mixture was stirred at room temperature for 16 hours in air. The black powder was isolated by filtration, washed with acetone and dried in vacuum. Anal. Calcd. for $(C_6H_4NH)_{0.77}V_2O_50.26H_2O$: C, 21.59%; H, 1.70%; N, 4.20%; V, 39.73%. Found: C, 21.59%; H, 2.02%; N, 4.07%; V, 39.51%. Changing the aniline/V_2O_5 ratio and solvent amount, different stoichiometric products can be obtained. The interlayer spacings of all samples calculated from X-ray powder diffraction are equal to 13.94Å.

Preparation of (poly-2,6-dimethylaniline)$_{0.4}V_2O_5.5H_2O$.

0.1 g (0.83 mmol) of 2,6-dimethylaniline was mixed with 50 ml H_2O, followed by addition of 0.35 g (1.66 mmol) of film of V_2O_5

xerogel. The mixture was allowed to stand at room temperature without stirring for 14 hours. The black film was isolated by filtration, washed with acetone and dried in air. Elemental analysis Calcd. for $(C_8H_8NH)_{0.4}V_2O_50.5H_2O$: C: 16.13%, H: 1.91%; N: 2.35%, V: 42.85%. Found: C: 15.13%, H: 2.40%, N: 2.36%, V: 40.68%. The interlayer spacing calculated from X-ray diffraction is equal to 14.57Å.

Synthesis of Bulk Polyaniline.

103 g (452 mmol) of $(NH_4)_2S_2O_8$ was dissolved in 150 ml of water and then added to a solution containing 20.0 g (215 mmol) of aniline with 300 ml 1M HCl(aq). The mixture was stirred in air at 0°C for 1 hour, then at room temperature for 3 hours. The black precipitate was isolated by filtration, washed with water then acetone and dried in air. The product was identified by its characteristic infrared spectrum [7a].

Extraction of Polyaniline from $(PANI)_{0.5}V_2O_50.3H_2O$ in Basic Solution.

0.15 g (0.64 mmol) of $(PANI)_{0.50}V_2O_50.33H_2O$ was mixed with 100 ml 2 wt% NaOH(aq) and stirred at room temperature for 17 hours. The black residue was isolated by filtration, washed copiously with H_2O, 1.0 M HCl(aq), then H_2O again and acetone, dried in vacuum. The product was identified to be the emeraldine salt of polyaniline by infrared spectroscopy.

:0

b:

a:

em

III

in

rep

xC

V₂(

xC

Extraction of Polyaniline from $(PANI)_{0.5}V_2O_5 0.33H_2O$ in Acidic Solution.

0.17 g (0.73 mmol) of $(PANI)_{0.50}V_2O_5 0.33H_2O$ was mixed with 100 ml 2M HCl(aq) and stirred at room temperature for 2 days. The black residue was isolated by filtration, washed with H_2O then acetone and dried in vacuum. This residue was identified to be the emeraldine salt of polyaniline by its infrared spectrum.

III. Results and Discussion:

A. Reaction of Aniline with V_2O_5 Xerogel and Product Characterization.

The intercalation of aniline in V_2O_5 xerogel is a redox reaction in which aniline is oxidatively polymerized and V_2O_5 is reduced as represented in equations 2.1, 2.2 and 2.3.

$$xC_6H_5NH_2 \longrightarrow (C_6H_4NH)_x + 2.5\,xe^- + 2xH^+ \quad \ldots\ldots \text{eq (2.1)}$$

$$V_2O_5 nH_2O + 2.5xe^- \longrightarrow V_2O_5^{-2.5x}nH_2O \ldots\ldots \text{eq (2.2)}$$

$$xC_6H_5NH_2 + V_2O_5 nH_2O \longrightarrow (C_6H_4NH)_x H_{2x}V_2O_5 nH_2O \ldots \text{eq (2.3)}$$
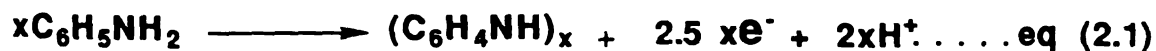
This redox intercalation is a facile reaction, which occurs instantly upon contact of the xerogel with aniline (aqueous solution), as evidenced by the immediate and dramatic color change to dark blue. However, the reaction takes several hours to go to completion because of the slow diffusion of the guest species into the inner layers of the host. Generally, if a solvent is able to swell the xerogel, the intercalation reaction occurs fast. In fact, V_2O_5 xerogel did not react with neat aniline presumably because it cannot be swelled by aniline. When solvents which swell the xerogel such as DMSO, NMF were used, we found significant amount of solvent was intercalated, while polymer formation was decreased. Thus far, water seems to be the most suitable solvent for this redox intercalation.

The black film isolated from the reaction of V_2O_5 xerogel film with aniline aqueous solution showed good crystallinity along the layer stacking direction but the homogeneity of the product was difficult to control. Reducing the particle size of the xerogel increases the reaction rate and avoids the homogeneity problem but at the same times decreases the crystallinity of the products, as judged by the XRD pattern. When a wet gel (preswollen) of V_2O_5 was used, the reaction was complete within minutes but the final product was amorphous and sometimes the V_2O_5 framework was destroyed as judged by the dramatic changes in the IR spectrum. Acetonitrile does not swell the V_2O_5 xerogel at room temperature and we observed no reaction between V_2O_5 film and aniline in this solvent at room temperature. Nevertheless, when a fine powder of V_2O_5 was used or the reaction was carried out at reflux temperature, the intercalation did occur. However, the products had relatively poor

crystallinity. Since CH_3CN does not swell the V_2O_5 xerogel, and all reactions were run in air, atmospheric H_2O may have been absorbed by the V_2O_5, causing some swelling of the xerogel, thus rendering it reactive towards aniline. Acetonitrile here is simply an inert solvent.

Strong evidence of formation of the emeraldine salt derives from the FTIR spectra shown in Figure 2.2. The FTIR spectrum of $(PANI)_xV_2O_5nH_2O$ shows the characteristic IR pattern of emeraldine salt [7a] occurring between 1000 cm^{-1} and 1600 cm^{-1}. The three strong peaks at wavenumber below 1000 cm^{-1} belong to the vibrations of V_2O_5 framework. The polyaniline inside can be easily extracted by digesting the V_2O_5 matrix with 2M HCl(aq) or 2% NaOH(aq). The IR spectrum of extracted polyaniline is similar to that of chemically polymerized bulk material (see Figure 2.2). Table 2.1 compares the most important absorption peaks of bulk polyaniline, $(PANI)_xV_2O_5nH_2O$ and extracted polyaniline.

The direct evidence for the formation of intercalated compound comes from the X-ray powder diffraction (XRD) data listed in Table 2.2. Upon intercalation, the interlayer spacing of V_2O_5 xerogel expands from 11.55Å to 13.94Å. Only several (001) reflections are observed as shown in Figure 2.3 which is a typical pattern for quasi-crystalline layered materials. The crystallite sizes (calculated from the Scherrer formula [13]) of V_2O_5 xerogel and $(PANI)_xV_2O_5nH_2O$ in the b-direction (ac plane) have the same order of magnitude (70Å and 80Å for V_2O_5 and $(PANI)_xV_2O_5nH_2O$ respectively). This indicates that the intralayer structure of V_2O_5 is preserved after intercalating polyaniline. The 2.39Å interlayer expansion is the result of removing one layer of H_2O (approximately 2.8Å) and inserting a

TRANSMITTANCE

(A)

(B)

(C)

2000 1820 1640 1460 1280 1100 920 740 560 380

WAVENUMBER (cm^{-1})
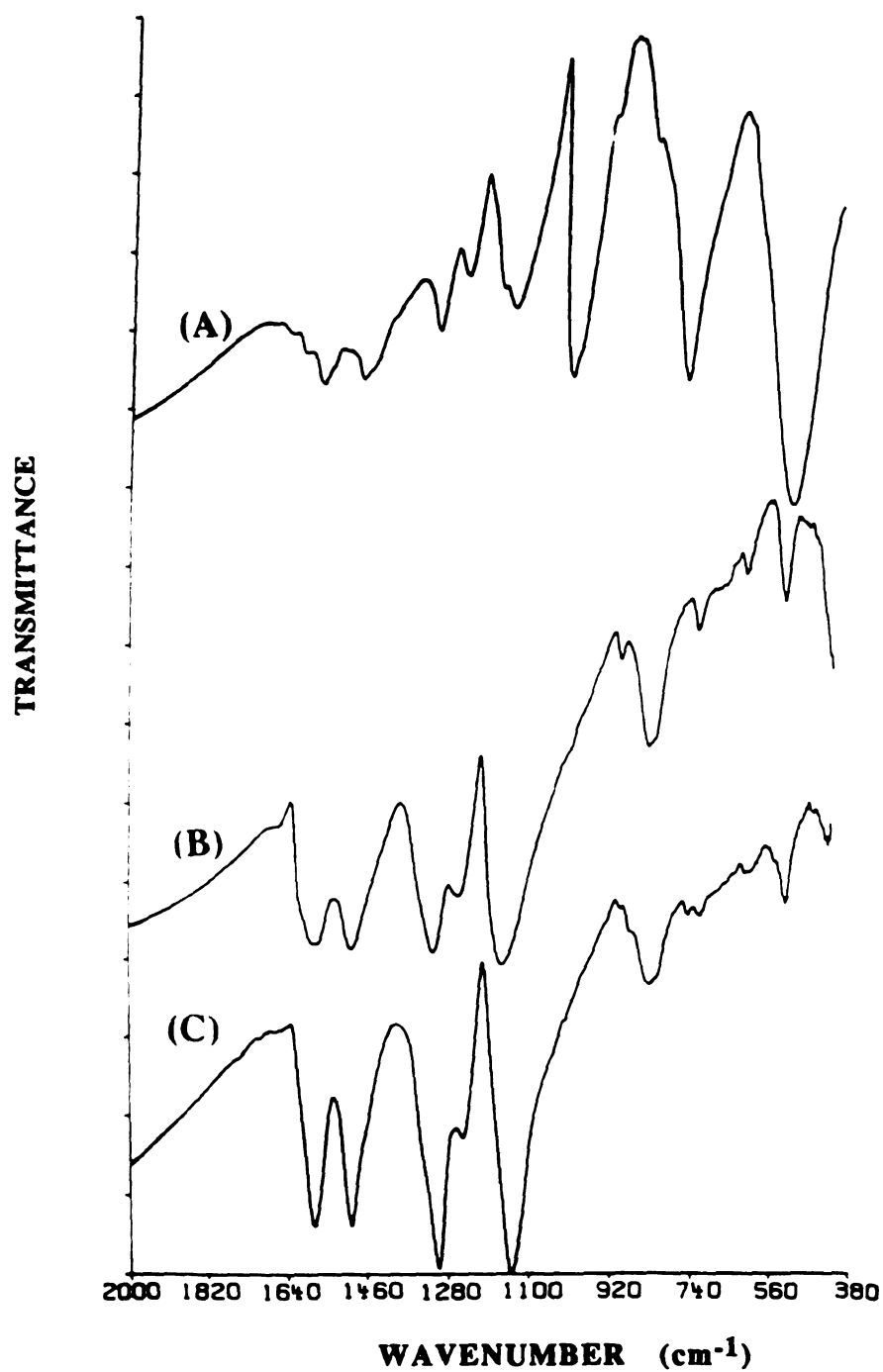
Figure 2.2. FT-IR spectra (KBr pellets) of (A) $(PANI)_x V_2 O_5 n H_2 O$ (B) Bulk polyaniline (emeraldine salt) (C) Polyaniline extracted from $(PANI)_x V_2 O_5 n H_2 O$.

Table 2.1. IR Vibration Energies of Bulk Polyaniline, (PANI)$_x$V$_2$O$_5$nH$_2$O and Extracted Polyaniline.

Modes[16]	*N=Q=N	*N-B-N OR C=N stretching	C-N in QBQ, QBB, BBQ and CH bending	C-N in BBB	Q=NH-B or CH deformation	CH on 1,4 ring bending or C-C stretching	CH on 1,2 ring bending	aromatic ring deformation
***Bulk polyaniline	1569 cm^{-1}	1478 cm^{-1}	1295 cm^{-1}	1249 cm^{-1}	1140 cm^{-1}	809 cm^{-1}	696 cm^{-1}	590 cm^{-1} 499 cm^{-1}
(PANI)$_x$V$_2$O$_5$	1566 cm^{-1}	1471 cm^{-1}	1298 cm^{-1}	1237 cm^{-1}	1131 cm^{-1}	**997 cm^{-1} **751 cm^{-1} **506 cm^{-1}		
Extracted polyaniline	1584 cm^{-1}	1492 cm^{-1}	1302 cm^{-1}	1239 cm^{-1}	1140 cm^{-1}	816 cm^{-1}	–	499 cm^{-1}

*: Q: quinone; B: benzene.

**: Vibration band belongs to V$_2$O$_5$ framework.

***: Emeraldine salt.

Table 2.2. Crystallographic Data of (CANL-X₂·XₐH₂O) and X₂O₅, Xₐ₀Xₐ₅):

Table 2.2. Crystallographic Data of $(PANI)_x V_2O_5 nH_2O$ and V_2O_5 Xerogel.

h k l	$(PANI)_x V_2O_5 nH_2O$		V_2O_5 xerogel	
	d(obsd) (Å),	d(calcd)* (Å)	d(obsd) (Å),	d(calcd) (Å)
0 0 1	14.198,	13.940	11.577,	11.550
0 0 2	7.019,	6.970	– – ,	5.775
0 0 3	4.605,	4.647	3.831,	3.850
0 0 4	3.456,	3.485	2.873,	2.898
0 0 5	2.766,	2.788	2.298,	2.310
0 0 6	2.297,	2.323	1.915,	1.925

*: Calculated values for orthorhombic cell; a=13.423Å, b=7.035Å, c=13.94Å

INTENSITY

Fig
of
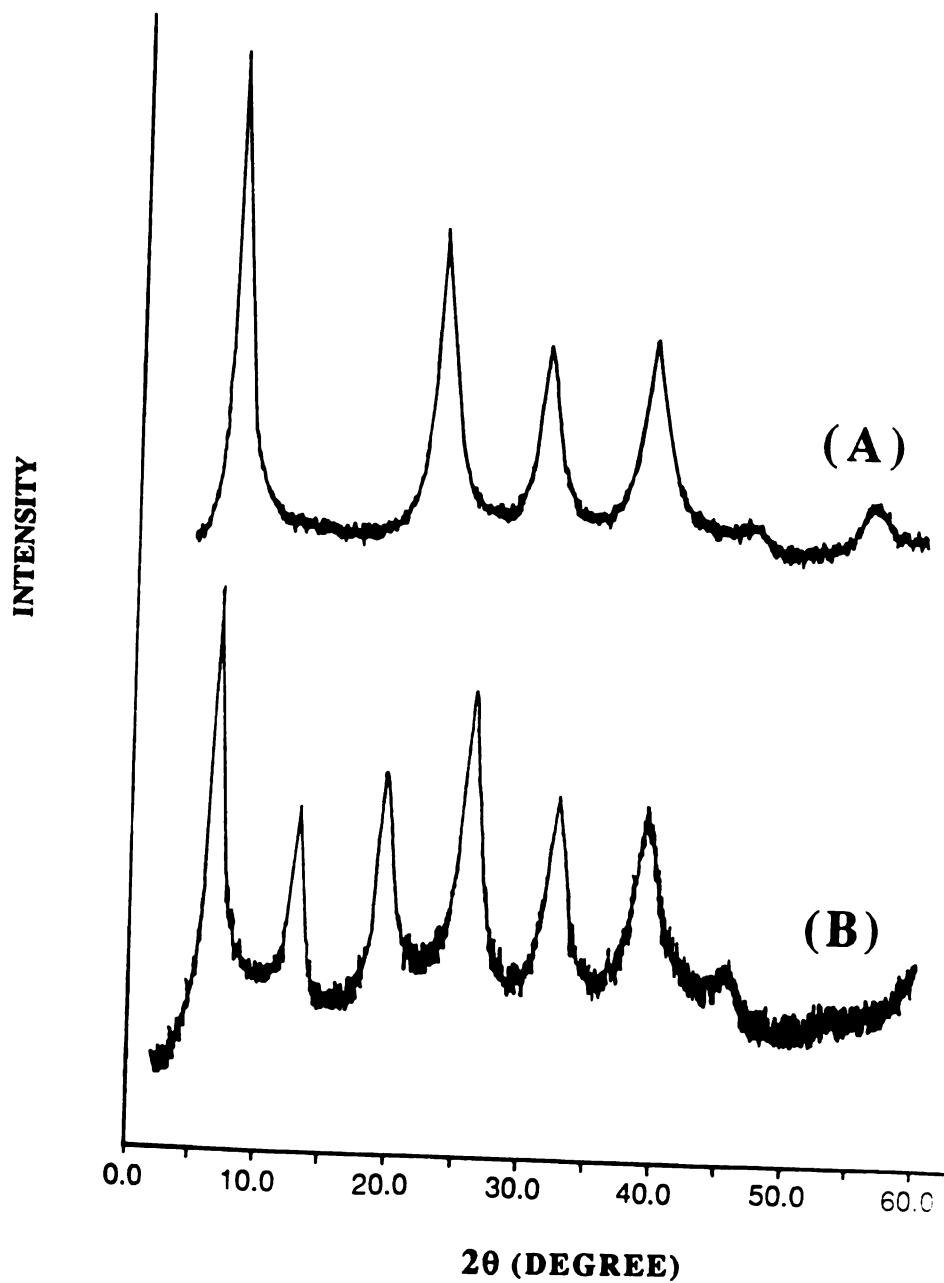
Figure 2.3. Reflection-mode X-ray diffraction patterns of films of(A) V_2O_5 xerogel (B) $(PANI)_{0.44}V_2O_50.7H_2O$.

no
m'a
val
mo
the
pro
C:Y
11

Sc

Th
in
an
d-
gr
su

monolayer of polyaniline. Therefore, the net expansion due to intercalated monolayer of polyaniline corresponds to 5.2Å. This value is comparable to that of $(pyridine)_{0.5}TaS_2$ in which the monolayer of pyridine and pyridinium ions are intercalated with their C_2 axis parallel to the TaS_2 slabs [14]. The same model can be proposed in $(PANI)_x V_2O_5 nH_2O$ where the two-fold axis bisecting the C-N-C angle is perpendicular to the V_2O_5 slabs as shown in Scheme 2.1.
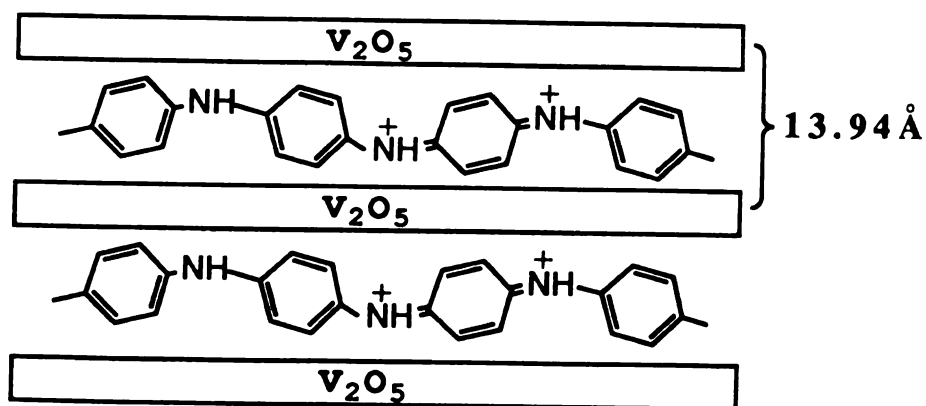
Scheme 2.1. Proposed arrangement of polyaniline in V_2O_5 layers

This model is further supported by insertion of 2,6-dimethyl aniline in V_2O_5. The resulting product (poly-2,6-dimethyl-aniline)$_x V_2O_5 nH_2O$ has an interlayer spacing of 14.57Å. This larger d-spacing compared to $(PANI)_x V_2O_5 nH_2O$ is due to the two methyl groups in 2,6 position of the benzene ring consistent with the structure shown in Scheme 2.2.

wit

2.4

im

two

fra

po

38

inte

is

geo

orh

tran

mo

V_2O_5

CH_3 CH_3 CH_3 CH_3

NH— —NH— —$\overset{+}{N}H$ = =$\overset{+}{N}H$ —

CH_3 CH_3 CH_3 CH_3

14.57 Å

V_2O_5

CH_3 CH_3 CH_3 CH_3

NH— —NH— —$\overset{+}{N}H$ = =$\overset{+}{N}H$ —

CH_3 CH_3 CH_3 CH_3
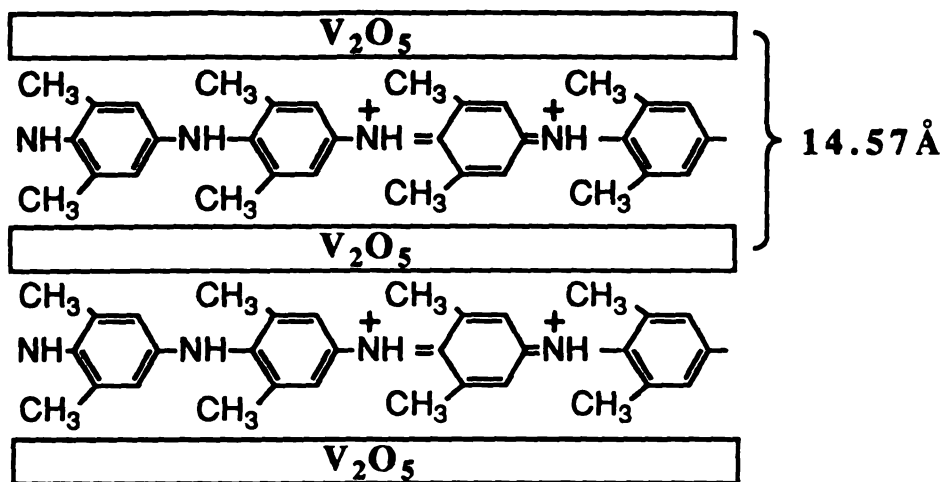
V_2O_5

Scheme 2.2. Proposed arrangement of poly-2,6-dimethyl aniline in V_2O_5 layers.

The X-ray diffraction patterns of $(PANI)_xV_2O_5nH_2O$ and V_2O_5 with the X-ray beam perpendicular to the layers are shown in Figure 2.4. This diffraction geometry allows us to examine the structural integrity and intra-layer atomic organization of the V_2O_5 slabs. The two diffraction patterns are similar indicating that the intralayer framework of V_2O_5 is structurally preserved after intercalating polyaniline. This is consistent with the IR data in the range of 380~1000 cm^{-1} which also show little change before and after intercalation. This proves that redox intercalation of aniline in V_2O_5 is topotactic. Based on the reflections observed in the two diffraction geometries, we have tentatively indexed them based on the orthorhombic unit cell. However, due the broadness of the peaks in transmission diffraction the reliable indices cannot be obtained.

When the reactions were carried out in high aniline/V_2O_5 molar ratio using a fine powder of xerogel, the resulting products
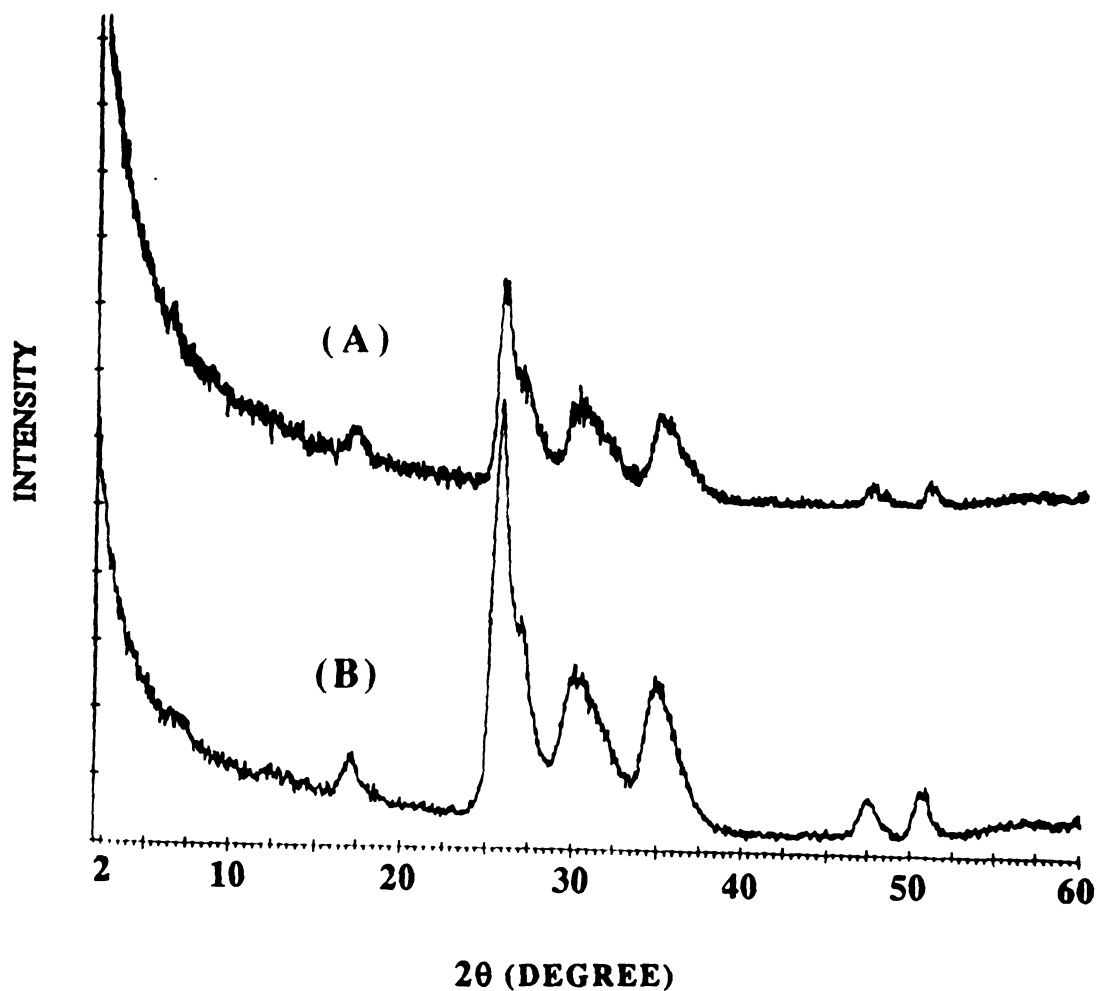
Figure 2.4. Transmission-mode X-ray diffraction patterns of films of (A) V_2O_5 xerogel (B) $(PANI)_{0.44}V_2O_50.7H_2O$. (In this experiment, the incident X-ray beam was perpendicular to the film. The detector is moving along the 2θ angle while the sample remains stationary.)

so

wl

ca

va

(b

ob

ag

pr

po

an

for

sa

ev

sh

du

sug

fra

aff

sug

und

air

Fur

can

sometimes absorbed anilinium molecules (in addition to polyaniline) which were identified in the infrared spectra. These anilinium ions cannot be removed by washing with acetone or pumping under vacuum at room temperature. However, they disappear upon aging (by staying in air for several months). This phenomenon was also observed in $(PANI)_xFeOCl$ (see page 231). Elemental analysis of the aged sample shows the same carbon content as those of freshly prepared sample, suggesting that the anilinium was either polymerized or oxidatively coupled to existing polymer chains. The anilinium molecules can be removed by heating the sample at 185°C for several days as judged by the lower carbon content of the heated samples. Interestingly, when the heating was performed in an evacuated sealed tube for 3 days, the polyaniline IR peaks did not change but the intensity of the peak at around 740 cm^{-1}, which is due to the V-O vibration of V_2O_5 host, decreased dramatically. This suggests that charge transfer from the guest polymer to the V_2O_5 framework may occur upon heating.

B. The Role of Ambient Oxygen.

At first, we did not expect the aniline/V_2O_5 reaction to be affected by ambient oxygen. Further observations however suggested that the products obtained from reactions carried out under nitrogen and under air were not the same. For example under air we observed that the reaction completion times were shorter. Further indications about the divergence of the two type of products came from the magnetic properties which showed a higher spin

ar

pro

no

int

Sin

cor

be

V

the

V

V

an

rew

xC

in

pol

sin

det

or

no

$(C$

number in the nitrogen prepared samples, and from the electrical properties, which showed that the samples prepared in air were more conductive. This is consistent with the aforementioned intriguing observation that trapped anilinium ions polymerize in air. Since samples prepared under air had better conductivities, we concentrated our efforts on those. The nitrogen based samples will be studied separately [15]. The detailed reaction steps of aniline and V_2O_5 in air are very complicated. Several reactions may be involved: the oxidative polymerization of aniline, the recombination of H^+ with V_2O_5, the acid-base interaction of H^+ and aniline, the reduction of V_2O_5, the reaction between V_2O_5 and O_2 and the reaction between aniline oligomers and O_2. A more accurate overall reaction can be rewritten as equation (2.4).

$$xC_6H_5NH_2 + V_2O_5 + (2x\text{-}3y)/4O_2 \longrightarrow (C_6H_4NH)_{x\text{-}y}(C_6H_4NH_3)_y V_2O_5 nH_2O$$

$$+ (2x\text{-}3y)/2H_2O_2 \text{(or } H_2O) \ldots eq \text{ (2.4)}$$
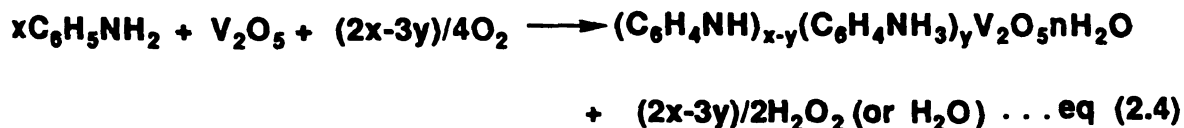
In some reactions, the anilinium molecules were not observed in the products (then y=0). In equation (2.4), when the polyaniline/anilinium ratio equals 0.5 (2x=3y), no oxygen is needed since all protons react with aniline to form anilinium. Attempts to determine the polyaniline/ anilinium ratio by ion exchange with Na^+ or K^+ according to equation 2.5 were not successful. EDS analysis did not show observable sodium and potassium concentration.

$$(C_6H_4NH)_{x\text{-}y}(C_6H_4NH_3)_y V_2O_5 nH_2O + K^+ \longrightarrow (C_6H_4NH)_{x\text{-}y}(K)_y V_2O_5 nH_2O$$

$$\text{(or } Na^+) \qquad + y\ C_6H_4NH_3^+ \ldots\ldots eq \text{ (2.5)}$$

H
fr
co
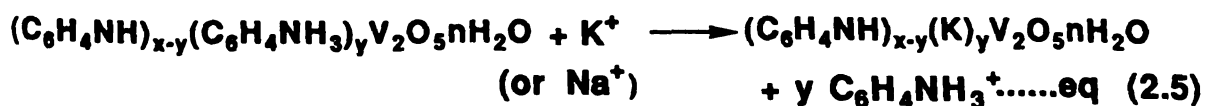
ex
co
as
th
exp
as
con
the
pol
ani
oxy
des
rea
salc
This
we

chan
Agra

However, this ratio was roughly estimated by isolating the polymer from the V_2O_5 matrix to be greater than 75% of the total organic component (polyaniline + anilinium).

Oxygen participation in the reaction was proven by using an oxygen monitor. The solvent was saturated with oxygen and its concentration was monitored as the aniline/V_2O_5 reaction proceeded as shown in Figure 2.5. The decreasing oxygen concentration, during the reaction indicates that oxygen is consumed. In a controlled experiment, V_2O_5 xerogel was reacted with alkali metal iodide, such as KI, and the oxygen concentration was monitored. No oxygen was consumed during the entire reaction period (30 minutes). Therefore, the consumption of oxygen must be related to the formation of polymer. The consumption of oxygen also depends on the aniline/V_2O_5 molar ratio. High aniline/V_2O_5 ratio consumed more oxygen as showed in Figure 2.6. Experiments have also been designed to quantify the amount of oxygen consumed during the reaction. Surprisingly, the results are much less than those calculated from the equation (2.4) and the magnetic data (vide infra). This implies that the reaction steps are more complicated than what we proposed in equation (2.4).

Oxygen is not only involved during the reaction but also changes the properties of the resulting products after isolation. Aging the sample in the presence of O_2, causes two separate reactions

Fi
du
sat
inc
rea
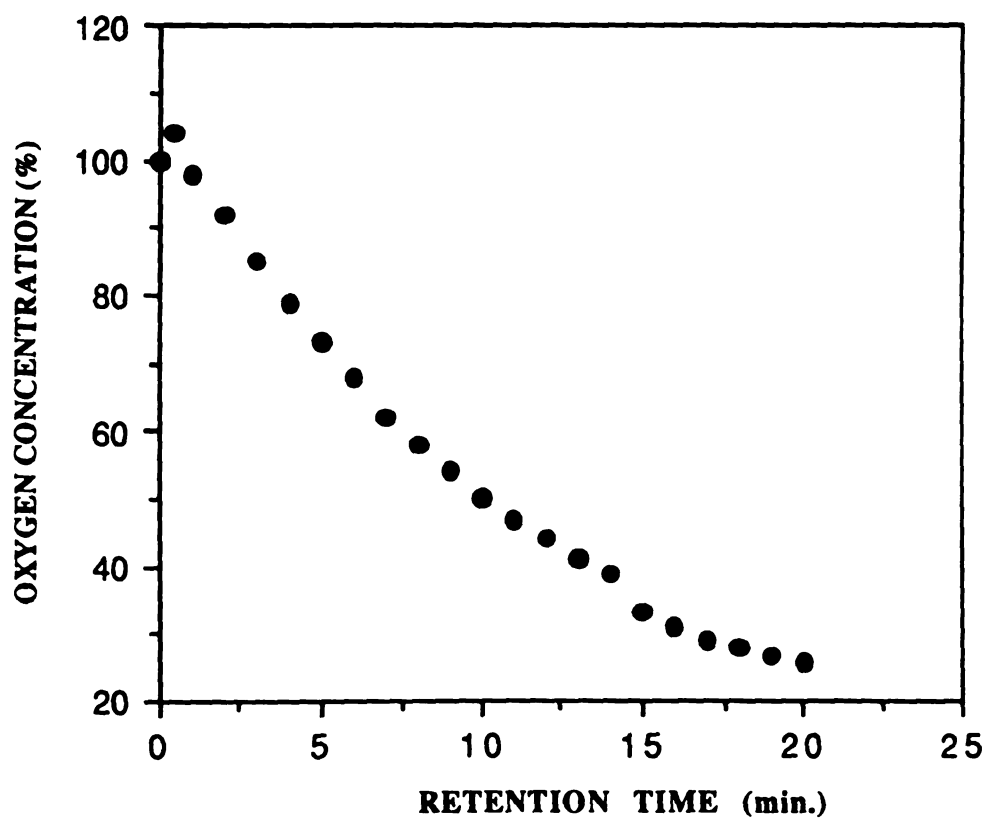
Figure 2.5. Oxygen concentration versus reaction time during the intercalation of aniline (aqueous solution saturated with oxygen) in V_2O_5 xerogel. (The 100% level indicated saturation and the aniline to V_2O_5 ratio in this reaction was 1)

Fig
At
oxy
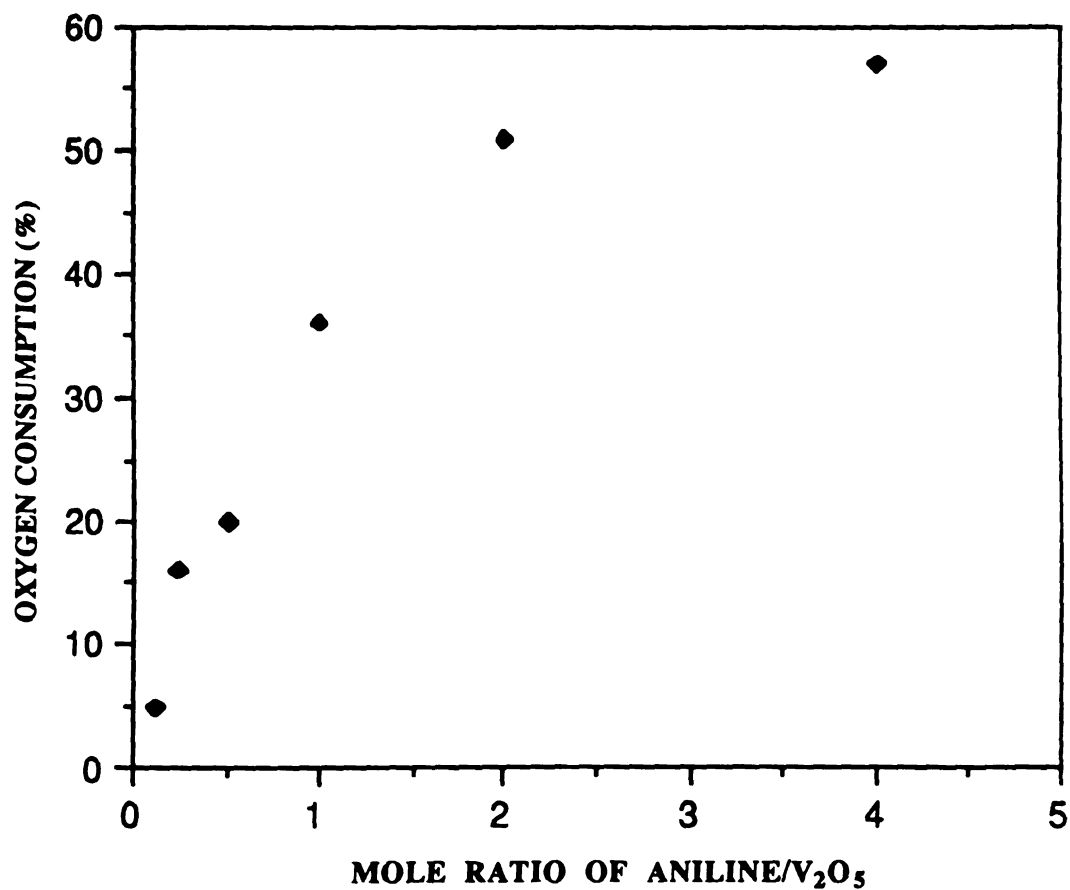
Figure 2.6. Oxygen consumption versus aniline/V₂O₅ ratio. (At 0% consumption, the aqueous solution is saturated with oxygen)

to

po

lor

y

The

dis

nor

unc

in

ten

ext

dis

to occur: first the reduced V_2O_5 framework is reoxidized and second polyaniline chains inside the V_2O_5 gallery oxidatively couple to form longer chains (see Scheme 2.3).
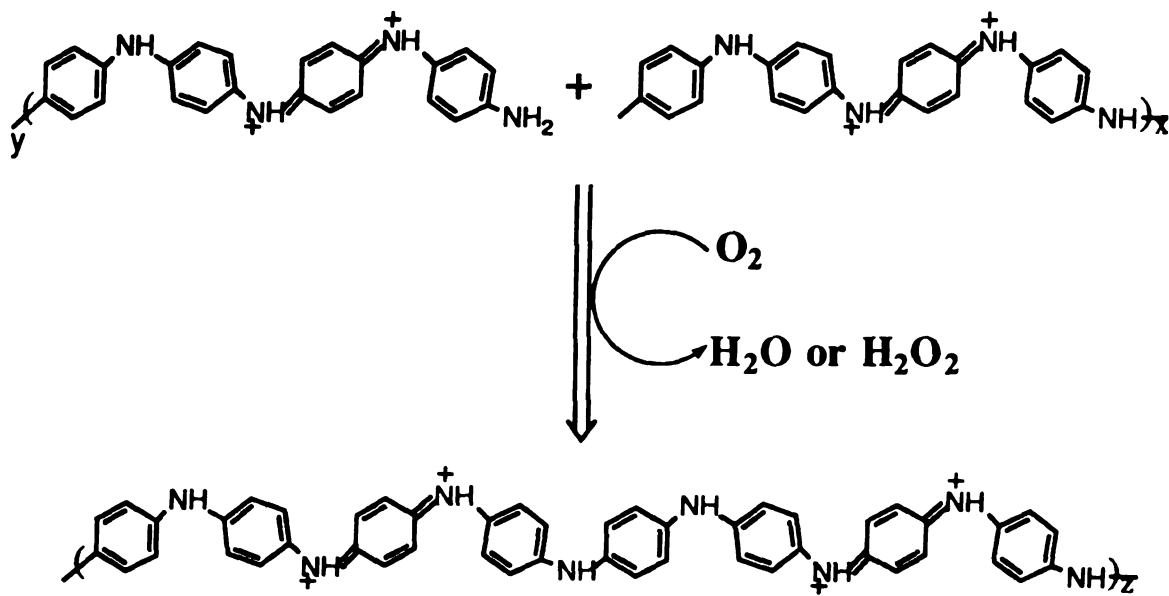
Scheme 2.3. Head to tail oxidative coupling of aniline oligomers.

The aged sample from now on will be called the β-phase in order to distinguish it from the fresh sample which is named the α-phase.

Pyrolysis mass spectroscopy studies of both α and β phases did not show any volatile low molecular weight species up to 350°C under vacuum. The polyaniline extracted from β-$(PANI)_xV_2O_5nH_2O$ in its base form, is less soluble in organic solvents, such as tetrahydrofuran, dimethyl-formamide and acetone, than polyaniline extracted from the α-phase. The anilinium peaks in the IR spectra disappeared in the β-phase which, as mentioned above, has the same

org
ma
cha
tha

mc
an
stu
mc
re
su
ida

bu
w
all
mc
sh
di
ex
bu
en
ki
po

organic content as α-phase. Furthermore, the thermal stability, magnetic susceptibility and charge transport properties are also changed significantly upon aging (vide infra). More direct evidence that PANI chains are longer in β-phase comes from the GPC results.

C. Gel Permeation Chromatography (GPC) Analysis.

The GPC technique is a common tool for the determination of molecular weights of polymers [16]. Recently, it has been applied to analyze the molecular weight of polyaniline [17]. Unfortunately, GPC studies on polyaniline are rare and a general consensus on its molecular weight (MW) has not yet been reached. This makes relevant MW comparisons difficult. Nevertheless, on a relative basis such comparisons are still useful especially when made under identical experimental conditions.

The polyaniline extracted from α-, β-$(PANI)_xV_2O_5nH_2O$ and bulk polyaniline were first converted to emeraldine base by treating with 1% NaOH(aq). The room temperature THF-extracted portion for all samples shows very low molecular weights (<600). However, the molecular weight of the NMP soluble portion was very high, as shown in Table 2.3. All samples show multi modal molecular weight distributions in GPC chromatograms as shown in Figure 2.7. As expected, the molecular weight of extracted polyaniline is lower than bulk polyaniline since it is formed in a structurally restricted environment which considerably slows down the polymerization kinetics. More interestingly, the highest molecular weight of polyaniline extracted from α-$(PANI)_xV_2O_5nH_2O$, α-polyaniline, is

Table 2.3.   Molecular Weight of Bulk Polyaniline, α-polyaniline and β-polyaniline.

Samples	Bulk polyaniline	α-polyaniline	β-polyaniline
Molecular weight	2,345,000 680,000 179,000 1,300	853,000 193,000 823 396	1,040,000 562,000 193,000 1,273

Figu
α·(]
poly
in

RETENTION TIME (min.)
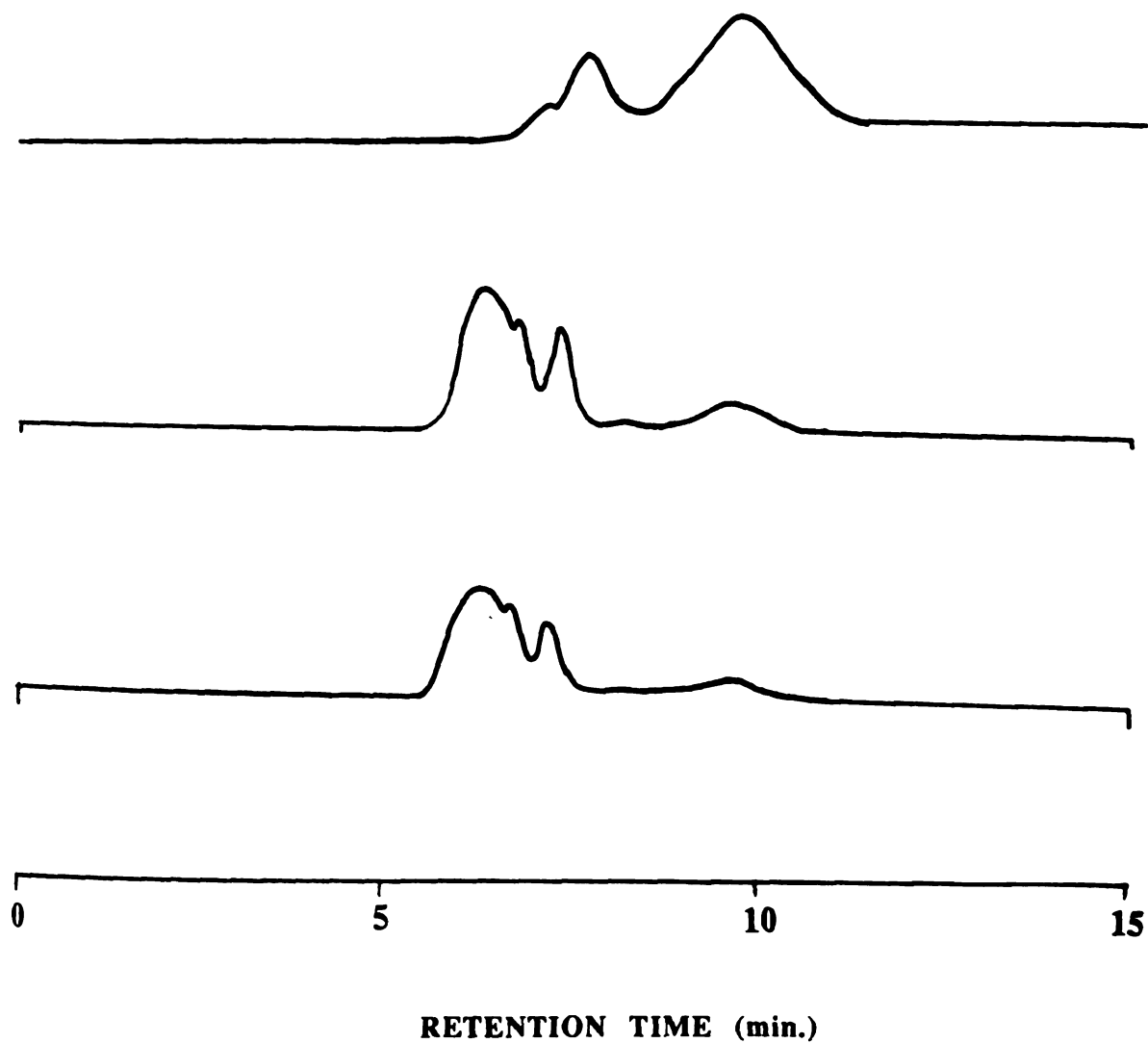
Figure 2.7   GPC diagrams of polyaniline extracted from (A)
α-$(PANI)_x V_2 O_5 n H_2 O$ (B) β-$(PANI)_x V_2 O_5 n H_2 O$ (C) Bulk
polyaniline. (The solvent was NMP and the polyanilines are
in their emeraldine base form.)

853

arou

PA

1,0

con

gro

fou

pro

MW

and

The

ass

pol

flo

bel

by

for

the

str

va

an

as

853,000 with a good portion of the sample at molecular weight around 1,300. On the other hand, polyaniline extracted from β-$(PANI)_x V_2 O_5 n H_2 O$, β-polyaniline, has molecular weights up to 1,040,000 and is a major portion of the extracted polymer. This is consistent with the proposal that the polyaniline chains continue to grow upon aging long after the intercalation reaction is over. We found that polyanilines extracted from various $(PANI)_x V_2 O_5 n H_2 O$ products had different MW distributions. It should be noted that the MW numbers reported here should be used only on a relative basis and we do not believe they represent the true MW of the polymers. The reason for the discrepancy lies in the (most probably false) assumption that polystyrene in NMP is a good model polymer for polyaniline in NMP.

D. Thermogravimetric Analysis (TGA) and Differential Scanning Calorimetry (DSC) Studies.

Typical TGA curves of α and β-$(PANI)_x V_2 O_5 n H_2 O$ under oxygen flow are shown in Figure 2.8. A small weight loss at temperatures below 100°C is probably due to absorbed moisture. This is followed by a continuous weight loss up to 700°C for the α-phase and 600°C for the β-phase. The weight loss between 100°C and 700°C is due to the decomposition of polymer and the loss of trace amounts of structural water from $V_2 O_5$. Since the degree of polymerization varies somewhat from sample to sample as suggested by GPC analysis, the weight loss patterns in the TGA diagrams vary slightly as well. The thermal stability of the α phase is better than that of β
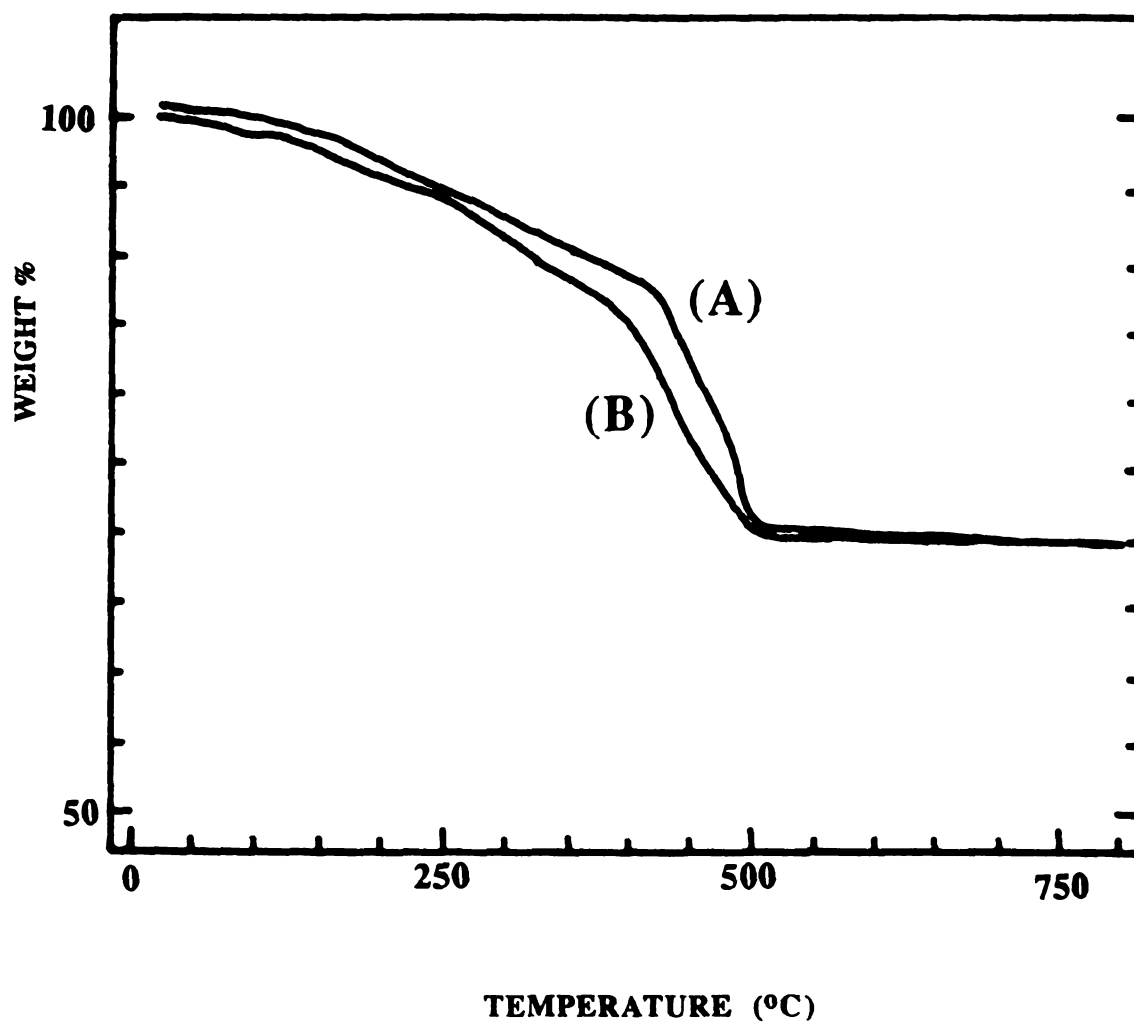
Figure 2.8. TGA curves (under oxygen flow) of (A) α-(PANI)$_{0.48}$V$_2$O$_5$0.71H$_2$O (B) β-(PANI)$_{0.48}$V$_2$O$_5$0.71H$_2$O. (The difference between the two curves is small but significant.)
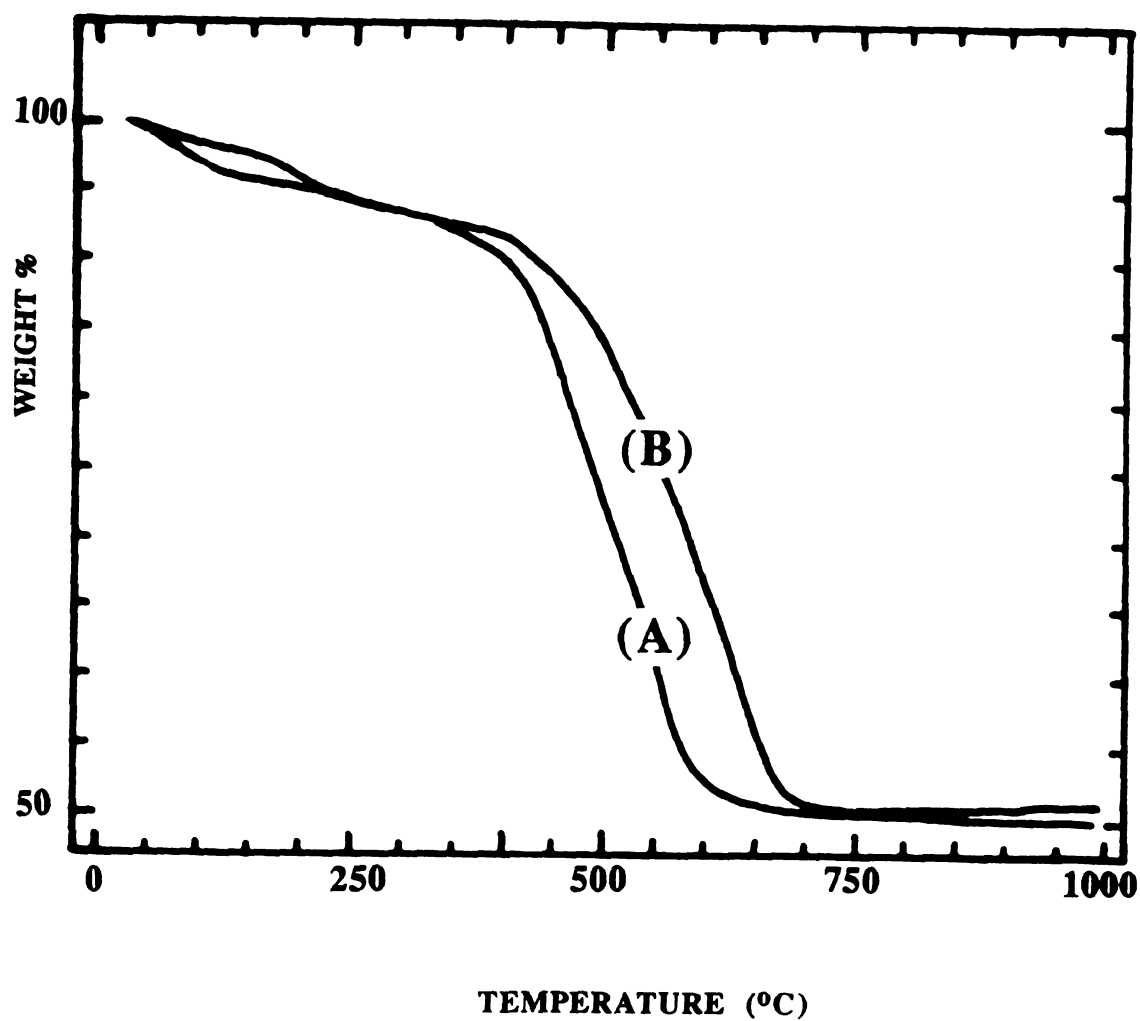
Figure 2.9. TGA curves (under nitrogen flow) of polyaniline extracted from (A) α-(PANI)$_{0.50}$V$_2$O$_5$0.33H$_2$O (B) β-(PANI)$_{0.50}$V$_2$O$_5$0.33H$_2$O.

ph

co

be

de

th

po

st

ex

(P

fr

th

m

(F

Th

co

st

n

E

{l

w

r

phase under either nitrogen or oxygen flow. At first, this might seem counter intuitive given the higher average MW in β-phase. As will became clear below, the aging process to the β-form results in a decreasing number of V^{4+} centers. The larger number of V^{5+} sites in the framework increase the oxidizing power which then degrades the polymer chains more easily. Under nitrogen flow the thermal stability of both α and β phases is better than under oxygen flow as expected.

The thermal stability of polyaniline extracted from β-$(PANI)_x V_2 O_5 n H_2 O$ under nitrogen flow is higher than that extracted from the α-form as shown in Figure 2.9 This is expected based on the higher average MW of the β-PANI.

E. Scanning Electron Microscopy (SEM) and Transmission Electron Microscopy (TEM).

Electron microscopy was used to study the morphology of these materials. Under the electron microscope, the surfaces of a $(PANI)_x V_2 O_5 n H_2 O$ films are continuous and relatively homogeneous. The layered nature can be observed clearly in Figure 2.10. This is consistent with a typical topotactic intercalation in which the layer structure and morphology is preserved after reaction. The topotactic nature of the reaction is further supported by TEM Selected Area Electron Diffraction (SAED) studies. Although the SAED patterns of $(PANI)_x V_2 O_5 n H_2 O$ did not show diffraction spots, several Bragg rings were observed. The d-spacings calculated from the observed Bragg rings are in good agreement with the d-spacings obtained by
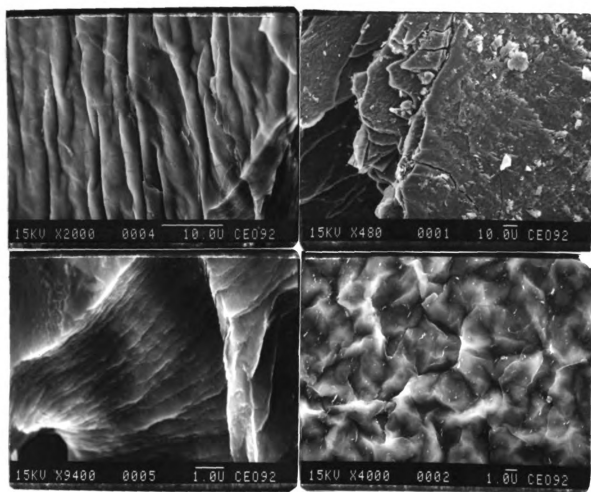
Figure 2.10. SEM micrographs of (PANI)$_{0.44}$V$_2$O$_5$0.5H$_2$O.
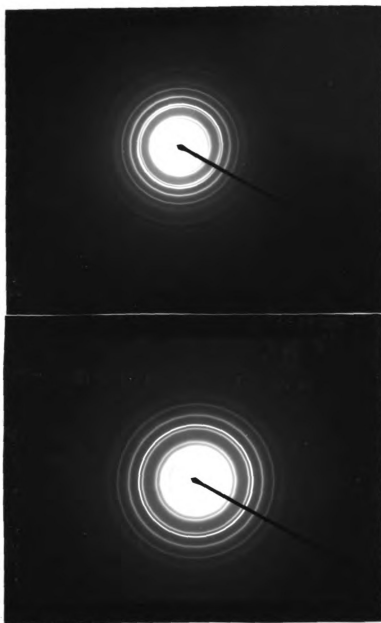
Figure 2.11. Selected area electron diffraction patterns of (A) $(PANI)_{0.44}V_2O_50.7H_2O$ (B) V_2O_5 xerogel

Figure 2.12. TEM micrograph of V_2O_5 gel.

transmission-mode X-ray diffraction (see page 69). The SAED pattern of $(PANI)_x V_2O_5 nH_2O$ is similar to that of pristine V_2O_5 xerogel or gel as shown in Figure 2.11. The TEM image of V_2O_5 xerogel and $(PANI)_x V_2O_5 nH_2O$ studied in our laboratory did not always show the fiber nature as seen by Livage and coworkers [18]. Most of the time the image obtained could be interpreted as folded sheets. This fiber morphology becomes very obvious in V_2O_5 wet gel as shown in Figure 2.12.

F. Electron Paramagnetic Resonance (EPR) Spectroscopy.

Since both emeraldine salt and reduced V_2O_5 are paramagnetic materials, we used EPR spectroscopy to study the nature of free spins in $(PANI)_x V_2O_5 nH_2O$. A representative EPR spectrum of $(PANI)_x V_2O_5 nH_2O$ is shown in Figure 2.13b. It features an intense, broad signal at g=1.975 with ΔH_{pp} in the range of 75~ 100 gauss. This signal comes from the reduced V_2O_5 framework. It is qualitatively similar to that observed in $A_x V_2O_5 nH_2O$ (A = Na, K, Cs) (Figure 2.13c) which is prepared from the reduction of the V_2O_5 xerogel with alkali metal iodides [15]. The original hyperfine splitting arising from the ^{51}V (I=7/2) nucleus disappeared after intercalation due to dipolar broadening. Interestingly, the typical strong and sharp EPR resonance arising from the massive polarons of bulk polyaniline was not observed [19]. This suggests that the polaron spins on polyaniline are in close proximity to the paramagnetic V^{4+} centers, so that magnetic exchange interaction
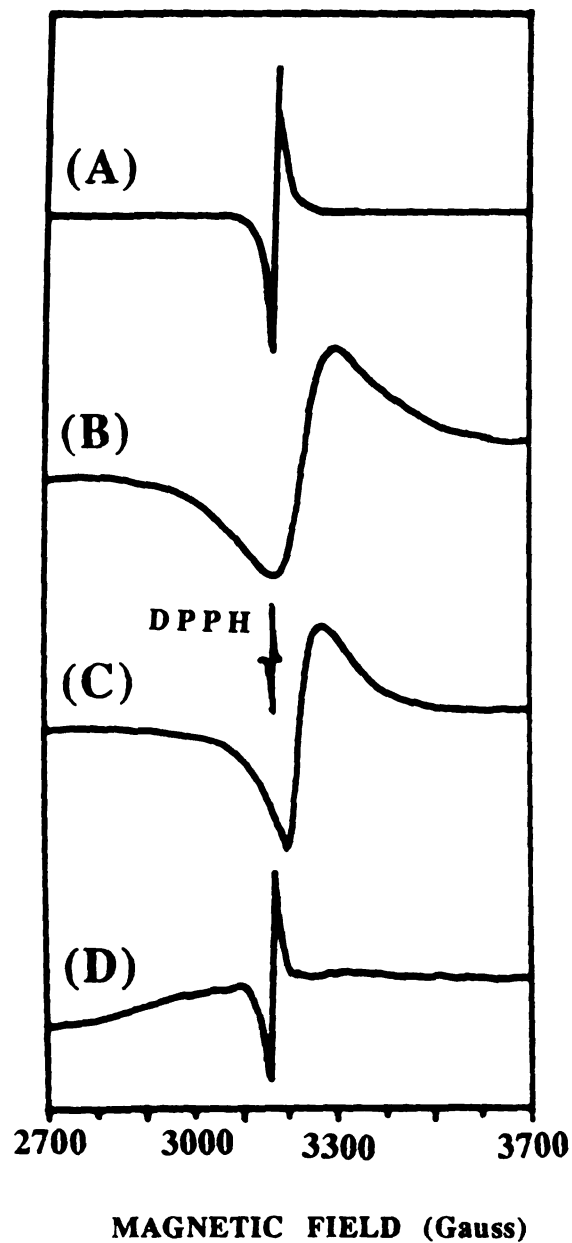
Figure 2.13. Room temperature EPR spectra of (A) Bulk polyaniline (emeraldine salt) (B) $(PANI)_{0.44}V_2O_50.7H_2O$ (C) $Na_{0.40}V_2O_5nH_2O$ (D) Extracted polyaniline.

between the two materials is significant. Therefore, in $(PANI)_x V_2O_5 nH_2O$ the mixing of polyaniline and V_2O_5 is at the molecular level and not simply a physical mixture. The characteristic EPR signal of polyaniline is observed after isolation by digesting away the V_2O_5 matrix (Figure 2.13d). It is similar to that of bulk polyaniline (Figure 2.13a). The same phenomenon has also been observed in polyaniline intercalated in zeolite [20], in $Ni(CN)_2NH_3$ [21] and in FeOCl (see page 245).

Lowering the temperature slightly enhanced the EPR peak intensity of $(PANI)_x V_2O_5 nH_2O$ but not the peak shape and width. The aged β-phase shows a similar but smaller EPR signal suggesting that the free spins on V_2O_5 decreased due to reoxidation of the V_2O_5 host. However, the g value and ΔH_{pp} did not change. Nevertheless, the reoxidation of V_2O_5 is not extensive enough to reach pre-intercalation levels since the hyperfine EPR signal is not observed even after two years. This is expected because the degree of reduction of V_2O_5 should be enough to balance the charge of protonated polyaniline. Part of the line broadening could arise from strong spin-spin interactions between polyaniline and the V_2O_5 framework despite the decrease of V^{4+} concentration.

G. Magnetic Susceptibility Studies.

Consistent with the EPR data, variable temperature magnetic susceptibility measurements from both fresh and aged $(PANI)_x V_2O_5 nH_2O$ show paramagnetic behavior. The magnetic susceptibility (χ_m) decreases with rising temperature as shown in

Figure 2.14. The paramagnetism from polyaniline is relatively small [22] and therefore the net magnetic moment comes mostly from V^{4+} species in V_2O_5 which probably are involved in some type of magnetic exchange interaction with the spins on polyaniline. We found that the best way to interpret the magnetic susceptibility data was to separate it into two components: Curie-Weiss paramagnetism and temperature independent paramagnetism (TIP) as represented in equation 2.6.

$$\chi_m = \chi_{Curie-Weiss} + \chi_{TIP} \quad \text{...............eq (2.6)}$$

$$\chi_{Curie-Weiss} = \frac{c}{T-\theta} \quad \theta : \text{Weiss constant}$$

The TIP is found in transition metal ions where the interacting d levels have been split by the ligand field [23]. This TIP susceptibility is rather small and is usually observed at high temperature where the Curie paramagnetism is relatively small. χ_{TIP} depends on the energy gap between the HOMO and LUMO orbitals as shown in equation 6.3 [23b].

$$\chi_{TIP} = \frac{16 \, N\beta^2}{\Delta} \quad \text{...............eq (2.7)}$$

N : Avogadro's number, β : Bohr Magneton, $\Delta = E_n - E_0$

The coordination of V in V_2O_5 xerogel is assumed to be a distorted square pyramid geometry of approximate C_{2v} symmetry [18]. The
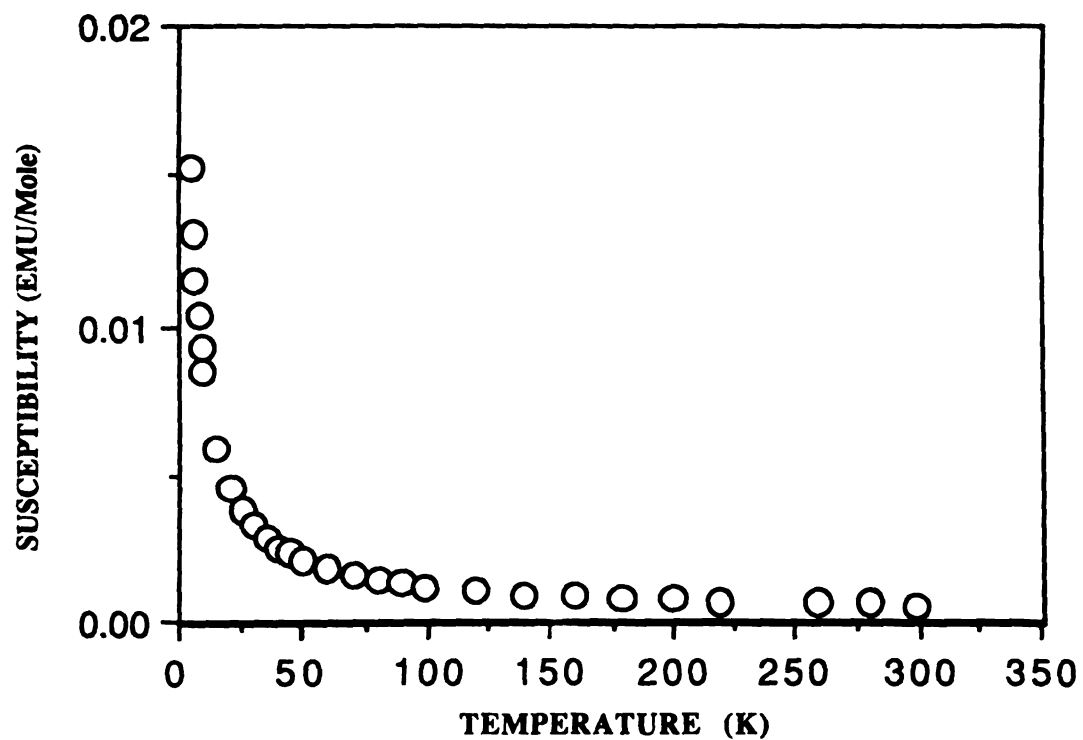
Figure 2.14. Variable temperature magnetic susceptibility (χ_m) data of $(PANI)_{0.24}V_2O_50.71H_2O$ at 5000 gauss applied field.

molecular orbital diagram of V^{4+} in square pyramidal ligand field can be expressed as Scheme 2.4. The Δ is very small in this case, therefore the χ_{TIP} can be observed at high temperature. This temperature independent paramagnetism was also observed in reduced V_2O_5 such as $M_xV_2O_5nH_2O$ (M = K, CS) [24] and was found to depend on the degree of reduction of V_2O_5 [24]. Figure 2.15 shows the variation of $1/\chi_m$ as a function of temperature of $(PANI)_{0.24}V_2O_5nH_2O$. The Weiss constant of Curie-Weiss susceptibility is -1.35. Variable temperature effective spin-only magnetic moment of $(PANI)_{0.24}V_2O_5nH_2O$ is basically constant except at very low temperature (<15K) as shown in Figure 2.16. This may be due to the paramagnetic impurity or there is an antiferromagnetic coupling between the V^{4+} centers as seen in other V^{4+} compounds [24,25]. The room temperature magnetic moments, μ_{eff}, of $(PANI)_xV_2O_5nH_2O$ with various x values are shown in Table 2.4. Two observations become immediately obvious from this Table. First, there is no direct relationship between the polymer content and magnetic moment (both Curie-Weiss μ_{eff} and total μ_{eff}). Second, the total μ_{eff} is always smaller than the theoretically expected value assuming all the electrons released from aniline during oxidative polymerization, were transferred to V_2O_5. The lower μ_{eff} values are consistent with our findings presented above that part of the released electrons are transferred to oxygen and not to V_2O_5. The complicated interactions between oxygen (or polyaniline) and reduced V_2O_5 makes it is difficult to quantitate the degree of reduction of V_2O_5 in all $(PANI)_xV_2O_5nH_2O$ simply using μ_{eff} values.
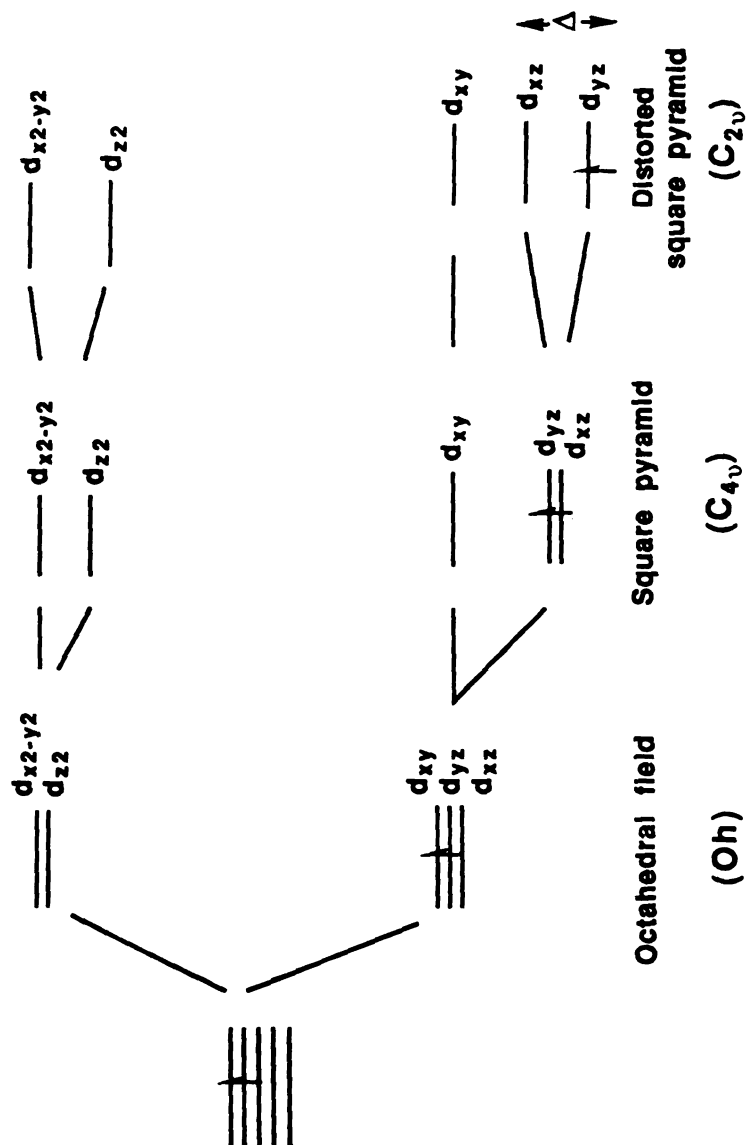
Scheme 2.4: Simplified orbital diagrams of V^{4+} in distored square pyramid ligand field. (Δ is the energy separation between d_{xz} and d_{yz} orbitals.)
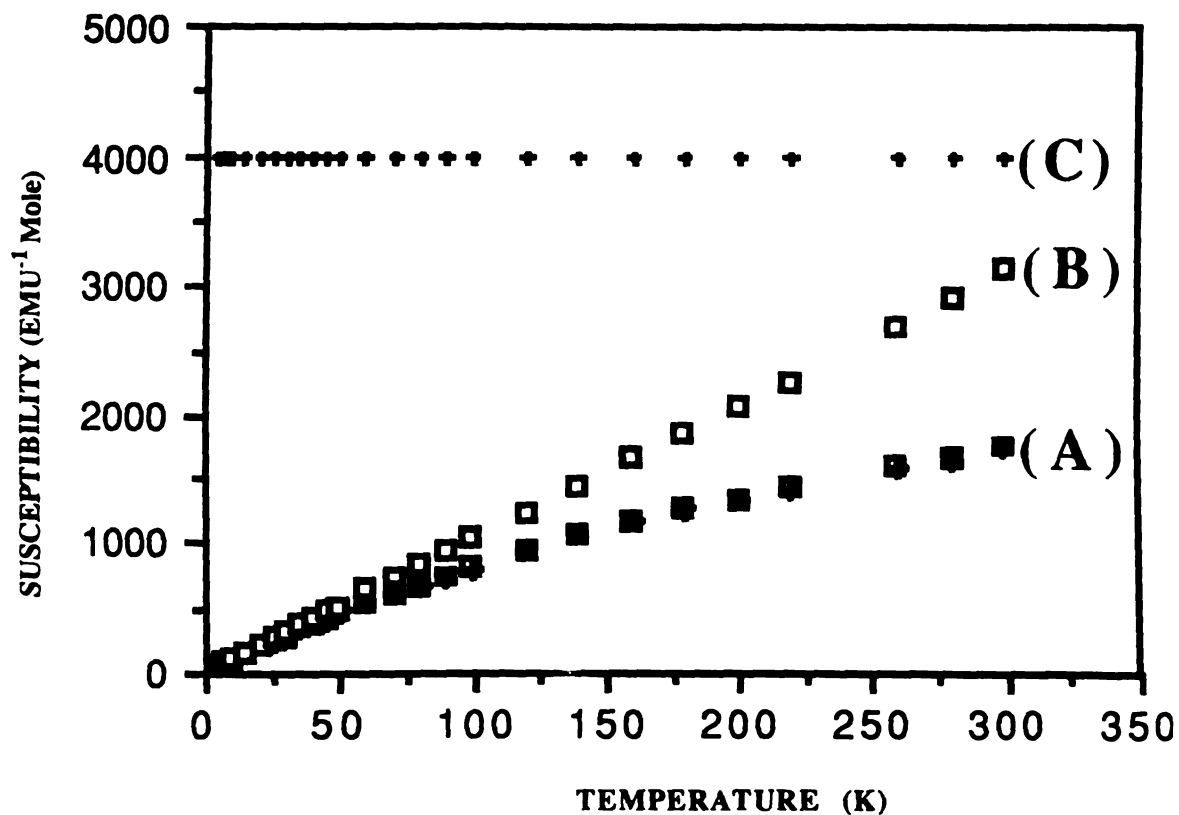
Figure 2.15.   Variable temperature magnetic data ($1/\chi_m$) of α-$(PANI)_{0.24}V_2O_50.71H_2O$ (A) Total magnetic susceptibility (B) Curie-Weiss susceptibility (C) Temperature independent paramagfnetism.
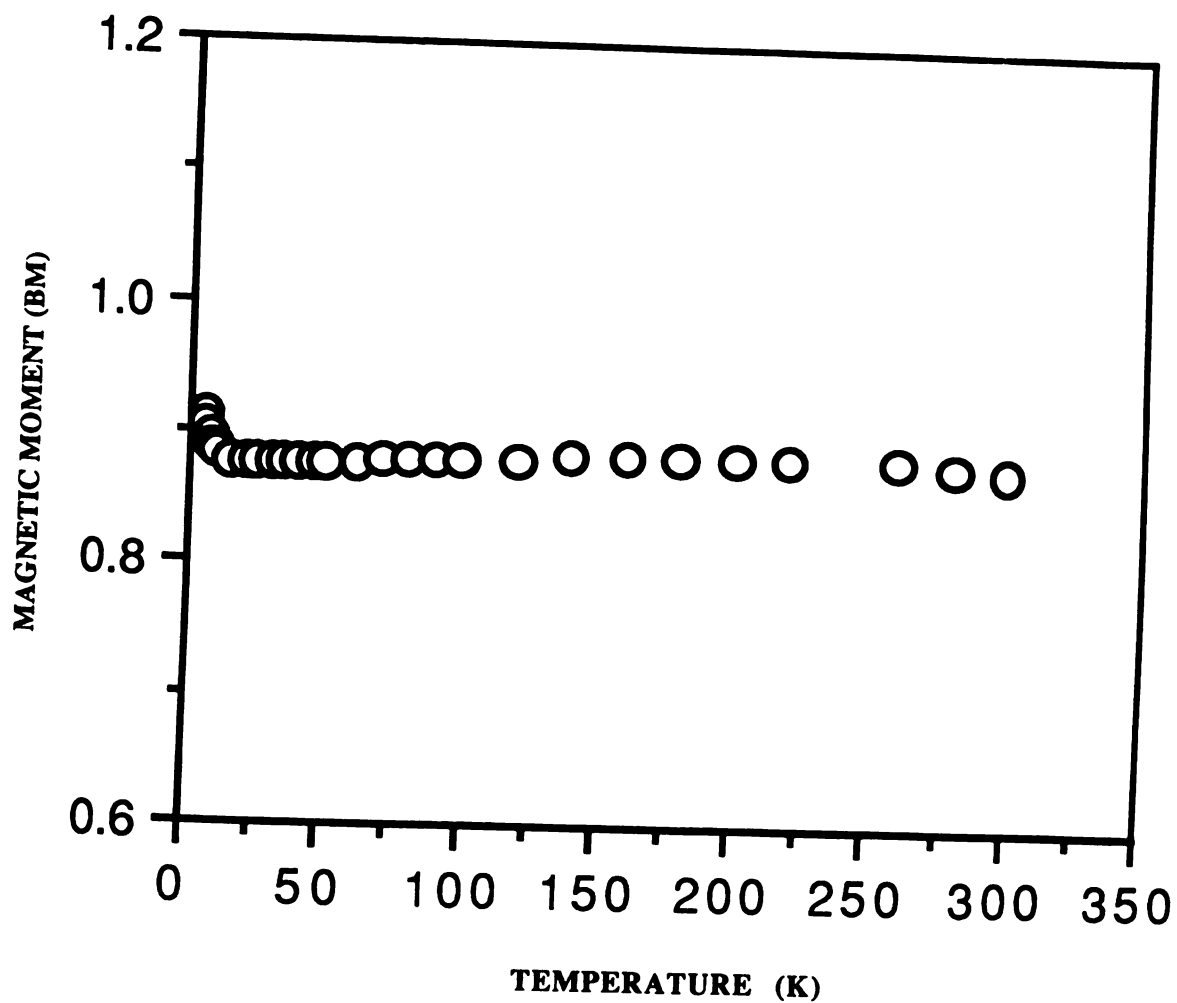
Figure 2.16. Variation of effective spin-only magnetic moment (Curie-Weiss) as a function of temperature of $\alpha\text{-}(PANI)_{0.24}V_2O_5 0.71H_2O$.

Table 2.4.   Room Temperature Magnetic Moment and Temperature Independent Paramagnetism of $(PANI)_xV_2O_5nH_2O$ versus x.

x	Total $\mu_{eff}(BM)$	*Curie-Weiss $\mu_{eff}(BM)$	$\chi_m \times 10^4$ (TIP)
0.21	0.97	0.88	0.75
0.24	1.21	0.98	2.0
0.25	1.17	0.87	2.5
0.29	1.02	0.90	1.0
0.44	0.87	0.61	1.6
0.48	1.25	0.78	4.0
0.72	0.92	0.75	1.2

*: Corrected for TIP Van Vleck paramagnetism.

We have attempted to quantitate the degree of reduction of V_2O_5 host by X-ray photoelectron spectroscopy (XPS). The V^{5+} peak of $(PANI)_x V_2O_5 nH_2O$ has a broad shoulder which is not observed in V_2O_5 xerogel. This shoulder is due to the overlapping of V^{5+} and V^{4+} peaks. However the change of the bonding energy, the peak shape of V^{4+} and significant overlap between V^{5+} and V^{4+} peaks, poses serious difficulties in determining a reliable V^{4+}/V^{5+} ratio, the exactly quantity of V^{4+} can not be performed.

Upon aging the samples show decreased magnetic susceptibility as shown in Figure 2.17. The decreasing of the magnetic susceptibility is probably due to the reoxidation of some V^{4+} centers to V^{5+}. The reoxidation process is slow and the degree of V_2O_5 reduction reaches a limiting value. As mentioned before, the aging process not only reoxidizes the host but also causes oxidative coupling of aniline oligomers inside the V_2O_5 layers to form longer chain of polymers. However, when the sample was stored in vacuum, the magnetic moment remains constant suggesting no further internal redox reaction between polyaniline and V_2O_5 at room temperature. The χ_{TIP} of $(PANI)_x V_2O_5 nH_2O$ also decreases upon aging (0.00025 and 0.0001 EMU/mole for fresh prepared $(PANI)_{0.48} V_2O_5 nH_2O$ and its aged samples respectively).
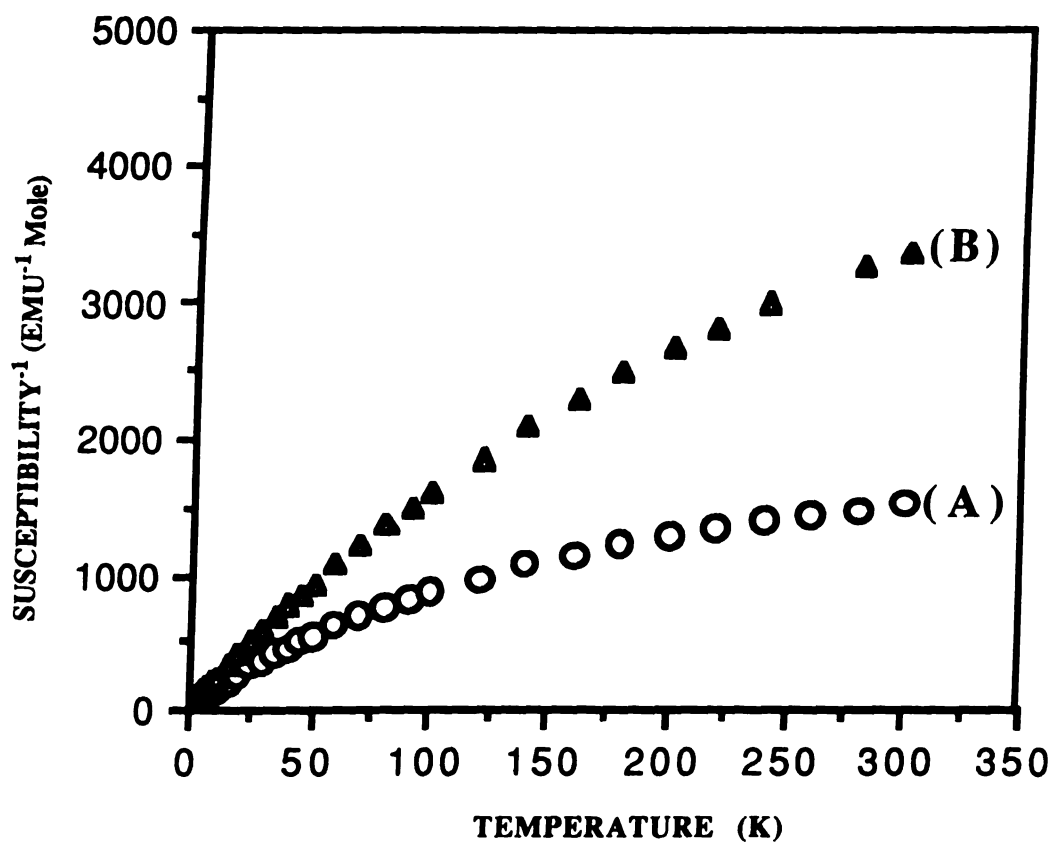
Figure 2.17. Variable temperature magnetic susceptibility data (5000 gauss field) of (A) α-$(PANI)_{0.48}V_2O_50.33H_2O$ (B) β-$(PANI)_{0.48}V_2O_50.33H_2O$.

H. Charge Transport Properties.

(1) Electrical Conductivity.

Upon intercalation of polyaniline, the charge transport properties of V_2O_5 xerogel changed significantly. The electrical conductivity of $(PANI)_xV_2O_5nH_2O$ is 10^4 times higher than pristine V_2O_5 as shown in Figure 2.18. In order to explore the effect of oxygen on the conductivity of $PANI/V_2O_5$ systems, the reactions were carried out both in air and nitrogen atmosphere. In the preliminary test, we found that for the similar polyaniline/V_2O_5 ratio, the material prepared in air has higher conductivity than that prepared under nitrogen as shown in Figure 2.19. Therefore, most of our attention was focused on the materials prepared in air. The materials prepared under nitrogen will be reported separately [15]. The room temperature conductivity of α-$(PANI)_xV_2O_5nH_2O$ is in the range of 10^{-4} to 10^0 $\Omega^{-1}cm^{-1}$ as listed in Table 2.5. Generally, there is no direct relationship between the conductivity and polyaniline/V_2O_5 ratios. This is probably due to the fact that the conjugation or chain length of polyaniline inside the V_2O_5 host most be taken into account. Thus short oligomers will give rise to lower conductivities than long ones. The highest conductivities will be expected in samples in which both the polymer content and polymer chain-length is high.

In all samples the conductivity increases with increasing temperature revealing a thermally activated behavior. This behavior is also observed in other intercalated compounds and conjugated

LOG CONDUCTIVITY (Ω^{-1}cm^{-1})

Fig
elec
(PA
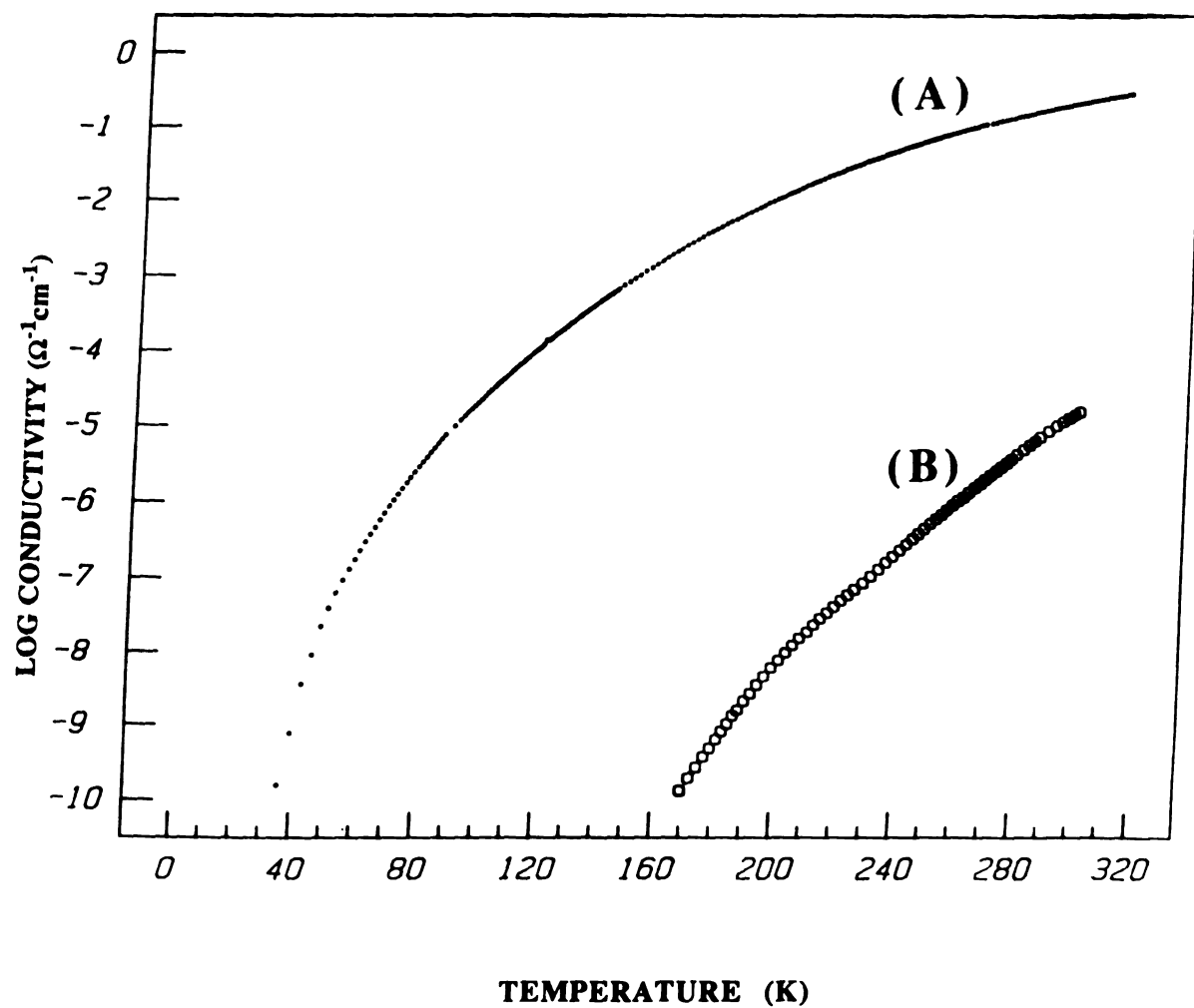
Figure 2.18. Four-probe variable temperature electrical conductivity data of films of (A) α-$(PANI)_{0.21}V_2O_50.56H_2O$ (B) PristineV$_2$O$_5$ xerogel.

LONG CONDUCTING TRANSITION LAYER... the

Fig
ele
(P.A
atm
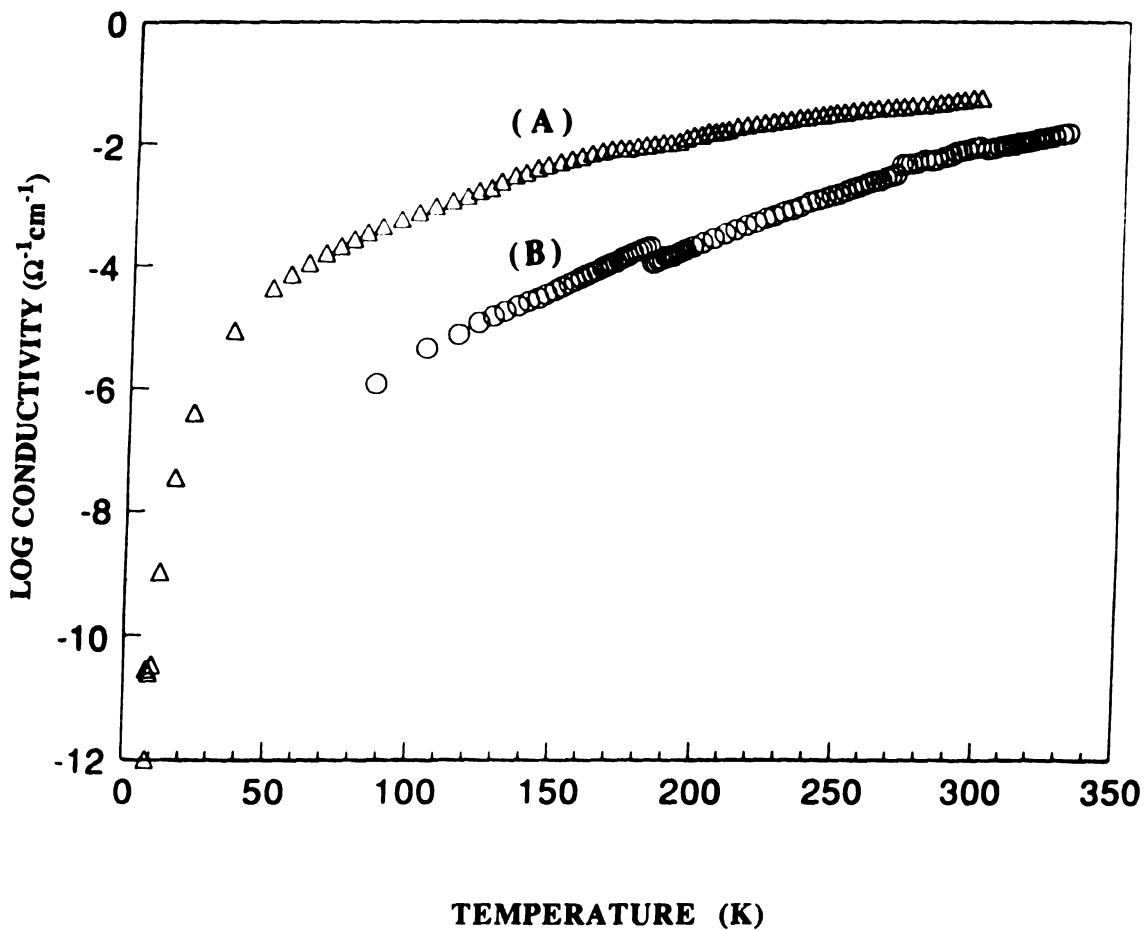
Figure 2.19. Four-probe variable temperature electrical conductivity data of films of α-(PANI)$_{0.29}$V$_2$O$_5$0.56H$_2$O prepared in (A) Air (B) N$_2$ atmosphere.

Table 2.5. Room Temperature Electrical Conductivity (σ) versus x of (PANI)$_x$V$_2$O$_5$nH$_2$O.

X	0.056	0.19[*]	0.21	0.29[*]	0.30[*]	0.37	0.44[*]
σ (Ω^{-1} cm^{-1})	$10^{-5}\sim10^{-4}$	$10^{-2}\sim10^{-1}$	$10^{-4}\sim10^{-3}$	$10^{-2}\sim10^{-1}$	$10^{-1}\sim10^0$	$10^{-2}\sim10^{-1}$	$10^{-1}\sim10^{-0}$
X	0.46	0.48	0.50	0.63	0.67	0.72	0.77
σ (Ω^{-1} cm^{-1})	10^{-2}	10^{-2}	$10^{-3}\sim10^{-2}$	$10^{-3}\sim10^{-2}$	10^{-2}	10^{-2}	$10^{-3}\sim10^{-2}$

*: Film sample

po
co
Nc
hi
be
at

tP
th
Th
m
re
in
de
to
sh
we
co
lon
air
wh
ox
st
co

polymers [26]. Figure 2.20 shows the typical variable temperature conductivity of α-$(PANI)_x V_2O_5 nH_2O$ in film and pressed pellet forms. Not surprising, the conductivities of film samples are 10 to 100 times higher than that of pressed pellet powder (see Table 2.5) because of better interparticle contact. The conductivity parallel to the layers is at least 10 times higher than perpendicular to the layers.

Upon aging for several months the conductivity of $(PANI)_x V_2O_5 nH_2O$ increased as shown in Figure 2.21. The increase in the conductivity with aging is slow and levels off to a certain value. The magnetic data showed that when $(PANI)_x V_2O_5 nH_2O$ is aged, its magnetic susceptibility decreases suggesting that V^{4+} centers are reoxidized to V^{5+}. The reoxidation of V_2O_5 framework will not increase the conductivity in the V_2O_5 layers since it results in a decrease of carriers [26]. Thus the observed increase should be due to the enhancements in the polymer conductivity. The GPC results show that polyaniline extracted from β-phase has higher molecular weight than from α-phase (see page 75). Therefore, the increased conductivity with aging most probably comes from the formation of longer chains of polyaniline via oxidative coupling after exposure to air. This is in contrast with conventional bulk conducting polymers which show a lower conductivity with aging. Apparently, the oxidative coupling of polyaniline continues to a certain level and then stops presumably when kinetic movement of the polymer chains comes to a halt.

Fi
co
a.
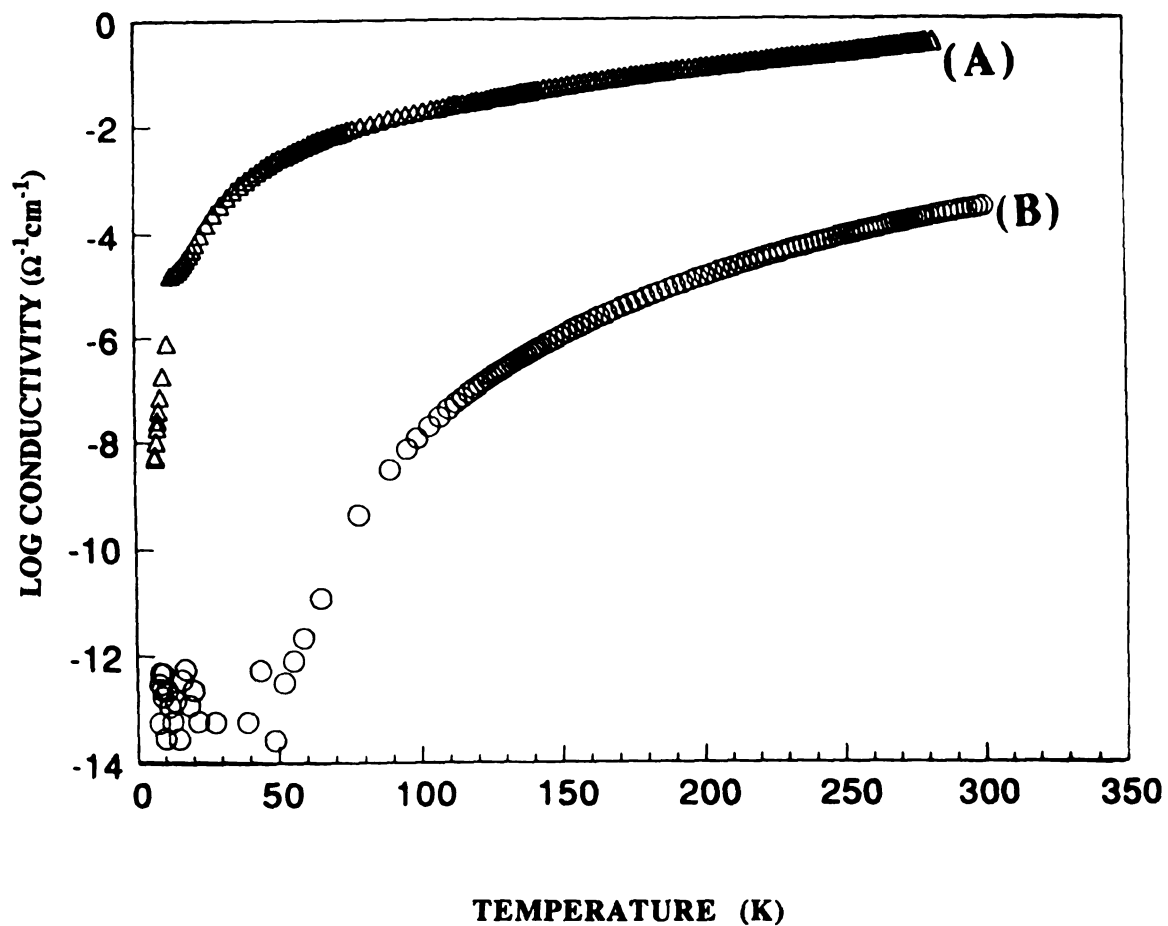
Figure 2.20. Four-probe variable temperature electrical conductivity data of (A) α-$(PANI)_{0.30}V_2O_51.3H_2O$ (film) (B) α-$(PANI)_{0.72}V_2O_50.33H_2O$ (pressed pellet).
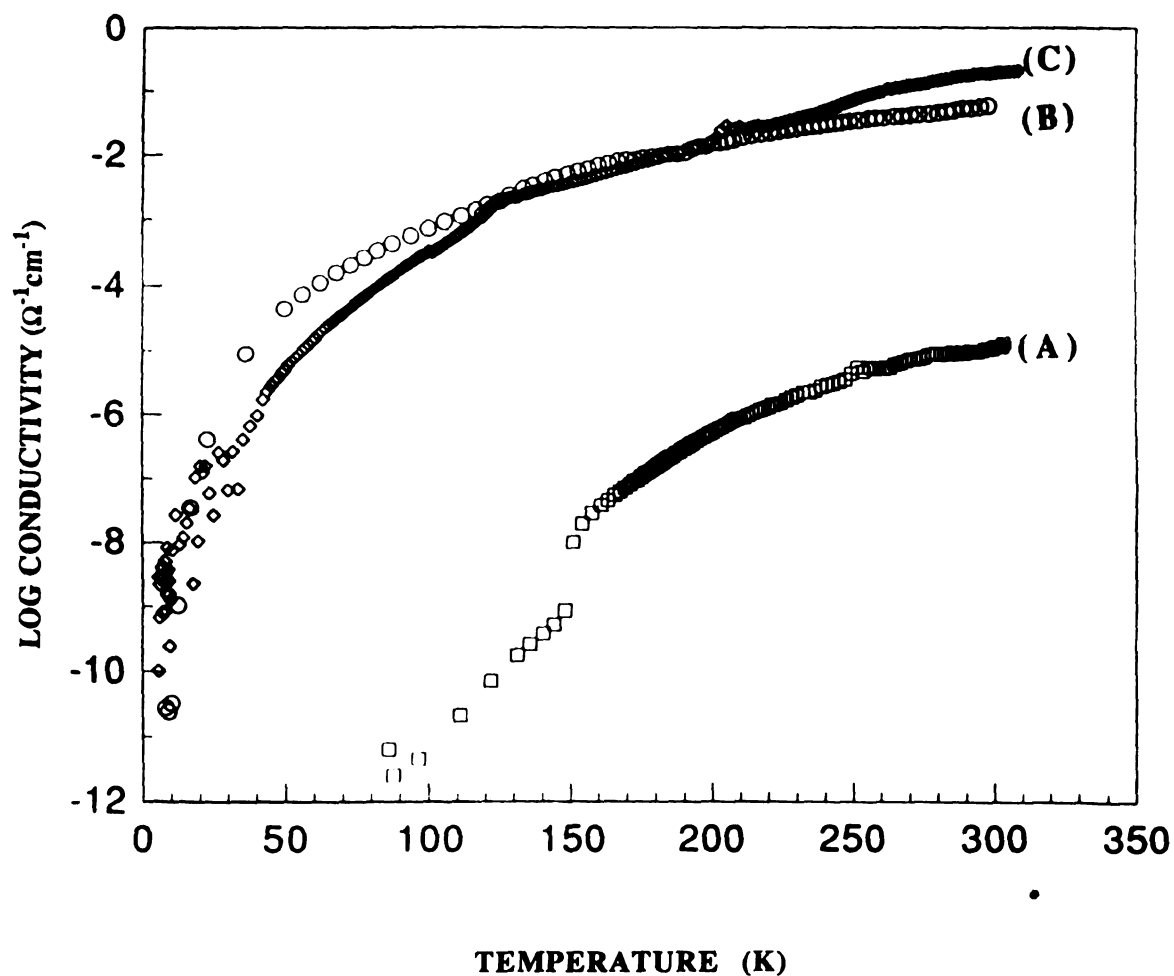
Figure 2.21. Four-probe variable temperature electrical conductivity data of pressed pellets of $(PANI)_{0.48}V_2O_5 0.33H_2O$ (A) Freshly prepared (B) Aging for 16 months (C) Aging for 31 months.

(2) Thermoelectric Power.

Unlike electrical conductivity, thermoelectric power (TP) which was measured as a function of temperature is not affected as much by interparticle contact resistance. It can provide valuable information as to the true nature of charge transport within the material. Typical variable temperature thermoelectric power of α-$(PANI)_xV_2O_5nH_2O$ in pressed pellet and film forms are shown in Figure 2.22. The thermoelectric power, TP (or called Seebeck coefficient, S), of pressed powder samples is large, negative and almost temperature independent from room temperature down to 250K. Below 250K, the exact Seebeck coefficient cannot be measured due to the high sample resistance. This is a n-type semiconductor behavior. The thermoelectric power of reduced V_2O_5 is independent of temperature but depends on the degree of reduction. This behavior was observed both in crystalline V_2O_5 [25] and V_2O_5 xerogel [27]. Therefore, the charge transport properties of powder α-$(PANI)_xV_2O_5nH_2O$ are dominated by the reduced V_2O_5 framework. This is consistent with the formation of short polymer chains which inhibit facile chain to chain charge transport. The charge transport appears more favorable through V_2O_5 layers although assistance via the polymer chains particularly in the direction perpendicular to the layers may be operative. Surprisingly, except for very low polyaniline/V_2O_5 ratio, the room temperature thermoelectric power of powder samples are independent on polymer content. As mentioned above oxygen was involved during the intercalation, and therefore the degree of reduction of V_2O_5 framework is not directly

relative to polymer/V_2O_5 ratio. Since the reduced V_2O_5 dominates the charge transport in these materials, the thermoelectric power is also independent on polymer/V_2O_5 ratio.

The TP of film samples is relative small compared to powder samples, see Figure 2.22a, and became more negative with rising temperature. This is a n-type conductor behavior although the S value is higher than typical metal. The TP of bulk (emeraldine salt) polyaniline shows metal-like behavior and its TP can be negative or positive depending on the degree of protonation [28]. Therefore, the polyaniline inside the V_2O_5 is probably responsible for the charge transport properties for the film samples. The difference of thermopower behavior between powder and film samples is not surprising. Since in film samples, the V_2O_5 have better continuity. The polyaniline chains inside the layers may have better arrangement, thus facile the chain to chain hoping, dominates the charge transport. Furthermore, the intercalation of polyaniline in V_2O_5 film is slower than in powder. The polyaniline in film sample may have less structure defects. Table 2.6 summarizes the room temperature TP of several α-$(PANI)_xV_2O_5nH_2O$ with various x.

Interestingly, the TP value of power samples of β-phase is relatively small, negative and becomes more negative as temperature increases revealing a n-type metal-like behavior as shown in Figure 2.23b. The transition form n-type semiconductor to n-type metal upon aging is a surprise. The polyaniline inside V_2O_5 layers did not degrade upon contact with air, instead it continued to polymerize forming longer polymer chains which changes dramatically the charge transport properties. These TP data are
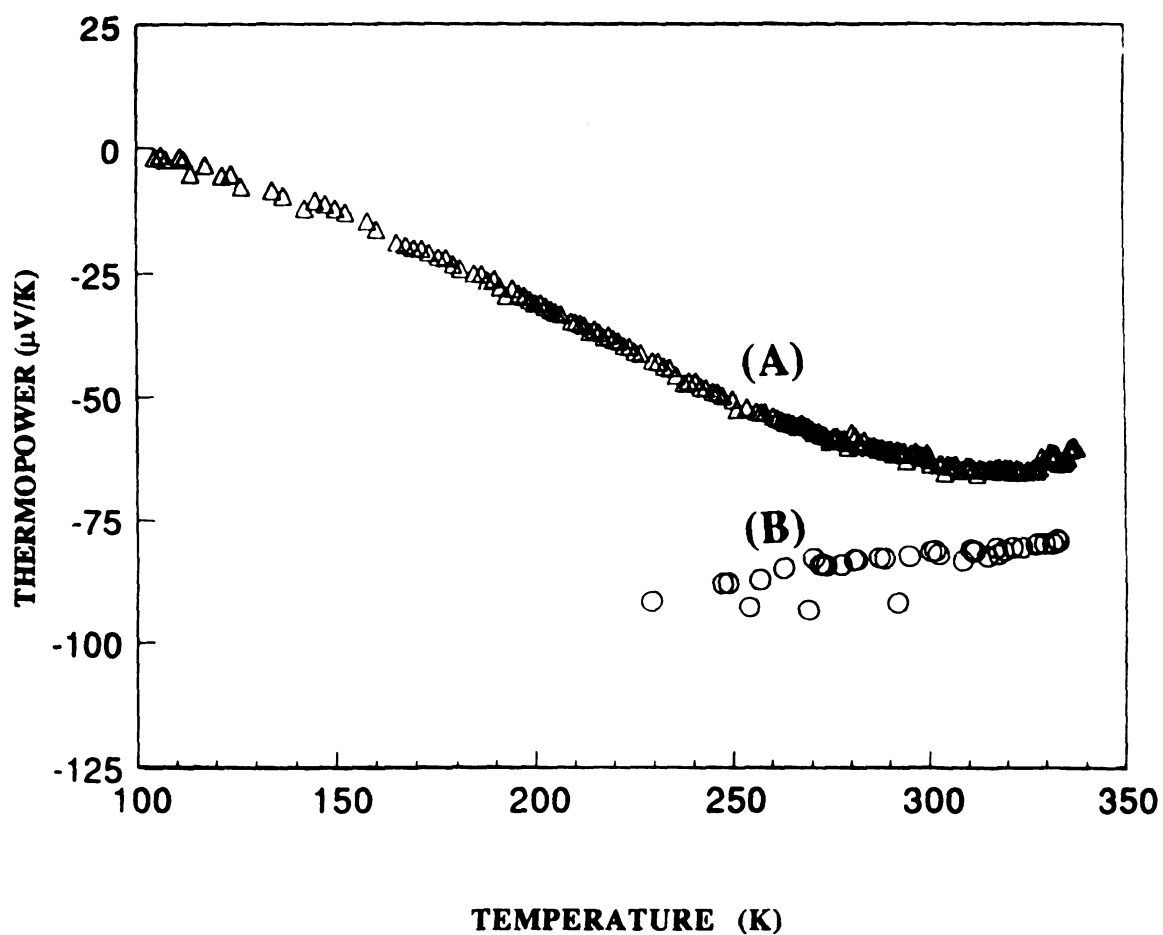
Figure 2.22. Variable temperature thermoelectric power data of (A) α-$(PANI)_{0.30}V_2O_5 1.3 H_2O$ (film) (B) α-$(PANI)_{0.72}V_2O_5 0.33H_2O$ (pressed pellet)

Table 2.6. Room Temperature Thermoelectric Power (S) versus x of $(PANI)_x V_2O_5 nH_2O$.

x	0.056	0.19[*]	0.21	0.29[*]	0.30[*]	0.37	0.44[*]
S $(\mu V/K)$	-300	-30	--	-150	-65	-60	-70
x	0.46	0.48	0.50	0.63	0.67	0.72	0.77
S $(\mu V/K)$	-78	-85	-95	-150	-50	-80	-30

[*]: Film sample.
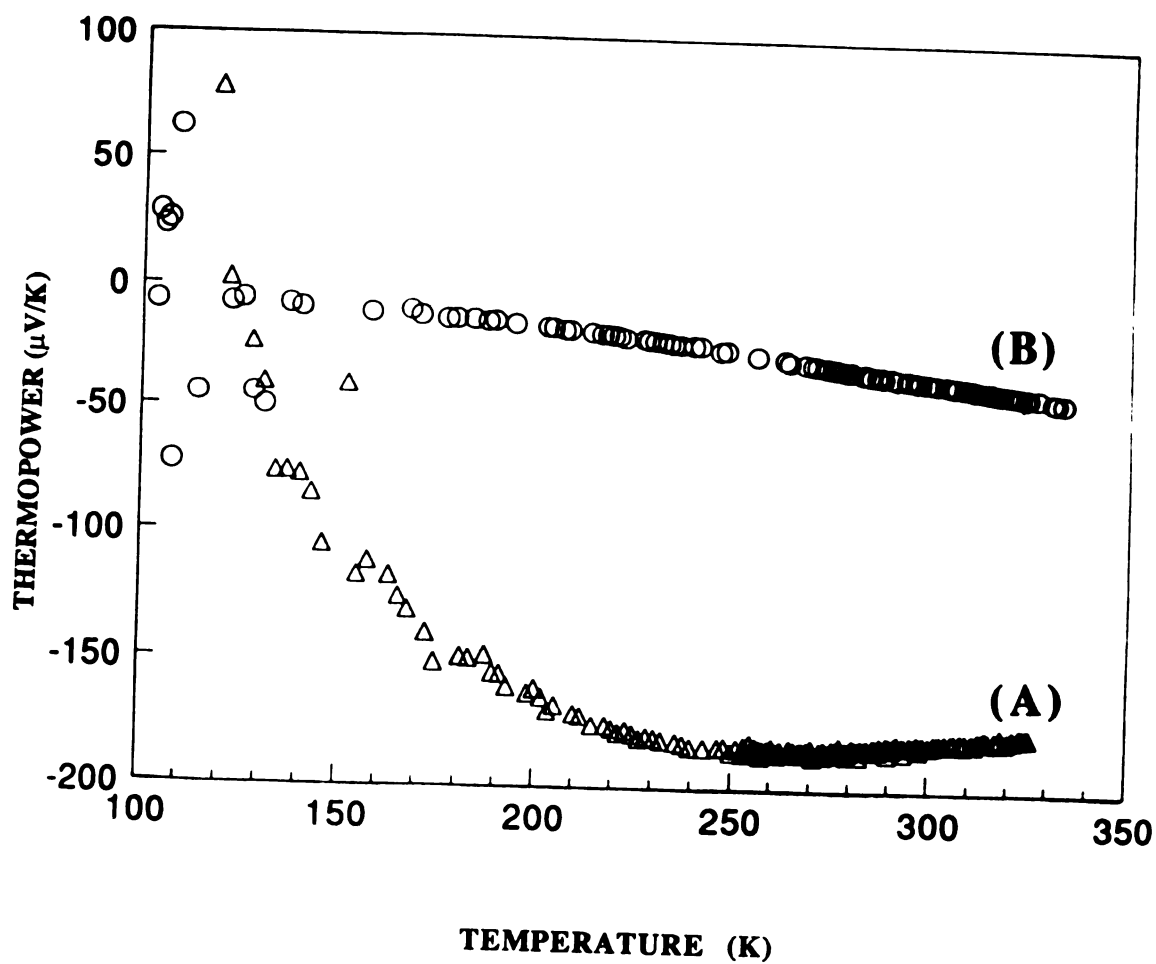
Figure 2.23. Variable temperature thermoelectric power data of pressed pellets of (A) α-$(PANI)_{0.50}V_2O_50.33H_2O$ (B) β-$(PANI)_{0.50}V_2O_50.33H_2O$.
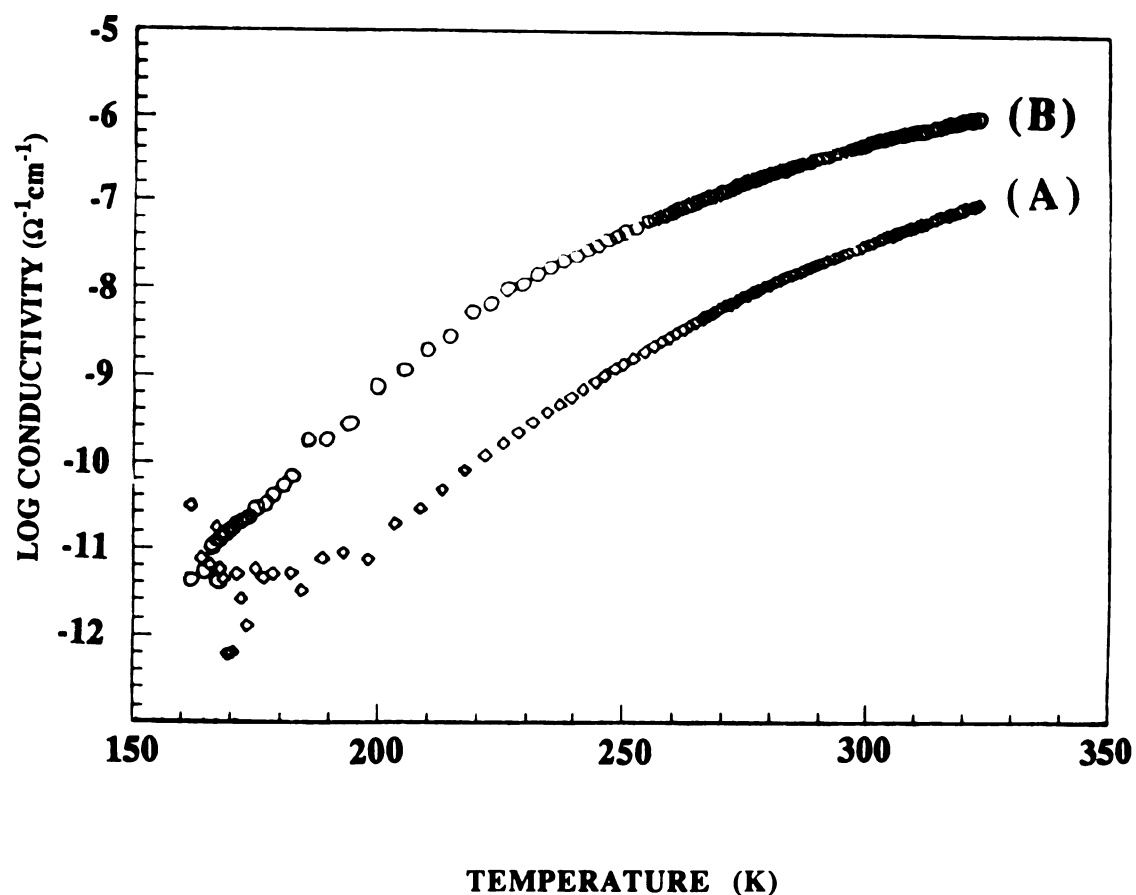
Figure 2.24. Four-probe variable temperature electrical conductivity data of pressed pellets of polyaniline extracted from (A) α-$(PANI)_{0.50}V_2O_5 0.33H_2O$ (B) β-$(PANI)_{0.50}V_2O_5 0.33H_2O$. (The low value of the conductivities is due to the low degree of protonation in the samples.)

consistent with our finding that higher molecular weight polyaniline is present in β-$(PANI)_x V_2O_5 nH_2O$. Longer polymer chains reduce the frequency of carrier hopping from chain to chain, thus facilitating charge transport through the intercalated polymer. However, the influence of V_2O_5 can not be ignored.

As expected, the conductivity of polyaniline extracted from β-$(PANI)_x V_2O_5 nH_2O$ is higher than that extracted from α-$(PANI)_x V_2O_5 nH_2O$ by an order of magnitude as shown in Figure 2.24. The overall low value of conductivity is due to the low degree of protonation and less water content [29] of the samples upon pumping under vacuum.

I. Polyaniline Prepared from Chemically Polymerized versus Extracted from $(PANI)_x V_2O_5 nH_2O$.

The strategies of intercalating conducting polymers in layered hosts have double purpose: to obtain more oriented polymers and to prepare new polymer-derived conducting materials. It is interesting to know the differences between polyaniline extracted from $(PANI)_x V_2O_5 nH_2O$ and bulk polyaniline polymerized with $(NH_4)_2 S_2 O_8$. Table 2.7 lists the comparison of some of the physical and conductivity data of these two materials. Generally, bulk polyaniline has higher molecular weight and therefore, higher conductivity. However, the V_2O_5 acts as a host and an oxidant which offers a more controllable reaction condition to synthesize conducting polyaniline by chemical polymerization. Furthermore, since V_2O_5 xerogel is an

Table 2.7. The Comparison of Extracted and Bulk Polyaniline.

	IR	XRD	EPR, ΔH_{pp} (Gauss)	μ_{eff} (R.T.) B. M.	Highest Molecular Weight	R.T. conductivity ($\Omega^{-1}cm^{-1}$)
Bulk polyaniline	1569 cm^{-1}, 1478 cm^{-1} 1295 cm^{-1} 1249 cm^{-1} 1140 cm^{-1}	amorphous	20	0.19	2,345,000	$10^{-1}\sim100$
Extracted polyaniline	1584 cm^{-1}, 1492 cm^{-1} 1302 cm^{-1}, 1239 cm^{-1} 1140 cm^{-1}	amorphous	20	0.74	1,040,000	$10^{-6}\sim10^{-5}$

electroactive material, interesting polymer-derived conducting composites can be prepared in this method.

VI. Conclusions:

The redox intercalation of aniline and V_2O_5 is a facile reaction. Products with variable $PANI/V_2O_5$ ratios can be obtained with good lamellar order in both film and powder form. All spectroscopic and physicochemical evidence shows that the conducting form of polyaniline is formed. The interlayer expansion calculated from XRD data corresponds to the insertion of a monolayer of polyaniline. The room temperature conductivity and thermoelectric power of as prepared samples are in the range of $10^{-4} \sim 10^0\ \Omega^{-1}cm^{-1}$ and $-30 \sim -300$ $\mu V/K$ respectively.

Upon aging, the reduced V_2O_5 framework of $(PANI)_x V_2O_5 nH_2O$ was partially reoxidized and the polyaniline inside the V_2O_5 interlamellar space continued to oxidatively couple forming longer polymer chains. This results in higher conductivity in the aged samples. The conductivity and molecular weight of polyaniline extracted from β-$(PANI)_x V_2O_5 nH_2O$ is higher than that from α-$(PANI)_x V_2O_5 nH_2O$. The thermoelectric power suggests that in the fresh samples the conductivity is dominated by the reduced V_2O_5 host whereas in the aged samples the polymer is responsible for the charge transport properties. The conductivity characteristic change from n-type semi-conducting to n-type metal-like base on the MW of the intercalated polymer.

LIST OF REFERENCES

LIST OF REFERENCES

1. (a) Genies, E. M.; Boyle, A.; Lapkowski, M.; Tsintavis, C. *Synth. Met*. **1990**, 36, 139-182. (b) Kanatzidis, M. G. *Chemical&Engineering News* **1990**, 68, 36-54.

2. Letheby, H. *J. Chem. Soc.* **1862**, 15, 161-163.

3. MacDiarmid, A. G.; Chiang, J.-C.; Halpern, M.; Huang, W.-S.; Mu, S. L.; Somasiri, N. L. D.; Wu, W.; Yaniger, S. I. *Mol. Cryst. Liq. Cryst.* **1985**, 121, 173-180.

4. (a) Oyama, N.; Kirabayashi, K.; Ohsaka, T. *Bull. Chem. Soc. Jpn.* **1986**, 59, 2071-2080. (b) Kitani, J.; Yano, J.; Kunai, A.; Sasaki, K. *J. Electroanal. Chem.* **1987**, 221, 69-82. (c) Diaz, A. F.; Logan, J. A. *J. Electroanal. Chem.* **1980**, 111, 111-114.

5. (a) Huang, W. S.; Humphrey, B. D.; MacDiarmid, A. G. *J. Chem. Soc. Faraday Trans. 1* **1986**, 82, 2385-2400. (b) Genies, E. M.; Lapkowski, M.; Penneau, J. F. *J. Electroanal. Chem.* **1988**, 249, 97-107. (c) Mohilner, D. M.; Adams, R. N.; Argersinger, W. J. *J. Am. Chem. Soc.* **1962**, 84, 3618-3622. (d) Stilwell, D. E.; Park, S.-M. *J. Elecrtochem. Soc.* **1988**, 135, 254-262. (e) Wang, B.; Tang, J.; Wang, F. *Synth. Met.* **1987**, 18, 323-328.

6. (a) MacDiarmid, A. G.; Chiang, J. C.; Richter, A. J.; Somasir, N. L. D.; Epstein, A. J. In "Conducting Polymers" Alcacer, L. Ed; Reidel Dordreck Holland **1987**. (b) Genies, E. M.; Tsintaris, C.; Syed, A. A. *Mol. Cryst. Liq. Cryst.* **1985**, 121, 181-185. (c) Hand, R. L.; Nelson, R. F. *J. Am. Chem. Soc.* **1974**, 96, 850-860.

7 (a) Harada, I.; Furukawa, Y.; Ueda, F. *Synth. Met.* **1989**, 29, E303-E312. (b) Tang, J.; Jing, X.; Wang, B.; Wang, F. *Synth. Met.* **1988**, 24, 231-238. (c) Cao, Y. *Synth. Met.* **1990**, 35, 319-332.

(d) Kim, Y. H.; Foster, C.; Chiang, J.; Heeger, A. J. *Synth. Met.* **1988,** 26, 49-59. (e) Ohira, M.; Sakai, T.; Takeuchi, M.; Kobayashi, Y.; Tsuji, M. *Synth. Met.* **1987,** 18, 347-352. (f) Wudl, F.; Augus, Jr R. O.; Lu, F. L.; Allemand, P. H.; Vachon, D. J.; Nowak, M.; Liu, Z. X.; Heeger, A. J. *J. Am. Chem. Soc.* **1987,** 109, 3677-3684. (g) Vachon, D.; Angus, R. O.; Lu, F. L.; Nowak, M.; Liu, Z. X.; Schaffer, H.; Wudl, F.; Heeger, A. J. *Synth. Met.* **1987,** 18, 297-302. (h) Lu, F.-L.; Wudl, F.; Nowak, M.; Heeger, A. J. *J. Am Chem. Soc.* **1986,** 108, 8311-8313.

8. (a) Kaplan, S.; Conwell, E. M.; Richter, A. F.; MacDiarmid, A. G. *Synth. Met.* **1989,** 29, E235-E242. (b) Menardo, C.; Nechtschein, M.; Rousseau, A.; Travens, J. P.; Hang, P. *Synth. Met.* **1988,** 25, 311-322. (c) Richter, A. F.; Ray, A.; Ramanathan, K. V.; Manohar, S. K.; Furst, G. T.; Opella, S. J.; MacDiarmid, A. G.; Epstein, A. J. *Synth. Met.* **1989,** 29, E243-E249. (d) Kaplan, S.; Conwell, E. M.; Richte, A. F.; MacDiarmid, A. G. *J. Am. Chem. Soc.* **1988,** 110, 7647-7651. (e) Tan, K. L.; Tan, B. T. G.; Kang, E. T.; Neoh, K. G. *Phys. Rev.* **1989,** 8070-8073. (f) Snauwart, P.; Lazzarani, R.; Riga, J.; Verbist, J. J. *Synth. Met.* **1987,** 18, 335-340. (g) Jozefowicz, M. E.; Epstein, A. J.; Pouget, J. P.; Masters, J. G.; Sun, A. R. Y.; Tang, X.; MacDiarmid, A. G. Proc. ICSM **1906** (Tubingen, Sept. **1990**) *Synth. Met.* **1991,** 41, 723-726. (h) Baughman, R. H.; Wolf, J. F.; Eckhardt, H.; Lagerstedt, I. *Synth. Met.* **1988,** 25, 121-137.

9. (a) Diel, B. N.; Inabe, T.; Lyding, J. W.; Schock, K. F. Jr.; Kannewurf, C. R.; Marks, T. J. *J. Am. Chem. Soc.* **1983,** 105, 1551-1567. (b) Lyding, J. W.; Marcy, H. O.; Marks, T. J.; Kannewurf, C. R. *IEEE. Trans. Instrum. Meas.* **1988,** 37, 76-80.

10. Chaikin, P. I.; Kwak, J. F. *Rev. Sci. Instrum.* **1975,** 46, 218-220.

11. (a) Huebener, R. P. *Phys. Rev.* **1964,** *136*, A1740-A1744. (b) Christian, J, W,; Jan, J. P.; Pearson, W. B. *I. B. Proc. R. Soc. A* **1958,** 213-221. (c) Rathnayaka, K. D. D. *J. Phys. E* **1985,** *18*, 380-381.

12. (a) Farges, J. P.; Brau, A. *Phys. Status Solidi B* **1974,** *64*, 269-275. (b) Andersen, H. H.; Nielson, M. *Phys. Lett.* **1963,** *6*, 17-

18. (c) Polák, J. *Czech. J. Phys. B* **1963**, 13, 616-618. (d) Kopp, J. *Solid State Commun.* **1974**, 14, 1059-1060.

13. Scherrer formula: $D = (0.9 \times \lambda)/\beta \cos\theta$. D: average crystallite size normal to the reflection plane in Å. λ: radiation wavelength (Å). β: halfwidth in radius. θ= Bragg angle in degree.

14. (a) Whittingham, M. S. *Mat. Res. Bull.* **1978**, 13, 775-782. (b) Ruthardt, R.; Schollhorn, R.; Weiss, A. *Z. Naturforsch* **1972**, 27, 1275-1276. (c) Ruitz-Hitzky, E.; Casal, B. *J. Chem. Soc. Faraday Trans. 1* **1986**, 82, 1597-1604.

15. Kanatzidis, M. G. et al work in progress.

16. (a) *"Size Exclusion Chromatography"* Provder, T. Ed. American Chemical Society, Washington, D. C. **1980**. (b) *"Detection and Data Analysis in Size Exclusion Chromatography"* Provder, T. Ed. American Chemical Society, Washington, D. C. **1987**.

17. (a) Genies, E,. M.; Syed, A. A.; Tsintavis, C. *Mol. Cryst. Liq. Cryst.* **1985**, 121, 181-185. (b) Watanbe, A.; Mori, K.; Iwasaki, Y.; Nakamura, J. *J. Chem. Soc. Chem Commun.* **1987**, 3-4. (c) Wei, Y.; Hsuech, K.; Tang, X.; Sun, Y. *Polym. Prepr.* **1989**, 30, 226-227. (d) MacDiarmid, A. G.; Epstein, A. J. in *"European Physical Society Industrial Workshop, Science and Applications of Conducting Polymers"* Lofthus, Norway **1990** IOP publishing.

18. Livage, J.; Gharbi, N.; Leroy, N. C.; Michaud, M. *Mat. Res. Bull.* **1978**, 13, 1117-1124.

19. (a) Ioffe, N. T.; Kogen, Y. L.; Mairanovskii, V. G. *Synth. Met.* **1990**, 37, 74-75. (b) Lapkosk, M.; Genies, E. M. *J. Electroanal. Chem.* **1990**, 279, 158-168. (c) Javadi, H. H. S.; Laversanne, R.; Epstein, A. J.; Kohli, R. K.; Scherr, E. M.; MacDiarmid, A. G. *Synth. Met.* **1989**, 29, E439-444.

20. (a) Enzel, P.; Bein, T. *J. Phys. Chem.* **1989**, 93, 6270-6272. (b) Bein, T.; Enzel, P. *Synth. Met.* **1989**, 29, E163-E168. (c) Enzel, P.;

116

Bein, T. *J. Chem. Soc. Chem. Commun.* **1989**, 1326-1327. (d) Kanatzidis, M. G.; Wu, C. G.; Marcy, H. O.; Kannewurf, C. R. *J. Am. Chem. Soc.* **1989**, <u>111</u>, 4139-4141. (e) Wu, C. G.; Kanatzidis, M. G.; Marcy, H. O.; DeGroot, D. C.; Kannewurf, C. R. *Polym. Mat. Sci. Eng.* **1989**, <u>61</u>, 969-973.

21. Wu, C.G.; Marcy, H. O.; DeGroot, D. C.; Schindler, J. L.; Kannewurf, C. R.; Kanatzidis, M. G. *Synth. Met.* **1991**, <u>41/43</u> 693-698.

22. (a) Fite, C.; Cao, Y.; Heeger, A. J. *Solid State Commu.* **1989**, <u>70</u>, 245-247. (b) Wudl, F.; Angus, R. O.; Lu, F. L.; Allemand, P. M.; Vachon, D. J.; Nowak, M.; Liu, Z. X.; Heeger, A. J. *J. Am. Chem. Soc.* **1987**, <u>109</u>, 3677-3684. (c) Javadi, H. H. S.; Laversanne, R.; Epstein, A. J.; Kohli, R. K.; Scherr, E. U.; MacDiarmid, A. G. *Synth. Met.* **1989**, <u>29</u>, E439-E444.

23. (a) Earnshaw, A. *"Introduction to Magnetochemistry"* Academic Press **1968**. (b) Boudreaux, E. A.; Mulay, L. N. *"Theory and Applications of Molecular Paramagnetism"*, John Wiley and sons New York **1976** P122-124. (c) Gladney, H. M.; Swalen, J. D. *J. Chem. Phys.* **1965**, <u>42</u>, 1999-2009. (d) Drago, R. S. *"Physicl Methods in Chemistry"* W. B. Sannders Co. Philadelphia, **1977** P417-426.

24 Liu, Y. J.; Wu, C>-G.; Kanatzidis, M. G. Manuscript in preparation.

25. (a) Villeneuve, G.; Lezama, L. *Mol. Cryst. Liq. Cryst.* **1989**, <u>176</u>, 495-506. (b) Pouchard, M. These de Doctorat es Sciences Physiques, Bordeaux, **1967**. (c) *"Non-stoichiometric Compounds, Tungsten Bronzes, Vanadium Bronzes and Related Compounds"* Bevan, D. J.; Hagemuller, P. Eds. Pergamon Press Oxford **1973**. (d) Murphy, D. W.; Christian, P. A.; DiSalvo, F. J.; Waszcak, J. V. *Inorg. Chem.* **1979**, <u>18</u>, 2800-2803.

26. (a) Kanatzidis, M. G.; Tonge, C. R.; Marks, T. J.; Marcy, H. O.; Kannewurf, C. R. *J. Am. Chem. Soc.* **1987**, <u>109</u>, 3797-3799. (b) Kanatzidis, M. G.; Marcy, H. O.; McCarthy, W. J.; Kannewurf, C. R.; Marks, T. J. *Solid State Ionics* **1989**, <u>32/33</u>, 594-608. (c) Caspar,

J. V.; Ramamurthy, V.; Corbin, D. R. *J. Am. Chem. Soc.* **1991,** 113, 600-610.

27. Unpublished results in this laboratory.

28. Park, Y. W.; Lee, Y. S.; Park, C.; Shacklette, L. W.; Baughman, R. H. *Solid State Commu.* **1987,** 63, 1063-1066.

29. (a) Angelopoulos, M.; Ray, A.; MacDiarmid, A. G.; Epstein, A. J. *Synth. Met.* **1987,** 21, 21-30. (b) Travers, J. P.; Nechtschein, M. *Synth. Met.* **1987,** 21, 135-141.

NA

CHAPTER 3

CONDUCTIVE POLYPYRROLE/VANADIUM OXIDE MOLECULAR NANOCOMPOSITES ‐ INTERCALATION OF POLYPYRROLE IN V_2O_5 XEROGEL

ABSTRACT

Polypyrrole can be successfully intercalated in V_2O_5 xerogel using pyrrole solutions of CH_3CN or H_2O at room temperature or refluxing (in CH_3CN). The reactions are facile and the resulting products, $(Ppy)_xV_2O_5nH_2O$ (I), revealed increased interlayer spacing. Variable stoichiometries can be achieved based on the reaction methods and mole ratios of pyrrole to V_2O_5. The expansion of interlayer spacing depends on the polymer content and preparation method. Transmission X-ray and electron diffraction patterns suggest the preservation of the layered V_2O_5 framework. Electron paramagnetic resonance (EPR) and variable temperature magnetic susceptibility data show that these materials are paramagnetic, the electron spin mostly comes from the reduced V_2O_5 framework. $(Ppy)_xV_2O_5nH_2O$ show room temperature conductivities up to $10^0 \Omega^{-1}cm^{-1}$ depending on the preparation methods. The materials prepared in aqueous solution have higher conductivity than those from acetonitrile solution. The thermoelectric power data of these composites depend not only on the reaction media but also on polypyrrole/V_2O_5 ratio. At low polypyrrole/V_2O_5 ratios, the Seebeck coefficient is large and negative (n-type conductivity). However, (I) prepared from aqueous solution with high polypyrrole/V_2O_5 ratio, showed a small and positive Seebeck coefficient (p-type conductivity). The electrical measurements suggest that charge transport properties in these materials are dominated by the V_2O_5 framework at the low polymer content limit while polypyrrole is responsible at high polymer concentration.

C

I

I

T

F

I

a

t

o

c

T

cl

ar

tr

to

bi

th

po

la

po

po

I. Introduction:

Currently, one of the interesting developments in intercalation chemistry are that conducting polymers, such as polypyrrole, polythiophene and polyaniline intercalate into the interlayer space of layered materials, such as FeOCl [1], V_2O_5 [2], zeolites [3] and clay [4]. Taking advantage of the *in-situ* oxidative intercalation/ polymerization, novel conducting polymer-inorganic hybrid laminated materials have been synthesized with good conductivity.

Conducting polymers have been attracting a great deal of attention from the scientific and technological community because of their potential applications in practical electronic devices [5,6]. Most of these polymers can be prepared by electrochemical [7,8] as well as chemical polymerization [9,10] of the corresponding monomers. There are indications of crosslinking which occurs during the chemical polymerization, particularly in the synthesis of polypyrrole and polythiophene [11]. This significantly affects the charge transport properties of these polymers.

The intercalation of pyridine in TaS_2 and FeOCl has been shown to proceed via oxidative coupling to yield significant amounts of 4,4'-bipyridine [12]. This selective coupling (regiospecific) is affected by the structural constraints of the lamellar hosts. Therefore, by using a polymerizable guest molecules regiospecific polymerization inside layered compounds could be envisioned to produce highly regular polymers.

Polypyrrole is one of the most widely studied heterocyclic polymers because of its high electrical conductivity. Its charge

transport mechanism has been rationalized by the bipolaron model [13]. The conductivity [14] and mechanical [15] properties of polypyrrole are largely dependent on the counter anion (dopant). The mechanical properties can be systematically modified by forming composites with polyvinyl alcohol or styrene [16]. Here we investigate the intercalation of polypyrrole in metal oxide and using the host as counter anion.

II. Experimental Section:

Reagents: NaOH, HCl, NH$_4$OH(aq), NaVO$_3$, FeCl$_3$, DMSO, NMF, catechol, pyrrole, 2,5-dimethyl-pyrrole and N-methyl-pyrrole were purchased from commercial sources and used without further purification. CH$_3$CN was dried under CaH$_2$ and distilled in air prior to use. All reaction were carried out in air.

Physicochemical methods.
See chapter 2.

Preparation of V$_2$O$_5$nH$_2$O Xerogel.
See page 55.

Preparation of (Ppy)$_{0.44}$V$_2$O$_5$0.5H$_2$O Film.

0.30 g (1.42 mmol) V$_2$O$_5$ xerogel film was added to 20 ml of saturated pyrrole aqueous solution. An immediate color change from red to blue occurred. The mixture was allowed to stand at room

temperature for 24 hours. The black film was picked up from the pyrrole aqueous solution and washed with acetone, then dried under vacuum. Elemental analysis: calcd. for $(C_4H_2NH)_{0.44}V_2O_50.5H_2O$: C, 9.62%; H, 1.06%; N, 2.89%; V, 46.44%. Found: C, 8.40%; H, 1.24%; N, 2.73%; V, 40.64%. The water content was obtained from thermal gravimetric analysis under oxygen flow. Different stoichiometric products are obtained by changing the pyrrole/V_2O_5 ratios. When we used powdered V_2O_5 xerogel (either in H_2O or CH_3CN), a black powder was produced and isolated by filtration and washed with acetone. An example is given below.

Preparation of $(Ppy)_{0.73}V_2O_50.90H_2O$ Powder.

0.64 g (9.55 mmol) of pyrrole was dissolved in 30 ml acetonitrile, and to the solution was added 1.0 g (4.70 mmol) of V_2O_5 xerogel fine powder. The mixture was stirred at room temperature for 4 hours. The resulting black powder was isolated by filtration, washed with acetone and dried in vacuum. Elemental and thermogravimetric analysis: calcd for $(Ppy)_{0.73}V_2O_5.0.9H_2O$: C, 14.26%; H, 1.62%; N, 4.12%; V, 41.52%. Found: C, 14.24%; H, 1.34%; N, 3.92%; V, 41.44%. Upon changing the reagents' ratios, the polypyrrole/ V_2O_5 can vary from 0.18 to 0.73.

Synthesis of Bulk Polypyrrole.

A literature procedure was followed [17]. To a solution of 50 ml 5.6 wt% of $FeCl_3$ aqueous solution was added 0.5 g (7.5 mmol)

pyrrole. The mixture was stirred at room temperature for 2 hours under nitrogen. The black precipitate was isolated by filtration, washed with acetone and dried in vacuum. Polypyrrole was identified by its characteristic IR spectrum [18].

Isolation of Polypyrrole from $(Ppy)_x V_2 O_5 n H_2 O$.

0.15 g (0.67 mmol) of $(Ppy)_{0.56} V_2 O_5 n H_2 O$ was stirred for 22 hours in 50 ml 2 M HCl(aq) in which 0.50 mg (4.5 mmol) of catechol was dissolved. The black residue was isolated by filtration, washed with $H_2 O$ then acetone and dried under vacuum. It was identified to be polypyrrole by its characteristic IR spectrum [18].

III. Results and Discussion:

A. Synthesis and Characterization.

We made extensive attempts to identify the optimum preparation conditions of homogeneous, single phase $(Ppy)_x V_2 O_5 n H_2 O$. Several methods were used to intercalate polypyrrole into $V_2 O_5$ interlayer space: (a) $V_2 O_5$ xerogel was first swelled with a small amount of water and then reacted with pyrrole at room temperature, (b) pyrrole/water mixture was poured over a $V_2 O_5$ xerogel film and allowed to stand for one day, (c) $V_2 O_5$ xerogel was refluxed with dilute pyrrole/acetonitrile solution and (d) fine powder of $V_2 O_5$ reacted with pyrrole/acetonitrile solution at room temperature. In all reactions, upon contact of pyrrole with the

$V_2O_5nH_2O$, a dramatic color change of the V_2O_5 occurred from red to a bluish black with metallic luster. When V_2O_5 xerogel films were used, their use in the synthetic procedure yields free standing films of the $(Ppy)_xV_2O_5nH_2O$ materials. Pyrrole which has a low oxidation potential is easily oxidatively polymerized by the V^{5+} centers in the xerogel with simultaneous generation of V^{4+} centers as shown in equation 3.1.

$$xC_4H_4NH + V_2O_51.6H_2O \longrightarrow (C_4H_2NH)_xH_{2x}V_2O_5nH_2O \cdots eq(3.1)$$
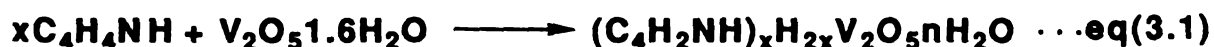
Reaction condition (a) always resulted in amorphous products because of the rapid redox reaction. Efforts to reduce the reaction rate by lowering the reaction temperature were not successful. Even the reaction carried out at ice water temperature, the black product was amorphous. Using method (b), (c) and (d) we were able to get good layered materials in which we can vary the stoichiometry by controlling the mole ratio of the reagents. Fourier transform infrared (FTIR) spectra of $(Ppy)_xV_2O_5nH_2O$ clearly showed the characteristic vibrations of the polypyrrole backbone as shown in Figure 3.1. When the reactions were carried out in refluxing acetonitrile solution using V_2O_5 film as starting material, in addition to the weak polypyrrole absorption, we observed new absorptions originating from intercalated acetamide which forms by acid-hydrolysis of CH_3CN. These acetamide peaks did not appear in the reaction of V_2O_5 powder under the same experimental conditions ($82°C$ 4 hours). The polypyrrole inside the V_2O_5 layers can be isolated by digesting the
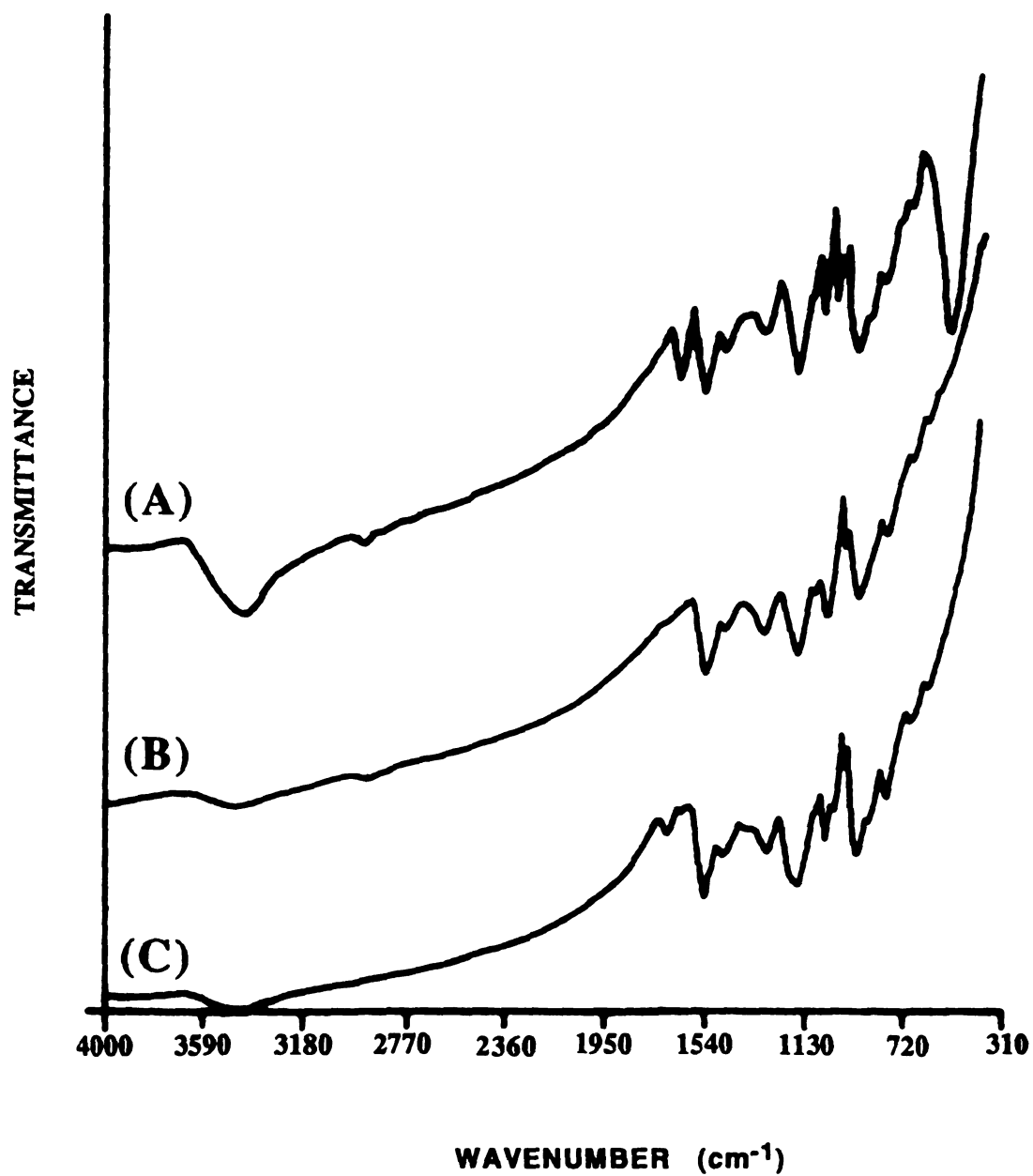
Figure 3.1. FT-IR spectra (KBr pellets) of (A) $(Ppy)_{0.56}V_2O_5nH_2O$ (B) Extracted polypyrrole (C) Bulk polypyrrole.

host layered framework with 2M HCl or 2% NaOH aqueous solution. Polypyrrole will degrade gradually in basic and acid medium and therefore isolating it intact proved to be difficult. To avoid the polymer degradation in acid we used catechol as a ligand for $(VO)^{3+}$ which is formed by reacting V_2O_5 with acid and is a known strong oxidant. The catechol complex formed is a considerably weaker oxidant and does not appear to attack the polymer. The IR spectra of extracted polypyrrole are very similar to bulk polypyrrole, see Figure 3.1b&3.1c. Although the IR spectra of $(Ppy)_x V_2O_5 n H_2O$ prepared from aqueous solution and acetonitrile solution are the same, we were unable to isolate the intact polypyrrole from the latter without adding catechol. This is probably because of the polymer in $(Ppy)_x V_2O_5 n H_2O$ prepared from acetonitrile solution has shorter chains. Therefore the extracted polymer degraded upon treating with acid or base in the presence of good oxidizing agent, $(VO)^{3+}$.

X-ray diffraction patterns (XRD) of these materials showed that the intercalation is accompanied by a large interlayer spacing (d) expansion. The increase of the interlayer spacing varies with the stoichiometry of the products and reaction conditions, as shown in Table 3.1 and Table 3.2 Generally, the $(Ppy)_x V_2O_5 n H_2O$ prepared from aqueous solution show higher d-spacings and vary slightly from sample to sample. This is probably due to the random arrangement of the polypyrrole molecules in V_2O_5 interlamellar space, caused by the fast redox intercalation reaction and perhaps due to some co-intercalated H_2O. This is suggested by the relatively weak and broad XRD peaks as shown in Figure 3.2. $(Ppy)_x V_2O_5 n H_2O$ are relatively

Table 3.1. The Interlayer Spacing (d) versus x of $(Ppy)_x V_2 O_5 n H_2 O$ Prepared from Acetonitrile Solution.

X	0.18	0.36	0.56	0.73
d(Å)	12.42	12.81	12.68	15.30

Table 3.2. The Interlayer Spacing (d) versus x of $(Ppy)_x V_2 O_5 n H_2 O$ Prepared from Aqueous Solution.

X	0.17	0.25	0.26	0.32	0.42	0.56
d(Å)	13.10	13.33	14.71	14.56	13.14	15.91
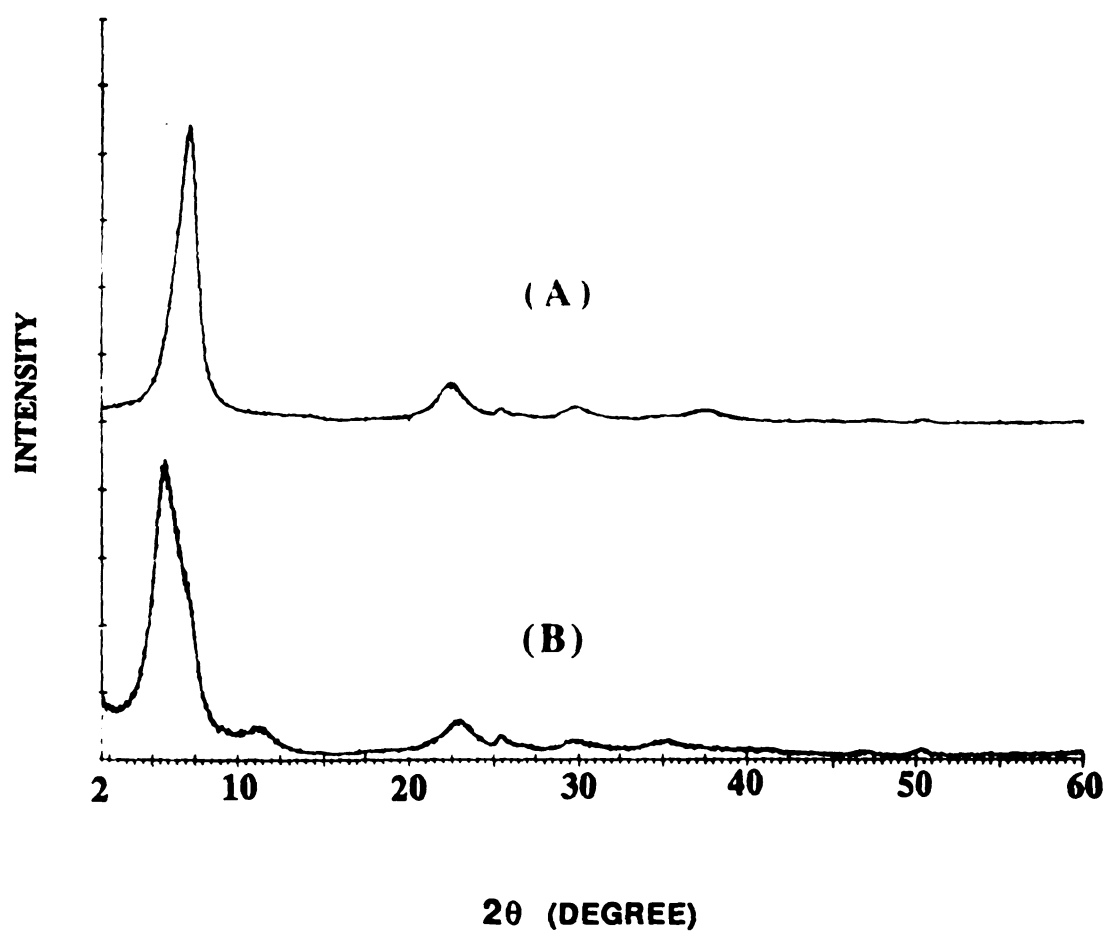
Figure 3.2. X-ray diffraction patterns of $(Ppy)_x V_2O_5 n H_2O$ prepared from acetonitrile solution (compressed powder) (A) $(Ppy)_{0.18}V_2O_5 n H_2O$ (B) $(Ppy)_{0.73}V_2O_5 n H_2O$.

porous as they absorb moisture and increase their interlayer spacing. Therefore, the variation of interlayer spacings may be due to the presence of differing amounts of water.

For $(Ppy)_x V_2O_5 nH_2O$ prepared from acetonitrile solution, there are two major phases, one with interlayer spacing of $15.20(\pm 20)$Å for high polymer content, and another with a spacing of $12.42(\pm 20)$Å for low polymer content, as shown in Figure 3.3. After intercalation of polymer most of the interlayer water in V_2O_5 xerogel is lost. The d-spacing expansions of the two phases due to the insertion of polypyrrole correspond to 6.4Å $(15.20-11.55+2.8)$Å and 3.72Å respectively. These values can be rationalized as intercalation of a monolayer of polypyrrole with the five member ring perpendicular to the V_2O_5 layers for the first phase and parallel to V_2O_5 slabs for the second phase as shown in Scheme 3.1. The transmission XRD patterns of all $(Ppy)_x V_2O_5 nH_2O$ films with the X-ray beam perpendicular to the film are identical to that of pristine V_2O_5 xerogels, see Figure 3.4. This confirms our belief that we are dealing with a topotactic reaction in which the host framework is preserved after intercalation.

The SEM micrographs of $(Ppy)_x V_2O_5 nH_2O$ are very similar to that of $(PANI)_x V_2O_5 nH_2O$ and $(Pth)_x V_2O_5 nH_2O$ [19]. Intercalation of polypyrrole into the V_2O_5 film created some defects on the surface of the film. However there was no observable separate phase and the layered nature was preserved after intercalation, even at this macroscopic level, as shown in Figure 3.5. Selected Area Electron

INTENSITY

Figu
prep
(Pp
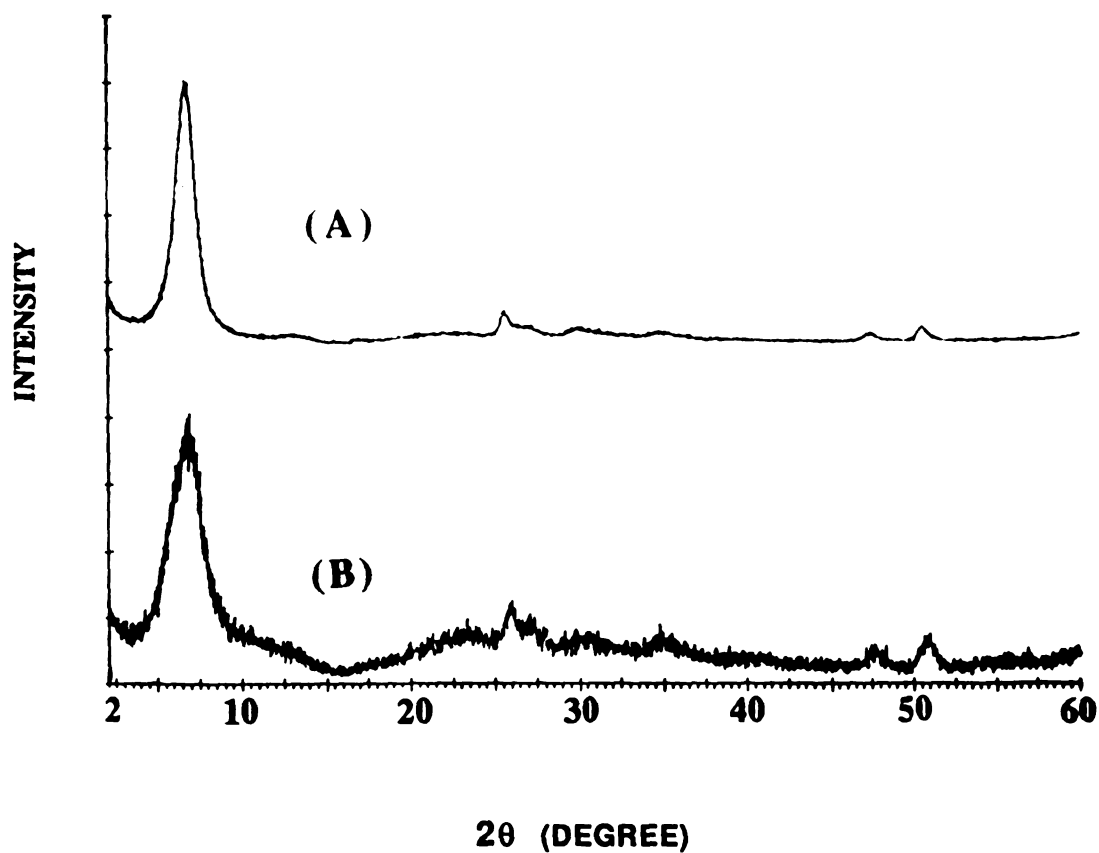
Figure 3.3. X-ray diffraction patterns of $(Ppy)_x V_2O_5 n H_2O$ prepared from aqueous solution (compressed powder) (A) $(Ppy)_{0.30}V_2O_5nH_2O$ (B) $(Ppy)_{0.56}V_2O_5nH_2O$.
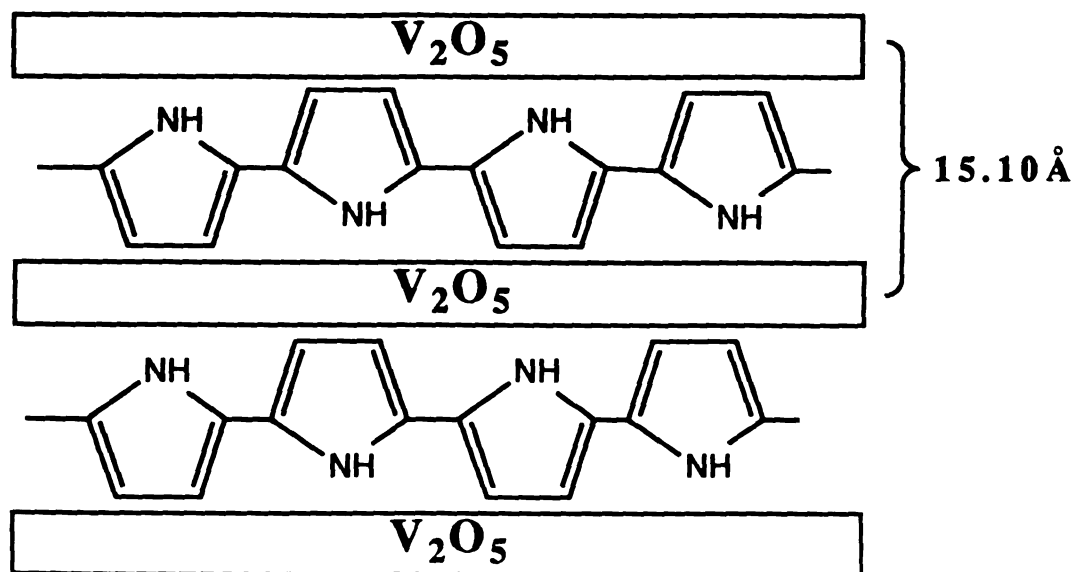
(A)
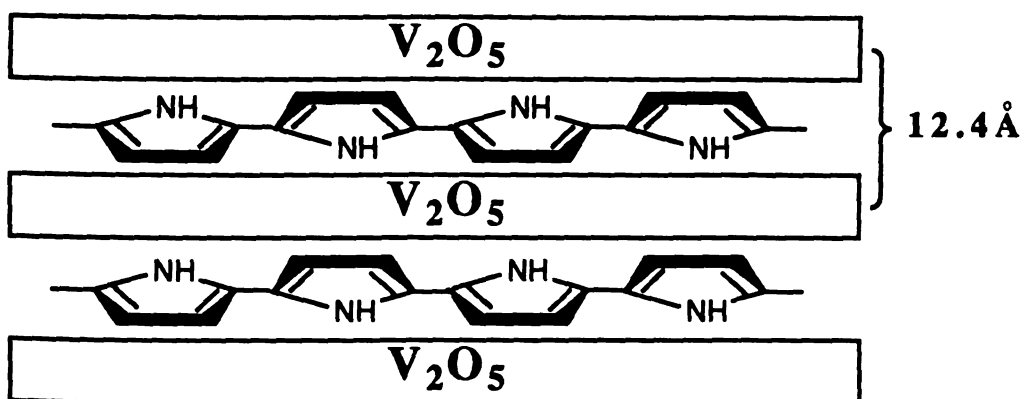
(B)

Scheme 3.1   Proposed arrangement of polypyrrole chains in V_2O_5 layers (A) Perpendicular. (B) Parallel to layers.

INTENSITY

2

Figure
of (A)
experim
the film
sample
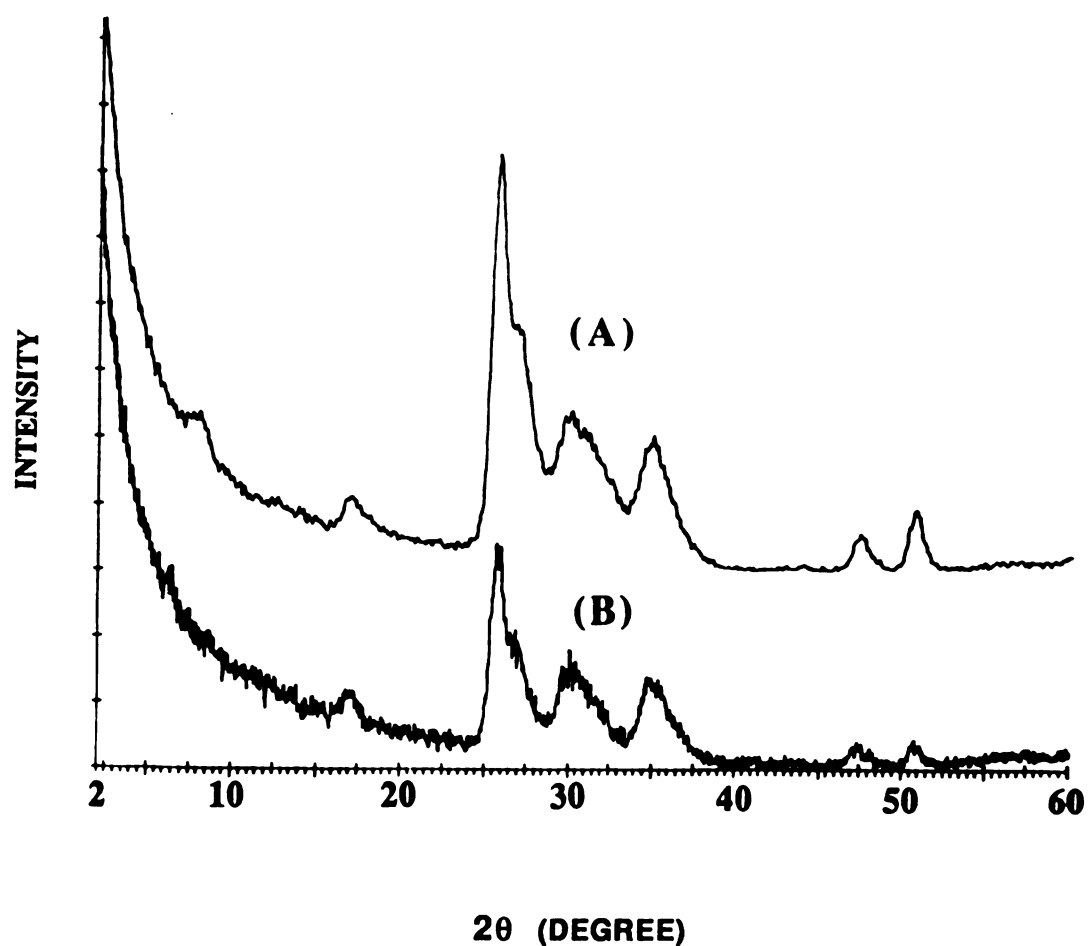
Figure 3.4. Transmission-mode X-ray diffraction patterns of (A) $(Ppy)_x V_2O_5 n H_2O$ (B) V_2O_5 xerogel. (In this experiment, the incident X-ray beam was perpendicular to the film. The detector is moving along the 2θ angle while sample remains stationary.)
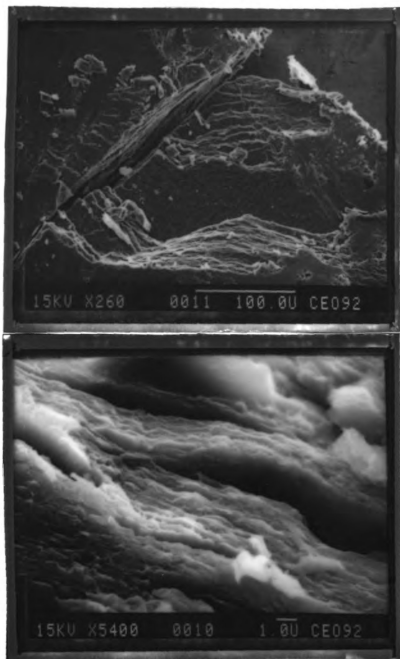
Figure 3.5. SEM micrographs of $(Ppy)_x V_2 O_5 n H_2 O$.
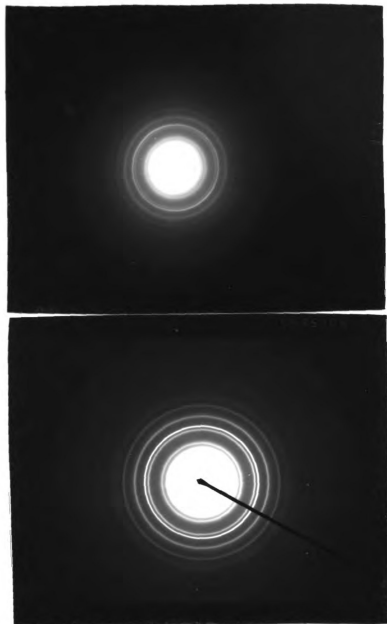
Figure 3.6. Selected area electron diffraction patterns of
(A) $(Ppy)_x V_2 O_5 n H_2 O$ (B) $V_2 O_5$ xerogel.

Dif

bea

3.6

(P

sin

go

pau

the

wi

ac

Du

di

m

th

be

is

th

co

Su

co

sy

hi

ox

Diffraction (SAED) patterns of $(Ppy)_x V_2O_5 nH_2O$ with the electron beam approximately perpendicular to the layers is shown in Figure 3.6a. It showed several weak rings as seen early in $(PANI)_x V_2O_5 nH_2O$, see page 83. The corresponding spacings are similar to that of pristine V_2O_5 xerogel (see Figure 3.6b) and are in good agreement with the X-ray data. The similar electron diffraction patterns of V_2O_5 xerogel and $(Ppy)_x V_2O_5 nH_2O$ further supported that the V_2O_5 framework was preserved after the reaction, consistent with the XRD results.

B. Oxygen Effects.

As we discussed in chapter 2, oxygen acts as an electron acceptor during the intercalation of polyaniline in V_2O_5 xerogel. During the course of our work with the polypyrrole system we discovered that oxygen plays a similar role. This phenomenon was monitored by using an oxygen electrode. As the reaction proceeds, the oxygen concentration in the solvent decreases very rapidly in the beginning and then levels off as the reaction nears completion. This is shown in Figure 3.7. The amount of oxygen consumed depends on the ratio of reagents. At higher pyrrole/V_2O_5 ratio (V_2O_5 kept constant), more oxygen was consumed as shown in Figure 3.8. Surprisingly, higher V_2O_5/pyrrole ratio (pyrrole keep constant) also consumed more oxygen. This implied that V_2O_5 in this reaction system acts as an oxidant as well as a catalyst. The oxygen oxidizes highly reactive (reducing) intermediates generated by the initial oxidation of the pyrrole itself. Such intermediates could be radical
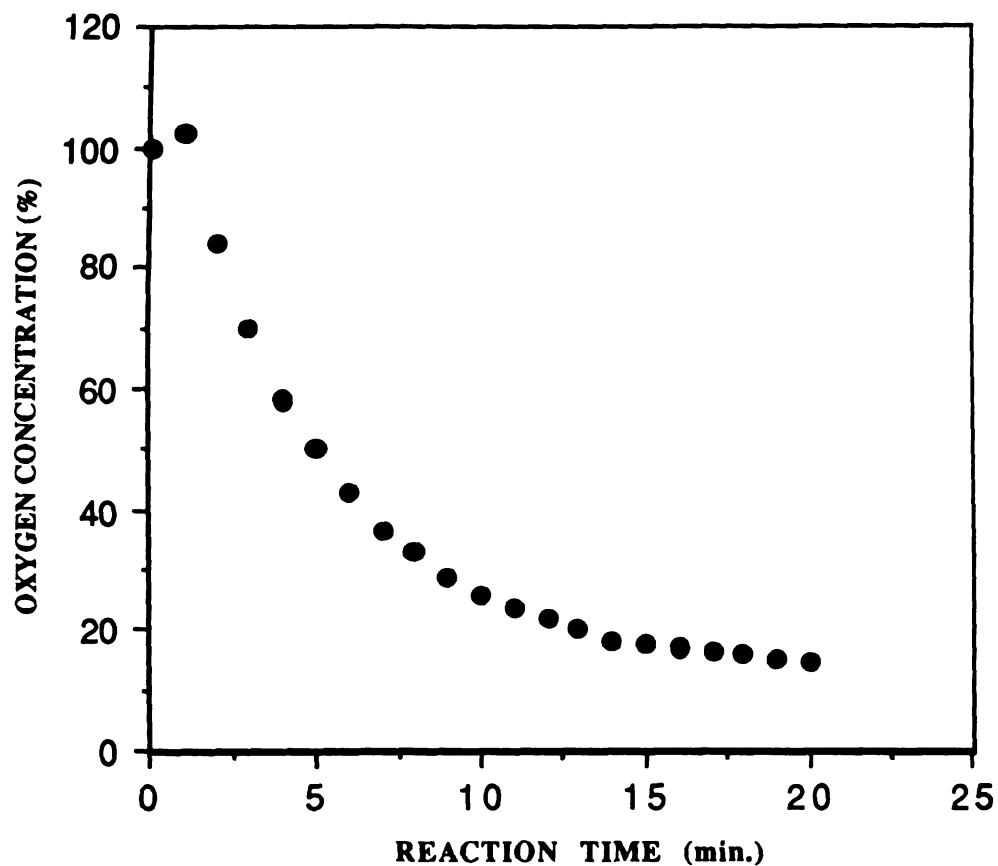
Figure 3.7. Oxygen concentration versus reaction time during the intercalation of pyrrole in V_2O_5 xerogel. (The oxygen concentration of pyrrole aqueous solution, before adding V_2O_5 xerogel, is set at 100%. In this reaction the pyrrole to V_2O_5 ratio was 1)

OXYGEN CONSUMPTION (%)

Fi
ra
co
ox
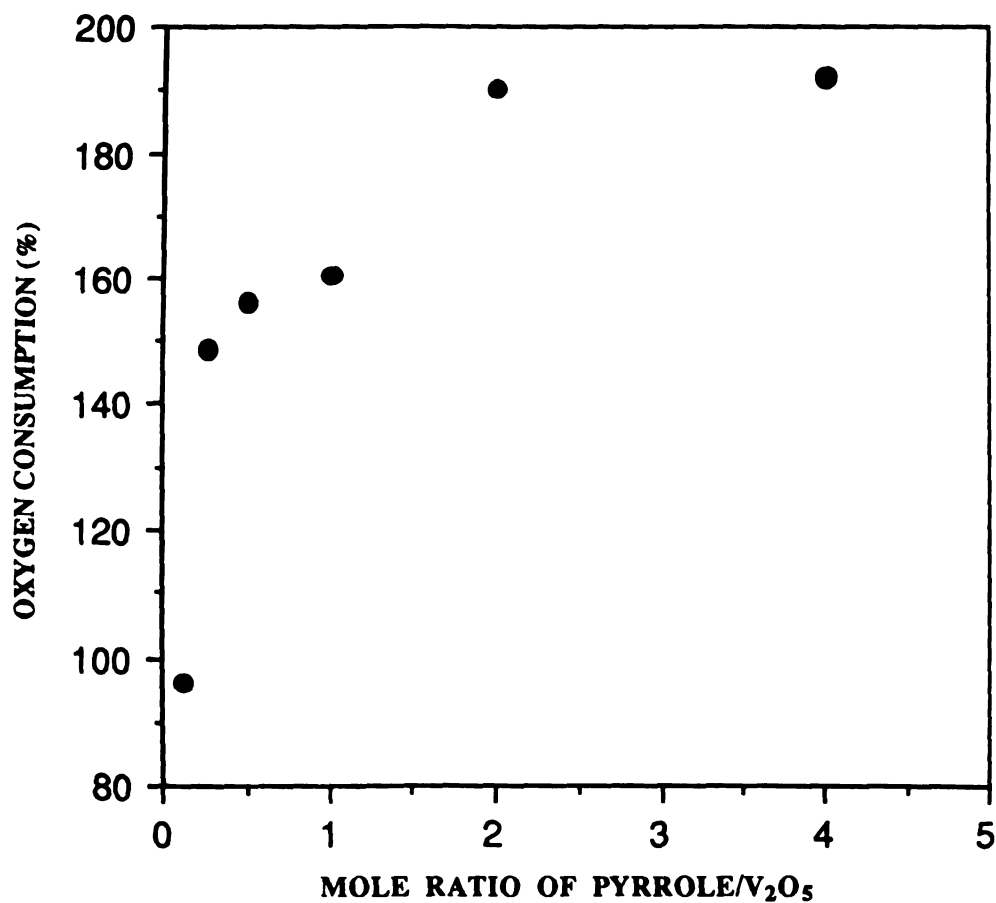
Figure 3.8. Oxygen consumption versus pyrrole/V_2O_5 ratio of intercalation of pyrrole in V_2O_5 xerogel. (At.0% consumption, the aqueous solution is saturated with oxygen)

cation oligomeric species. In a controlled experiment, V_2O_5 xerogel was reacted with alkali metal iodide, such as KI, and monitored the oxygen concentration of the system. We found no oxygen was consumed during the entire reaction period (30 minutes). Therefore, the consumption of oxygen must related to the formation of polypyrrole. Therefore, the more accurate reaction for this redox intercalation can be represented in equation 3.2.

$$xC_4H_4NH + V_2O_51.6H_2O + x\text{-}y/2O_2 \longrightarrow (C_4H_2NH)_xH_yV_2O_5nH_2O$$
$$+ \; x\text{-}y/2H_2O_2 \; \ldots \ldots eq(3.2)$$
$$(or \; H_2O)$$
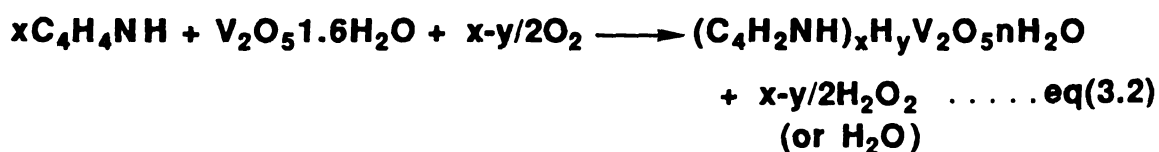
Oxygen is not only involved during the reaction but also affects the products after isolation. Upon standing in air (aging) for several months, the magnetic moment of $(Ppy)_xV_2O_5nH_2O$ decreases as observed in $(PANI)_xV_2O_5nH_2O$, see page 87. We found that polypyrrole in $(Ppy)_xV_2O_5nH_2O$ degrades gradually upon aging. This can be clearly detected by the small but significant change in the FTIR spectra. No change in the XRD pattern is observed. The samples are stable in sealed evacuated tubes, as judged by the IR and magnetic susceptibility data. Unlike $(PANI)_xV_2O_5nH_2O$, oxygen here did not cause continuing oxidative polymerization of pyrrole oligomers in the interlamellar space of V_2O_5 but instead it reacted the V_2O_5 and perhaps with polypyrrole and destroyed its conjugating structure. Another cause for the degradation of polypyrrole could be the V_2O_5 framework after it has been reoxidized. Pyrolysis mass

spectra of both aged and fresh samples showed no volatile species at temperature up to 350°C under vacuum. This suggested that the degradation did not seriously reduce the polymer chain length. This polymer degradation results in a decrease in electrical conductivity (vide infra).

The oxidative degradation is accelerated at higher temperature. When $(Ppy)_x V_2O_5 nH_2O$ was heated at 175°C in air for 3 days, IR spectra showed changes consistent with degradation of polypyrrole. No change was observed in the V_2O_5 framework. However, when the sample was heated in vacuum at 175°C, we observed IR spectra changes associated with changes both in the polymer as well as V_2O_5 structures. The V_2O_5 is reduced and Ppy is oxidized consistent with internal redox chemistry between the two species.

C. Thermogravimetric Analysis (TGA) and Differential Scanning Calorimetry (DSC) Studies.

Typical thermogravimetric diagrams of fresh and aged $(Ppy)_x V_2O_5 nH_2O$ under oxygen flow are shown in Figure 3.9. A less than 2% weight loss is observed at temperatures below 100°C probably due to absorbed and intercalated water. A continuous weight loss was observed between 100°C to 470°C and stabilized thereafter. The decreasing weight between 100°C and 470°C (differs slightly from sample to sample) is due to the decomposition of the polymer and loss of trace amount of residual structural water. The thermal stability of fresh samples is better than that of aged samples. This is because the aged samples have more V^{5+} sites in
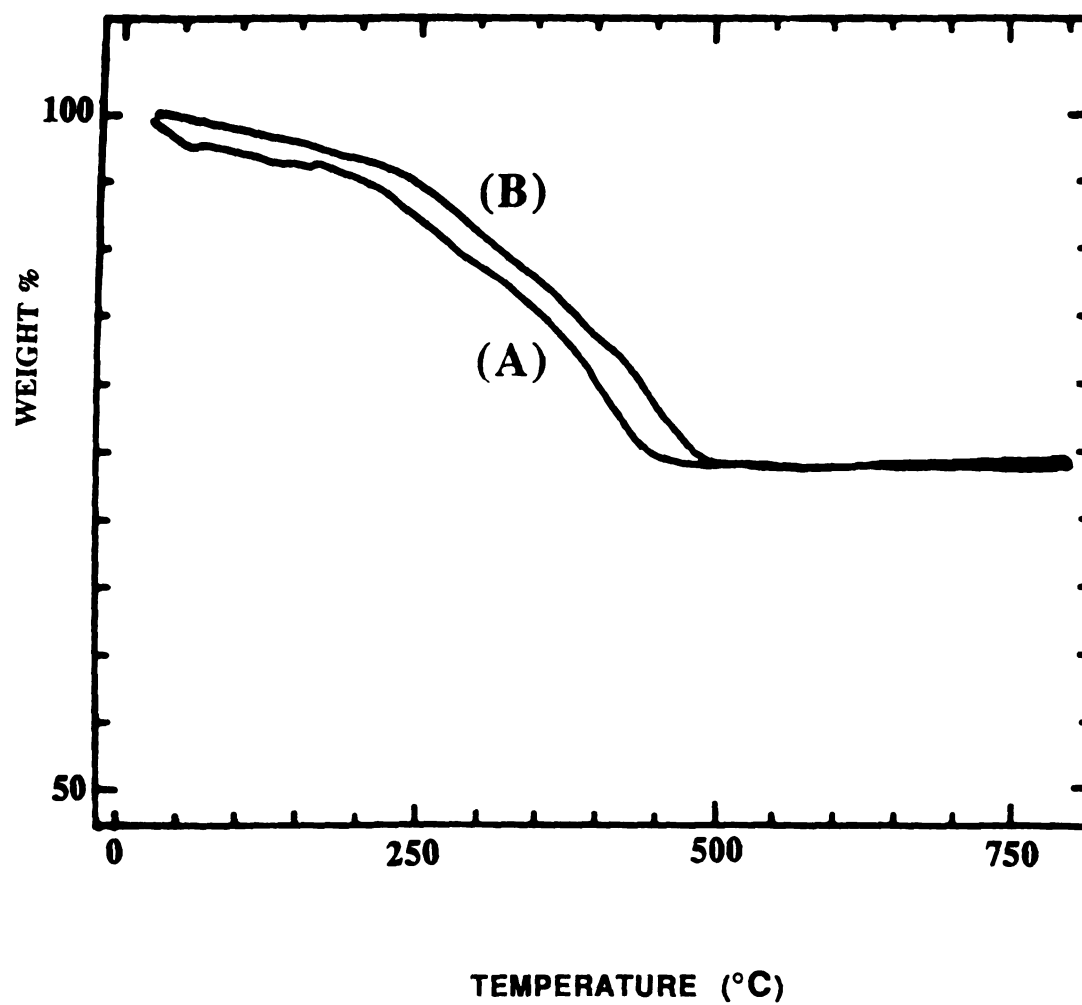
Figure 3.9. TGA curves (under oxygen flow) of (A) Fresh $(Ppy)_{0.9}V_2O_5nH_2O$ (B) Aged $(Ppy)_{0.9}V_2O_5nH_2O$.

V_2O_5 layers which in turn are more oxidizing. The same reason explains why the material under nitrogen flow is more stable than that under oxygen flow. The thermal behavior of $(Ppy)_xV_2O_5nH_2O$ is similar to that of $(PANI)_xV_2O_5nH_2O$ and $(Pth)_xV_2O_5nH_2O$ systems, see page 78 and Page 182.

The DSC diagram of $(Ppy)_xV_2O_5nH_2O$ was featureless. Compared to that of pristine V_2O_5 xerogel which showed a strong, broad endothermic peak at temperature around 150°C which is due to the loss of the interlayer water [19]. The DSC result was consistent with the XRD data which showed that after intercalation, most of the interlayer water was expelled. When $(Ppy)_xV_2O_5nH_2O$ was placed in air for several months (aged), it absorbed moisture as judged the increase in interlayer spacing. The DSC diagram of aged sample showed a weak endothermic peak at temperature around 150°C.

D. Electron Paramagnetic Resonance (EPR) Spectroscopy.

The EPR spectra of all $(Ppy)_xV_2O_5nH_2O$ showed very broad signals (ΔH_{pp} = 100~200 G) centered at g = 1.9637 which was similar to that of reduced V_2O_5, such as $Na_xV_2O_5nH_2O$ [20]. This signal is due to the presence of V^{4+}, d^1 centers [21]. The typical narrow EPR peak arising from static defects of conducting polypyrrole [22] was not observed even at liquid nitrogen temperature. This suggests that either the unpaired spins on the static defects of polypyrrole are magnetically coupled to the electron spins in the reduced V_2O_5 framework or the number of such defects
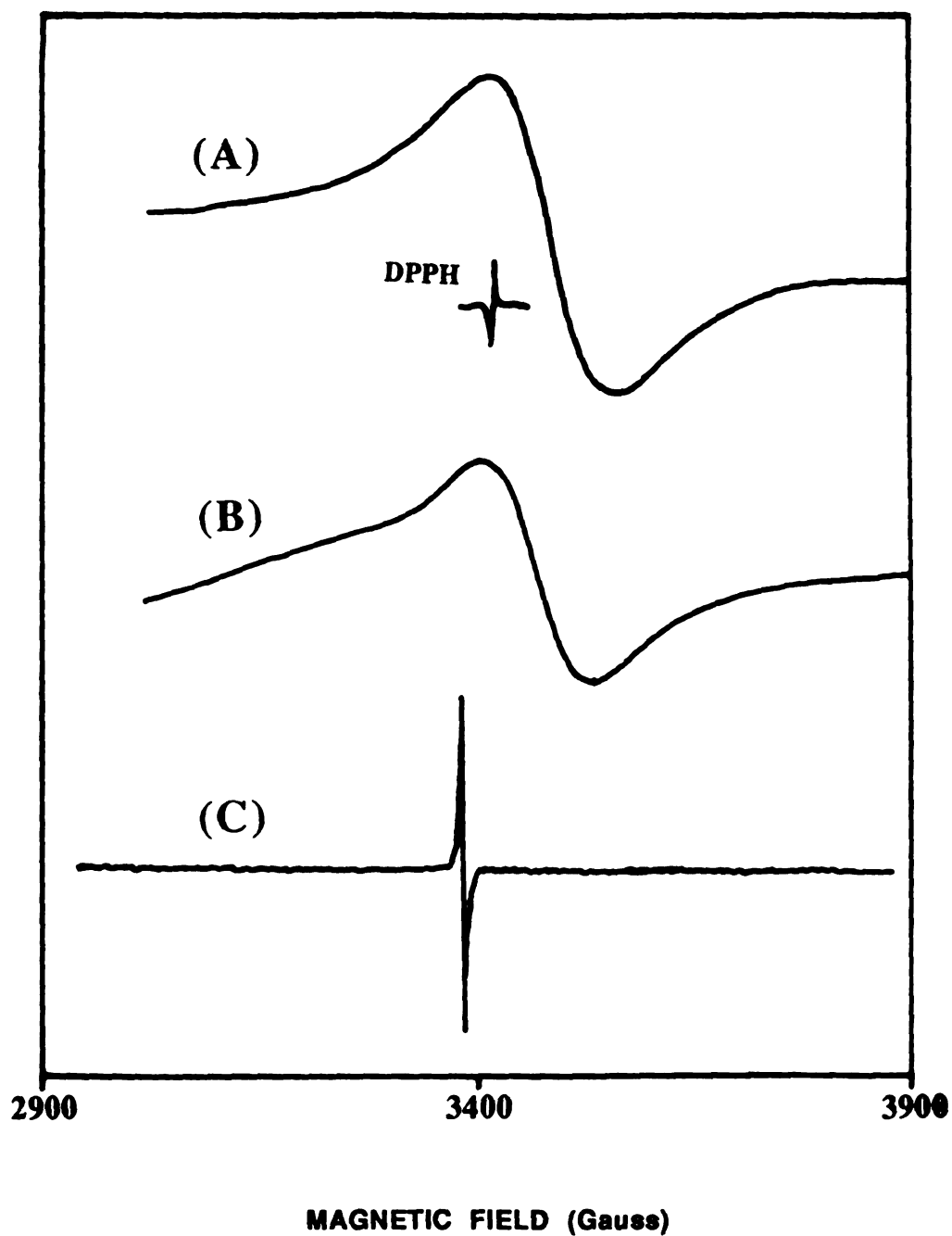
Figure 3.10. Room temperature EPR spectra of (A) $(Ppy)_{0.56}V_2O_5nH_2O$ (B) $Na_{0.4}V_2O_5nH_2O$ (C) Extracted polypyrrole.

in these materials considerably smaller than typical bulk Ppy or the defects are diamagnetic. The latter is unlikely since the narrow EPR signals of polypyrrole can be observed after extracting the polymer from the host matrix by acidic solution as shown in Figure 3.10. These results are consistent with the absence of any separate Ppy impurity phase. The EPR data show that the magnetic behavior of these polypyrrole "bronzes" is dominated by the V_2O_5 network.

Efforts to relate the spin quantity derived from the EPR signal to the degree of reduction of V_2O_5 framework were not pursued, as they could be unreliable, due to the strong spin-spin interaction between polypyrrole and V_2O_5 host and the large peak width of the signal.

E. Magnetic Susceptibility Studies.

Consistent with the EPR results, variable temperature magnetic susceptibility data showed $(Ppy)_xV_2O_5nH_2O$ to be a paramagnetic material. The susceptibility decreases with rising temperature as shown in Figure 3.11. The magnetic moment of polypyrrole is relatively small [20] and thus the magnetic moment of $(Ppy)_xV_2O_5nH_2O$ mostly comes from the reduced V_2O_5 host. Similar to $(PANI)_xV_2O_5nH_2O$ (see page 87), the susceptibility of $(Ppy)_xV_2O_5nH_2O$ can be separated into two components: Curie paramagnetism and Van Vleck paramagnetism (or temperature independent paramagnetism) as shown in Figure 3.12. For a discussion of TIP see chapter 2 above. Figure 3.13 shows the variable temperature effective spin-only (Curie) magnetic moment,
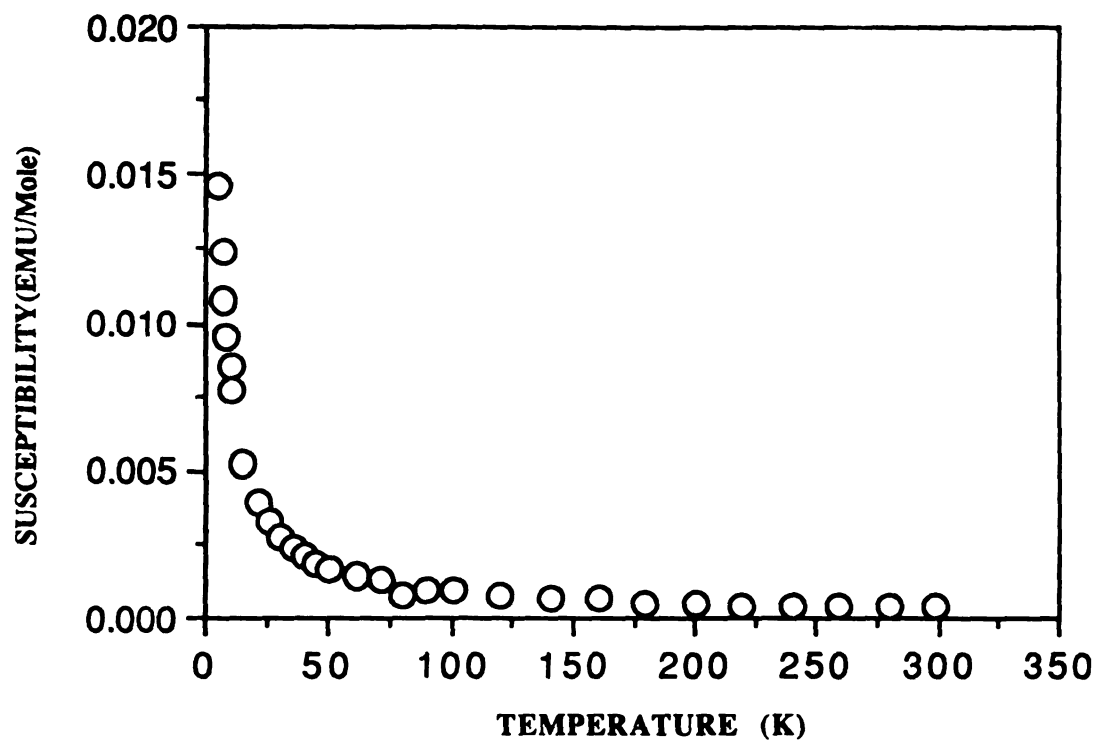
Figure 3.11. Variable temperature magnetic susceptibility (χ_m) data of $(Ppy)_{0.73}V_2O_5nH_2O$ at 5000 gauss applied field.
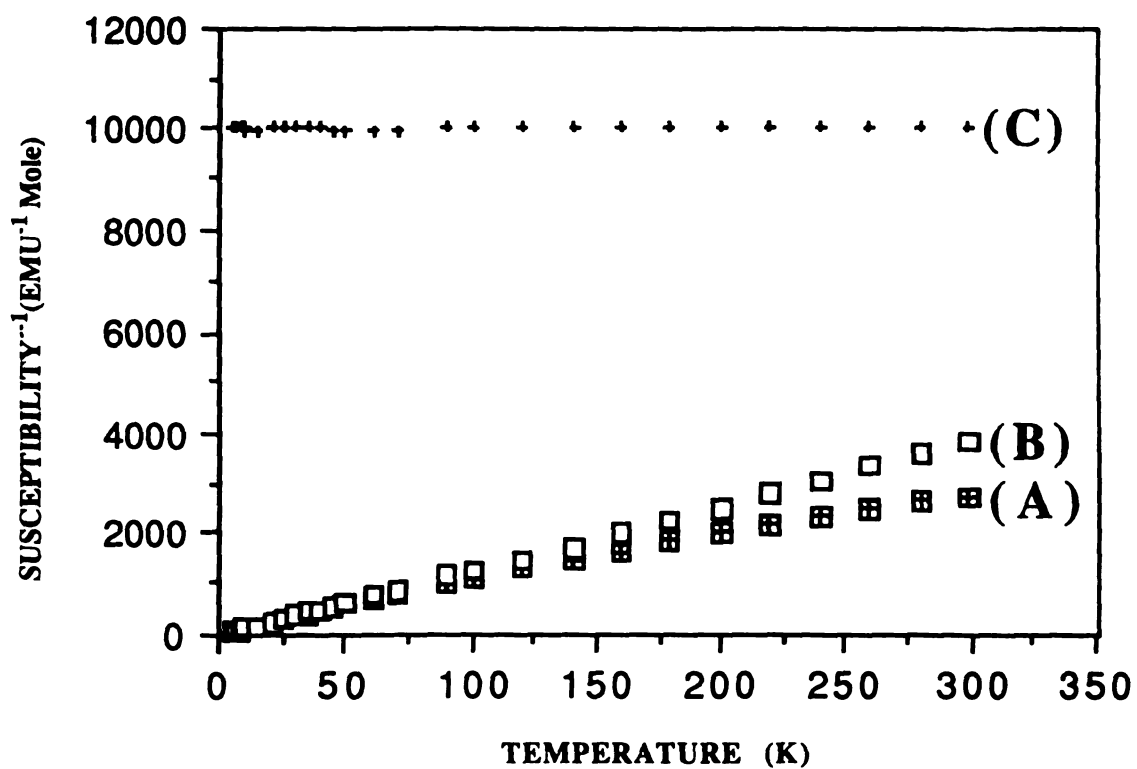
Figure 3.12. Variable temperature magnetic susceptibility data $(1/\chi_m)$ of $(Ppy)_{0.73}V_2O_5nH_2O$ at 5000 gauss applied field (A) Total magnetic susceptibility (B) Curie susceptibility (C) Temperature independent paramagnetism
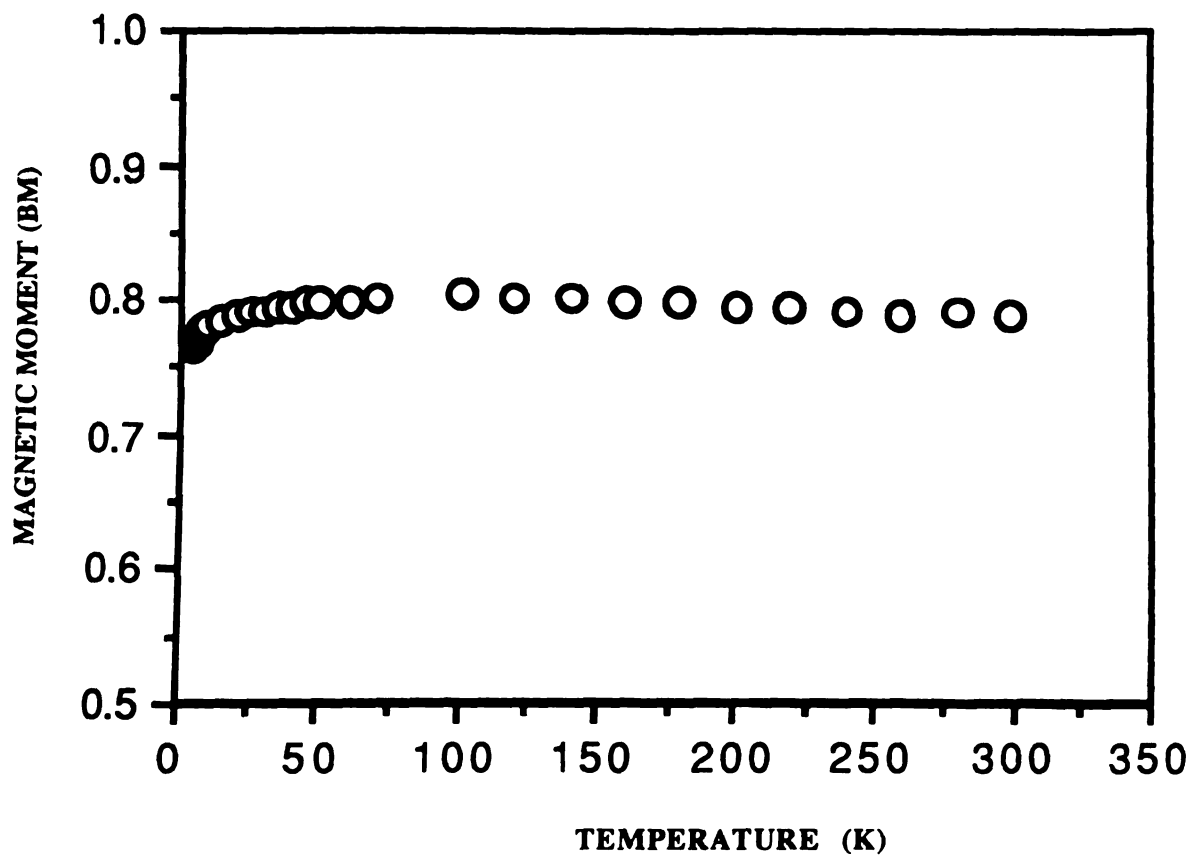
Figure 3.13. Variation of effective spin-only magnetic moment as a function of temperature for $(Ppy)_{0.73}V_2O_5nH_2O$ at 5000 gauss applied field.

μeff,

error

param

sever

3.3.

we

oxida

preli

Furth

numl

polyn

deca

10 d

repre

simil

samp

prepa

indic

forme

with

reoxi

oxyge

may

photc

obser

μ_{eff}, of $(Ppy)_{0.73}V_2O_5nH_2O$. The μ_{eff} is constant, within experimental error, in all measured temperature (5k~300K), consistent with the paramagnetic behavior. The room temperature magnetic moment for several $(Ppy)_xV_2O_5nH_2O$ with different x values are listed in Table 3.3. In all samples, the total μ_{eff} is lower than the value expected if we assume that all electrons released from the monomer during oxidative polymerization are transferred to V_2O_5 layers. This is preliminary due to the effect of oxygen as discussed above. Furthermore, the chain length of the polymer is also related to the number of electrons transferred to V_2O_5 during oxidative polymerization. For instance, for 20 monomer unit, to form 2 decamers, more electrons are transferred than by the formation of 10 dimers. Due to these complicated interactions the μ_{eff} does not represent fully the degree of reduction of V_2O_5. Generally, for similar x value in $(Ppy)_xV_2O_5nH_2O$, the magnetic moments of the samples prepared from aqueous solution are higher than those prepared from acetonitrile solution (see Table 3.3). This may indicate (qualitatively) that the degree of reduction of host in the former was higher than the latter.

Upon standing in air (aging), the magnetic moment decreased with time as shown in Figure 3.14. This is probably due to the reoxidation of V^{4+} centers to V^{5+}. However, in $(Ppy)_xV_2O_5nH_2O$, oxygen also degrades the polypyrrole inside the V_2O_5 layers, which may also effect the magnetic behavior.

We attempted to determine the V^{4+}/V^{5+} ratio by X-ray photoelectron spectroscopy (XPS). Although the V^{+4} peak was observed, due to the change of V^{4+} peak position and shape as well

Table 3.3.   Room Temperature Magnetic Moment and Temperature Independent Paramagnetism of $(Ppy)_x V_2 O_5 n H_2 O$ versus x.

X	$\mu_{eff}(BM)$ (Total)	$\mu_{eff}(BM)^*$ (Curie)	$\chi_m \times 10^4$ (TIP)
0.18	0.89	0.74	1.0
0.32	0.73	0.52	1.0
0.36	0.85	0.73	0.8
0.56	0.96	0.91	1.0
0.73	0.93	0.79	1.0
**0.17	1.14	0.91	0.911.6
**0.26	1.50	0.90	5.5
**0.56	1.67	0.93	8.0

*: Corrected for TIP Van Vleck paramagnetism.
**: Samples prepared in aqueous solution
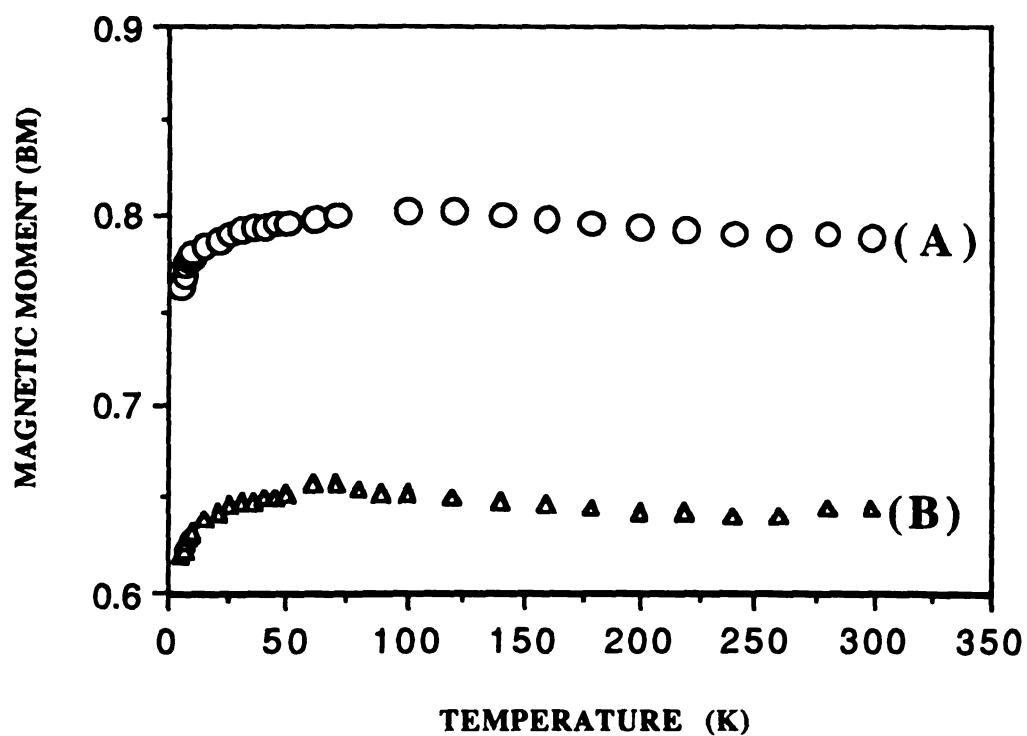
Figure 3.14. Variation of effective spin-only magnetic moment as a function of temperature for $(Ppy)_{0.73}V_2O_5nH_2O$ (A) Fresh prepared (B) Aged.

as serious overlap between V^{4+} and V^{5+} peaks, we were not able to do a complete quantitation of each species. Further investigation of XPS spectra is in progress.

F. Charge Transport Properties.

(1). Electrical conductivity.

The electrical conductivities of $(Ppy)_x V_2O_5 nH_2O$ were measured by the in-line four-probe method as a function of temperature. We found that the conductivity of film samples prepared in water increases 5 orders of magnitude compared to pristine V_2O_5 as shown in Figure 3.15. AC/DC measurements suggest that the charge-transport in these materials is electronic in nature. No ionic contribution was detected. Interestingly, the film samples of $(Ppy)_x V_2O_5 nH_2O$ prepared in H_2O show significantly higher conductivity than those prepared in CH_3CN, as shown in Figure 3.16. For all samples the conductivity increases with rising temperature. This is a typical thermally activated behavior dominated by interparticle contact resistance as well as intrinsic effects such as polymer conjugation length, interchain distance and V^{4+} to V^{5+} hopping barriers. Similar behavior was observed in $(PANI)_x V_2O_5 nH_2O$ and $(Pth)_x V_2O_5 nH_2O$ (see page 97 and 194). Thermally activated behavior is also existent in other intercalated compounds [22] and conducting polymers [23].

The higher conductivity for the samples prepared by using water as a solvent may be due to the formation of longer polymer
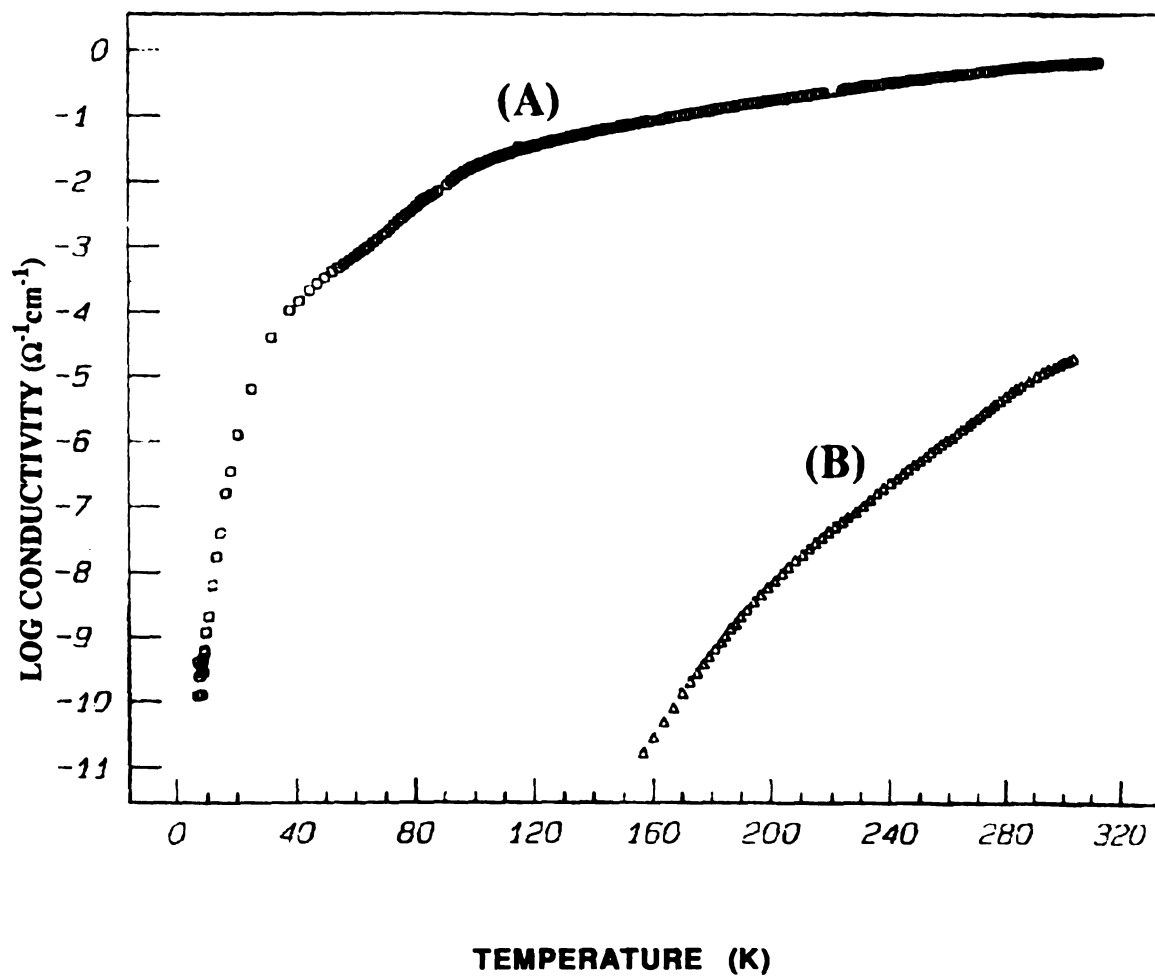
Figure 3.15. Four-probe variable temperature electrical conductivity data of films of (A) $(Ppy)_{0.26}V_2O_5 n H_2O$ (B) Pristine V_2O_5 xerogel.
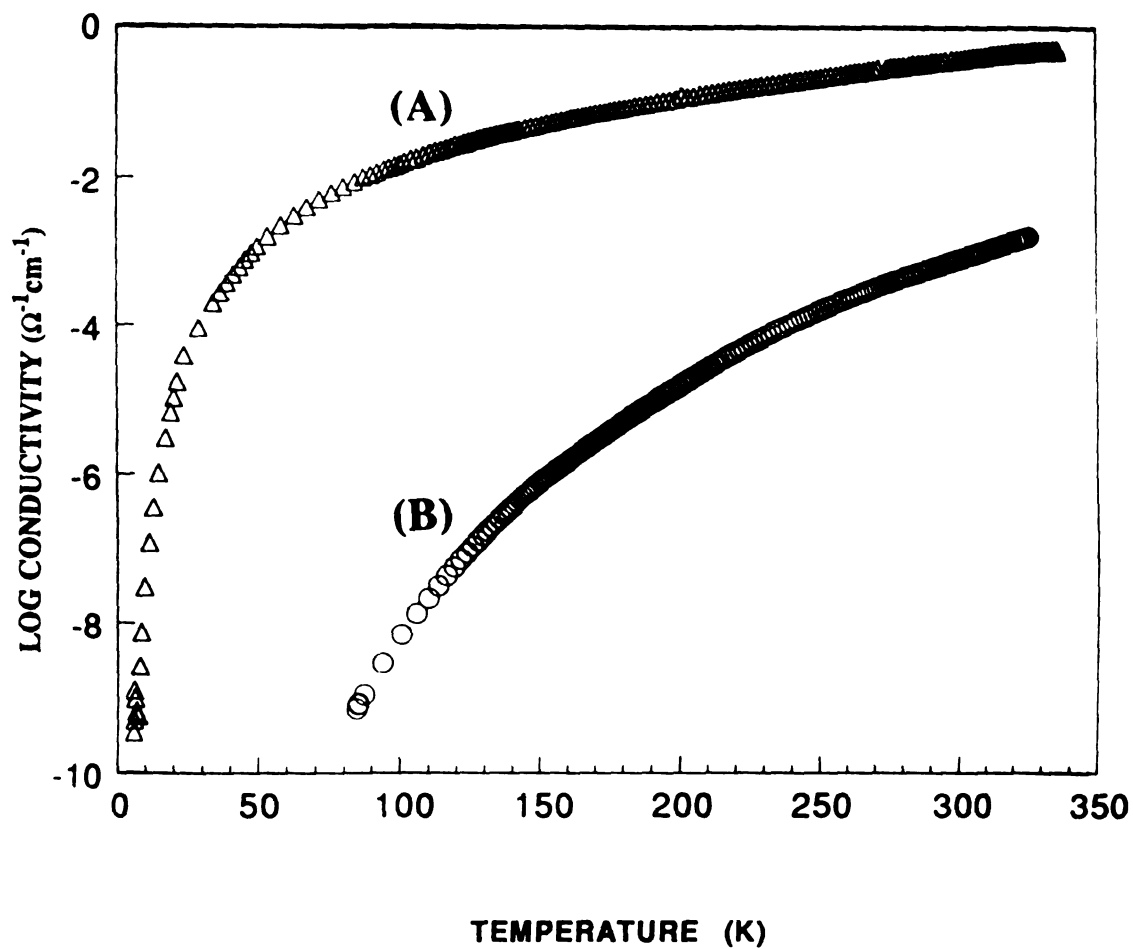
Figure 3.16. Four-probe variable temperature electrical conductivity data of films of (A) $(Ppy)_{0.26}V_2O_5nH_2O$ prepared from aqueous solution (B) $(Ppy)_{0.32}V_2O_5nH_2O$ prepared from acetonitrile solution.

chains or polymer with fewer structural defects and thus longer conjugation length. Also, according to the magnetic data, the V^{4+}/V^{5+} ratio in the water-prepared samples is higher than the acetonitrile based, meaning that the number of carriers in the former is greater than in the latter, and thus contribute to higher conductivity. It has been known that polypyrrole prepared from solvents having OH group exhibits higher conductivity [13], but the reason is not understood. Table 3.4 lists the room temperature conductivities of $(Ppy)_x V_2 O_5 n H_2 O$ prepared from CH_3CN solution with different x value. It is clear from this table that with exception of very low x values, the conductivity of film samples are similar to those of pressed pellets. It is also evident that the magnitude of the conductivity is more or less consistent. This is surprising since we would expect that the conductivity would be sensitive to the polymer/$V_2 O_5$ ratio. When current is passed through these materials, it either goes through the reduced $V_2 O_5$ framework or through the partially oxidized polymer blocks, depending on which way is more favorable. In low polymer/$V_2 O_5$ ratio, the distance between polymer chains should be large, and the current flow should be better mediated through the $V_2 O_5$ framework. In high polymer/$V_2 O_5$ ratio, the polymer chains should be closer together, and thus we might except the carriers to travel easier through the polymer. In our studies, all the $(Ppy)_x V_2 O_5 n H_2 O$ samples prepared from CH_3CN solution showed similar conductivity ($10^{-3} \sim 10^{-2}\ \Omega^{-1}cm^{-1}$) regardless of the polymer content. A possible explanation is that the polypyrrole chains inside the $V_2 O_5$ layers are low molecular weight

Table 3.4. Room Temperature Electrical Conductivity (σ) versus x of $(Ppy)_x V_2 O_5 n H_2 O$ Prepared from Acetonitrile Solution.

x	$\sigma_{R.T.}$ $(\Omega^{-1} cm^{-1})$	measured form
0.16	$< 10^{-4}$	pellet
0.18	$< 10^{-4}$	pellet
0.32	$10^{-3} \sim 10^{-2}$	film
0.36	$10^{-3} \sim 10^{-2}$	pellet
0.56	$10^{-3} \sim 10^{-2}$	pellet
0.64	10^{-2}	film
0.73	$10^{-3} \sim 10^{-2}$	pellet

Table 3.5. Room Temperature Electrical Conductivity (σ) versus x of $(Ppy)_x V_2 O_5 n H_2 O$ Prepared from Aqueous Solution.

x	$\sigma_{R.T.}$ $(\Omega^{-1} cm^{-1})$	measured form
0.17	$10^{-3} \sim 10^{-2}$	pellet
0.25	10^{-2}	pellet
0.26	10^{0}	film
0.40	10^{0}	film
0.42	$10^{-3} \sim 10^{-2}$	pellet
0.56	$10^{-3} \sim 10^{-2}$	pellet

polymers, and the charge transport is preliminarily through the vanadium oxide framework.

The conductivity of $(Ppy)_x V_2O_5nH_2O$ prepared from aqueous solution varied significantly between film samples and pressed pellets $(\sigma_{R.T.}: 10^0$ vs $10^{-3} \Omega^{-1}cm^{-1})$ as listed in Table 3.5. In this table we see no obvious correlation between conductivity and polymer/V_2O_5 ratios. The high conductivity of the film samples can be rationalized by the longer conjugation length of the intercalated polypyrrole and less structural defects. We emphasize however we do not have molecular weight information to substantiate this claim.

The Ppy inside the V_2O_5 degraded gradually upon aging as observed in FT-IR spectroscope. However, the room temperature conductivities of the aged samples are similar to those of fresh prepared as shown in Figure 3.17.

Although the conductivities of $(Ppy)_x V_2O_5nH_2O$ prepared from acetonitrile solution are approximately the same , the thermoelectric power (TP) data vary with different x values as shown in Figure 3.18. The Seebeck coefficient becomes steadily less negative as the Ppy content increases. The large and negative TP indicate that $(Ppy)_x V_2O_5nH_2O$ is a n-type semiconductor. Typical variable temperature thermoelectric power data are shown in Figure 3.19. The TP behavior is similar to alkali metal xerogel bronzes, $Cs_x V_2O_5$ [24] and suggest that the reduced V_2O_5 dominates the charge transport. This implies that the polymer chains in $(Ppy)_x V_2O_5nH_2O$ are short, not favorable for current flow. The decreasing of thermopower may be due to the increasing degree of reduction of V_2O_5 framework as the polymer/V_2O_5 ratio increases,.
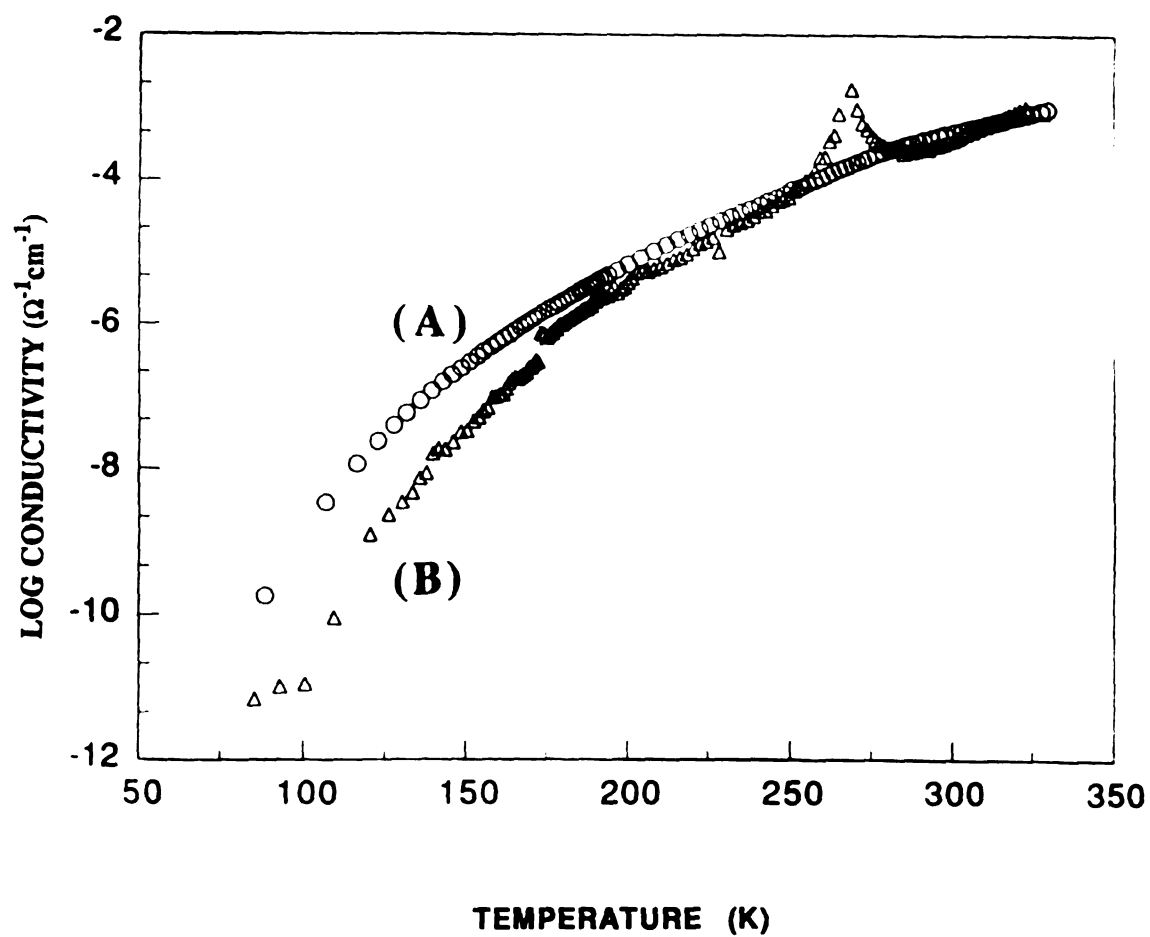
Figure 3.17. Four-probe variable temperature electrical conductivity data for $(Ppy)_{0.73}V_2O_5nH_2O$ (A) Fresh prepared (B) Aged. (The anomaly at ~270K is due to instrumental instability and no physical significant)
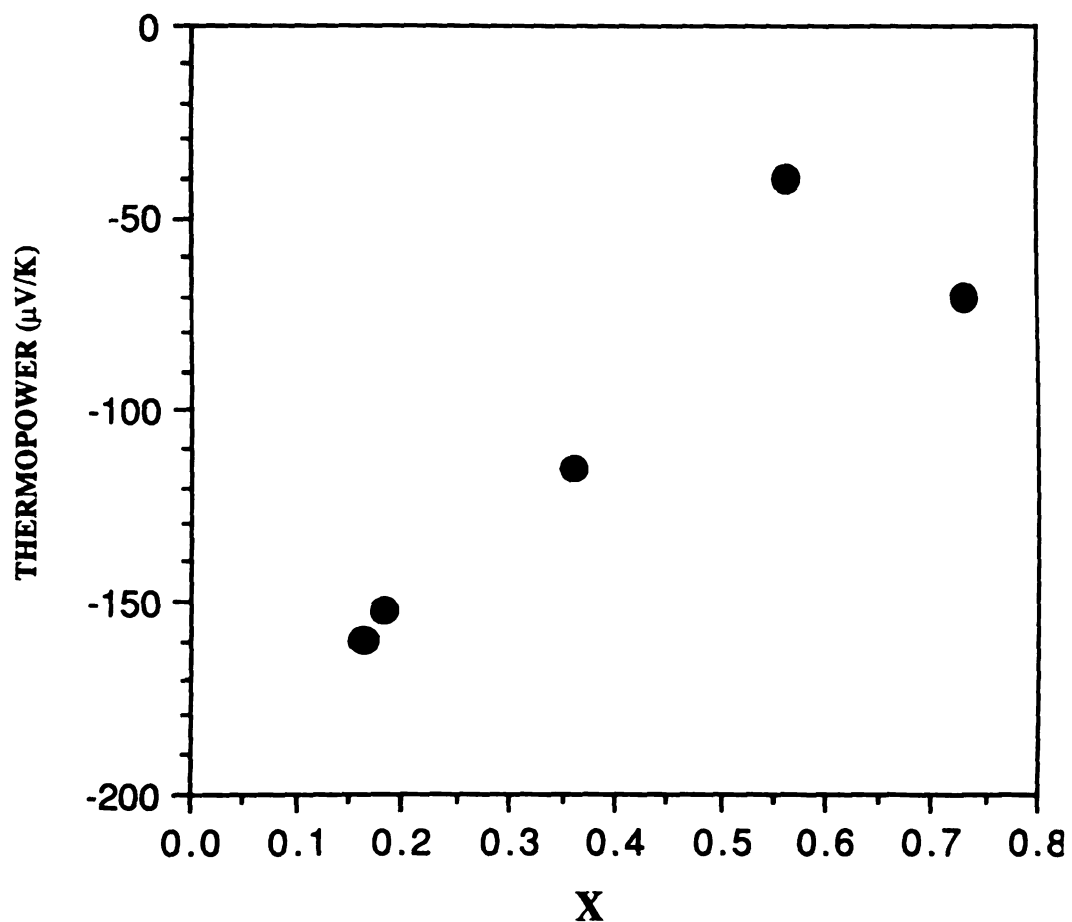
Figure 3.18. Variation of room temperature thermoelectric power as a function of x for $(Ppy)_x V_2 O_5 n H_2 O$ prepared from $CH_3 CN$ solution.
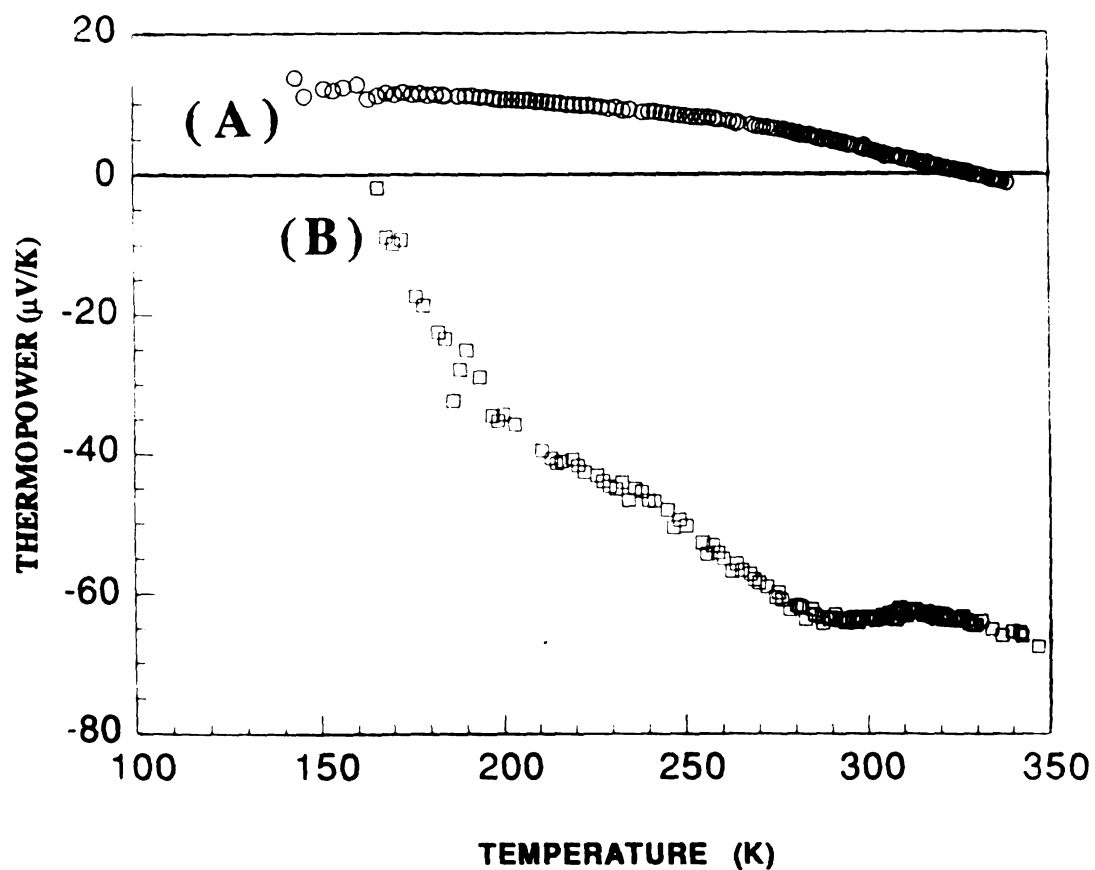
Figure 3.19. Variable temperature thermoelectric power data (pressed pellets) for (A) $(Ppy)_{0.26}V_2O_5nH_2O$ prepared in water (B) $(Ppy)_{0.32}V_2O_5nH_2O$ prepared in acetonitrile.

The TP of $(Ppy)_x V_2O_5 nH_2O$ prepared from aqueous solution show very interesting behavior. The Seebeck coefficients are relatively small compared to those prepared from CH_3CN solution (with similar polymer content) and become less negative as the polymer/V_2O_5 ratio increases as shown in Figure 3.20. At low polymer/V_2O_5 ratio, the Seebeck coefficient is almost temperature independent as seen in reduced V_2O_5. This indicates that for the low x values the reduced V_2O_5 is responsible for the charge transport properties. Near the high x limit, the sample shows a n-type to p-type transition at 175K (see Figure 3.20a). This behavior is not observed in either reduced V_2O_5 or polypyrrole. The p-type conductivity is not possible for V_2O_5 alone while n-type conductivity is not possible for partially oxidized polypyrrole. Furthermore the slope of the TP in the polypyrrole-rich samples is opposite to what is observed in conventional p-doped polymer. Therefore, the charge transport property of this composite is a hybrid of both components. In contrast to the CH_3CN derived samples, the film samples of $(Ppy)_x V_2O_5 nH_2O$ prepared from aqueous solution show small and positive TP in all temperature range (4.2K~300K), consistent with p-type metallic behavior, see Figure 3.19b. The fact that the TP decreases as temperature increases makes it different from polypyrrole, and it is another demonstration that we are looking at hybrid behavior. The charge transport through the polypyrrole is more favorable despite the fact that the polymer content is not high. This implies that the polymer chains may be much longer than those in the samples prepared in CH_3CN. This also consistent with the conductivity data.
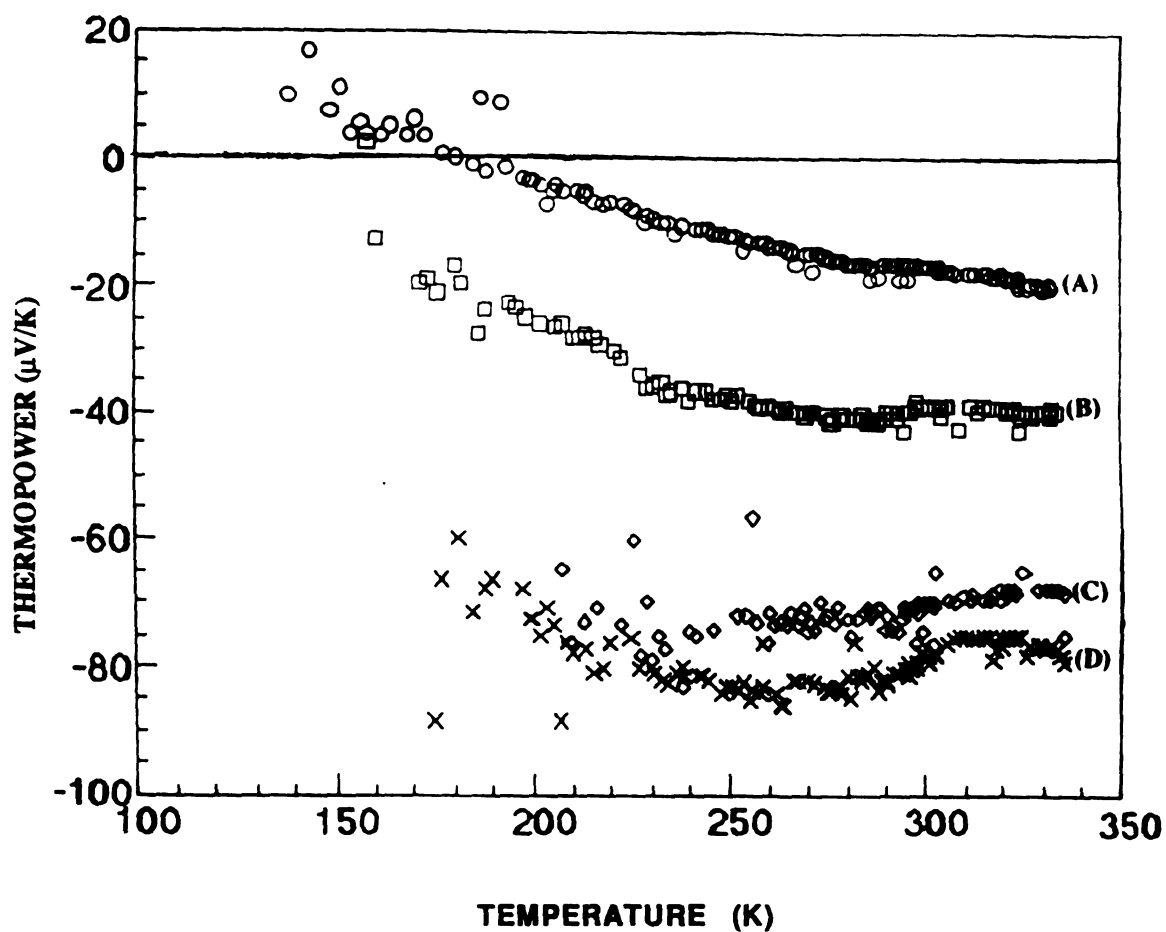
Figure 3.20. Variable temperature thermoelectric power data (pressed pellets) of $(Ppy)_x V_2 O_5 n H_2 O$ prepared in $H_2 O$ solution (A) $(Ppy)_{0.56} V_2 O_5 n H_2 O$ (B) $(Ppy)_{0.42} V_2 O_5 n H_2 O$ (C) $(Ppy)_{0.17} V_2 O_5 n H_2 O$ (D) $(Ppy)_{0.25} V_2 O_5 n H_2 O$.
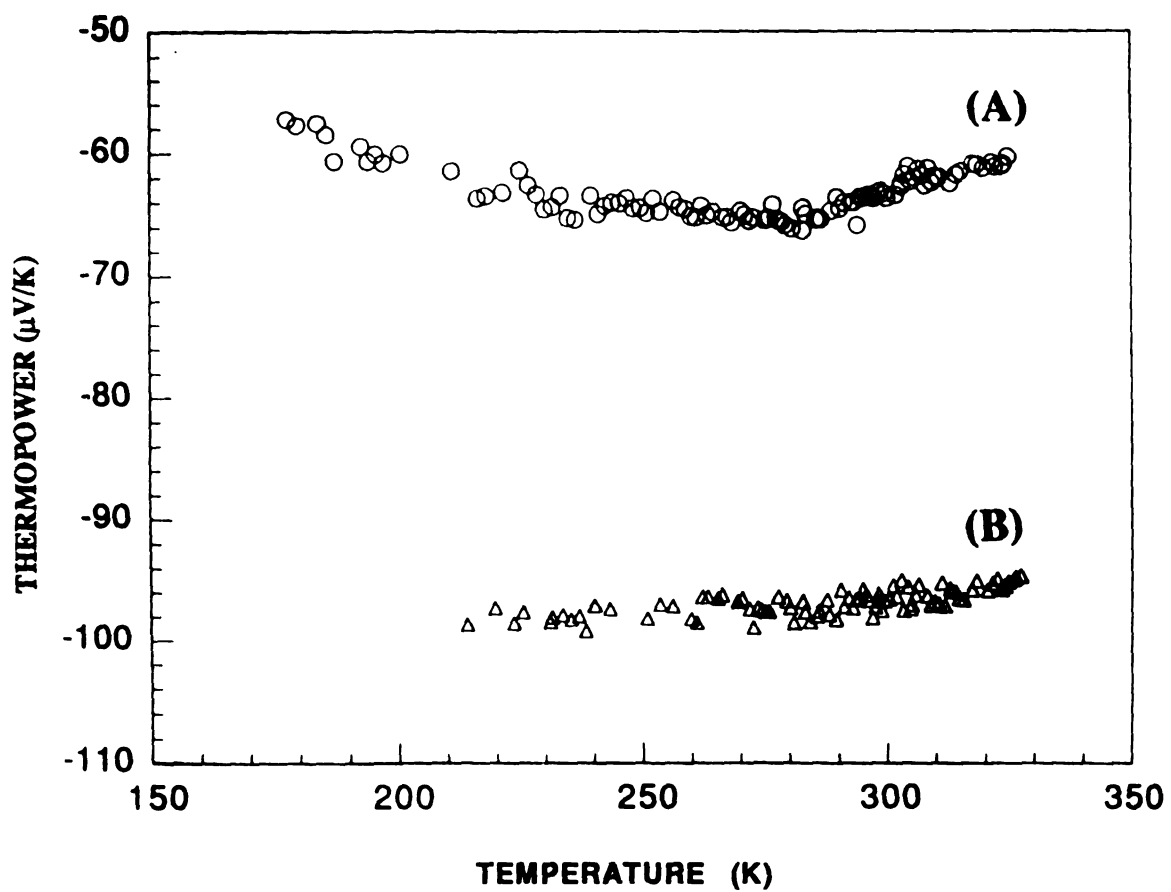
Figure 3.21. Variable temperature thermoelectric power data (pressed pellets) for $(Ppy)_{0.73}V_2O_5 n H_2O$ (A) Fresh prepared (B) Aged.

Not surprising, the TP of aged samples became more negative and almost can not be measured at temperature below 230K due to high contact resistance as shown in Figure 3.21. This is due to reoxidation of the V_2O_5 framework and degradation of the polypyrrole as evidenced by the IR and magnetic data (vide supra).

IV. Conclusions:

The $(Ppy)_x V_2O_5 nH_2O$ composites consist of alternating monolayers of metal oxide and conductive polymer and thus they may be called molecular nanocomposites. The charge transport properties of $(Ppy)_x V_2O_5 nH_2O$ does not depend on polymer/V_2O_5 ratios but rather on the reaction media in which they are prepared. The charge carriers can switch from electrons to holes, and the behavior can be changed from semiconducting to metal-like by varying the reaction conditions. This coupled with the ability to synthesize different polymer/V_2O_5 ratios with variable charge transport properties, suggest possible applications as multi-functional materials and devices that take advantage of both organic and inorganic components. *In-situ* oxidative intercalation/ polymerization reaction may provide a new strategy to synthesize interesting conducting polymer-derived electroactive materials in a relatively controlled way.

LIST OF REFERENCES

LIST OF REFERENCES

1. (a) Kanatzidis, M. G.; Tonge, L. M.; Mark, T. J.; Mercy, H. O.; Kannewurf, C. R. *J. Am. Chem. Soc.* **1987**, 109, 3797-3799. (b) Kanatzidis, M. G.; Mercy, H. O.; MaCarthy, W. J.; Mark, T. J.; Kannewurf, C. R. *Solid State Ionics* **1989**, 32/33, 594-608.

2. (a) Kanatzidis, M. G.; Wu, C.-G.; Marcy, H. O.; Kannewurf, C. R. *J. Am. Chem. Soc.* **1989**, 111, 4139-4141. (b) Kanatzidis, M. G.; Wu, C.-G.; Marcy, H. O.; DeGroot, D. C.; Kannewurf, C. R. *Chem. of Mat.* **1990**, 2, 222-224. (c) Wu, C.-G.; Marcy, H. O.; DeGroot, D. C.; Kannewurf, C. R.; Kanatzidis, M. G. *Mat. Res. Soc. Symp. Proc.* **1990**, 173, 317-322. (d) Wu, C.-G.; Kanatzidis, M. G.; Marcy, H. O.; DeGroot, D. C.; Kannewurf, C. R. NATO Advanced Study Institute *"Low Dimensional Systems and Molecular Devices"* R. M. Metzger Ed. Plenum Press Inc **1991**, 427-433. (e) Wu, C.-G.; Kanatzidis, M. G.; Marcy, H. O.; Kannewurf, C. R.; DeGroot, D. C. *Polym. Mat. Sci. Eng.* **1989**, 61, 969-973.

3. (a) Enzel, P. Bein, T. *J. Phys. Chem.* **1989**, 93, 6270-6272. (b) Bein, T.; Enzel, P. *Synth Met.* **1989**, 29, E163-E168. (c) Enzel, P.; Bein, T. *J. Chem. Soc. Chem. Commun.* **1989**, 1326-1327. (d) Bein, T.; Enzel, P. *Mol. Cryst. Liq. Cryst.* **1990**, 181, 315-324. (e) Bein, T.; Enzel, P.; Benueu, F.; Zuppiroli, L. *Adv. Chem.* **1990**, 226, 433-449.

4. Mehrotra, V.; Giannelis, E. R. *Mat. Res. Soc. Symp. Proc.* **1990**, 171, 39-44.

5. (a) Genies, E. M.; Hany, P.; Santier. C. *J. Appl. Electrochem.* **1988**, 18, 751-756. (b) Nakajima, T.; Kawogoe, T. *Synth. Met.* **1989**, 28, C647-C654. (c) MacDiarmid, A. G.; Mu, S.-L.; Spmasir, N.L.D.; Wu, W. *Mol. Cryst. Liq. Cryst.* **1985**, 121, 187-190. (d) Inganas, O.; Lundstroem, I. *Synth. Met.* **1987**, 21, 13-19. (e) Burroughes J. H.; Jones, C. A.; Friend, R. H. *Nature* **1988**, 335, 137-141. (f)

164

Yoshino, K.; Kaneto, K.; Tekeda, S. *Synth. Met.* **1987**, <u>18</u>, 741-746.

6. (a) Simon, R. A.; Ricco, R. A.; Wrighton, M. S. *J. Am. Chem. Soc.* **1982**, <u>104</u>, 2031-2034. (b) Frank, A. J.; Glenis, S.; Nelson, A. J. *J. Phys. Chem.* **1989**, <u>93</u>, 3815-3825. (c) Horowitz, G.; Tourillon, G.; Garnier, F. *J. Electrochem. Soc.* **1984**, <u>131</u>, 151-156. (d) Frank, A. J.; Honda, K. *J Phys. Chem.* **1982**, <u>86</u>, 1933-1935. (e) Honda, K.; Frank, A. J. *J. Phys. Chem.* **1984**, <u>88</u>, 5577-5582.

7. (a) Kanazawa, K.; Diaz, A. F.; Geiss, R. H.; Gill, W. D.; Kwak, J. F.; Logan, J. A.; Rabolt, J. F.; Street, G. B. *J. Chem. Soc. Chem. Commun.* **1979**, 854-855. (b) Kanazawa, K.; Diaz, A. F.; Gill, W. D.; Grant, P. M.; Street, G. B. *Synth. Met.* **1979/1980**, <u>1</u>, 329-336. (c) Satoh, M.; Kaneto, K.; Yoshino, K. *Synth. Met.* **1986**, <u>14</u>, 289-296.

8. (a) Tourillon, G.; Garnier, F. *J. Electroanal. Chem.* **1983**, <u>149</u>, 101-113. (b) Letheby, H. *J. Chem Soc.* **1962**, <u>15</u>, 161-163. (c) Diaz, A. F.; Logan, J. A. *J. Electroanal. Chem.* **1980**, <u>111</u>, 111-114.

9. (a) Dall'Olio, A.; Dascola, Y.; Varacco, V.; Bocchi, C. R. *C.R Seances, Acad. Sci. Paris Ser. C* **1968**, <u>267</u>, 433-435. (b) Salmon, M.; Kanazawa, K.; Diaz, A. F.; Krounbi, M. *J. Polym. Sci. Polym. Lett.* **1982**, <u>20</u>, 187-193.

10. (a) MacDiarmid, A. G.; Chiang, J. C.; Richter, A. F.; Somasiri, N. L. D.; Epstein, A. J. In *Conducting Polymers* Alcacer, L. Ed. Reidel Dordrecht, Holland, **1987**. (b) MacDiarmid, A. G.; Chiang, J. C.; Halpern, M.; Huang, W. S.; Mu, S. L.; Somasiri, N. L. D.; Wu, W.; Yaniger, S. I. *Mol. Cryst. Liq. Cryst.* **1985**, <u>121</u>, 173-180.

11. (a) Yamamoto, T.; Sanechika, K.; Yamamoto, A. *J. Polym. Sci., Polym. Lett.* **1980**, <u>8</u>, 9-12. (b) Kossmehl, G.; Chatzitheodorou, G. *Mol. Cryst. Liq. Cryst.* **1982**, <u>83</u>, 291-296. (c) Lapkowski, M.; Genies, E. M. *Polimery*, **1989**, <u>34</u>, 45-52. (d) MacDiarmid, A. G.; Asturias, G. E.; Kershner, D. L.; Manohar, S. K.; Ray, A.; Scherr, E.

M.; Sun. Y.; Tang, X.; Epstein, A. J. *Polym. Prepr.* **1989**, 30(1) 147-148.

12. (a) Whittingham, M. S. *Mat. Res. Bull.* **1978**, 13, 775-782. (b) Ruthard, R.; Schollhorn, R.; Weiss, A. *Z. Naturforsch* **1972**, 27, 1275-1276. (c) Ruitz-Hitzky, E.; Casal, B. *J. Chem. Soc. Faraday Trans. 1* **1986**, 82, 1597-1604.

13. (a) Bredas, J. L.; Street, G. B. *Acc. Chem. Res.* **1985**, 18, 309-315. (b) Patil, A. O.; Heeger, A. J.; Wudl, F. *Chem Rev.* **1988**, 88, 183-200.

14. Walker, J. A.; Warren, L. F.; Witucki, E. F. *J. Polym. Sci. Part A: Polym. Chem.* **1988**, 26, 1285-1294.

15. Diaz, A. F.; Hall, B. *IBM J. Res. Dev.* **1983**, 27, 342-347.

16. (a) Lindsey, S. E.; Street, G. B. *Synth. Met.* **1985**, 10, 67-69. (b) Nazzal, A.; Street, G. B. *J. Chem. Soc. Chem. Commun.* **1985**, 375-376.

17. Machida, S.; Miyata, S.; Techagumpuch, A. *Synth. Met.* **1989**, 31 311-318.

18. (a) Street, G. B.; Clarhe, T. C.; Krounbi, M.; Kanazawa, K.; Lee, V.; Pfluger, P.; Scott, J. C.; Weiser, G. *Mol. Cryst. Liq. Cryst.* **1982**, 83, 253-264. (b) Neugebauer, H.; Sariciftci, N. S. *"Low Dimensional Systems and Molecular Electronics"* Ed. R. M. Metzger et al Plenum Press New York **1991**, P401-406.

19. Aldebert, P.; Baffier, N.; Gharbi, N.; Livage, J. *Mat. Res. Bull.* **1981**, 16, 669-676.

20. Genoud, F.; Guglielmi, M. *Phys. Rev. Lett.* **1985**, 55, 118-121.

21. *"Non-Stoichiometric Compounds, Tungsten Bronzes, Vanadium Bronzes and Related Compounds"* Bevan, D. J.; Hagemuller, P. Eds. Pergamon Press Oxford **1973**.

22. Babonneau, P. F.; Barboux, P.; Josien, F. A.; Livage, J. *J. de Chim. Phys.* **1985**, 82, 761-766.

23. Maddison, D. S.; Roberts, R. B.; Unsworth, J. *Synth. Met.* **1989**, 33, 281-287.

24. Kanatzidis, M. G. et al work in progress.

CHAPTER 4

SYNTHESIS AND CHARACTERIZATION OF CONDUCTING POLYTHIOPHENE/V_2O_5 BRONZE ~ *In-situ* INTERCALATION OF POLYTHIOPHENE IN V_2O_5 XEROGEL

ABSTRACT

Polythiophene (Pth) can be easily intercalated in V_2O_5 xerogel by reacting 2,2'-bithiophene with V_2O_5 in acetonitrile. The resulting products, $(Pth)_xV_2O_5nH_2O$, have interlayer spacing of 14.7Å. The polymer formed inside the layers can be extracted by digesting away the V_2O_5 framework with the assistance of chelating agent, catechol. The EPR spectra of $(Pth)_xV_2O_5nH_2O$ show a broad signal ($\Delta H_{pp}=155$ gauss) centered at $g=1.9623$. The typical sharp radical-based peak of polythiophene was not observed due to the spin-spin interaction between polythiophene and V_2O_5 host. Variable temperature magnetic susceptibility revealed Curie paramagnetism mixed with temperature independent paramagnetism. The conductivity of $(Pth)_xV_2O_5nH_2O$ increased continuously with increasing x at the same time the thermopower also changed. The Seebeck coefficient, S, of high x value samples reveals p-type metal-like behavior. Samples with low x show a relative large S and negative suggesting n-type semiconductor behavior. Upon aging, the magnetic moment of $(Pth)_xV_2O_5nH_2O$ decreased and the room temperature electrical conductivity slightly decreased compared to the fresh sample. The thermoelectric power of the aged sample with high polymer content still remain small and positive, but decreases as temperature increases which is different from all the fresh samples.

I. Introduction:

The redox intercalation of conducting polymers into various layered hosts is the subject of intense investigation in our laboratory. The resulting compounds can be viewed as polymer bronzes by analogy to the alkali metal [1] or molecular [2] bronzes. It has been mentioned that in molecular scale organic/inorganic composites, the interaction between the two components can give a new set of properties which is not possible from either component separately [3]. Therefore, by inserting polymers in structurally restricted and electrically active hosts, two goals may be achieved: preparing oriented polymers and synthesizing new interesting polymer/ inorganic conducting molecular composites.

Polythiophene, (Pth) is one of the prototype conducting polymers with excellent environmental stability and good electroactivity [4]. It can be prepared by either electrochemical or chemical polymerization of thiophene or 2,2'-bithiophene respectively. Neutral polythiophene is a red-colored semiconductor with band gap (E_g) of 2.2 eV [5]. Upon doping, the electrical conductivity of the polymer film can be increased over 10 orders of magnitude, to the metallic state [6]. The color of the doped material is black. This semiconductor to metal transition is also accompanied by important modifications of mass [7], volume [8] and chain geometry [9]. The conductivity of polythiophene is not determined only by the chain length, but the abundance of long conjugated segment is required [10]. In other words, the extension of the monomer ring planarity (without ring opening) will affect the

conductivity [11]. It has been known that electrochemically polymerized polythiophene contains some impurities and structural defects [12], such as cross-links and C-C coupling through the β-positions of the thiophene ring. However, a highly regular polymer backbone can be obtained by varying the nature of dopants [13] during polymerization. A good synthetic strategy to prepare well oriented polythiophene is by *in-situ* oxidative polymerization/ intercalation of polythiophene in layered hosts. Here the host also acts as oxidant as well as dopant.

II. Experimental Section:

Reagents: NaOH, HCl, NH$_4$OH(aq), NaVO$_3$, FeCl$_3$, DMSO, NMF, catechol, thiophene and 2,2'-bithiophene were purchased from commercial sources and used without further purification. CH$_3$CN was dried under CaH$_2$ and distilled in air prior to use.

Physicochemical Methods.
See chapter 2.

Preparation of V$_2$O$_5$nH$_2$O Xerogel.
See page 56.

Preparation of (Pth)$_{0.87}$V$_2$O$_5$0.54H$_2$O Film.

0.4 g (1.9 mmol) film of V$_2$O$_5$ xerogel was added to 30 ml of 0.04 M acetonitrile solution of 2,2'-bithiophene. The mixture was

refluxed for 12 hours. The black film was isolated by filtration, washed with acetone and dried in vacuum. Elemental analysis: Calcd for $(C_4H_2S)_{0.87}V_2O_50.54H_2O$: C, 15.87%; H, 1.07%; S, 10.58%; V, 38.77%. found: C, 14.98%; H, 1.25%; S, 8.12%; V, 36.48%. Water content was obtained from thermal gravimetric analysis under oxygen flow. The interlayer spacing calculated from X-ray diffraction is equal to 14.70Å.

Preparation of $(Pth)_{0.16}V_2O_50.58H_2O$ Film.

0.1 g (0.60 mmol) of 2,2'-bithiophene was dissolved in 20 ml CH_3CN. To the solution, added 2 drops of H_2O followed by 0.4 g (1.9 mmol) of film of V_2O_5 xerogel. The mixture stood at room temperature without disturbing for 24 hours. The black film was isolated by filtration, washed with acetone and dried in vacuum. Elemental analysis: Calcd for $(C_4H_2S)_{0.16}V_2O_50.58H_2O$: C, 3.74%; H, 0.72%; S, 2.49%; V, 49.62%. Found: C, 3.41%; H, 1.72%; S, 3.04%; V, 44.53%. The water content was obtained from thermal gravimetric analysis under oxygen flow. The interlayer spacing determined from X-ray diffraction is equal to 14.50Å.

Preparation of $(Pth)_{0.72}V_2O_51.10H_2O$ Powder.

To a 0.62 g (3.73 mmol) 2,2'-bithiophene solution in 30 ml acetonitrile was added 1.0 g (4.74 mmol) of V_2O_5 xerogel (fine powder). The mixture was stirred at room temperature for 20 hours. The resulting black powder was isolated by filtration, washed with

acetone and dried in vacuum. Anal. Calcd. for $(C_4H_2S)_{0.72}V_2O_51.1H_2O$: C, 7.47%; H, 1.26%; S, 4.98%; V, 44.09%. Found: C, 13.80%; H, 0.82%; S, 7.31%; V, 40.61%. Changing the 2,2'-bithiophene/V_2O_5 ratio, the x value of $(Pth)_xV_2O_5nH_2O$ can be varied from 0.30 to 0.72.

Synthesis of Bulk Polythiophene.

In an inert atmosphere glove box, 3.0 g (18.50 mmol) of $FeCl_3$ was dissolved in 50 ml acetonitrile. To this was added 1.25 g (7.53 mmol) 2,2'-bithiophene and the mixture was stirred at room temperature for 4 hours. The black precipitate was isolated by filtration, washed with acetone, dried in vacuum and characterized by Infrared spectroscopy [14].

Extracting Polythiophene from $(Pth)_{0.45}V_2O_50.93H_2O$ in Acidic solution.

0.15 g (0.63 mmol) of $(Pth)_{0.45}V_2O_5nH_2O$ with 0.50 g (4.5 mmol) catechol was stirred in 100 ml 1M HCl(aq) for 40 hours or in 2 weight % NaOH(aq) for 15 hours. The black residue was isolated by filtration, washed with acetone, dried under vacuum and identified by FTIR spectroscopy.

III. Results and Discussion:

A. Preparation and Characterization.

In our initial attempts for intercalation of polythiophene in V_2O_5 xerogel, we used thiophene as monomer. However, thiophene cannot be oxidatively polymerized by V_2O_5 xerogel due to its high oxidation potential. Although upon contact of V_2O_5 xerogel with thiophene acetonitrile solution, a color change to green is observed FTIR spectroscopy revealed that no organic product was intercalated. Therefore, we used 2,2'-bithiophene which has lower oxidation potential.

The intercalation of polythiophene into V_2O_5 xerogel was achieved by refluxing 2,2'-bithiophene with V_2O_5 xerogel in acetonitrile. 2,2'-bithiophene was oxidatively polymerized and V_2O_5 is reduced as showed in equation 4.1 and 4.2. The total reaction is listed in equation 4.3.

$$xC_8H_6S_2 \longrightarrow (C_8H_4S_2)_x^{+d} + 2xe^- + \delta e^- + 2xH^+ \cdots\cdots\cdots eq(4.1)$$

$$V_2O_5nH_2O + 2xe^- + de^- \longrightarrow V_2O_5^{-(2x+d)}nH_2O \cdots\cdots\cdots eq(4.2)$$

$$xC_8H_6S_2 + V_2O_5nH_2O \longrightarrow (C_8H_4S_2)_xV_2O_5nH_2O \cdots\cdots eq(4.3)$$
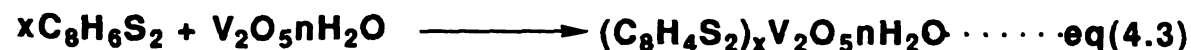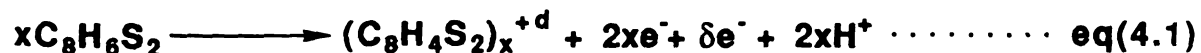
This reaction is relatively slow compared to that of aniline and pyrrole with V_2O_5. Higher oxidation potential and higher molecular weight of 2,2'-bithiophene could be the reasons. The solvent used with 2,2'-bithiophene was acetonitrile. Unlike water, acetonitrile cannot swell V_2O_5 xerogel at room temperature. Even though the red color of V_2O_5 turns black immediately upon contacting 2,2'-bithiophene solution, complete intercalation requires more than 4 hours depending on the reagent ratios. When mixed CH_3CN/H_2O was used as a solvent, the reaction rate increased but often the products were not homogeneous and exhibited amorphous character. The reaction principles of intercalating polythiophene in V_2O_5 xerogel are similar to that of polyaniline and polypyrrole analog. Use of other solvents, such as DMF and DMSO yielded products in which solvent molecules were inserted with very little polymer inside. Primary alcohols seem unsuitable as solvents because they are oxidized gradually by V_2O_5.

The polythiophene formed between the slabs of V_2O_5 xerogel can be detected easily from FTIR spectra as shown in Figure 4.1a. The three strong peaks at frequencies below 1000 cm^{-1} belong to V_2O_5 framework which does not change after intercalation. The IR spectra of polythiophene in V_2O_5 interlamellar space show slightly different frequencies compared to that of bulk polythiophene (see Table 4.1). The vibration energies are shifted to higher frequency and the relative intensities are altered. This may be due to a different degree of polymerization and oxidation or the effect of the counter anion (in this case $([V_2O_5nH_2O]^{x-})$. However, the polythiophene inside the V_2O_5 layers can be extracted by digesting
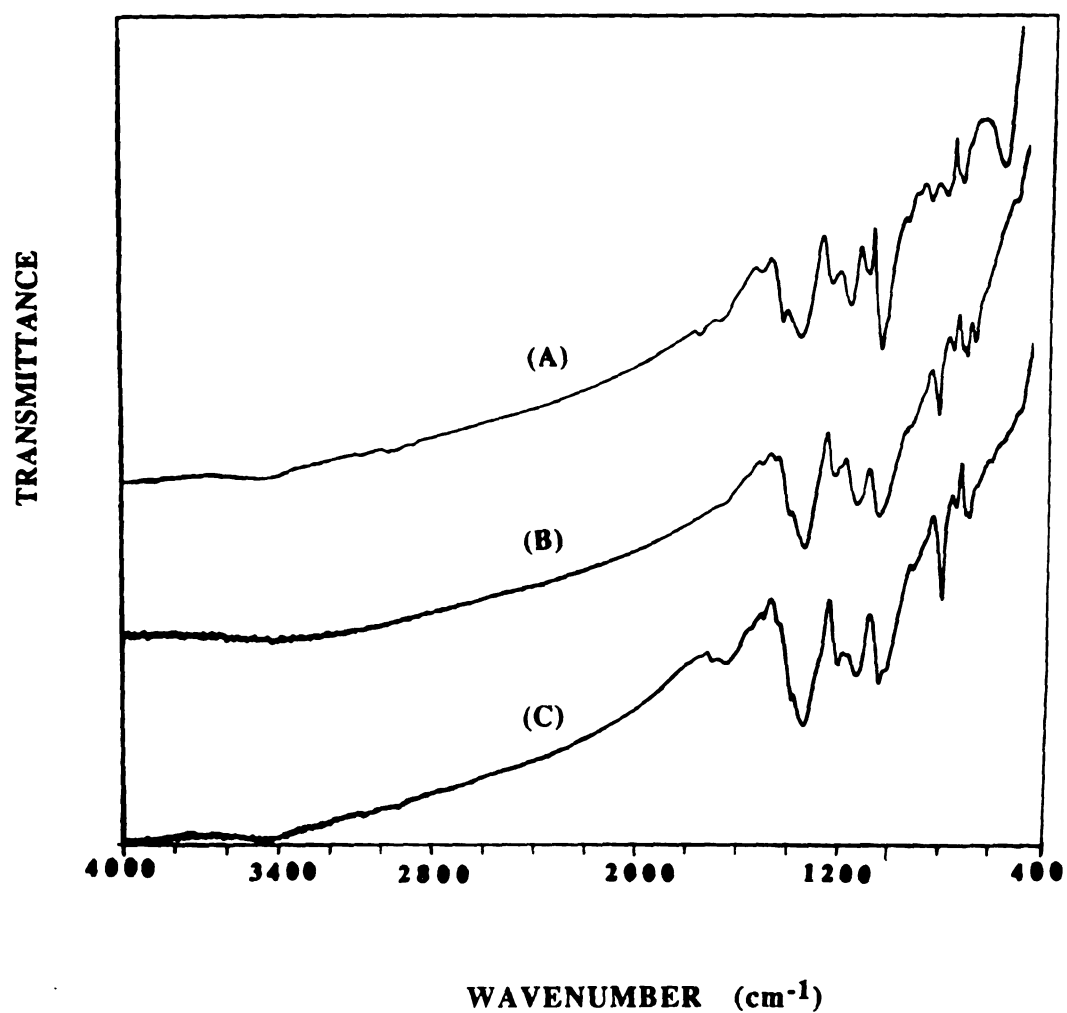
Figure 4.1. FT-IR spectra (KBr pellets) of (A) $(Pth)_{0.45}V_2O_5 0.93H_2O$ (B) Extracted polythiophene (C) Bulk polythiophene.

176

Table 4.1. Infrared Vibration Modes of Bulk Polythiophene, $(Pth)_{0.16}V_2O_5 0.58H_2O$ and Extracted Polythiophene

Modes[14]	C=C antisymmetric stretching	C=C symmetric stretchings	C-H in plane vibrations	C-H out of plane vibrations	V_2O_5 framework
Bulk polythiophene	$1478cm^{-1}$(vW)	$1323cm^{-1}$(vS) $1196cm^{-1}$(M)	$1105cm^{-1}$(S) $1025cm^{-1}$(S)	$790cm^{-1}$(M)* $717cm^{-1}$(W) $668cm^{-1}$(W)	
$(Pth)_{0.16}V_2O_5nH_2O$	$1485cm^{-1}$(W)	$1394cm^{-1}$(M) $1344cm^{-1}$(S) $1196cm^{-1}$(M)	$1126cm^{-1}$(M) $1048cm^{-1}$(W)	$725cm^{-1}$(S) $668cm^{-1}$(M)	$999cm^{-1}$(vS) $752cm^{-1}$(S) $503cm^{-1}$(vS)
Extracted polythiophene	$1488cm^{-1}$(vW)	$1324cm^{-1}$(vS) $1191cm^{-1}$(M)	$1105cm^{-1}$(S) $1020cm^{-1}$(S)	$779cm^{-1}$(S)* $715cm^{-1}$(W) $668cm^{-1}$(W)	

* C-H out of plane vibration of 2, 5 disubstituted thiophene

vW: very weak; W: weak; M: medium; S: strong; vS: very strong.

away the V_2O_5 framework with dilute acid or base (with the assistance of catechol). Polythiophene is damaged slowly both in concentrated basic solution and also in acidic solution during isolation, where the strong oxidizing power of V^{5+} species, which are released in solution, react with it. Intact polythiophene was successfully extracted from $(Pth)_xV_2O_5nH_2O$ from an acidic solution in which catechol was added. The catechol acts as a chelating ligand to arrest the aquated V^{5+} ions and reduce their oxidation potential, thus rendering them unreactive towards polythiophene. The IR pattern of extracted intact polythiophene is virtually the same as that of bulk polythiophene (see Figure 4.1). It has been proposed that the vibration bands of polythiophene are independent of the doping species [15]. The difference in IR pattern of bulk polythiophene and polythiophene inside the V_2O_5 host is because of the latter was probably bound, at least electrostatically, to a structurally restricting framework.

The XRD pattern of $(Pth)_xV_2O_5nH_2O$ prepared from 2,2'-bithiophene with V_2O_5 in refluxing acetonitrile is shown in Figure 4.2. Only several 00l reflections are observed consistent with the turbostratic nature of the product. Upon intercalation, the 00l peaks shift to lower Bragg angles. The interlayer spacing calculated from the average of several 00l reflections are equal to $14.70(\pm 20)$Å which corresponds to an interlayer expansion of 5.95Å. This interlayer expansion was smaller (by 0.3Å) in the low polymer content samples (interlayer spacing of $(Pth)_{0.45}V_2O_50.93H_2O$ is 14.50Å compared to 14.80Å for $(Pth)_{0.87}V_2O_50.54H_2O$). When the reactions were carried out at room temperature using fine powder of V_2O_5 xerogel, the
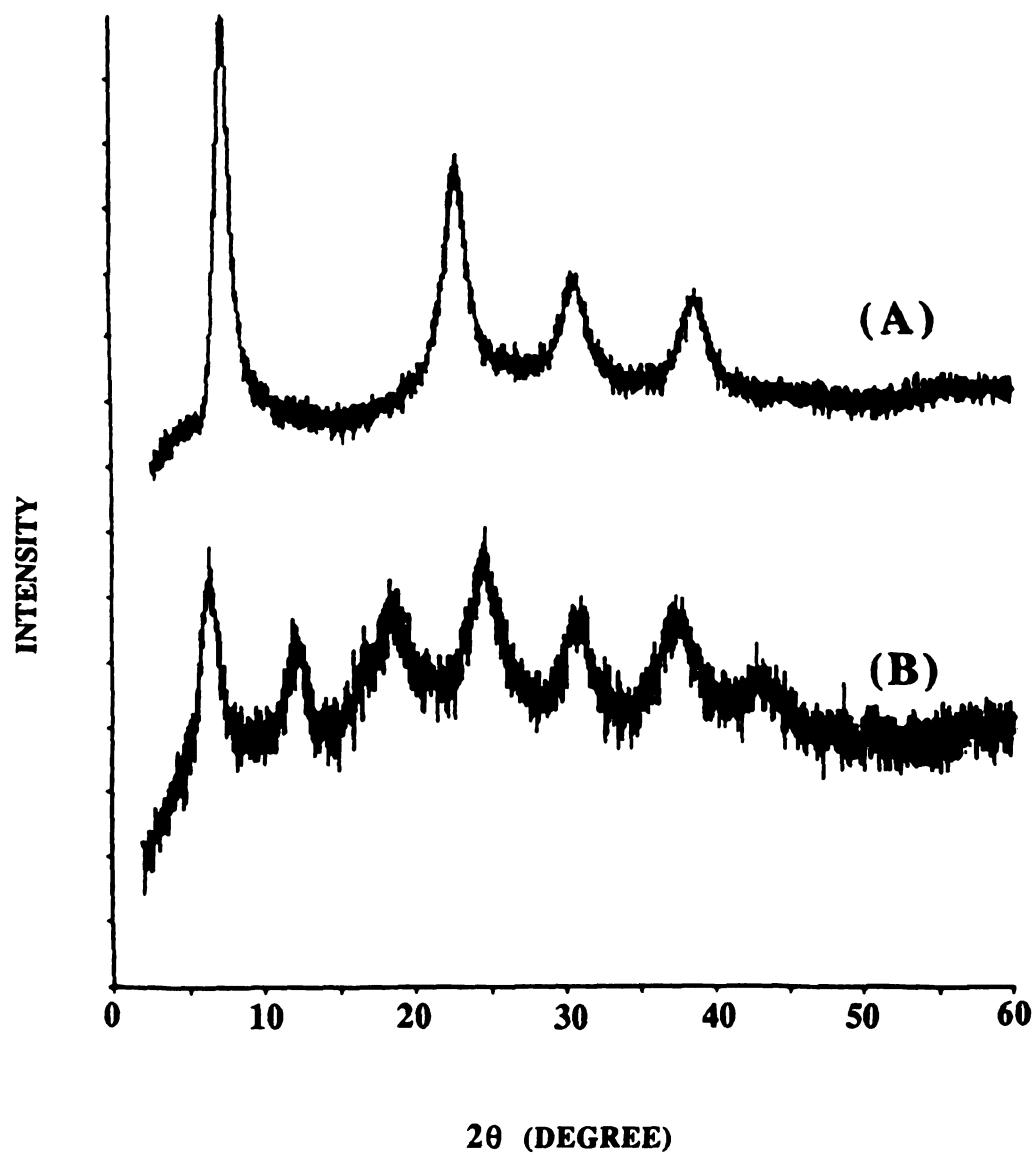
Figure 4.2. Reflection-mode X-ray diffraction patterns of (A) V_2O_5 xerogel (film) (B) $(Pth)_{0.87}V_2O_5 0.54H_2O$ (pressed pellet).

resulting black powder had similar interlayer spacing although the diffraction peaks are relatively broad and weak. We found that $(Pth)_xV_2O_5nH_2O$ is a relatively porous materials, which upon sitting in air absorb moisture and increase their interlayer spacing as evidenced by corresponding changes in the XRD pattern.

It will be interesting to know the arrangement of polythiophene in V_2O_5 layers. There are two most common proposed structures of polythiophene, linear chain [12,16] and coil [17] arrangements. The dimension of coil arrangement is larger than 10Å. Therefore, the 5.95Å interlayer expansion due to the intercalation of polymer can be regarded as insertion of a monolayer of linear polythiophene chain with the five member rings perpendicular to the V_2O_5 slabs as shown in Scheme 4.1.
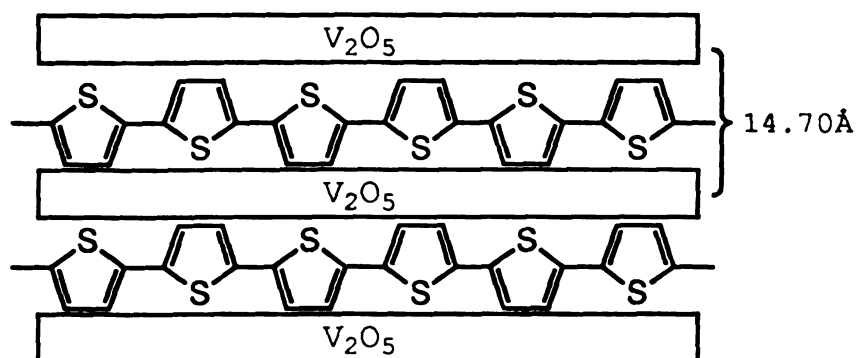
Scheme 4.1. Proposed arrangement of polythiophene chain in V_2O_5 layers.

The same arrangement has also been proposed in $(Pth)_xFeOCl$ [18], $(PANI)_xV_2O_5nH_2O$ and $(PANI)_xFeOCl$, see chapter 2&5. The slightly different interlayer spacing for each sample may be due to the

imperfect arrangement of polythiophene chains in $(Pth)_x V_2O_5 nH_2O$ layers. To study the alteration of V_2O_5 layers after intercalation, x-ray diffraction with the X-ray beam perpendicular to the $(Pth)_x V_2O_5 nH_2O$ film was performed. The XRD pattern of $(Pth)_x V_2O_5 nH_2O$ is identical to that of pristine V_2O_5 as shown in Figure 4.3. This implies that there is a topotactic intercalation in which the host framework is preserved after the reaction.

During *in-situ* insertion/ polymerization of aniline and pyrrole in V_2O_5, we found that ambient oxygen was intimately involved in the reaction. In the PANI/V_2O_5 system it even continues to oxidatively polymerize aniline oligomers to longer chain of polymer long after $(PANI)_x V_2O_5 nH_2O$ is isolated. The oxygen effects on $(Pth)_x V_2O_5 nH_2O$ are not as obvious as seen in $(PANI)_x V_2O_5 nH_2O$ and there is no direct evidence showing that significant quantity of oxygen is consumed during the reaction. It is difficult to document the role of oxygen because the intercalation is relatively slow compared to polyaniline and polypyrrole systems. However, if we look at equation 4.3 carefully, when the polymer/V_2O_5 ratio is equal to 0.5, then more than 50% of V^{5+} were reduced to V^{4+}. In this case, the V_2O_5 framework will change as observed by Livage and coworkers [19]. However, in $(Pth)_x V_2O_5 nH_2O$ the IR and XRD data showed the structural preservation of V_2O_5 layers implying that some oxygen must be involved. The more accurate reaction is written as equation 4.4.

$$xC_8H_6S_2 + V_2O_5 + (x-y/2)O_2 \longrightarrow (C_8H_4S_2)_x H_y V_2O_5$$
$$+ (x-y/2)H_2O_2 \cdots\cdots eq(4.4)$$
$$(or\ H_2O)$$
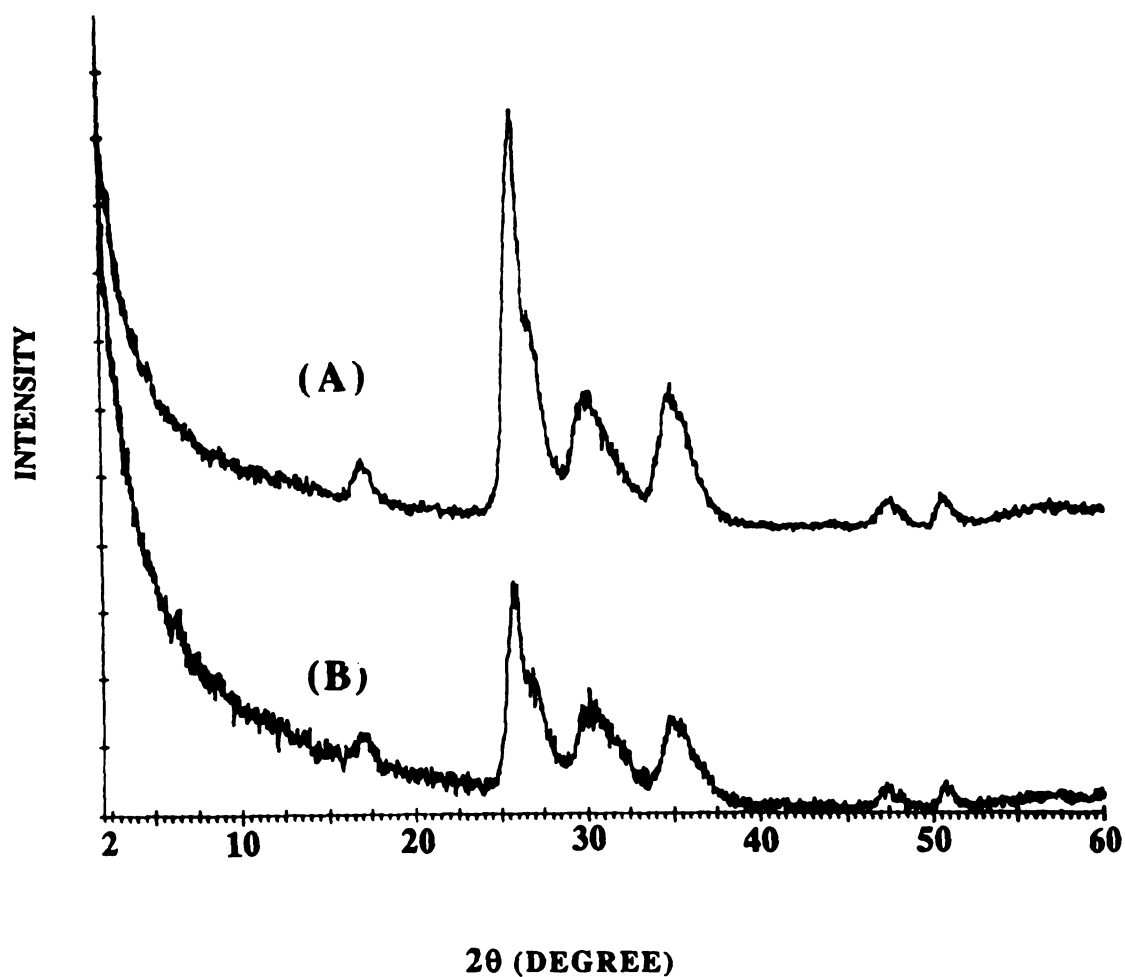
Figure 4.3. Transmission-mode X-ray diffraction patterns of (A) $(Pth)_{0.87}V_2O_5 0.54H_2O$ (B) V_2O_5 xerogel. (In this experiment, the incident X-ray beam was perpendicular to the film. The detector is moving along the 2θ angle while the sample remains stationary)

There is also no firm evidence showing that the polythiophene continues to couple upon sitting in air (aging). The pyrolysis mass of both fresh and aged samples did not show any volatile species up to 350°C under vacuum. The IR and XRD spectra did not change upon aging although the conductivity slightly decreased (vide infra).

B. Thermogravimetric Analysis (TGA) and Differential Scanning Calorimetry (DSC) Studies.

Polythiophene is stable up to 350°C in air and 950°C under inert atmosphere [13b,4b]. However, the thermal stability of $(Pth)_x V_2 O_5 n H_2 O$ is similar to that of $(PANI)_x V_2 O_5 n H_2 O$. Typical TGA diagrams of fresh and aged $(Pth)_x V_2 O_5 n H_2 O$ under oxygen flow are shown in Figure 4.4. A small amount of weight-loss (1~2%) is observed below 100°C (belong to the absorbed moisture), followed by a continuous weight loss up to 500°C. A slight weight-increase between 500°C and 700°C is observed and stabilized after 700°C. The weight loss between 100°C and 500°C is primarily due to the decomposition of polythiophene chains. The slight weight gain is because during the decomposition of polymer, some oxygen of $V_2 O_5$ is lost to form $V_2 O_{5-x}$. Oxygen is regained when the residue is heated at high temperature under oxygen atmosphere.

The molecular weight of polythiophene inside the $V_2 O_5$ interlamellar space is currently not known. The lower thermal stability of $(Pth)_x V_2 O_5 n H_2 O$ compared to bulk polythiophene does not imply that the polymer in $(Pth)_x V_2 O_5 n H_2 O$ has lower molecular weight. Since the polymer is in intimate contact with a strong
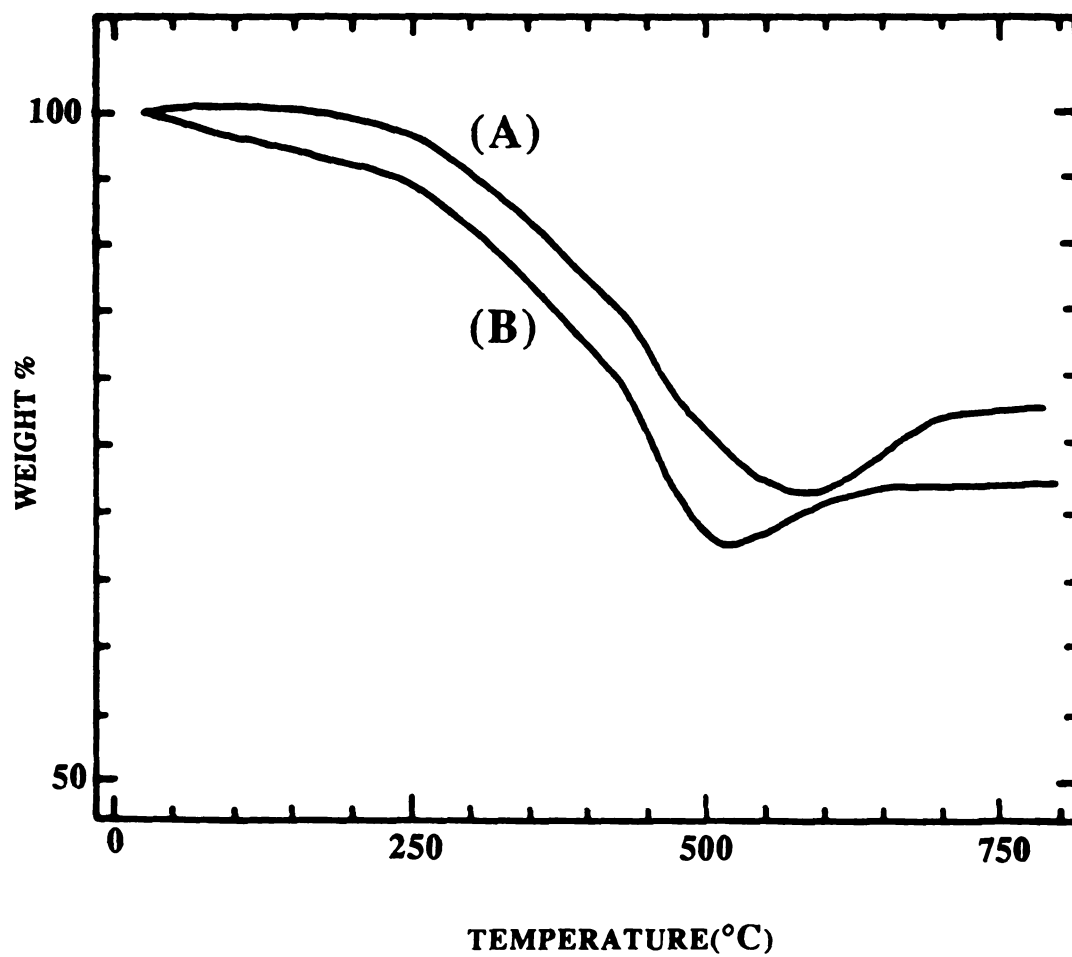
Figure 4.4. TGA curves (under oxygen flow) of $(Pth)_{0.72}V_2O_5 0.52H_2O$. (A) Fresh prepared (B) Aged

oxidant V_2O_5, the thermal stability of polythiophene will be affected by V_2O_5 even under nitrogen atmosphere. This argument can be further supported by the fact the thermal stability of fresh sample is higher than that of the aged sample (see Figure 4.4). In aged samples, the V^{5+}/V^{4+} ratio is increased due to the reoxidation of V^{4+} centers by oxygen (vide infra). This increases the oxidizing power of V_2O_5 framework which in turn degrades faster the polythiophene chains.

The DSC diagram of $(Pth)_xV_2O_5nH_2O$ is almost featureless. A very broad exothermal peak start at room temperature all the way to 200°C is due to the decomposition of polymer.

C. Scanning Electron Microscopy (SEM) and Selected Area Electron Diffraction (SAED).

The SEM micrographs of $(Pth)_xV_2O_5nH_2O$ films are similar to that of $(PANI)_xV_2O_5nH_2O$ and $(Ppy)_xV_2O_5nH_2O$ as shown in Figure 4.5. They reveal the layered nature of the materials and do not show obvious separate phases. The electron diffraction patterns of $(Pth)_xV_2O_5nH_2O$ showed only Bragg rings with weak intensities. Although the pattern of $(Pth)_xV_2O_5nH_2O$ is not as sharp as $(PANI)_xV_2O_5nH_2O$, the corresponding d-spacings of the Bragg rings are similar to that of the V_2O_5 xerogel. This further proves that this is a topotactic intercalation reaction. The relatively weak diffraction may be due to the more random orientation of the polymer inside the layers and more disordering in the V_2O_5 framework. This disordered structure was also observed in XRD data which also
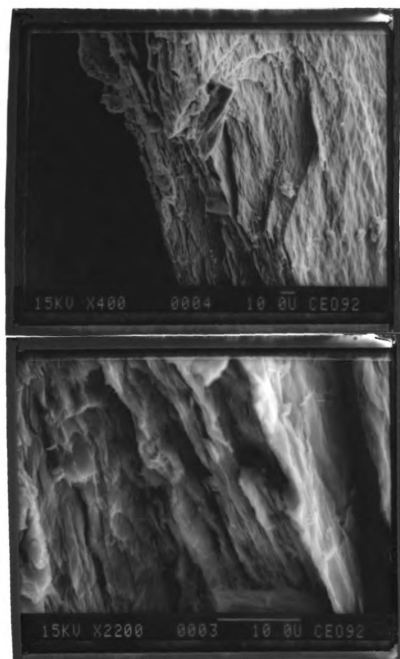
Figure 4.5. SEM micrographs of $(Pth)_{0.72}V_2O_5 n H_2O$.

showed rather broad peaks and slight variation in the interlayer spacing for different samples.

D. Electron Paramagnetic Resonance (EPR) Spectroscopy.

In order to understand the spin-spin interactions between polythiophene and V_2O_5 host, EPR studies were carried out at room temperature and liquid nitrogen temperature. Typical EPR spectra of $(Pth)_xV_2O_5nH_2O$ show a broad peak centered at g value equal to 1.9632 with ΔH_{pp} = 125~155 gauss as shown in Figure 4.6a. This signal comes from the reduced V_2O_5 layers as observed in $Na_xV_2O_5$ (Figure 4.6b). The sharp peaks which belongs to the resonant spins which are carried by delocalized charge in partially oxidized polythiophene did not show up. This is probably due to the exchange broadening by the strong magnetic interaction between polythiophene and V_2O_5. The same phenomenon is also observed in $(PANI)_xV_2O_5nH_2O$ and $(Ppy)_xV_2O_5nH_2O$. This confirmed the intimate contact between polythiophene and reduced V_2O_5 as expected for intercalated polymer. However, the sharp polythiophene signal can be recovered when the V_2O_5 framework was digested away by acid or base solution (see Figure 4.6c). At lower temperature, the EPR signal of $(Pth)_xV_2O_5nH_2O$ was more intense but the peak shape and width does not change.
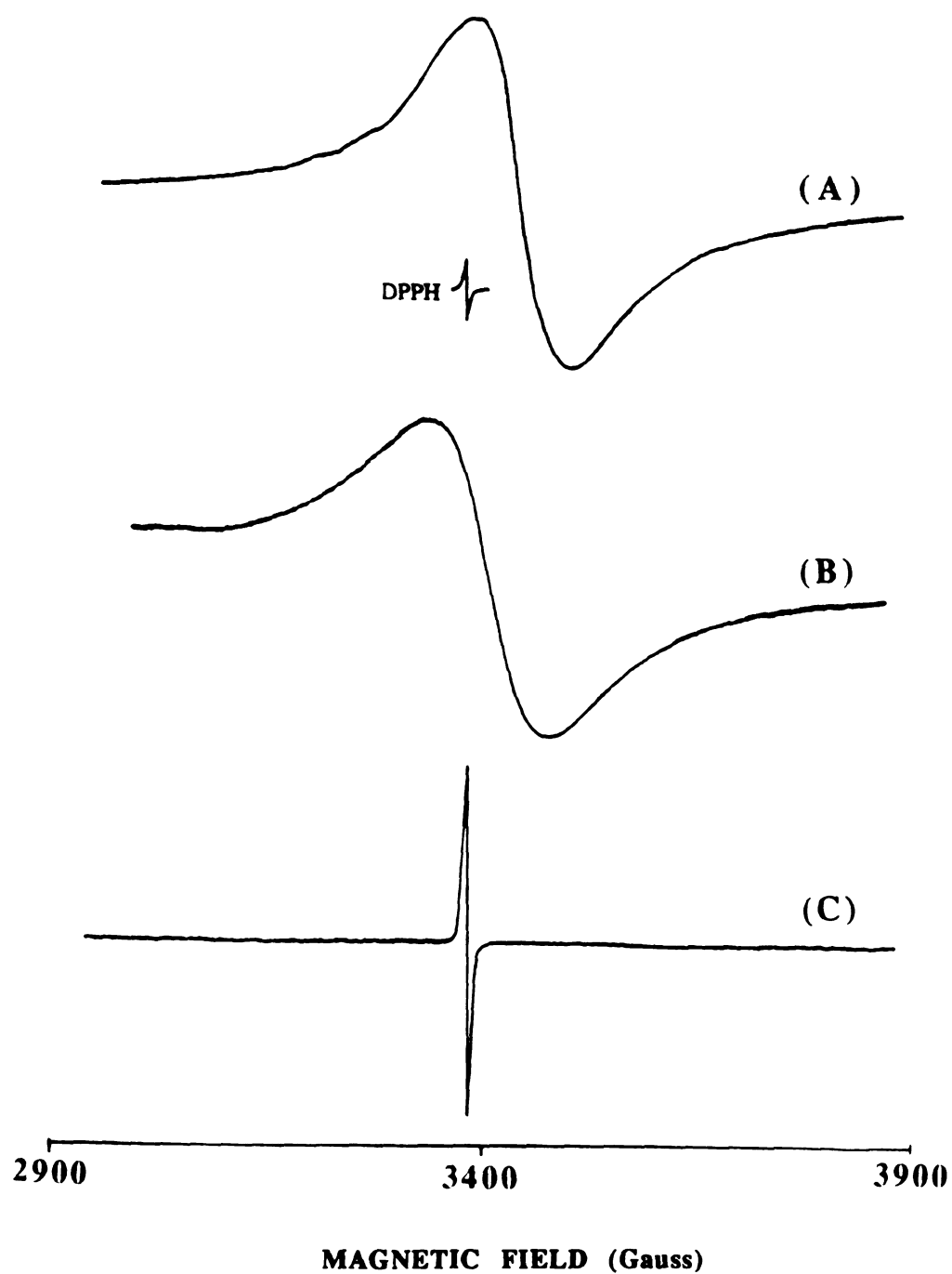
Figure 4.6. **Room temperature EPR spectra of (A)** $(Pth)_x V_2 O_5 n H_2 O$ **(B)** $Na_{0.40} V_2 O_5 n H_2 O$ **(C) Extracted polythiophene.**

E. Magnetic Susceptibility studies.

The magnetic behavior of $(Pth)_x V_2O_5nH_2O$ is similar to those of $(PANI)_x V_2O_5nH_2O$ and $(Ppy)_x V_2O_5nH_2O$. The magnetic moment in $(Pth)_x V_2O_5nH_2O$ mostly is due to the reduced V_2O_5 layers. The susceptibility (χ) decreases as the temperature increases, indicates a paramagnetic behavior as shown in Figure 4.7. The susceptibility is a summary of two individual components: Curie susceptibility and temperature independent paramagnetism (TIP) as represented in equation 4.5.

$$\chi_m = \chi_{Curie} + \chi_{TIP} \quad\text{............eq (4.5)}$$

Variation of susceptibility as a function of temperature of each component is shown in Figure 4.8. The effective spin-only magnetic moment, μ_{eff}, is constant from 5K to 300K as shown in Figure 4.9. This is consistent with Curie paramagnetic behavior. Table 4.2 lists the room temperature magnetic moment versus x of several $(Pth)_x V_2O_5nH_2O$. There was no linear relationship between the magnetic moment and polymer content. The magnetic moment is always smaller than theoretical value which assumed that all electrons released from oxidative polymerization of monomers are transferred to V_2O_5 framework. These may be due to a couple of reasons: first, oxygen may also be involved in this reaction as observed in $(PANI)_x V_2O_5nH_2O$ and $(Ppy)_x V_2O_5nH_2O$, see page 69, 135. Second, the molecular weight of polythiophene in different
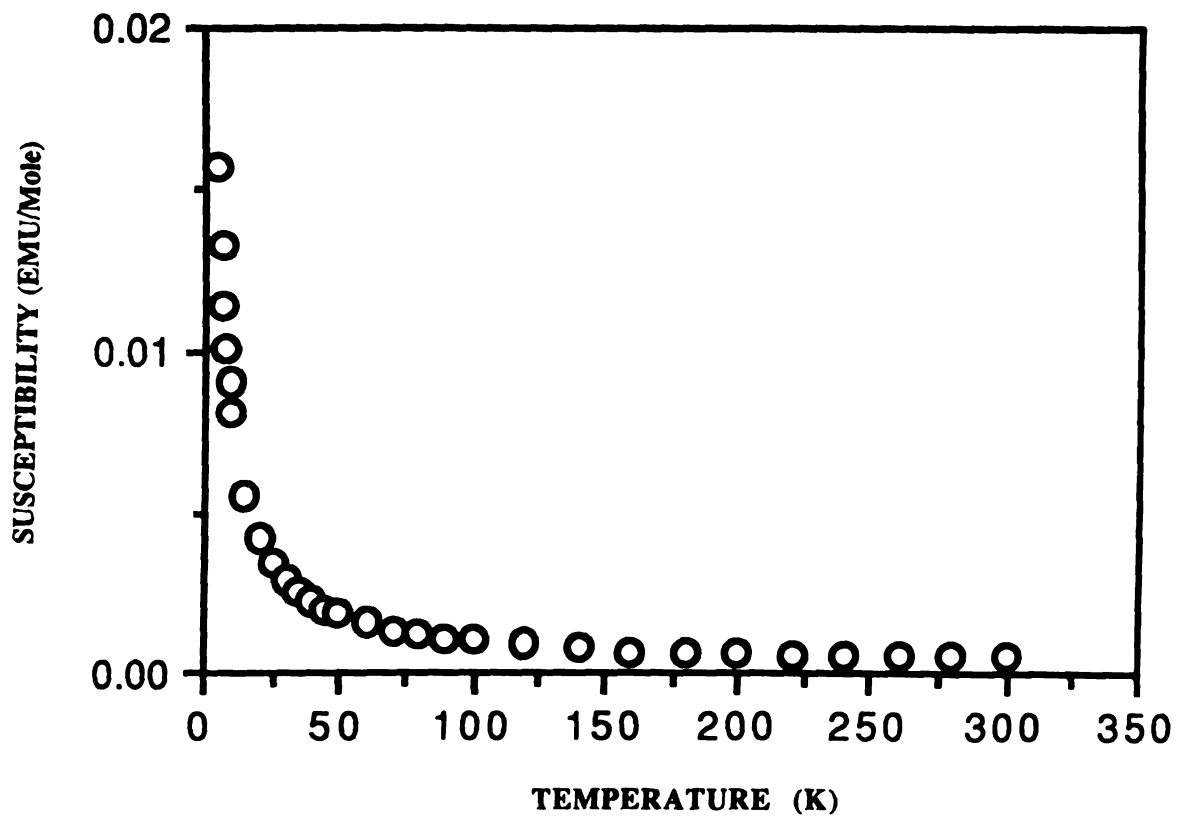
Figure 4.7. Variable temperature magnetic susceptibility data (c_m) for $(Pth)_{0.72}V_2O_5 0.52H_2O$.
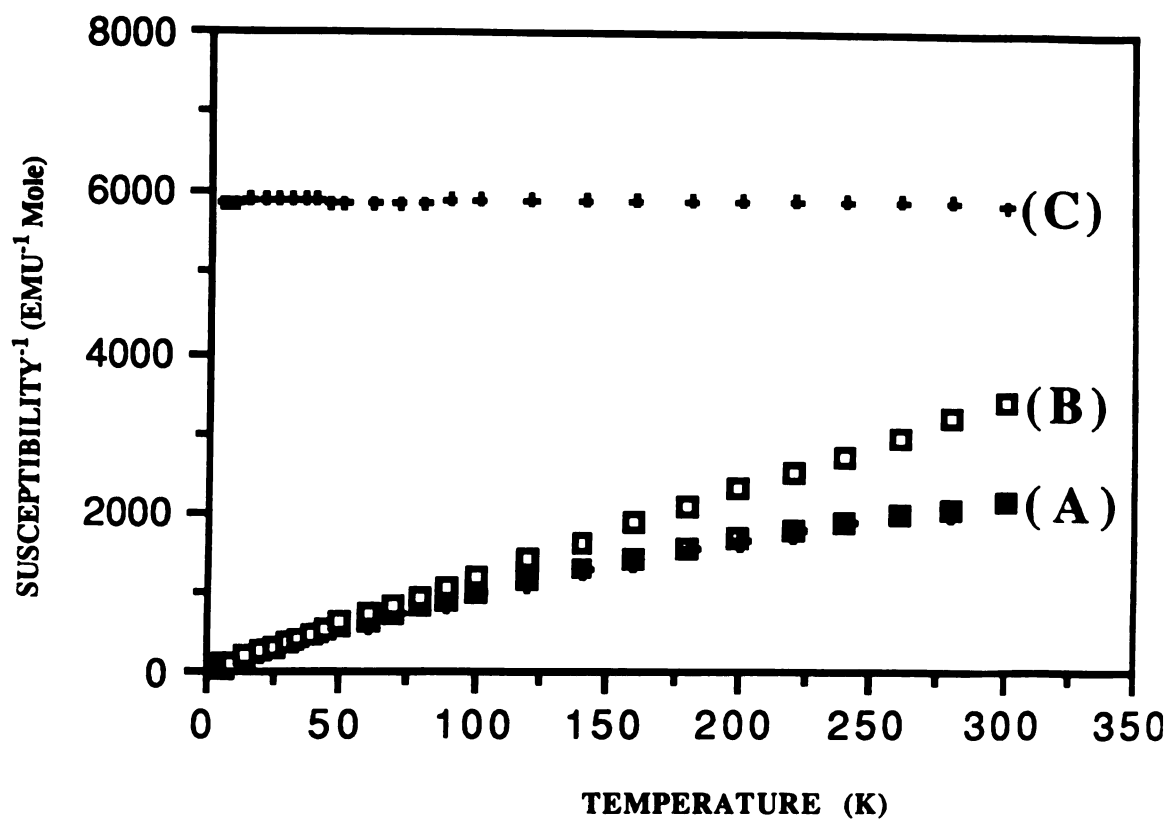
Figure 4.8. Variable temperature magnetic susceptibility data $(1/\chi_m)$ of $(Pth)_{0.72}V_2O_5.0.52H_2O$. (A) Total magnetic susceptibility (B) Curie susceptibility (C) Temperature independent paramagnetism.
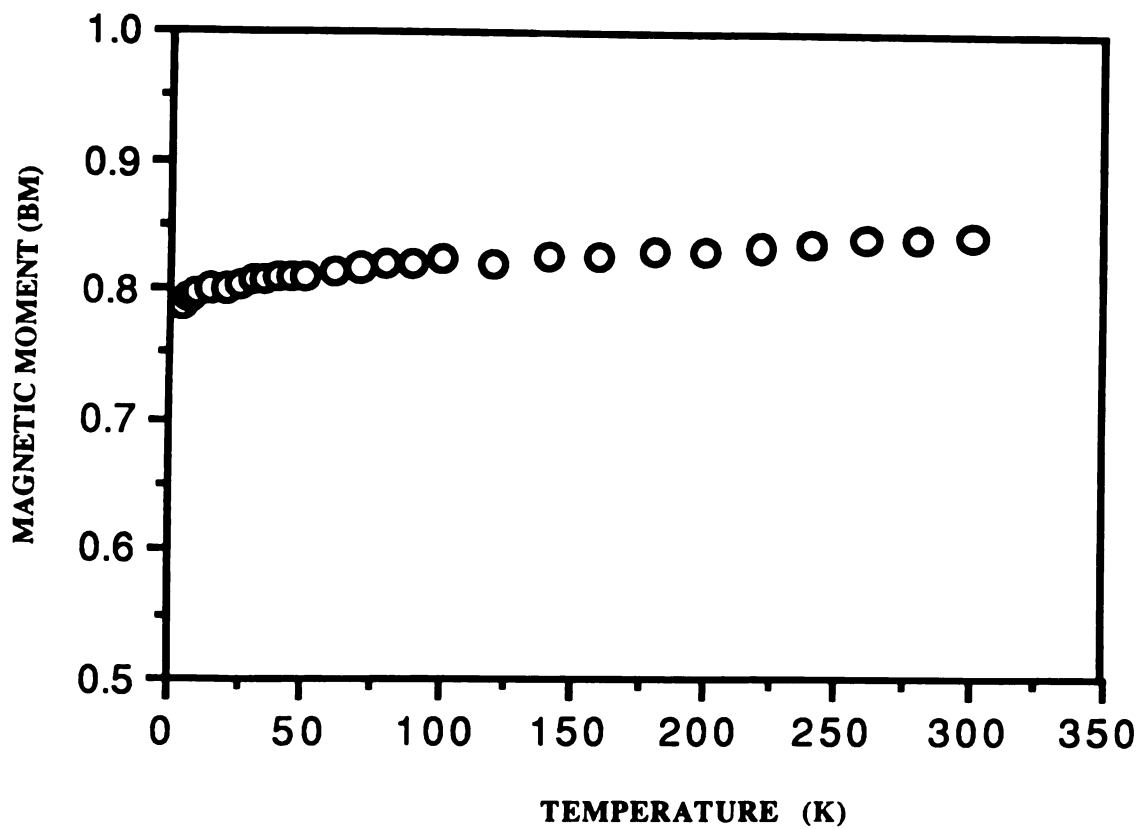
Figure 4.9. Variation of effective spin-only
magnetic moment as a function of temperature
for (Pth)$_{0.72}$V$_2$O$_5$.0.52H$_2$O

Table 4.2. The Room Temperature Magnetic Moment and Temperature Independent Paramagnetism of $(Pth)_xV_2O_5nH_2O$ versus x.

X	μ_{eff} (BM) (Total)	μ_{eff} (BM) (Curie)	χ_m x 10^4 (TIP)
0.16	0.87	0.62	1.5
0.30	0.94	0.80	1.0
0.45	0.93	0.77	3.2
0.57	1.20	0.77	3.5
0.58	0.96	0.77	1.3
0.72	1.06	0.84	1.7
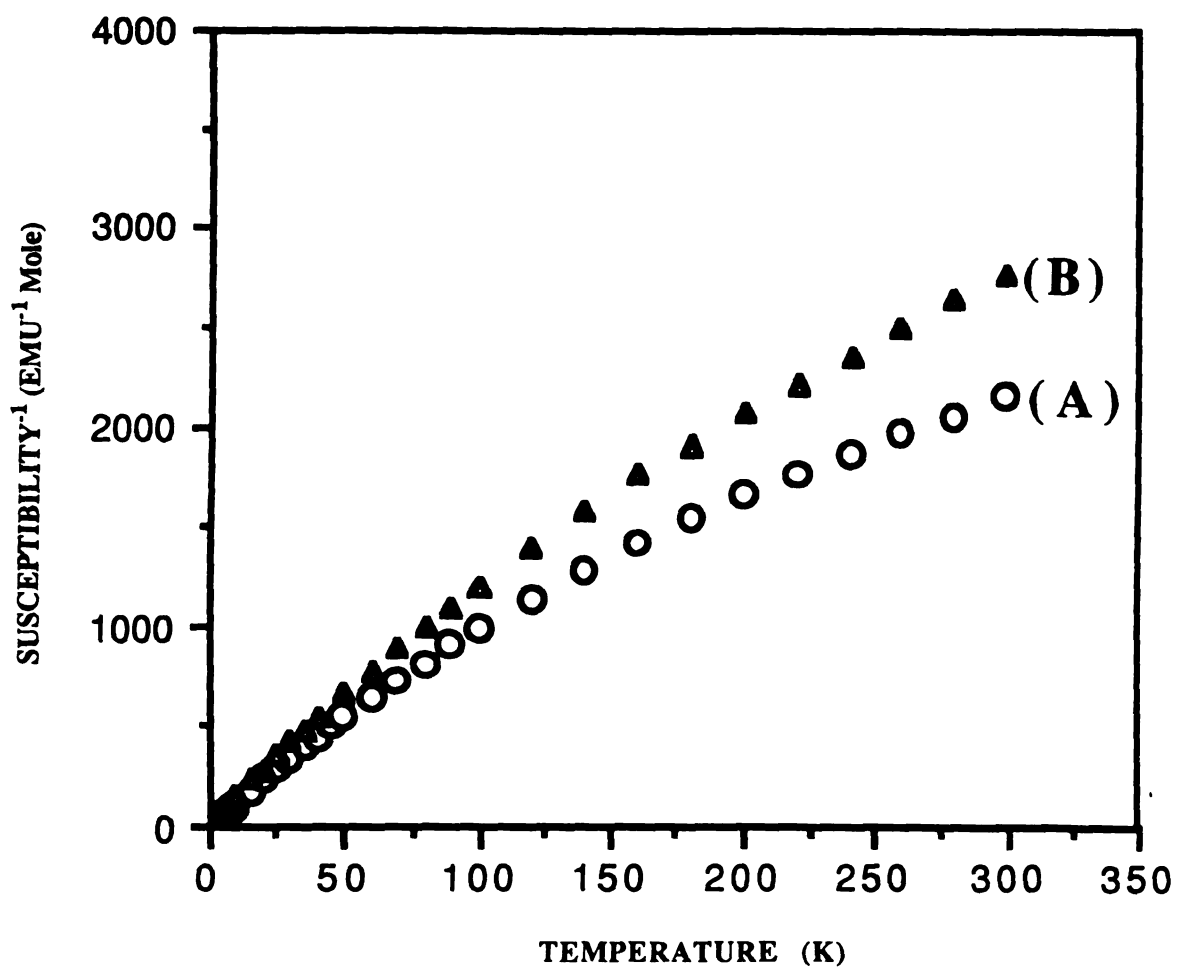
Figure 4.10. Variable temperature magnetic susceptibility data $(1/\chi_m)$ of $(Pth)_{0.72}V_2O_5.0.52H_2O$. (A) Fresh prepared (B) Aged.

samples could be different, therefore the degree of reduction of V_2O_5 xerogel could vary even for samples with the same carbon content. Therefore the magnetic data alone can not determine the precise degree of reduction of V_2O_5 framework. We note here that carbon content found from elemental analysis does not necessarily give the polymer length and thus cannot give the expected V^{4+}/V^{5+} ratios. Attempted to quantify the degree of reduction of V_2O_5 host by X-ray Photoelectron Spectroscopy (XPS). Although the V^{4+} peak is observed, due to the large change in the chemical shift and shape of V^{4+} peak and serious overlap between V^{4+} and V^{5+} peaks, the exact V^{4+}/V^{5+} ratio could not be obtained.

Upon sitting in air (aging), the magnetic susceptibility of $(Pth)_xV_2O_5nH_2O$ decreased gradually as shown in Figure 4.10. This is due to the reoxidation of the V^{4+} sites to V^{5+} presumably by ambient oxygen as observed in $(PANI)_xV_2O_5nH_2O$ (page 96) and $(Ppy)_xV_2O_5nH_2O$ (page 149).

F. Charge Transport Properties.

The charge transport properties of the $(Pth)_xV_2O_5nH_2O$ system varied widely with polymer/V_2O_5 ratio. The room temperature conductivities vary from 0.2 to 10^{-4} $\Omega^{-1}cm^{-1}$ depending on the polymer content, with higher polymer content materials exhibiting higher conductivity. Generally, the conductivities of films are 10 to 100 times higher than those of pressed pellets and the conductivities measured parallel to the layer are 10 times higher than perpendicular to the layers. Figure 4.11 shows the variable
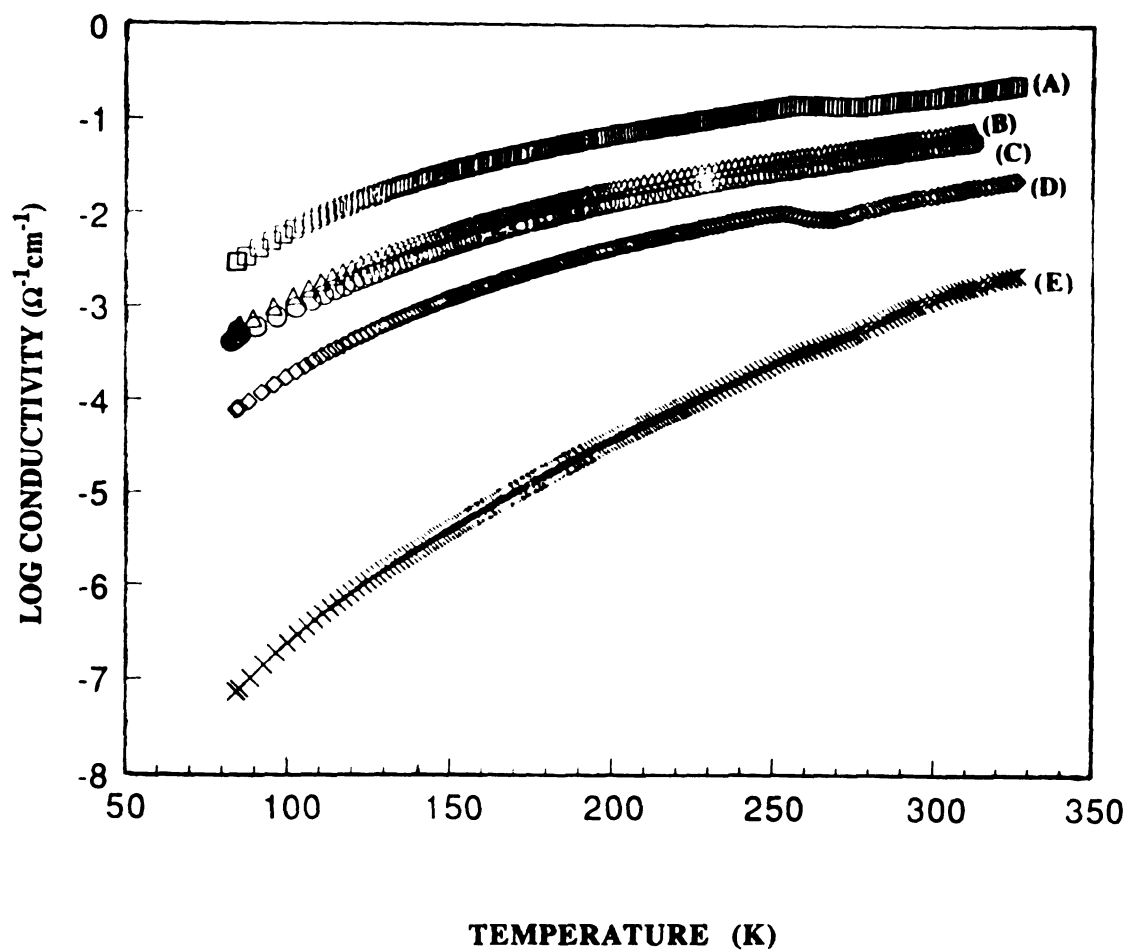
Figure 4.11. Four-probe variable temperature electrical conductivity data of (A) $(Pth)_{0.72}V_2O_5nH_2O$ (B) $(Pth)_{0.58}V_2O_5nH_2O$ (C) $(Pth)_{0.57}V_2O_5nH_2O$ (D) $(Pth)_{0.45}V_2O_5nH_2O$ (E) $(Pth)_{0.30}V_2O_5nH_2O$.

temperature conductivities of $(Pth)_x V_2O_5 nH_2O$ with different x values. The conductivities increase with rising temperature showing typical thermally activated behavior, most likely associated with the interparticle contact resistance, as observed in $(PANI)_x nH_2O$ and $(Ppy)_x V_2O_5 nH_2O$ (vise supra).

For similar polymer content, $(Pth)_x V_2O_5 nH_2O$ has higher conductivity than $(Ppy)_x V_2O_5 nH_2O$, but has similar magnetic moment. Since we used 2,2'-bithiophene as monomer, for the same degree of electron transfer, the chain length of polythiophene will be doubled the size of that of polypyrrole as showed in equation 4.6, 4.7 and 4.8.

$$\text{pyrrole} \longrightarrow \text{polypyrrole}_x + 2xe^- \quad \cdots \text{eq (4.6)}$$

$$\text{bithiophene} \longrightarrow \text{polythiophene}_{2x} + 2xe^- \quad \cdots \text{eq (4.7)}$$

$$V_2O_5 + 2xe^- \longrightarrow (V_2O_5)^{-2x} \quad \cdots \cdots \text{eq (4.8)}$$
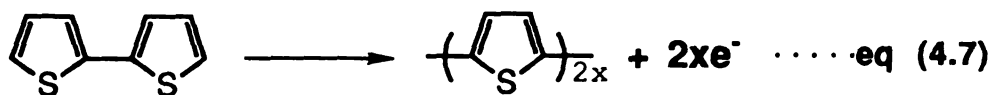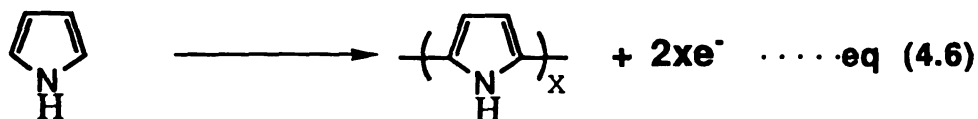
On the other hand, the higher oxidation potential and molecular weight of 2,2'-bithiophene, reduced the reaction rate, compared to pyrrole, and may have increased selectivity of the more thermodynamic stable 2,5 coupling. Higher molecular weight and less crosslinking in intercalated polythiophene may also be responsible for the higher conductivity.

Not surprising, the conductivity of $(Pth)_x V_2 O_5 n H_2 O$ did not increase upon aging. On the contrary, it slightly decreased upon sitting in air as shown in Figure 4.12. This is probably due to the reoxidation of the V_2O_5 framework and some oxidative degradation of polythiophene Although the IR spectra of aged $(Pth)_x V_2 O_5 n H_2 O$ did not show any significant difference compared to the fresh sample, polythiophene may react with oxygen to create structural defects in low concentration which cannot be detected by IR. Those structural defects decreases the conjugation length of the polymer, thus decreasing the conductivity. Possible oxidative degradation pathways may be the epoxidation of C-C double bonds and the oxidation of sulfur atoms to a sulfoxide or sulfone.

To determine the carrier type and understand the conducting behavior in detail, thermoelectric power (TP) measurements were carried out at Professor Kannewurf's laboratory. The variable temperature thermoelectric power of $(Pth)_x V_2 O_5 n H_2 O$ with different x values are shown in Figure 4.13. They can be separated into three categories: (a) when the polymer/V_2O_5 is very low (<0.3), the thermoelectric power (TP) is large, negative and becomes more negative as temperature increases (see Figure 4.13e). This is a n-type semiconductor with metal-like behavior, presumably due to the reduced V_2O_5, which is responsible for the charge transport properties of this material; (b) at medium polymer/V_2O_5 ratio, the Seebeck coefficient (S) is positive at temperature below 170°C and decreased as temperature increased, a typical p-type semiconductor behavior. Above 170°C the S became negative and kept constant eventually up to 350°C, as shown in Figure 4.13d. This mixed
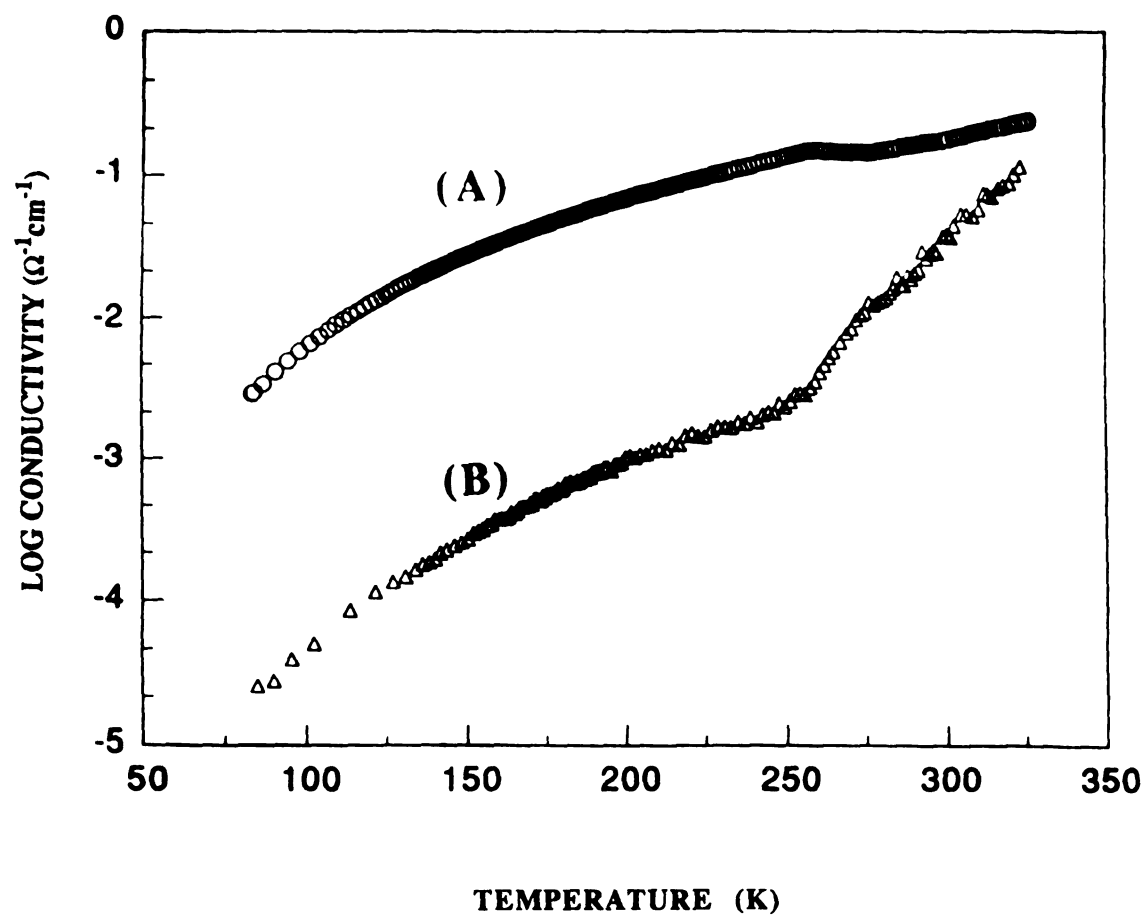
Figure 4.12. Four-probe variable temperature electrical conductivity data of $(Pth)_{0.72}V_2O_5nH_2O$. (A) Fresh prepared (B) Aged.
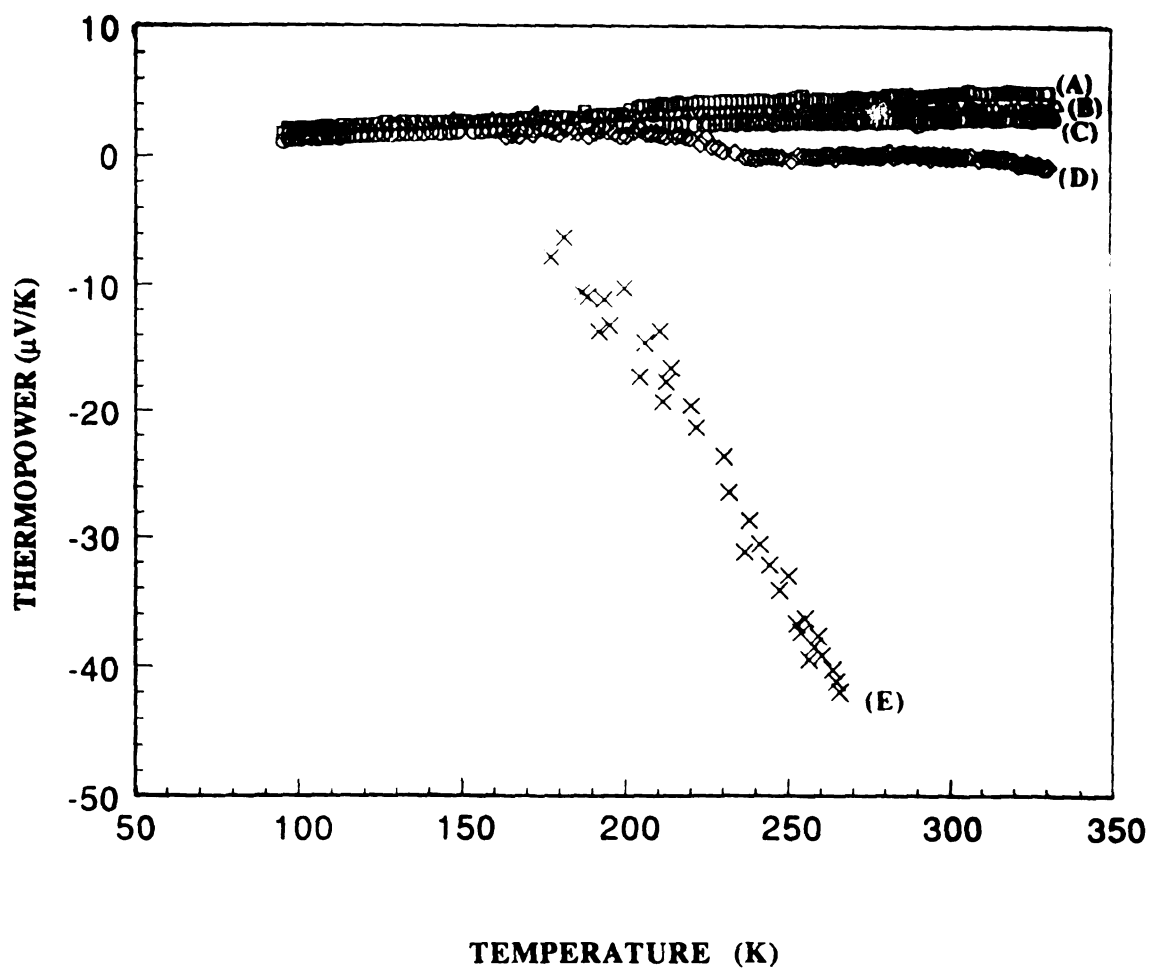
Figure 4.13. Variable temperature thermoelectric power data of (A) $(Pth)_{0.72}V_2O_5nH_2O$ (B) $(Pth)_{0.58}V_2O_5nH_2O$ (C) $(Pth)_{0.57}V_2O_5nH_2O$ (D) $(Pth)_{0.45}V_2O_5nH_2O$ (E) $(Pth)_{0.30}V_2O_5nH_2O$.

semiconductor and metal behavior did not occur in $(PANI)_x V_2 O_5 n H_2 O$, $(Ppy)_x V_2 O_5 n H_2 O$, $M_x V_2 O_5$ or bulk polythiophene [20]. Therefore the charge transport properties of these materials are the hybrid of reduced $V_2 O_5$ host and polythiophene. The semiconductor-metal switch temperature was also dependent on polythiophene/$V_2 O_5$ ratios. (c) the TP of higher polymer content samples (x>0.57) showed typical p-type metallic behavior. The S was small and positive (+3 $\mu V/K$ at room temperature for $(Pth)_{0.72} V_2 O_5 n H_2 O$) and decreased smoothly as temperature decreased (see Figure 4.13a, 4.13b and 4.13c). Since polythiophene has p-type metallic property [4d,21], the charge transport properties of high polymer content samples must be dominated by the polythiophene inside the $V_2 O_5$ layers.

Interestingly, although the conductivities of aged samples did not change dramatically, the thermopower varied and showed unusual behavior as shown in Figure 4.14. The S of aged sample was relatively small and positive but became less positive as the temperature increases to 200K. The small and positive TP values indicated p-type conductor with holes being the predominant charge carriers. However, the slope of the variable temperature thermoelectric power data suggested a semi-conducting behavior. This property was also not observed in either polythiophene or $V_2 O_5$. Therefore, the charge transport properties of aged $(Pth)_x V_2 O_5 n H_2 O$ with high polymer content are a hybrid of those of polymer and reduced $V_2 O_5$ but not dominated by polythiophene. This may be because upon aging the V^{4+} centers are reoxidized to V^{5+}, and at the same time, the doping level of polythiophene may have decreased.
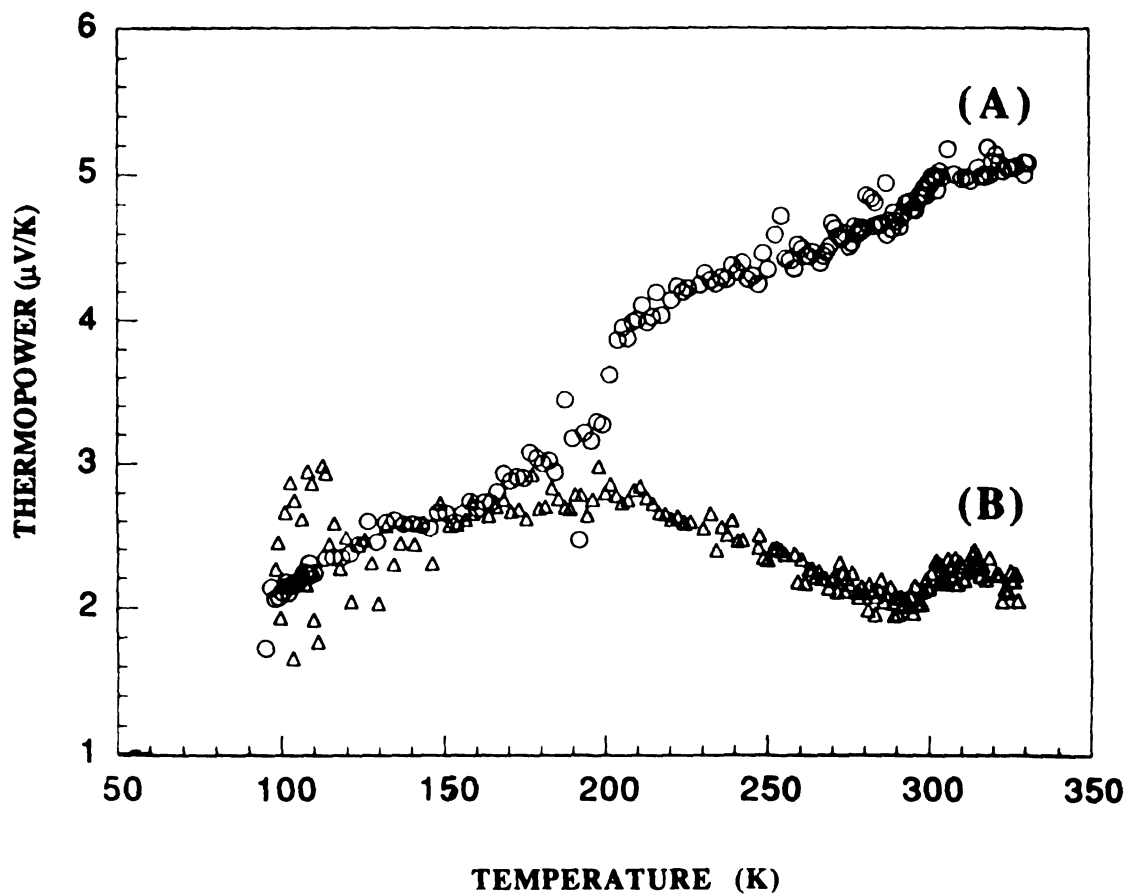
Figure 4.14. Variable temperature thermoelectric power data of $(Pth)_{0.72}V_2O_5nH_2O$. (A) Fresh prepared (B) Aged.

Another possibility is the degradation of the polymer with time in air.

VI. Conclusions.

The *in-situ* oxidative polymerization/ intercalation of polythiophene in layered V_2O_5 host can be achieved by refluxing 2,2'-bithiophene with V_2O_5 xerogel in CH_3CN. It is a topotactic reaction with 5.95Å interlayer spacing expansion. Both X-ray and electron diffraction data confirmed the intactness of the layered framework. EPR spectra of $(Pth)_xV_2O_5nH_2O$ revealed only one broad signal at g=1.9623 which comes from reduced V_2O_5 layers. The typical sharp peak of polythiophene did not appear which indicated that there is an intimate contact and strong spin-spin interaction between polymer and host. This magnetic interaction phenomenon is also observed in the magnetic data. $(Pth)_xV_2O_5nH_2O$ is a paramagnetic material with magnetic susceptibility followed the Curie law. The room temperature conductivity of $(Pth)_xV_2O_5nH_2O$ falls in a wide range $(10^{-4}\sim10^0\,\Omega^{-1}cm^{-1})$ and the thermopower can be positive or negative. The carrier type and conductivity can be varied by simply changing the polythiophene/V_2O_5 ratios under the same reaction condition. These unique properties open a new avenue for preparing electroactive materials with controllable charge transport properties.

LIST OF REFERENCES

LIST OF REFERENCES

1. *"Non-Stoichiometric Compounds, Tungsten Bronzes Vanadium Bronzes and Related Compounds"* Bevan, D. J.; Hagemuller P. Eds Pergamon Press Oxford **1973**, P 569-601.

2. (a) Alderbert P.; Baffier, N.; Legendre, J. J.; Livage, J. *Rev. Chim. Min.* **1982**, 19, 485-495. (b) Lemordant, D.; Bouhaouss, A.; Alderbert, P.; Baffier, N. *J. Chim. Phys.* **1986**, 83, 105-113. (c) Ruitz-Hitzky, E.; Casal, B. *J. Chem. Soc. Faraday Trans. 1* **1986**, 82, 1579-1604.

3. Day, P. *Phil. Trans. R. Soc. Lond. A* **1985**, 314, 145-158.

4. (a) Yamamoto, T.; Sanachika, K.; Yamamoto, A. *Bull Chem. Soc. Jpn.* **1983**, 56, 1497-1502. (b) Tourillon, G.; Garnier, F. *J. Electrochem. Soc.* **1983**, 130, 2042-2044. (c) Tourillon, G.; Garnier, F. *J. Phys. Chem.* **1983**, 87, 2289-2292. (d) Kaneto, K.; Yoshino, K. *Solid State Commun.* **1983**, 46, 389-391. (e) Hotta, S.; Hosaka, T.; Shimotsuma, W. *Synth. Met.* **1983**, 6, 317-318. (f) Horowitz, G.; Tourillon, G.; Garnier, F. *J. Electrochem. Soc.* **1984**, 131, 151-156. (g) Alcacer, L. Ed. Proc. Workshop, Sintra, Portugal, July 28-31 1. *"Polymers Special Applications"* Reidel, Dordrecht, **1987**.

5. Glenis, S.; Tourillon, G.; Garnier, F. *Thin Solid Films* **1984**, 122, 9-17.

6. Ofer, D.; Wrighton, M. S. *J Am. Chem. Soc.* **1988**, 110, 4467-4468.

7. Kaufman, J. H.; Kanazawa, K. K.; Street, G. B. *Phys. Rev. Lett.* **1984**, 53, 2461-2464.

8. Tourillon, G.; Garnier, F. *J. Polym. Sci. Polym. Phys. Ed.* **1984**, 22, 33-39.

9. Heinze, J.: Meinze, J.; Störzbach, M. *Ber. Bunsen-Ges, Phys. Chem.* **1986**, 90, 1043-1048.

10. (a) Akimoto, M.; Furukawa, Y.; Takeuchi, H.; Harada, I.; Soma, Y.; Soma, M. *Synth. Met.* **1986**, 15, 353-360. (b) Furukawa, Y.; Akimoto, M.; Harada, I. *Synth. Met.* **1987**, 18, 189-194.

11. Daniell, R.; Taliani, C.; Zamoni, R.; Giro, G. *Synth. Met.* **1986**, 13, 325-328.

12. (a) Yamamoto, T.; Sanechika, K.; Yamamoto, A. *J. Polym. Sci. Polym. Lett. Ed.* **1980**, 18, 9-12.

13. *"Handbook of Conducting Polymers"* T. A. Skotheim Ed. Marcel Dekker Inc. New York **1986**, Vol. 1 293-350.

14. (a) Hotta, S.; Hosaka, T.; Saga, M.; Shimotsuma, M. *Synth. Met.* **1984/1985**, 10, 95-99. (b) Yamamoto, T.; Sanachika, K.; Yamamoto, A. *Bull. Chem. Soc. Jpn.* **1983**, 56, 1497-1502. (c) Tourillon, G.; Gariner, F. *J. Phys. Chem.* **1983**, 87, 2289-2292.

15. Hotta, S.; Shimotsuma, W.; Taketani, M. *Synth. Met.* **1984/1985**, 10, 85-94.

16. (a) Hotz, C. Z.; Kovacic, P.; Khoury, I. A. *J. Polym. Sci. Polym. Chem. Ed.* **1983**, 21, 2617-2628. (b) Tourillon, G.; Garnier, F. *J. Electroanal. Chem.* **1982**, 135, 173-178.

17. Tourillon, G.; Garnier, F. *J. Electroanal. Chem.* **1984**, 161, 51-58.

18. (a) Kanatzidis, M. G.; Tonge, C. R.; Marks, T. J.; Marcy, H. O.; Kannewurf, C. R. *J. Am. Chem. Soc.* **1987**, 109, 3797-3799. (b) Kanatzidis, M. G.; Marcy, H. O.; McCarthy, W. J.; Kannewurf, C. R. Marks, T. J. *Solid State Ionics* **1989**, 32/33, 594-608.

19. Babonneau, F.; Barboux, P.; Josien, F. A.; Livage, J. *J. De Chim. Phy.* **1985**, 82, 761-766.

20. Koboyashi, M.; Chen, J.; Chung, T.-C.; Morase, F. ; Heeger, A. J.; Wudl, F. *Synth. Met.* **1984**, 9, 77-86.

21. (a) Bredas, J. L.; Themans, B.; Fripiat, J. G.; Andre, J. A. *Phys. Rev. B* **1984**, 29, 6761-6773. (b) Kobayashi, M.; Chen, J.; Cheng, T.-C.; Moraes, F.; Heeger, A. J.; Wudl, F. *Synth. Met.* **1984**, 19, 77-86.

CHAPTER 5

FORMATION OF CONDUCTING POLYANILINE IN A CRYSTALLINE LAYERED HOST ~ *IN-SITU* OXIDATIVE INTERCALATION OF ANILINE IN FeOCl

ABSTRACT

Polyaniline was inserted into FeOCl, to yield a black microcrystalline product, α-(PANI)$_x$FeOCl, α-(I). The observed 5.94Å interlayer spacing expansion, corresponds to the insertion of one layer of polyaniline chains inside the intralamellar space of FeOCl. The reaction rate can be accelerated by the presence of oxygen. The Infrared spectrum of α-(I) show the characteristic peaks of conducting polyaniline. The room temperature conductivity of powder samples (in pressed pellet form) are 10^{-3} to 10^{-2} $\Omega^{-1}cm^{-1}$ (single crystal samples show conductivities of $\sim 10^{-1}$ $\Omega^{-1}cm^{-1}$) with thermally activated behavior. Variable temperature thermoelectric power shows typical p-type semiconductor behavior. When polyaniline was intercalated in single crystal FeOCl, a superlattice phenomenon was observed indicating the polyaniline chains in FeOCl layers are oriented.

Upon standing in air, two separated processes were occur: the FeOCl framework was hydrolyzed to form β-FeOOH and the polyaniline chains continue to oxidatively couple to longer chains. The obtained product is a composite of polyaniline and β-FeOOH which remain intimately mixed. This composite we called the "β"-(I) phase. The physicochemical and charge transport properties of decomposition products, "β"-(I) are dramatically different from those of α-(I). The conductivity of "β"-(I) is 10 times higher and thermopower measurements show metallic behavior which is

entirely due to polyaniline. The room temperature effective spin-only magnetic moment, μ_{eff}, of α-$(PANI)_{0.20}FeOCl$ is 2.8 B.M. The observed antiferromagnetic behavior is similar to that of FeOCl.

I. Introduction:

Electrically conducting polymers have received a great deal of attention due to their promising electrical properties and their potential applications in a variety of devices [1,2]. A prototype conductive polymer, polyaniline, known for more than a century [3], has attracted renewed interest during the last decade [4]. Its conducting form exhibits excellent environmental stability and can be used in various electronic devices and sensors [5]. There has been extensive investigation of its chemical structure by various spectroscopy methods [5]. However, our understanding of the structure is still fragmentary due to the amorphous or poor crystalline nature and insolubility in common organic solvents. Important structural problems associated with single chain and their macromolecular aggregation remain to be solved. The systematic control and modification of its physical, structural and electronic properties is an active area of research [6]. Goals include the optimization of the charge transport properties and the better understanding of the relationship between electronic and lattice structure. This has been approached by preparing oriented or crystalline polymers. Progress in this area has been made recently by MacDiarmid, Epstein and coworkers [7] who studied a microcrystalline form of polyaniline and proposed a crystal structure, based on X-ray powder diffraction data, similar to that of polyethylene-sulfide. Further progress in determining structural details is hampered by the small X-ray coherence length of polycrystalline polyaniline ($\sim$50-150Å) as larger crystallites are not

available. Also key structural features of acceptor-doped polyaniline were deduced from the single crystal structure determinations of the ClO_4^- and BF_4^- dication salts of $H-(C_6H_4-NH)_4-C_6H_5$, radical cation salts of shorter oligomers and neutral $H_5C_6-N=C_6H_4=N-C_6H_5$ [8].

One way to obtain orientation of the polymer chains would be to grow them inside a structurally organized host framework. The framework could be either three dimensional with large oriented tunnels or two dimensional with accessible interlayer space. We have proved that conductive polymers can be inserted in layered V_2O_5 xerogel, see chapter 2,3&4. Recently, conductive polymers were also reported to insert in other layered materials such as montmorillonite [9], three dimensional matrices [10] and zeolites [11]. FeOCl is another excellent layered system for intercalation reactions [12]. Growing polymers in FeOCl would result in intercalated compounds with alternating monolayers of polymer chains and FeOCl monolayers. These compounds, if crystalline, may enable us to further characterize the polymer structure by crystallographic and spectroscopic methods. This work follows previous studies of *in-situ* intercalative polymerization of pyrrole [13a] and thiophene [13b] in FeOCl and complements our studies of polyaniline intercalation in the layered V_2O_5 xerogel. The products obtained in the latter system are turbostratic, contrary to the FeOCl-derived products which are crystalline [14].

II. Experimental Section:

Reagents. $FeCl_3$, Fe_2O_3, KPF_6, toluene, nitrobenzene, ethanol, dimethoxy-ethane, acetone and HPLC grade N-methyl-2-pyrrolidinone (NMP) were purchased from commercial sources and used without further purification. Aniline, methanol and acetonitrile were dried over CaH_2 and distilled prior to use (aniline was distilled under vacuum).

Physicochemical Methods.

See chapter 2.

Synthesis of FeOCl.

FeOCl was prepared by mixing 9.69 g (59.7 mmol) $FeCl_3$ with 7.20 g (45.1 mmol) Fe_2O_3 in a evacuated pyrex tube at 380°C for 40 hours. The product was washed with acetone to remove excess $FeCl_3$, dried in vacuum and characterized by X-ray powder diffraction [15]. During the reaction, some large single crystals of FeOCl were formed on the edge of the tube away from the bulk material. They were separated carefully from the powder for single crystal reaction studies.

Preparation of Microcrystalline α-(PANI)$_x$FeOCl.

(a) *α-(PANI)$_{0.16}$FeOCl:* 60 ml of a 5% aniline solution (32.3 mmol) in acetonitrile was stirred with 0.50 g (4.66 mmol) FeOCl

in air for a week. The black shiny microcrystalline product was isolated by filtration, washed with acetone and dried in vacuum. The yield was quantitative.

The intercalation reaction was deemed complete when the (0k0) peak of the starting FeOCl disappeared from the X-ray powder diffraction pattern. Elemental analysis: Calcd. for $(C_6H_4NH)_{0.16}FeOCl$: C, 9.45%; H, 0.66%; N, 1.84%; Fe, 45.83%. Found: C, 8.53%; H, 1.75%; N, 1.59; Fe, 40.12%.

(b) α-$(PANI)_{0.20}FeOCl$:   50 ml of a 4% aniline solution (21.5 mmol) in acetonitrile was mixed with 0.34 g of (3.17 mmol) FeOCl. The mixture was stirred in air for 8 days. The black product was isolated in the same way as in (a). Elemental analysis: Calcd. for $(C_6H_4NH)_{0.20}FeOCl$: C, 11.47%; H, 0.80%; N, 2.23%; Fe, 44.50%. Found C,11.04%; H, 1.59%; N, 1.89%; Fe, 42.07%. Other compounds with different stoichiometries were prepared the same way with different ratios of the reagents (the particle size of FeOCl also affect the PANI/FeOCl ratio of the products). The PANI to FeOCl ratio typically varied between 0.16 and 0.28.

Intercalation with single crystals of FeOCl.

(a) α-$(PANI)_{0.28}FeOCl$:   0.30 g (2.80 mmol) of single crystals of FeOCl were mixed with 2.00 g (21.51 mmol) of aniline in 50 ml acetonitrile. Upon standing in air at room temperature without any disturbance for 30 days black shiny crystals of $(PANI)_{0.28}FeOCl$ were obtained. This product was isolated by filtration, washed with

acetone and dried in vacuum. Elemental analysis: Calcd. for $(C_6H_4NH)_{0.28}FeOCl$: C, 15.18%; H, 1.06%; N, 2.95%; Fe, 41.99%. Found: C, 15.05%; H, 1.66%; N, 4.29%; Fe, 41.50%.

(b) *α-(PANI)$_{0.23}$FeOCl:*   Mixed 0.34 g (3.17 mmol) of single crystals of FeOCl with 2.00 g (21.51 mmol) of aniline in 50 ml acetonitrile. The mixture, upon standing in air at room temperature without disturbance for 60 days, afforded black single crystals of $(PANI)_{0.23}FeOCl$. The isolation procedure was the same as above in (a). Elemental analysis: Calcd. for $(C_6H_4NH)_{0.23}FeOCl$: C, 12.91%; H, 0.90%; N, 2.51%; Fe, 43.55%. Found: C, 12.63%; H, 1.61%; N, 2.76%; Fe, 41.70%.

Isolation of polyaniline from α- and "β"-(PANI)$_x$FeOCl

2.50 g of α- or "β"-$(PANI)_{0.28}FeOCl$ were stirred with 400 ml 2M $HCl_{(aq)}$ at room temperature for 3 days. The black solid, polyaniline, was isolated by filtration, washed with H_2O then acetone and dried in vacuum. It was characterized by infrared spectroscopy [16].

III. Results and Discussion:

The objective of this study was the detailed characterization of the redox intercalation reaction of aniline with FeOCl and the subsequent polymerization chemistry associated with this system. We begin with a discussion of the synthetic chemistry and polymer

characterization, followed by magnetic and charge transport studies of the products α-(PANI)$_x$FeOCl. We then discuss the nature of the so-called "β"-phase (which is the decomposition product of α-phase) and its ultimate characterization.

A. Syntheses: The Reaction of Aniline with FeOCl.

The reaction of aniline with FeOCl can yield poorly defined products, if not done properly and in one occasion was reported not to occur [17]. For this reason, we investigated the reaction in detail in order to determine the optimum synthetic conditions. Several solvents such as toluene, nitrobenzene, acetone, ethanol, acetonitrile and even aniline itself were used. No reaction occurred in refluxing nitrobenzene. When the reactions were carried out in refluxing toluene, acetone, ethanol and aniline, intercalation was observed early in the reaction, but the products decomposed to a brown material before the reaction went to completion. After careful experimentation, we found acetonitrile to be the most suitable solvent in this reaction system. Violet crystals of FeOCl react with excess aniline in CH$_3$CN at room temperature, in air to form black microcrystalline products of the general formula α-(PANI)$_x$FeOCl. The reaction is simply represented as equation 5.1 in which the aniline is oxidatively polymerized and FeOCl is reduced.

$$C_6H_5NH_2 + FeOCl \xrightarrow[\text{R.T., 1~2 week}]{\text{CH}_3\text{CN}} (C_6H_4NH)_xH_{2x}FeOCl \ldots eq(5.1)$$

The reaction is typically complete after one to two weeks depends on aniline to FeOCl ratio and FeOCl particle size. In general, the mole ratio of aniline to FeOCl must be larger than seven in order to drive the reaction to completion, without losing too much crystallinity in the product. Raising the temperature accelerates the reaction, but at the same time can accelerate decomposition of the products. It is interesting that reactions performed under air are much faster than those under nitrogen, indicating that oxygen is involved in the reaction. It most likely acts as an electron acceptor and reacts with H^+ released from the oxidative polymerization of aniline as observed in polyaniline/V_2O_5 system. Therefore, the H^+ content of the product is much less than what represented in equation 5.1. Not surprising, when large single crystals of FeOCl are used, the reaction is much slower, but the resulting products contain similar amounts of PANI as the microcrystalline samples. It is nevertheless remarkable that single crystals as long as 0.5 mm can be intercalated completely under the conditions used. Elemental analyses showed various stoichiometries ($0.16<x<0.30$) depending on reaction conditions and FeOCl particle size. This is consistent with the maximum theoretical stoichiometry calculated based on the molecular sizes of FeOCl and polyaniline, $(PANI)_{0.32}FeOCl$. Regardless of stoichiometry the products exhibited very similar properties.

Reactions were also carried out in evacuated sealed tubes using ethanol, methanol, acetone, acetonitrile or dimethoxyethane as a solvent at 80-110°C. Methanol was found to be the most suitable solvent, always yielding single phase products. In the other solvents, the products either decomposed before the reaction went to

completion or resulted in multiple phases. The products isolated from sealed tube reactions were black shiny microcrystalline solids with a slightly higher interlayer expansion than those isolated from reactions in open systems. Furthermore, we found that the methanothermally made materials trapped a lot of solvent inside, making it difficult to determine the actual polymer content by elemental analysis. These products are also slightly different (electronically and compositionally) from those prepared in acetonitrile, at ambient pressure, most likely differing in the degree of reduction of the FeOCl layer and the degree of aniline polymerization. We also believed that the FeOCl framework was changed by covalent attachment of MeO groups as observed in polyfuran/FeOCl system [18]. Thus these products should be considered different compounds from those prepared at ambient temperature and pressure. The spectroscopic studies were focused on the products isolated from reactions in air at room temperature using acetonitrile as a solvent.

B. Infrared Spectroscopy and X-ray Powder Diffraction Studies.

Unequivocal evidence for the formation of conducting polyaniline in the interlamellar space of FeOCl is derived from the FTIR spectra, given in Figure 5.1, which show the characteristic fingerprint of the emeraldine salt form [19]. This form is positively charged and requires a counter anion which in this case is the reduced FeOCl. By comparison, the counterion in bulk emeraldine
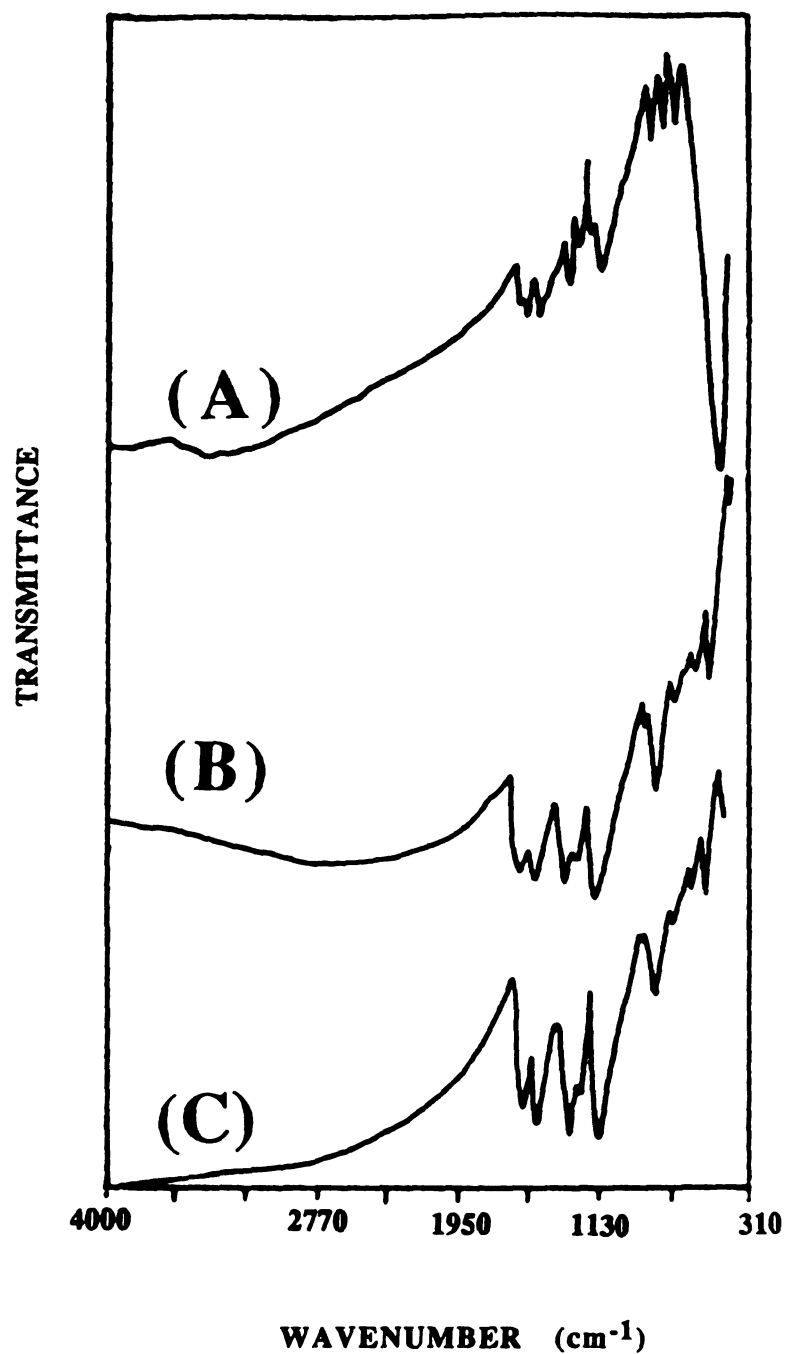
Figure 5.1. FT-IR spectra (KBr pellets) of (A) α-(PANI)$_x$FeOCl (B) Bulk polyaniline (emeraldine salt) (C) Extracted polyaniline.

salt (prepared by aniline oxidation with $(NH_4)_2S_2O_8$ in 0.1M HCl) is Cl^-. The broad rising absorption at 2000-4000 cm^{-1} which continues into the near-IR is due to the continuum of overlapping electronic transitions, originating from both the mixed valence FeOCl [20], and emeraldine salt [21] components. The peak at around 470 cm^{-1} is the vibration of FeOCl framework which did not change after reaction. The polyaniline can be extracted from α-$(PANI)_x$FeOCl, by digesting the FeOCl framework with 2 M aqueous HCl solution for 20 hours. The IR spectrum of the extracted polyaniline is identical with that of an authentic bulk polyaniline sample (see Figure 5.1). It is interesting to note that the absorptions of intercalated PANI generally occur at higher energies than of bulk PANI, suggesting that the former is found in a more rigid environment and/or possesses a lower average molecular weight than bulk PANI (vide infra).

Consistent with intercalation, the interlayer spacing of the host lattice expands along the b axis. As the reaction proceeds, the XRD peak intensities *0k0, hk0, 0kl* and *hkl* of FeOCl decrease gradually and new broader peaks appear at lower 2θ angles. At the same time the color of FeOCl turns black. The reaction was judged complete by the total disappearance of FeOCl *0k0* reflections. During the reaction we observe basal *0k0* reflections from both the product and the pristine FeOCl consistent with an *inhomogeneous* intercalation mechanism. The XRD patterns of FeOCl and α-$(PANI)_x$FeOCl are shown in Figure 5.2 for comparison. The interlayer spacing of α-$(PANI)_x$FeOCl is 13.86Å, corresponding to an interlayer expansion of 5.94Å, sufficient to accommodate the monolayer of polyaniline molecules. We found that the magnitude of expansion varies slightly
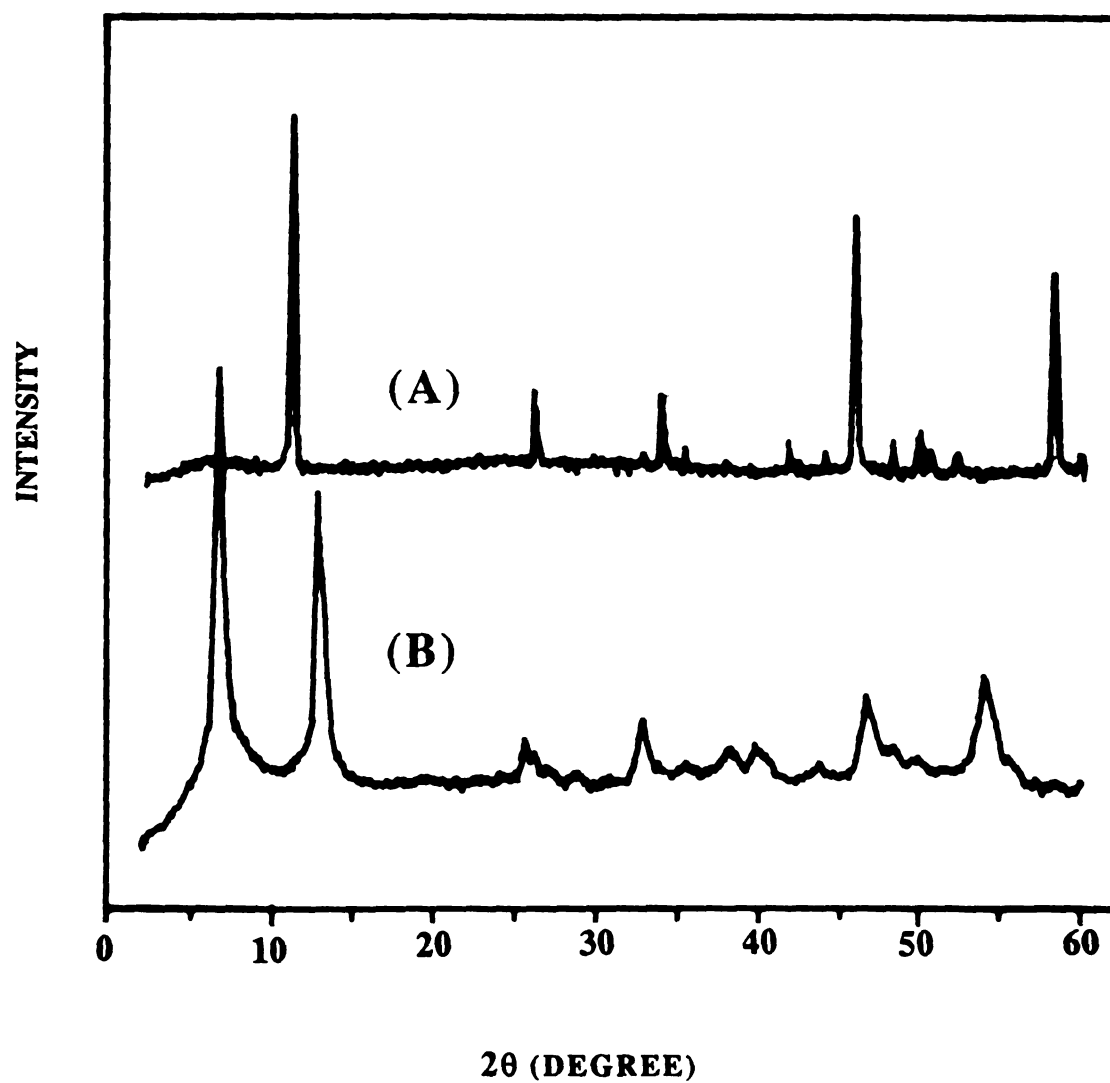
Figure 5.2. Reflection-mode X-ray powder diffraction patterns of (A) Pristine FeOCl (B) α-(PANI)$_x$FeOCl.

(around 0.6Å) between single crystal and powder samples (the interlayer spacing of single crystal is 14.46Å). This may be due to the imperfect arrangement of molecules in the layer gallery which also can be seen from the broadness of the peaks. The magnitude of interlayer expansion suggests the presence of a monolayer of polymer. This is also consistent with the two-fold axis, bisecting the C-N-C angle, being oriented roughly perpendicular to the FeOCl layers as shown in Scheme 5.1.
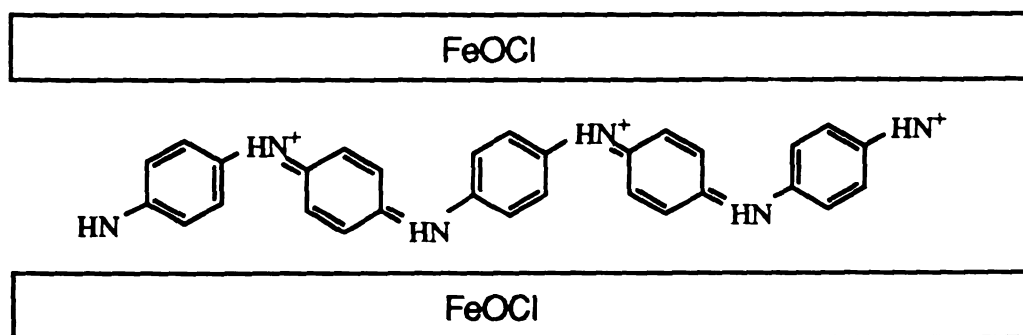
Scheme 5.1. Proposed orientation of polyaniline chain in FeOCl layers.

During intercalation, a few aniline molecules fail to polymerize and are trapped inside the interlamellar space as anilinium (AnH^+) ions. The latter can form by reaction of aniline with released H^+ during polymerization. The AnH^+ are easily identified by their characteristic vibrations in the FTIR spectra of the products (1492, 745, 687 cm^{-1}). Subjecting the material to vacuum does not remove the AnH^+ ions. However, upon standing in air the AnH^+ vibrations disappear without decrease in the carbon to iron ratio, suggesting

that they polymerize or incorporate to existing polymer chains in the interlamellar space. Oxygen must act as an oxidant and proton acceptor. The polymerization of AnH^+ ions can be accomplished by heating the α-$(PANI)_xFeOCl$ sample at 140°C in air or oxygen for several days, as judged by the disappearance of the anilinium peaks from the infrared spectrum while the peaks of FeOCl and polyaniline remain intact. This phenomenon was also observed in polyaniline/V_2O_5, and is the first example of *post-intercalative* oxidative polymerization of a monomer in a layered host induced by molecular oxygen. This observation raises important implications of broad applicability to other systems which contain molecular, but oxidatively polymerizable guests, in host matrices.

In order to determine how much anilinium was present, we attempted ion exchange with K^+ according to equation 5.2.

$$(AnH^+)_x(C_6H_4NH)_yFeOCl + nK^+ \longrightarrow K_x(C_6H_4NH)_yFeOCl + nAnH^+ ...eq(5.2)$$
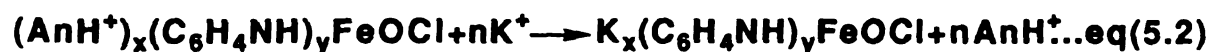
This is based on the assumption that anilinium, being the smallest species in the interlamellar space, and thus the most mobile, would ion exchange faster than its less mobile oligomers and polymers. Based on nearly complete ion-exchange, the amount of K^+ in the product of eq. 5.2 would correspond to the amount of unpolymerized AnH^+ (ignore the trace amount of proton in the α-$(PANI)_xFeOCl$).

The reaction was carried out in CH_3CN with KPF_6 for 20 hours. Indeed, ion-exchange is successful as judged by disappearance of the anilinium derived peaks in the FTIR spectrum. EDS analysis

confirmed the presence of 0.017 mole of potassium per mole of FeOCl. This corresponds to ~8-10% of aniline to be in the form of AnH^+ in freshly prepared α-$(PANI)_xFeOCl$. Interestingly, the interlayer spacing of the K^+ exchanged product is slightly smaller than that of the starting material by 0.6Å. This can be explained via a structural model in which the anilinium ions are oriented with their C-N bonds perpendicular to the FeOCl layers acting as pillars while the PANI chains lie parallel to the layers, as shown in Scheme 5.2.
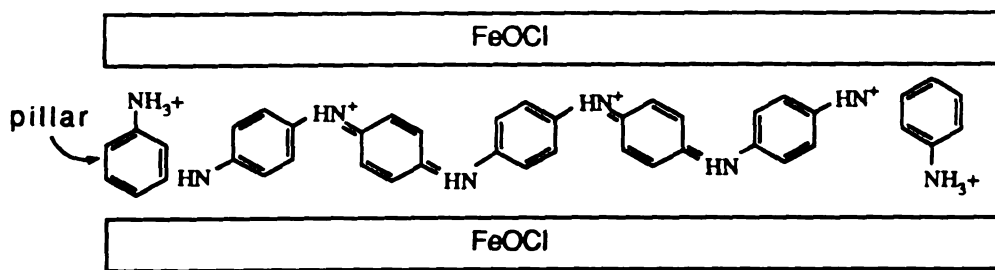
Scheme 5.2. The pillar effect of anilinium in $(PANI)_xFeOCl$

C. Insertion of Polyaniline in FeOCl Single Crystals and Crystallographic Studies.

The intercalation of single crystals of many materials at room temperature is known to be very slow, it is seldom complete, and usually it destroys the crystals. Nevertheless we still attempted the reaction of FeOCl with aniline to see if similar difficulties existed in this system. After several unsuccessful tries, we have been able to insert polyaniline into single crystals of FeOCl by careful slow reaction using a CH_3CN solution of aniline in air at room temperature.

Surprisingly, the resulting compound, (polyaniline)$_{0.28}$FeOCl, retains significant single crystal character, despite the fact that the overall crystallinity has decreased and most crystals appear to have been exfoliated. The crystals cleave perpendicular to the [010] direction, consistent with their lamellar structure. This can be observed clearly in the SEM photographs of (I) which are shown in Figure 5.3. The insertion of polyaniline causes an interlayer expansion of 6.54Å. The formation of polyaniline (emeraldine salt) in the interlayer space can be easily confirmed by FTIR spectroscopy.

Examination of crystals of (I) by X-ray diffraction revealed that the crystal quality, though inferior to that of starting FeOCl, was sufficiently good for preliminary X-ray diffraction experiments. Oscillation photographs of such crystals show broad but intense diffraction peaks. The broadest peaks are those of the $0k0$ class of reflections. This is to be expected considering that the FeOCl crystals have undergone a topotactic intercalation reaction. Axial X-ray photographs from single crystals are shown in Figure 5.4.

Interestingly, the diffraction pattern of the $h0l$ zone reveals a set of strong reflections associated with the parent 3.30Å x 3.78Å cell, and a set of several weak reflections half way between the strong ones, suggesting that the periodicity along the a- and c- axes have doubled relative to the original FeOCl unit cell. The new unit cell is orthorhombic with a=6.60Å, b=28.86Å, c=7.56Å and V=1459Å^3. The origin of this superlattice must be due to substantial long-range order of polyaniline in FeOCl. Long range order of
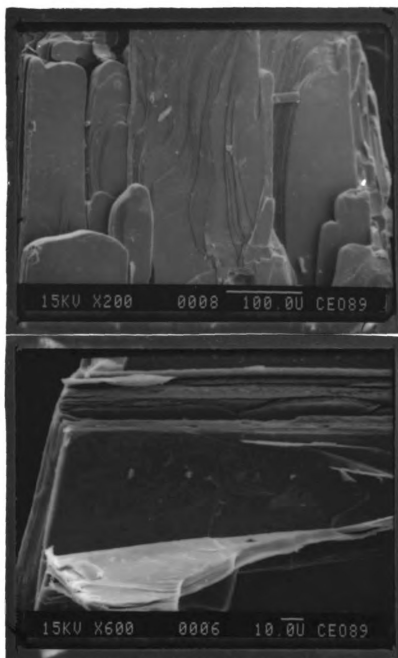
Figure 5.3. SEM micrographs of single crystal α-(PANI)$_{0.28}$FeOCl.

rotation photograph

c-axis

a-axis

b-axis (perpedicular to the layers)
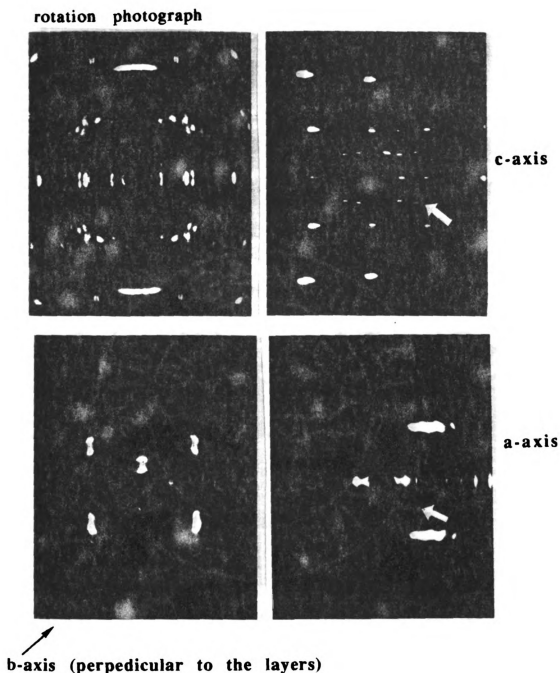
Figure 5.4. Single crystal X-ray random orientation rotation photograph (upper left) and axial oscillation photographs along the three crystallographic axes of α-$(PANI)_{0.28}FeOCl$. (White arrows indicated superlattice reflections responsible for the doubling of the unit cell in the a- and c- direction.)

polyaniline could be achieved by orientation of the polymer chains along certain crystallographic directions, such that a doubling of the periodicity of a- and c- axes is caused by the special arrangement of polyaniline chains in FeOCl (vide infra).

Although the structure of polyaniline is not yet known in detail, it has been proposed, based on X-ray diffraction studies on powders, that it is similar overall to that of poly-phenyleneoxide [22]. This is shown in Scheme 5.3.
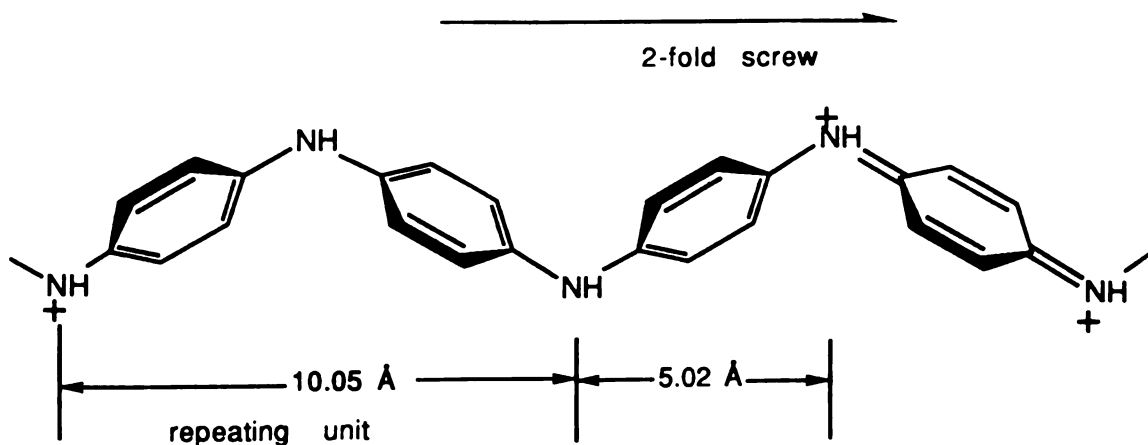
Scheme 5.3. Proposed structure of polyaniline.

Based on single crystal crystallographic studies of aniline oligomers, by Baughman et al [22] the repeating unit of polyaniline is estimated to be 10.05Å (ignoring the details in individual phenyl groups). The highest symmetry possible for the polymer chain corresponds to a 2-fold screw axis in the chain direction. The step of the 2-fold screw axis is 10.05/2=5.02Å. If we now attempt to orient such a chain along either the a- or the c-axis of the FeOCl layer, as

shown in Figure 5.5, we see that the repeating unit of the polymer and the inorganic layers are not commensurate. A doubling of the a- or c- axes cannot be achieved. A close examination of the structural details of FeOCl reveals that the minimum Cl---Cl' distance along the [101] direction (diagonal to the a-,c- axes) is 5.03Å, almost one-half of the repeating unit of polyaniline. By orienting parallel to the [101] direction, polyaniline can provide each of his NH units with a Cl "partner" thus establishing H---Cl hydrogen bonding which can act as an additional stabilizing force. The main stabilizing force, of course, being the coulombic attraction of the positively charged polymer to the negatively charged FeOCl layers, as given in Scheme 5.4.
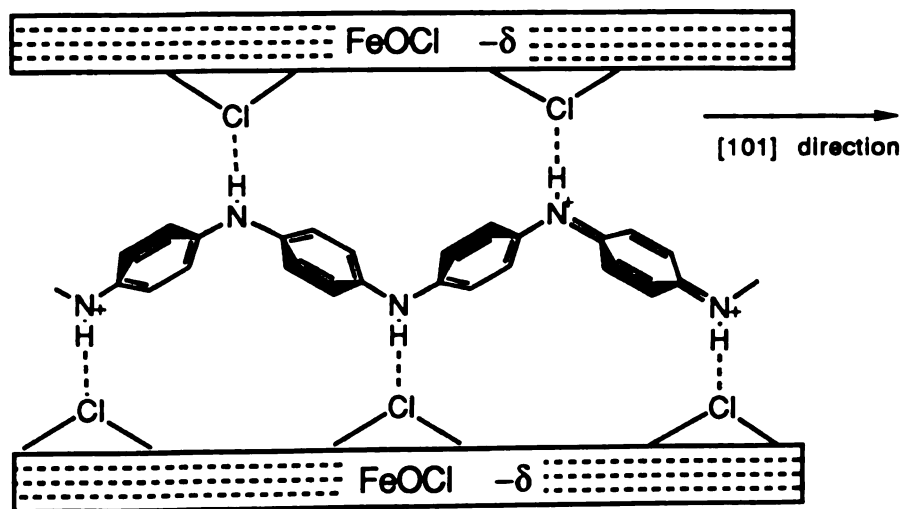
Scheme 5.4. Proposed hydrogen bonding between polyaniline chains and FeOCl framework.

Figure 5.6 shows that a diagonal orientation of polyaniline produces a system in which the positions of the NH groups are commensurate
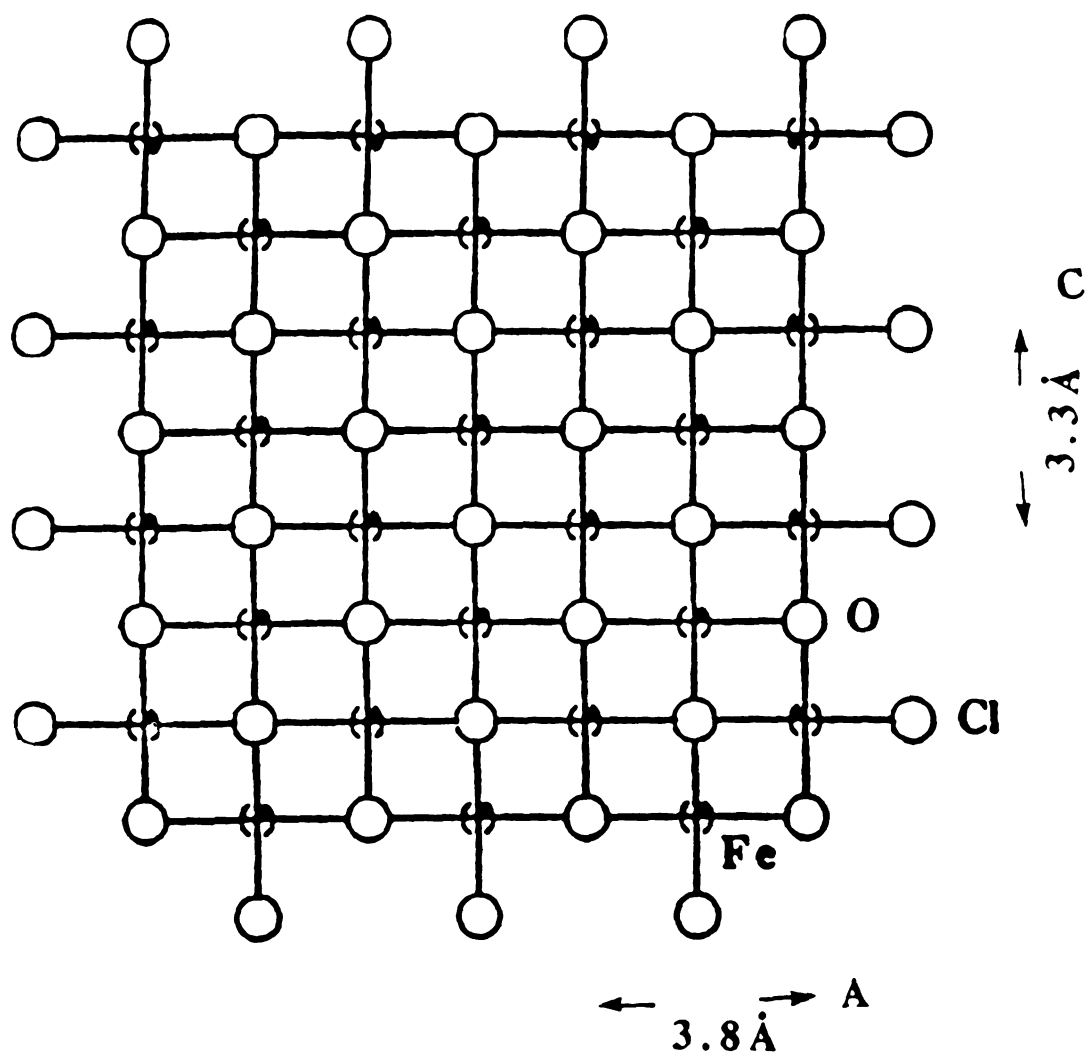
Figure 5.5. **The ac plane of FeOCl (looking down b axis).**
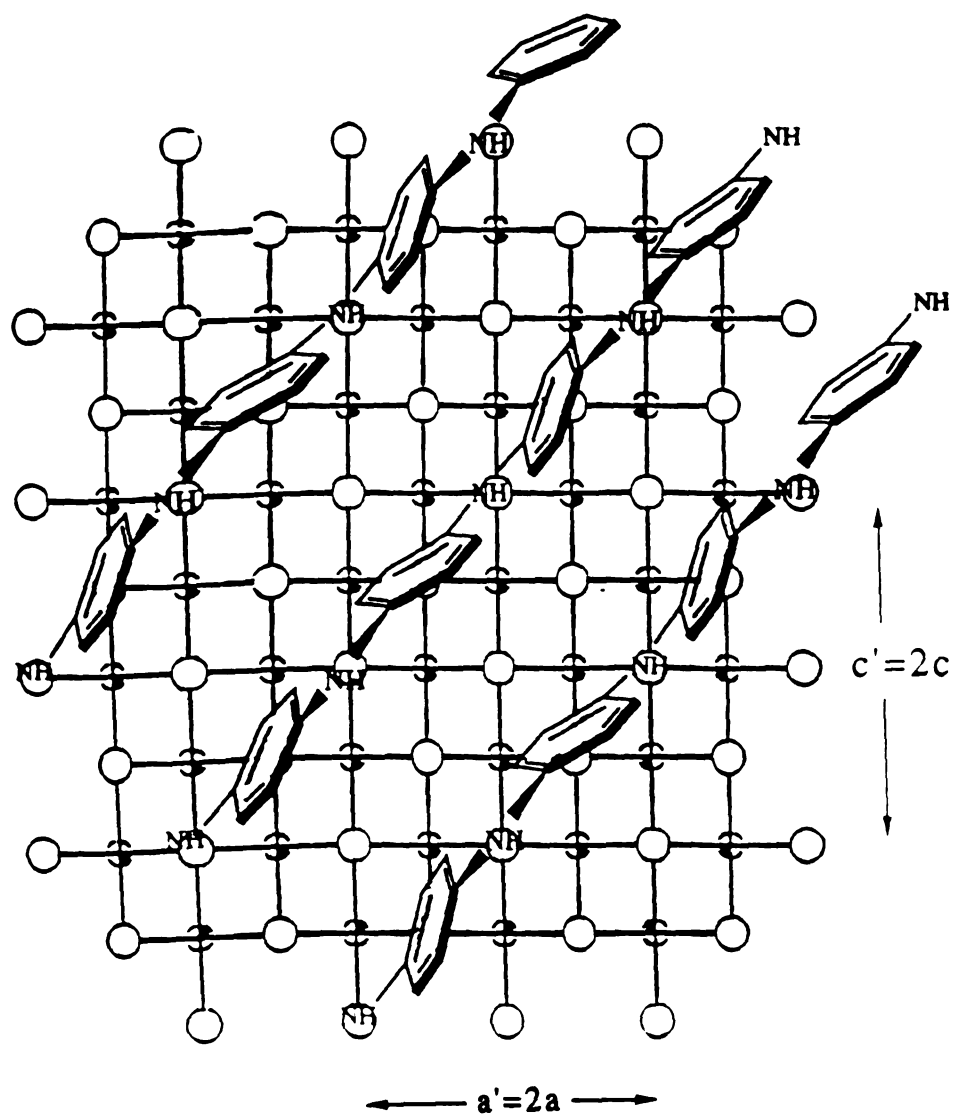
Figure 5.6. Possible relative position of polyaniline chains and FeOCl layers.

with those of the Cl atoms in the layers. This produces a new orthorhombic unit cell with crystallographic axes a'=2a and c'=2c. In this fashion, the polymer chains can stack side by side lying above every other row of Cl atoms with an interchain distance of ~5Å. Because the doubling of the unit cell is caused by the light carbon and hydrogen atoms, the superlattice reflections would be weak, consistent with the experimental data. What the experimental data cannot tell us is how the polyaniline chains are oriented (i.e. along the [101] or [-101]) in the interlayer space below and above the one shown in Figure 5.6. Work along these lines is continuing.

D. Aerial Oxidation: α-(I) and the Nature of the "β" Phase.

Early on in this investigation it became evident that oxygen plays an important role in the intercalation of aniline into FeOCl. The first noticeable observation was that intercalation is slower under nitrogen than under air. In fact, reactions carried out under nitrogen, often resulted in decomposition before they went to completion. We later determined that decomposition was due to over-reduction of FeOCl. Based on our own observation and those from the literature, we now recognize that the reductive capacity of this host material is 0.1e per Fe. Reduction beyond this value results in decomposition by virtue of structural change.

During the reaction, aniline is oxidatively polymerized while FeOCl is reduced. An electron-balanced equation for this redox intercalation reaction (assuming that aniline and FeOCl are the only

reactants) is shown for each component separately in equation 5.3 and equation 5.4. The overall reaction is shown in equation 5.5.

$$xC_6H_5NH_2 \longrightarrow [(C_6H_4NH)(C_6H_4NH^+)]_{0.5x} + (2.5X)e^- + 2xH^+....eq(5.3)$$

$$FeOCl + (2.5X)e^- \longrightarrow FeOCl^{(2.5x)-} ....eq(5.4)$$

$$xC_6H_5NH_2 + FeOCl \longrightarrow [(C_6H_4NH)(C_6H_4NH^+)]_{0.5x}H_{2x}FeOCl....eq(5.5)$$
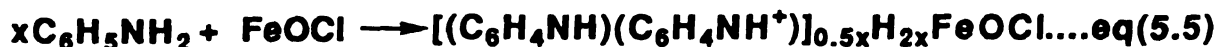
Equation 5.5 demands that all the protons released from aniline are retained in the product and that FeOCl accepts all the transferred electrons. Thus, in a product with 0.20 equivalents of aniline monomer per FeOCl the oxidation state of Fe should be $\sim+2.5$. In other words, 50% of the Fe^{3+} sites should be reduced to Fe^{2+}. This conclusion is contrary to two experimental facts: the quantitation of Fe^{2+}/Fe^{3+} by Mössbauer spectroscopy shows that only 10% of the Fe atoms are in the Fe^{2+} state, regardless of stoichiometry; the inability of FeOCl lattice to sustain more than $\sim$10% of the Fe atoms in +2 state without structural decomposition [23]. Furthermore attempts to carry the reaction out in nitrogen resulted in decomposition of FeOCl before the reaction could go to completion. Given that α-$(PANI)_xFeOCl$ is crystalline and that we have no evidence for excess H^+ ions in the products, it appears that only part of the electrons are transferred to the host while the rest end up somewhere else. We believe the latter is molecular oxygen, which acts not only as electron acceptor but also as proton acceptor, forming either H_2O or H_2O_2.

Oxygen could participate in the reaction by either oxidizing generated Fe^{2+}, thus increasing the oxidation state of FeOCl, or by oxidizing directly intermediate aniline oligomers which themselves might be more reducing than aniline. We have obtained sufficient evidence that the intercalative oxidation of aniline by V_2O_5 xerogel also consumes ambient oxygen, suggesting a similar intercalation mechanism.

α-$(PANI)_x$FeOCl is a moisture and air sensitive material, upon standing in air for several months, it gradually transforms to a different product. This change is associated with considerable changes in the physicochemical and electrical properties of the material. No change is observed when the samples are stored in evacuated sealed tubes. Here we would like to specially define the so called α phase and "β" phase. The material obtained upon standing in air for several month is defined as the "β" phase, "β"-(I) or "β"-$(PANI)_x$FeOCl. At this stage, the product is very weakly crystalline or X-ray amorphous. Based on the data given below, the phase change can be rationalized by assuming that the polyaniline chains in the interlamellar space, couple further to form higher molecular weight polymer. However, attempts to accelerate the transformation by heating the sample under oxygen flow at 140~200°C were not successful presumably due to the slow coupling of aniline oligomers and the absence of water. At this temperatures the structure of polyaniline changed, as evidenced by the IR spectra. At the same time, independent of the polymer oxidation, a hydrolysis take place at the FeOCl framework. This change is not abrupt but slow and continuous. Certainly, there are infinite stages of oxidation

in between, as this is a continuous oxidation/hydrolysis. If the oxidation is allowed to continue, we observe the slow but steady appearance of diffraction peaks which correspond to crystalline β-FeOOH as shown in Figure 5.7. For simplicity, we define the "β"-(I) by the complete fading of the IR peak of α-phase at 480 cm^{-1} which is due to the Fe-O vibration in FeOCl framework. The infrared spectra of α-(I) and "β" phase of $(PANI)_x FeOCl$ are shown in Figure 5.8. Table 5.1 lists the IR vibration modes of polyaniline extracted from α-(I) and "β"-(I), compared with extracted polyaniline and bulk polyaniline. The term "β" phase here is used with caution being cognizant of the fact that *this material is not a pure compound* (vide infra) and lies between the α-(I) and its oxidative decomposition product. The full characterization of both the α- and "β" phases was accomplished with a variety of experimental techniques, as described below.

E. PANI Extracted from α-(I) and "β"-(I) versus Bulk PANI.

The PANI extracted from "β"-(I) differs from bulk PANI in several respects. First, in its base form, the sample is more soluble in tetrahydrofuran (THF) and dimethylformamide (DMF) than the corresponding bulk PANI. Second, the salt form has room temperature conductivity of 0.1 $\Omega^{-1}cm^{-1}$ compared to 1-5 $\Omega^{-1}cm^{-1}$ of the corresponding bulk emeraldine salt. These data suggest that the intercalated polyaniline contains significantly shorter chains than bulk PANI and thus correspondingly smaller average MW. This is
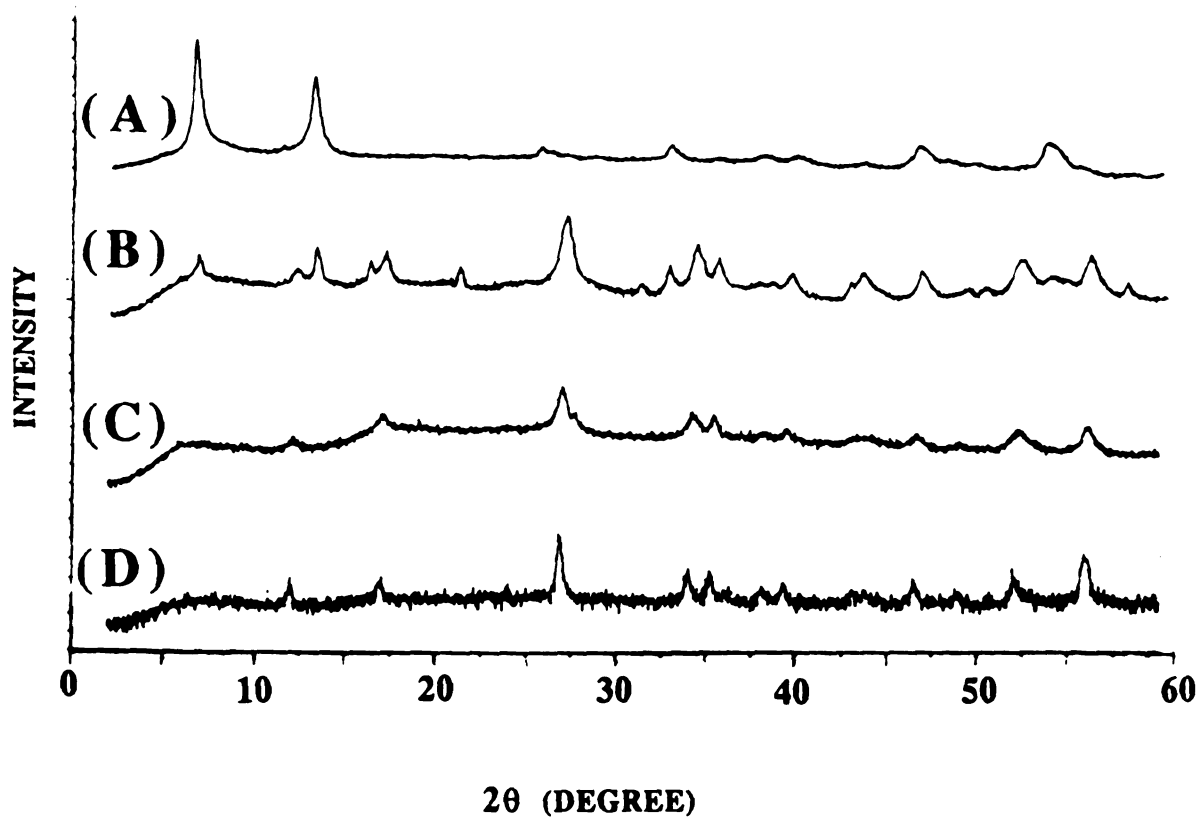
Figure 5.7. Reflection-mode X-ray powder diffraction patterns of (A) α-$(PANI)_x FeOCl$ (B) Partially decomposed phase (C) "β"-$(PANI)_x FeOCl$ (D) β-FeOOH.
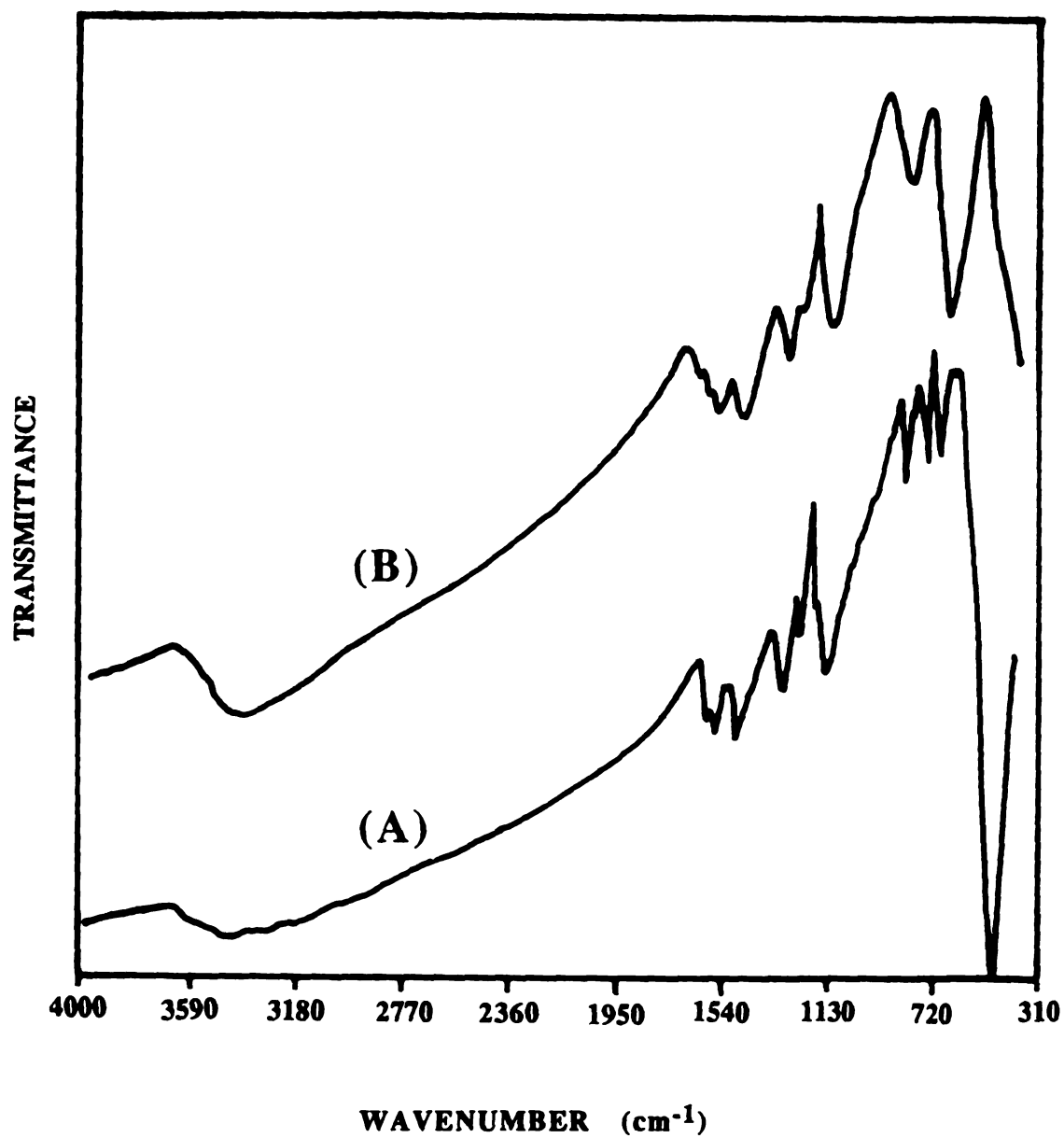
Figure 5.8.   FT-IR spectra (KBr pellets) of (A) α-
(PANI)$_x$FeOCl   (B) "β"-(PANI)$_x$FeOCl.

Table 5.1. The Major Vibration Modes of α-, "β"-(PANI)$_x$FeOCl and Extracted Polyaniline Compared with Bulk Polyaniline.

Mode	α	"β"	Bulk	Extracted
N=Q=N	1556cm^{-1}	1557cm^{-1}	1569cm^{-1}	1563cm^{-1}
benzene ring	1478cm^{-1}	1479cm^{-1}	1478cm^{-1}	1485cm^{-1}
C-N in QBQ*, QBB, BBQ	1302cm^{-1}	1301cm^{-1}	1295cm^{-1}	1295cm^{-1}
C-N in BBB	1239cm^{-1}	1241cm^{-1}	1246cm^{-1}	1239cm^{-1}
C-H bending	1140cm^{-1}	1129cm^{-1}	1140cm^{-1}	1119cm^{-1}
C-H on 1,2,4. subst. benzene			879cm^{-1}	
p-substituted benzene ring	809cm^{-1}	822cm^{-1}	809cm^{-1}	802cm^{-1}
C-H on 1,2 subs. benzene ring		702cm^{-1}	696cm^{-1}	700cm^{-1}
FeOCl or β-FeOOH	478cm^{-1}	675cm^{-1}		

Subs.: substitution, *: B: benzene; Q: quinone
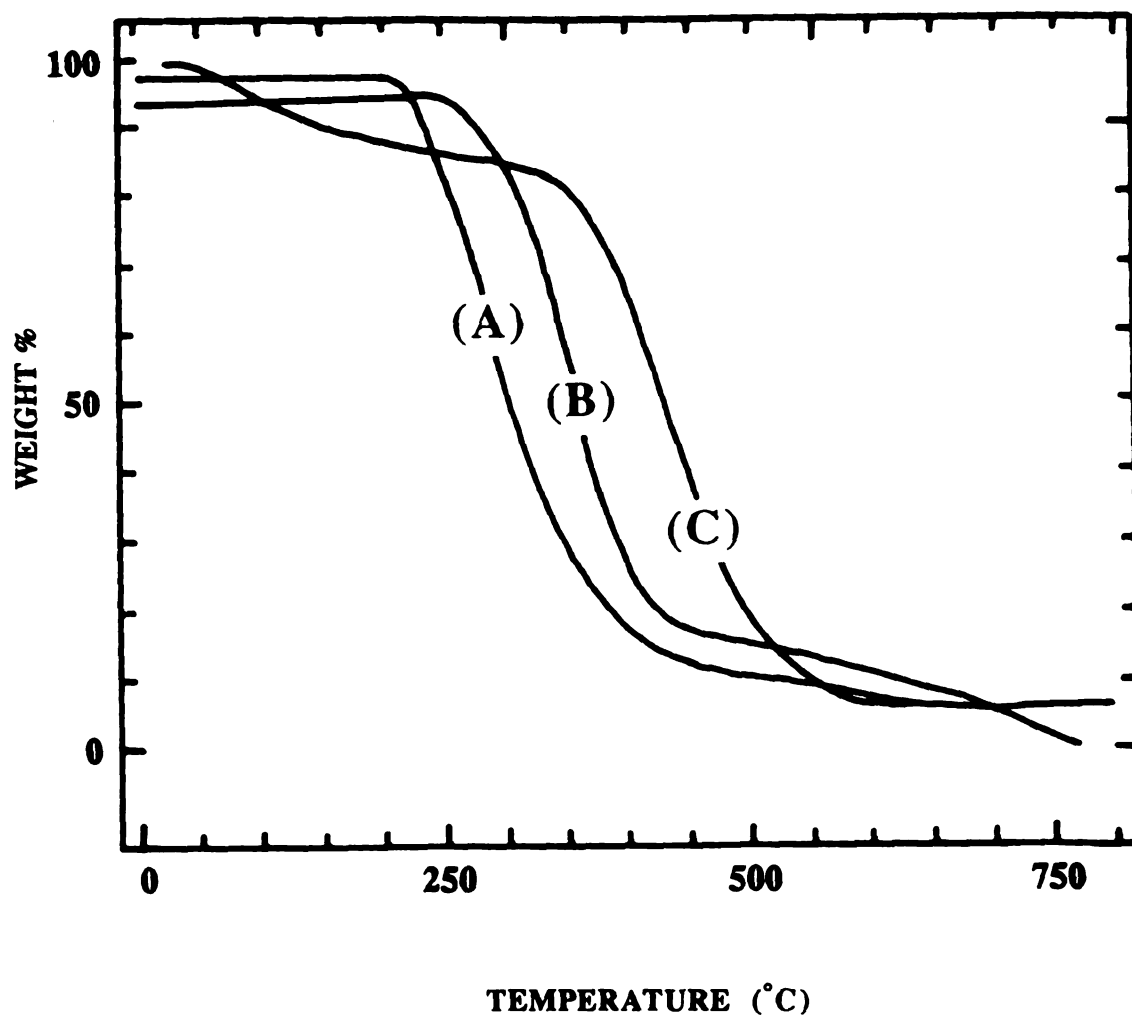
Figure 5.9. TGA curves (under nitrogen flow) of polyaniline extracted form (A) α-(PANI)$_x$FeOCl (B) "β"-(PANI)$_x$FeOCl (C) Bulk polyaniline. (The heating rate was 5°C/min)

rationalized by the slower-kinetics of polymerization of aniline in FeOCl due to the constrained environment in which it must occur, thus yielding smaller chains. Efforts are under way to obtain more quantitative data regarding the MW distribution of PANI chains in α-(I) and "β"-(I) using gel permeation chromatography (see below for preliminary data). The thermal stability of the three PANI's was compared by examining the TGA diagrams under oxygen, shown in Figure 5.9. We found that the extracted PANI from α-(I) decomposes at a lower temperature than from "β"-(I) and bulk polyaniline, consistent with the smaller MW of PANI in α-(I). The direct evidence of formation of longer polyaniline chain in "β"-(I) comes from the gel permeation chromatography analyses.

F. Gel Permeation Chromatography (GPC) Analysis.

GPC graphs were obtained by using N-methyl-2-pyrrolidinone as an eluent at room temperature. The molecular weight distribution observed in the GP chromatographies of bulk polyaniline and polyaniline extracted from both α- and "β"-(I) (α- and β-polyaniline) were multi-modal, similar to those of extracted PANI from $(PANI)_x V_2 O_5$ (vide supra). Interestingly, the polyaniline extracted from "β"-(I) and bulk polyaniline have similar molecular weight. As expected, the molecular weight of polyaniline extracted from "β"-(I) is higher than that from α-(I) as shown in Figure 5.10.
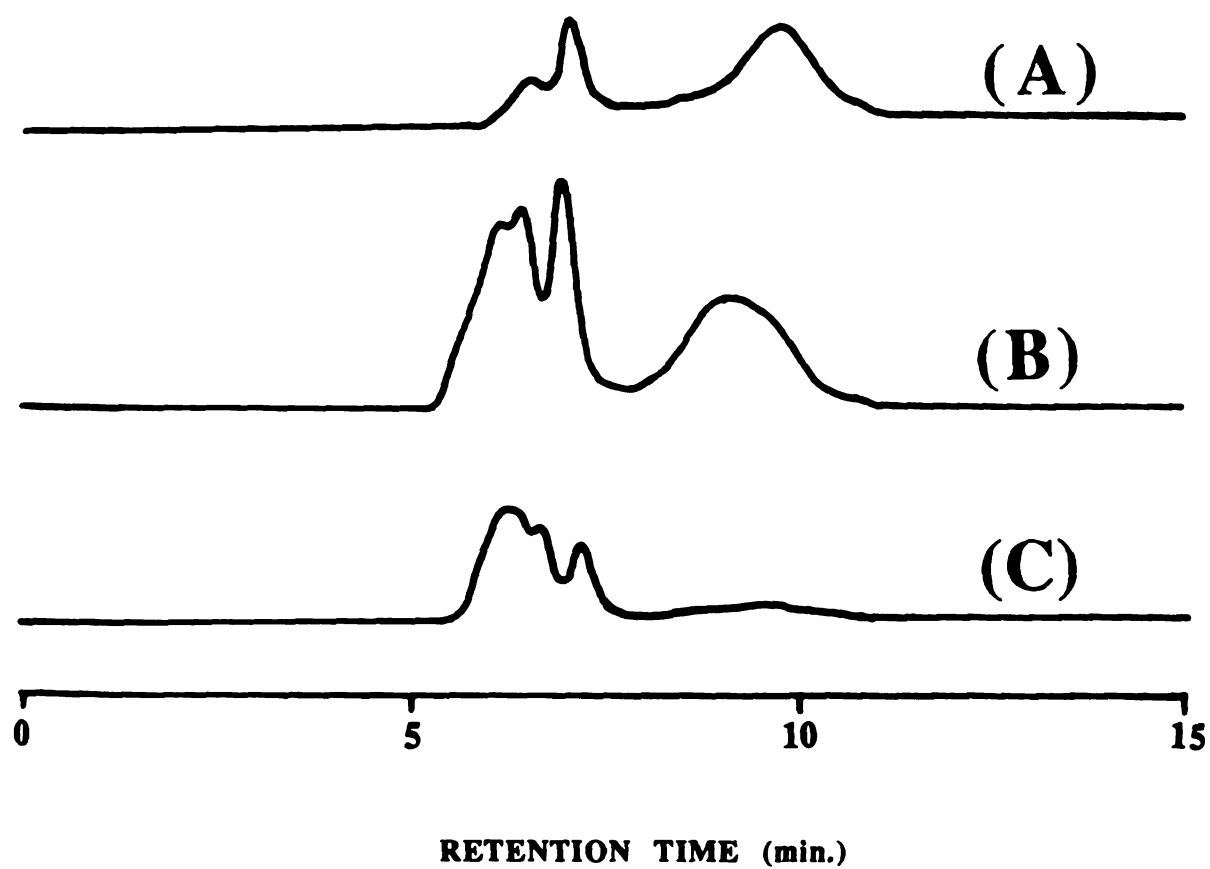
Figure 5.10. GPC diagrams of polyaniline extracted from (A) α-$(PANI)_x FeOCl$ (B) "β"-$(PANI)_x FeOCl$ (C) Bulk polyaniline.

G. Scanning Electron Microscopy (SEM) and Selected Area Electron Diffraction (SAED).

SEM microscopy of α-(PANI)$_x$FeOCl reveals a clearly lamellar nature and is consistent with a topotactic intercalation reaction in which the host framework remains intact. We found no morphological differences between the α- and "β" phases as shown in Figure 5.11. The topochemical reaction can be further confirmed by TEM SAED patterns. The SAED patterns of α-(PANI)$_x$FeOCl with the electron-beam perpendicular to the [0k0] planes showed the same (h0l) diffraction patterns as that of pristine FeOCl as shown in Figure 5.12. α-(PANI)$_x$FeOCl is a very beam sensitive material. However, electron diffraction studies on single crystals occasionally also showed interesting superlattice phenomena which quickly fades due to beam damage. Further investigations in this direction are in progress.

H. Thermogravimetric Analysis (TGA).

The thermal stabilities of α-, "β"-(PANI)$_x$FeOCl and FeOCl are different from one another. TGA diagrams of both α- and "β"-(PANI)$_x$FeOCl, under nitrogen, show two step decomposition patterns. A slow weight loss from 50°C to 625°C and a sharp weight loss at around 625°C are observed. In contrast, FeOCl is stable up to 450°C before it decomposes to Fe_2O_3 and $FeCl_3$ in one step.

Unlike FeOCl, the thermal stability of α-(PANI)$_x$FeOCl decreases significantly when oxygen is used as a carrier gas. Under oxygen the
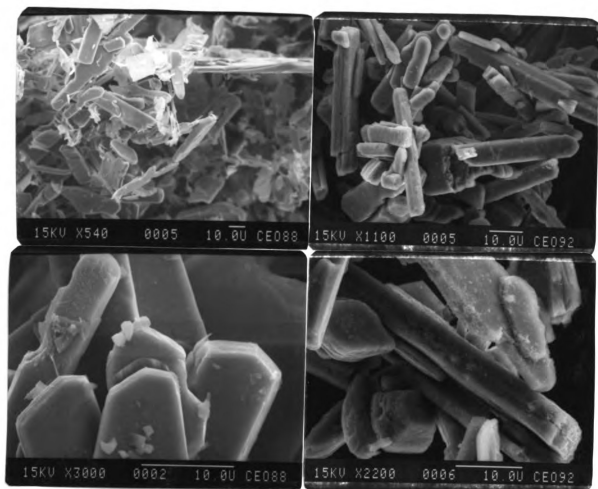
Figure 5.11. SEM micrographs of microcrystalline α- and "β"-(PANI)$_x$FeOCl.
left: α-(PANI)xFeOCl ; right: "β"-(PANI)$_x$FeOCl

Figure 5.12. Selected area electron diffraction pattern of α-(PANI)$_{0.20}$FeOCl.
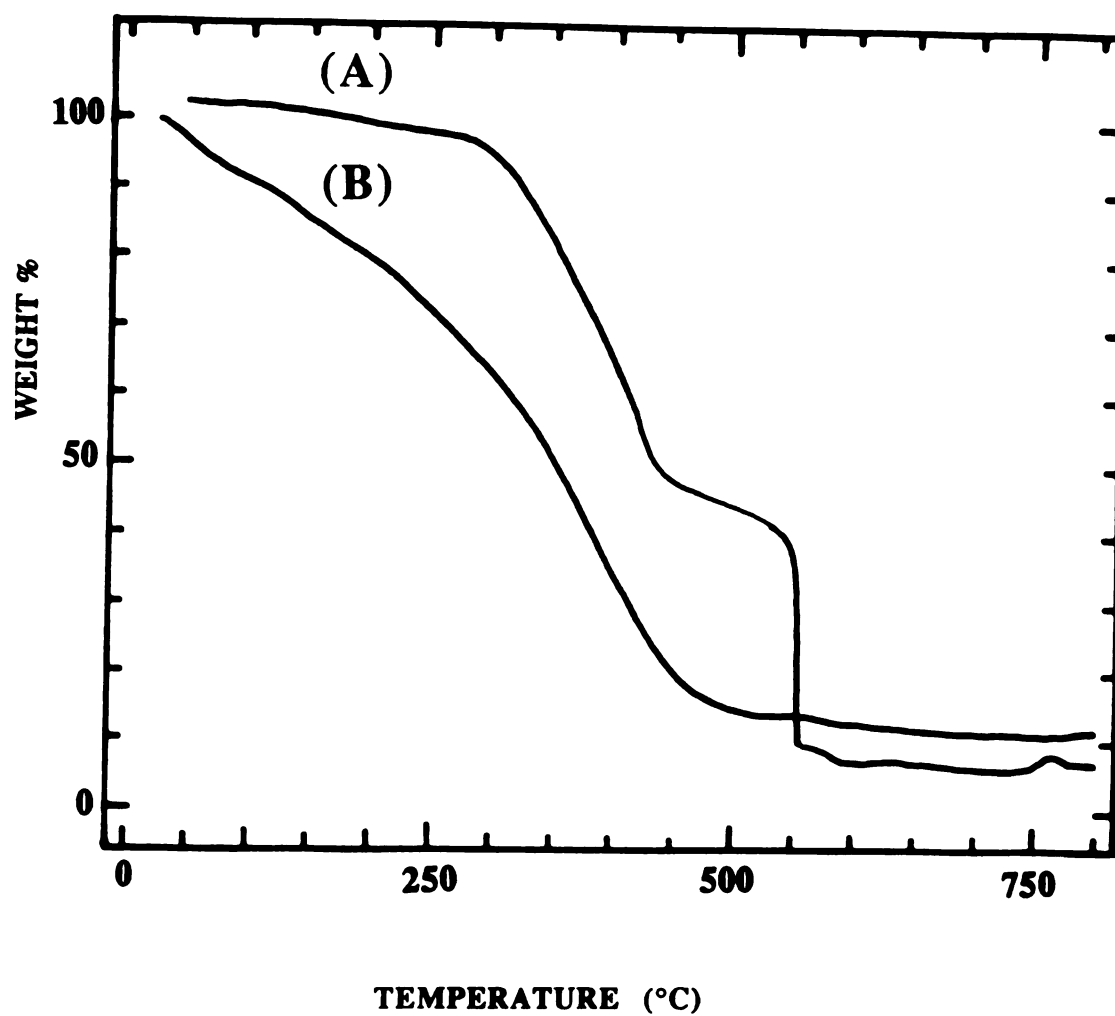
Figure 5.13. TGA curves (under nitrogen flow) of (A) α-(PANI)$_x$FeOCl (B) "β"-(PANI)$_x$FeOCl. (The heating rate was 5°C/min.)

α-(PANI)$_x$FeOCl loses weight slowly from 50°C to 350°C while a faster weight loss is observed from 350°C to 500°C. On the other hand, the "β" phase shows continuous weight loss from 50°C to 500°C as shown in Figure 5.13. Pyrolysis mass-spectroscopy of both α- and "β"-(PANI)$_x$FeOCl did not show any aniline or aniline oligomers at temperatures up to 350°C under vacuum. The weight loss at low temperature probably is due to the absorbed moisture or solvent and polymer backbone at high temperature.

I. Electron Paramagnetic Resonance (EPR) Spectroscopy.

The EPR spectra of α- and "β"-(PANI)$_x$FeOCl are very broad and complex to be of real characterization value. We examined these spectra in order to see whether we could observe the typical EPR S=1/2 singlet of polyaniline (emeraldine salt). Interestingly, the characteristic sharp EPR polaron signal did not show up in either α- or "β"- phase as shown in Figure 5.14, presumably due to exchange broadening with the paramagnetic FeOCl layers. In a control experiment, finely divided mixtures of (PANI)Cl/FeOCl and (PANI)Cl/α-(PANI)$_x$FeOCl showed the narrow characteristic S=1/2 signal of PANI at g=2.0023. The absence of PANI signal from "β"-(I) indicates that the polymer is very close to (<~15 Å) the ferromagnetic centers, Fe atoms. This indicates that "β"-(I) is a composite with intimate mixed polyaniline and β-FeOOH, although it is not a single phase.

(A)

DPPH

(B)

(C)

2900   3400   3900

MAGNETIC FIELD (Gauss)
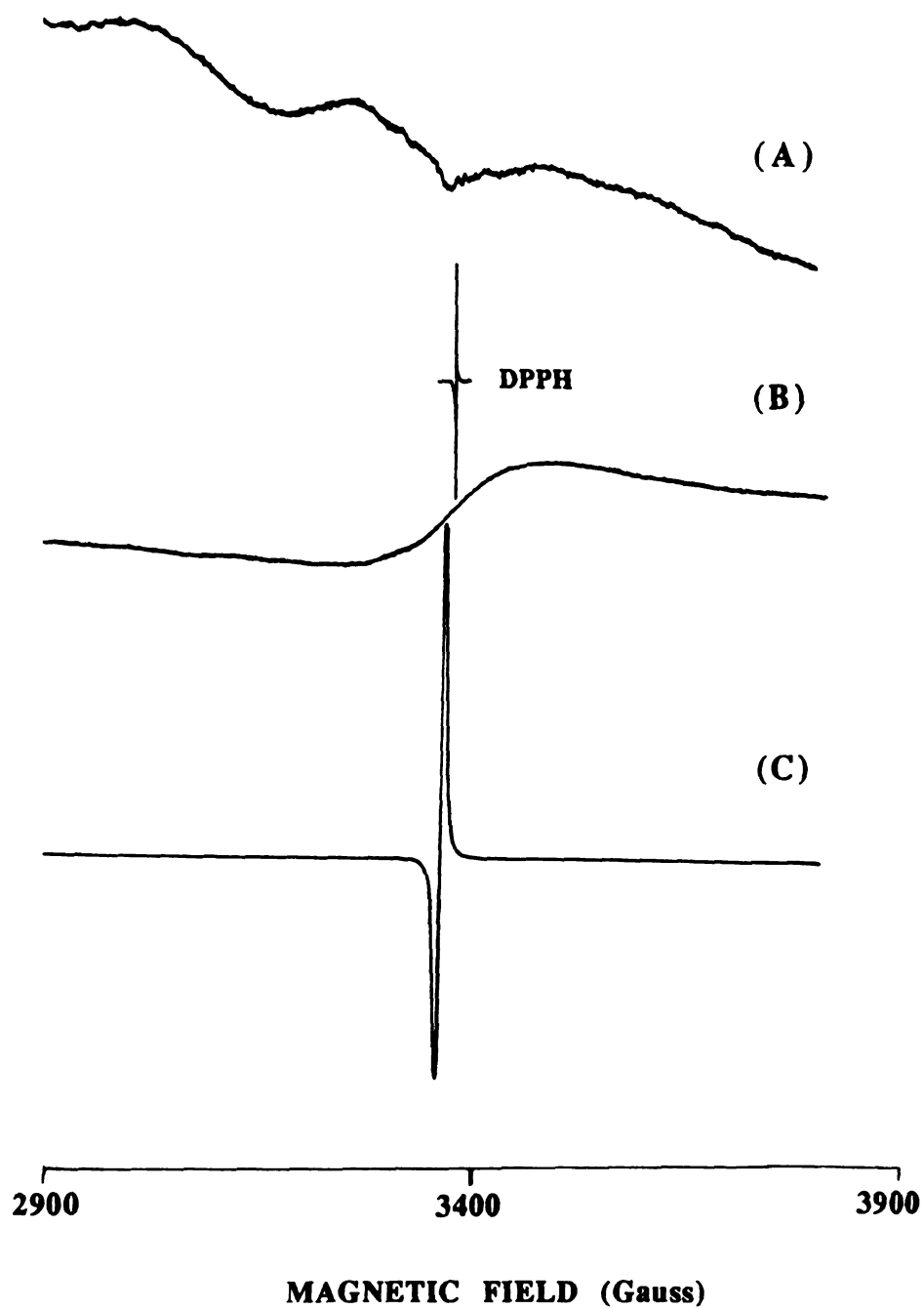
Figure 5.14.   Room temperature EPR spectra of (A) α-(PANI)$_x$FeOCl (B) "β"-(PANI)$_x$FeOCl   (C) Extracted polyaniline.

J. Magnetic Susceptibility Studies.

FeOCl is a quasi-two-dimensional antiferromagnetic compound. The temperature dependence of the magnetic susceptibility of microcrystalline FeOCl has been studied extensively by several groups [24], yet it remains ill-understood. Bizette and Adam [23] reported a characteristic Curie-Weiss antiferromagnetic behavior, with a large anomaly at 22 K. However, in the investigation by Halbert [23,25] et al., the susceptibility displayed a small cusp at 15 K and a broad maximum at approximately 350 K. A recent study on single crystals by Herber and coworkers [19], reported a slow increase in susceptibility to a broad maximum at 310 ± 10 K and a discontinuity in the $d(\chi T)/dT$ curve at 84 ± 1 K. We note that to date no fundamental understanding of the magnetic behavior of pristine FeOCl exists which complicates further the understanding of the magnetism of its intercalation compounds.

In the present work, the susceptibility data were recorded from 5 K to 300 K in a constant field (5000 gauss). Variable temperature magnetic susceptibility data of the α-(I) and "b"-(I) are shown in Figure 5.15. The magnetic behavior of α-(I) is similar to that of FeOCl except for a low temperature Curie tail. The similar susceptibilities suggest that the short range magnetic interactions observed in FeOCl are also present in α-(I). The spin-only magnetic moment (μ_{eff}) of the α-(I) is 2.8 BM, at room temperature, which is slightly higher than that of FeOCl, but much lower than the theoretical high-spin Fe^{3+} (5.9 BM) or Fe^{2+} (4.9 BM) value. Table 5.2 lists the room temperature μ_{eff} of $(PANI)_x FeOCl$ with various x.
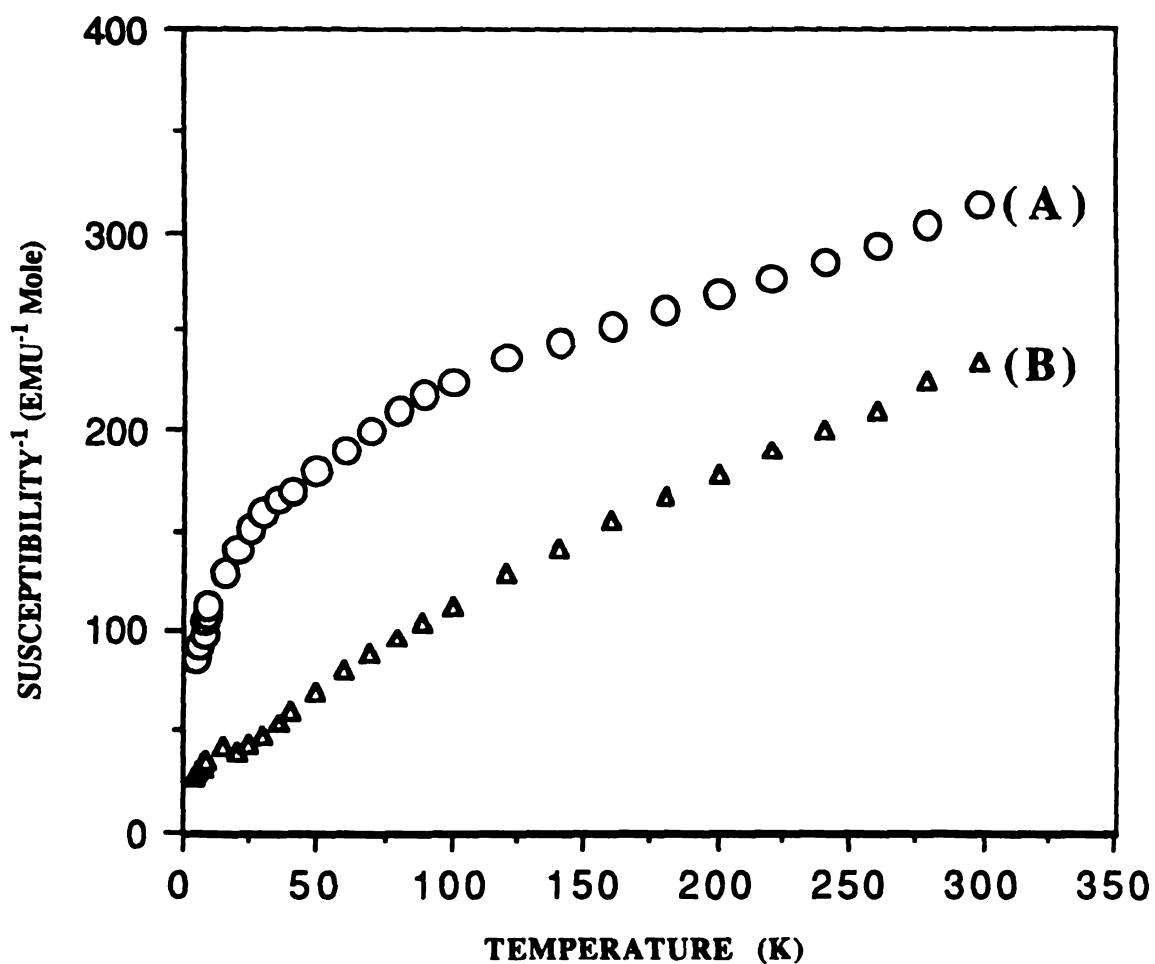
Figure 5.15. Variable temperature magnetic susceptibility data($1/\chi_m$) of (A) α-(PANI)$_{0.2}$FeOCl (B) "β"-(PANI)$_{0.2}$FeOCl.

Table 5.2. **Room Temperature Spin-only Magnetic Moment** (μ_{eff}) **versus x of** α- **and** "β"-$(PANI)_xFeOCl$

Compounds	$\mu_{eff(R. T.)}$ (BM)
α-$(PANI)_{0.16}FeOCl$	2.77
"β"-$(PANI)_{0.16}FeOCl$	3.19
"β"-$(PANI)_{0.17}FeOCl$	3.05
α-$(PANI)_{0.20}FeOCl$	2.77
"β"-$(PANI)_{0.20}FeOCl$	3.21
α-$(PANI)_{0.28}FeOCl$	2.87

The "β" phase shows paramagnetic behavior, with the susceptibility decreasing with increasing temperature with a slight deviation from Curie-Weiss law, Figure 5.15b. The room temperature μ_{eff} is equal to 3.2 BM. The long range magnetic order is observed in a wide temperature range (5~300 K). The μ_{eff} for both phases varies with temperature as shown in Figure 5.16. The steady increase of μ_{eff} with temperature indicates antiferromagnetic coupling of the magnetic spins located in polyaniline and in FeOCl. In general the "β" phase has higher magnetic moment than α-(I). The magnetic behavior of α-(I) is similar to FeOCl (antiferromagnetic) while the behavior of the "β" phase is closer to polyaniline (paramagnetic). It is known that protonated polyaniline is a paramagnetic material due to the proton induced spin generation (polarons) and its susceptibility depends on the degree of protonation [24] with highest Pauli susceptibility (χ^{Pauli}) equal to 100×10^{-6} (emu/mole 2 rings). This χ^{Pauli} is relatively small compare to the susceptibility of "β"-(I). Therefore, the magnetic moments of both α- and "β"-(PANI)FeOCl mostly comes from FeOCl.

K. Charge Transport Properties.

(a). Electrical Conductivity Studies.

α-(PANI)$_x$FeOCl: Samples of α-(I) were studied in a pressed pellet and single crystal form by ac and dc electrical conductivity measurements using the four-probe geometry. Room temperature conductivities for pressed pellets and single crystals for several α-
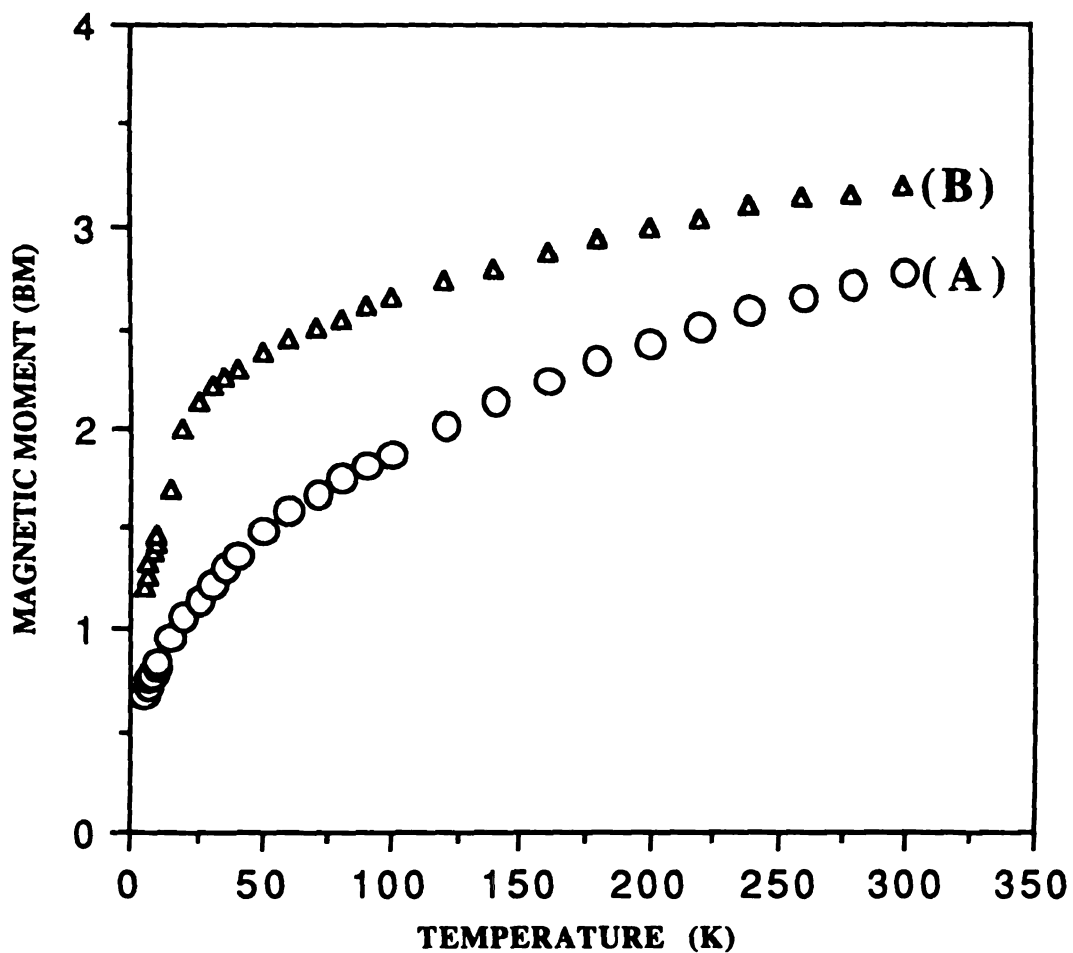
Figure 5.16. Variable temperature effective spin-only magnetic moment of (A) α-$(PANI)_{0.20}FeOCl$ (B) "β"-$(PANI)_{0.16}FeOCl$.

and "β"- $(PANI)_x FeOCl$ samples are given in Table 5.3. We found, by X-ray diffraction, that in pressed pellets significant orientation effects are present which cause the crystallites to orient with their crystallographic ac-planes perpendicular to the pressing axis. Thus, the measurements were carried out parallel to the ac-plane. Interestingly, the observed conductivities of the pressed pellets were not dramatically lower than those obtained from single crystal samples. Figure 5.17 shows the temperature dependence of the electrical conductivity of α-(I) in pressed pellet and single crystal form. The latter is only 10 times greater, $7.5x10^{-2}$ $\Omega^{-1}cm^{-1}$ at room temperature, than the polycrystalline value even though at lower temperatures this difference becomes greater. A significant feature of the single crystal data is the thermally activated temperature dependence of the conductivity, suggesting that the material is a semiconductor. The powder-like conductivity behavior of α-(I) may be due to several factors, including domain boundaries in the crystals due to fracture upon intercalation and most likely the finite length of polyaniline chains in the interlamellar space which may generate large activation barriers for carrier hopping from chain end to chain end. Overall, the electrical conductivity of α-(I) is lower than that of bulk polyaniline by approximately two orders of magnitude. This disparity probably reflects the differences in morphology between the two samples (films of polyaniline are smoother and more continuous) and the higher carrier density per unit volume in bulk polyaniline compared to α-(I) which is only ~15% polyaniline by weight. Furthermore, the molecular weight of the polyaniline chains in α-(I) is expected to be lower and thus more carrier hopping

Table 5.3. Room Temperature Electrical Conductivity (σ) of α- and "β"-$(PANI)_xFeOCl$.

Samples	Conductivity ($\Omega^{-1}cm^{-1}$)	Sample form
α-$(PANI)_{0.20}FeOCl$	$10^{-3} \sim 10^{-2}$	powder
α-$(PANI)_{0.23}FeOCl$	$10^{-3} \sim 10^{-2}$	powder
α-$(PANI)_{0.32}FeOCl$	$10^{-3} \sim 10^{-2}$	powder
α-$(PANI)_{0.24}FeOCl$	$10^{-2} \sim 10^{-1}$	single crystal
α-$(PANI)_{0.28}FeOCl$	$10^{-2} \sim 10^{-1}$	single crystal
"β"-$(PANI)_{0.16}FeOCl$	$10^{-2} \sim 10^{-1}$	powder
"β"-$(PANI)_{0.17}FeOCl$	$10^{-2} \sim 10^{-1}$	powder
"β"-$(PANI)_{0.20}FeOCl$	10^{-1}	powder
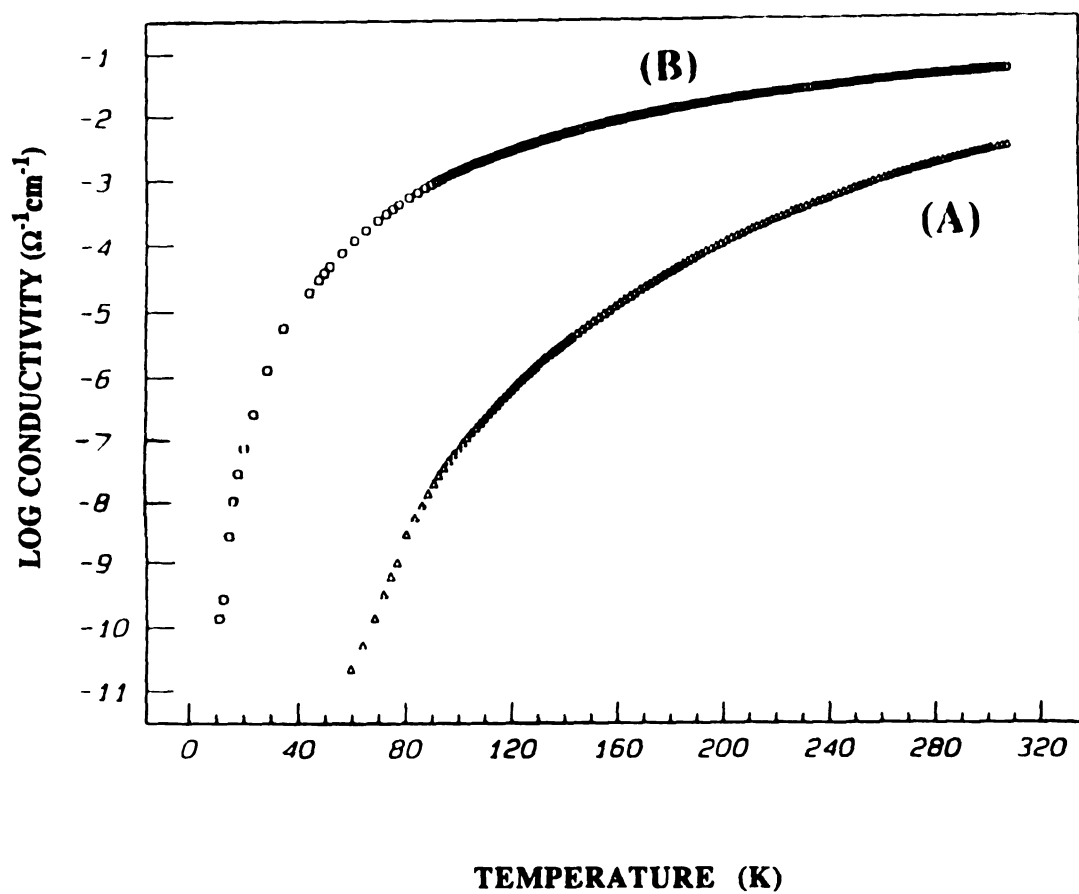
Figure 5.17. Four-probe variable temperature electrical conductivity data of α-$(PANI)_{0.23}FeOCl$ in (A) Pressed pellet (B) Single crystal form.

barriers are present resulting in lower conductivity. Another reason for the lower conductivity may be the lower intrinsic conductivity of FeOCl layers themselves which in single crystal intercalated form exhibit only $\sim 10^{-3}$ $\Omega^{-1}cm^{-1}$ at room temperature. The reduced FeOCl layers could act as barriers for electron hopping between polyaniline chains. α-(I) has lower conductivity than $(Ppy)_{0.34}FeOCl$ [12] and $(Pth)_{0.24}FeOCl$ [13] by an order of magnitude. This parallels the trend observed in the corresponding bulk samples which show that polyaniline is always less conductive than polypyrrole and polythiophene. However, α-(I) is significantly more conductive than other FeOCl intercalation compounds containing molecular guests as listed in Table 5.4. In considering the electrical properties of α-(I), the conductivity of the reduced FeOCl framework must be considered. A good representation of the ability of reduced FeOCl to transport electrical charge comes from the electrical properties of molecular intercalates of this host. For example, samples of $(pyridine)_{0.33}FeOCl$ [26], $(TTF)_{0.125}FeOCl$ [26] and $(ferrocenium)_{0.5}FeOCl$ [27] display maximum conductivities at room temperature of 10^{-3} $\Omega^{-1}cm^{-1}$. The electrical conductivity of FeOCl is due to the small but finite mobility of 3d electrons in Fe^{2+} and Fe^{3+} in FeOCl slabs [28]. The pristine FeOCl (all Fe^{3+}) is an insulator. Since FeOCl layers alternate with PANI in α-(I) the overall conductivity will be limited by the ability of the carriers to transport in a direction perpendicular to the layers. This ability is higher parallel to the layers, which makes α-(I) a very anisotropic material. The true conductivity of the confined PANI chains is difficult to assess but it is expected to be much higher than the observed values.

Table 5.4. The Interlayer Spacing (d) and Room Temperature Electrical Conductivity (σ) of Several Intercalation Compounds of FeOCl.

Compounds	d (Å)	σ ($\Omega^{-1}cm^{-1}$)	Reference
$(TTF)_{0.1}FeOCl$	13.63	3.5×10^{-3}	26
$(TTT)_{0.14}FeOCl$	15.22	2.2×10^{-4}	26
$(TTN)_{0.5}FeOCl$	15.31	5.5×10^{-4}	26
$(TMTTF)_{0.08}FeOCl$	11.32	1.6×10^{-2}	31
$(Ppy)_{0.34}FeOCl$	13.21	1.5×10^{-1}	13
$(Pth)_{0.28}FeOCl$	13.31	5.0×10^{0}	14
$(Ferrocene)_{0.17}FeOCl$	14.92	1.0×10^{-4}	27
$(Perylene)_{0.11}FeOCl$	16.69	2.3×10^{-2}	32
$(TSF)_{0.12}FeOCl$	13.52	5.0×10^{-3}	33
$(TMTSF)_{0.10}FeOCl$	13.82	5.4×10^{-3}	33
$(ET)_{0.25}FeOCl$	22.18	2.6×10^{-3}	34
$(PANI)_{0.20-0.28}FeOCl$	13.92	$10^{-3} \sim 10^{-1}$	this work

Attempts to extract the PANI chains from single crystal α-(I) and still keep them oriented failed, giving rise to an amorphous polymer. The room temperature conductivity of extracted polymer is 8.5×10^{-1} $\Omega^{-1}cm^{-1}$. The conductivity of polyaniline extracted from both α- and "β"-(I) is lower than that extracted from single crystal α-(I), imply that the latter may contain longer conjugated segments. More work is needed to confirmed this assertion. It would be interesting to know whether the electrical properties of these materials originate from either of the individual components (is FeOCl, PANI) or are the result of a combined, cooperative effect. Thermoelectric power measurements may provide a better insight into this question (vide infra).

"β"-$(PANI)_x$FeOCl: The conductivity of "β"-(I) is ten times higher than that of α-(I) as shown in Figure 5.18. This suggests the presence of longer chains of polyaniline in the oxidized product. The IR and GPC data support this hypothesis (vide supra). Direct evidence comes from the comparison of the conductivity of polyaniline extracted from α-(I) and "β" phase as shown in Figure 5.19. The polymer extracted from "β" phase is 100 times more conductive than that from the corresponding α-phase, consistent with longer chain lengths of polymer in "β" phase.

(b).Thermoelectric Power (Seebeck coefficient) Studies.

The conductivity measurements alone can not unequivocally characterize the electrical behavior of α-(I). A complementary probe to address this issue is thermoelectric power (TP) measurements as a
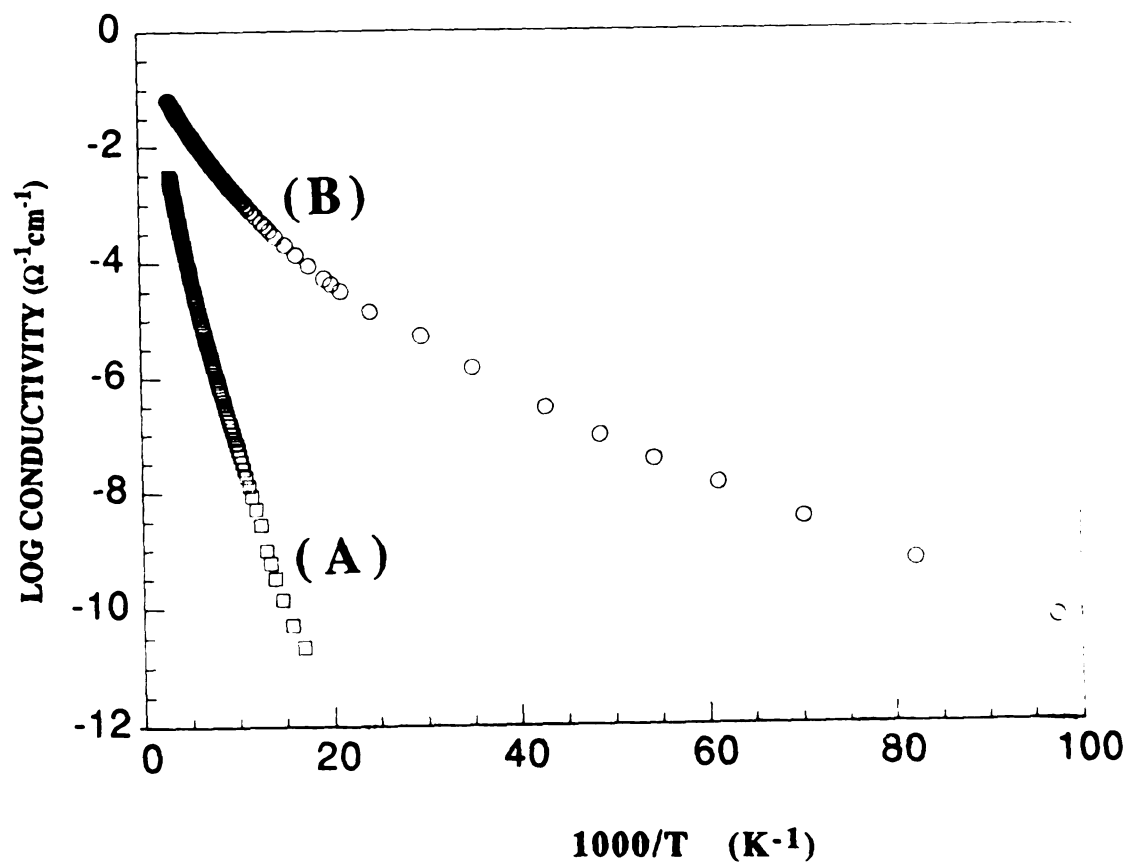
Figure 5.18. Four-probe variable temperature electrical conductivity data of pressed pellets of (A) α-(PANI)$_{0.17}$FeOCl (B) "β"-(PANI)$_{0.17}$FeOCl.
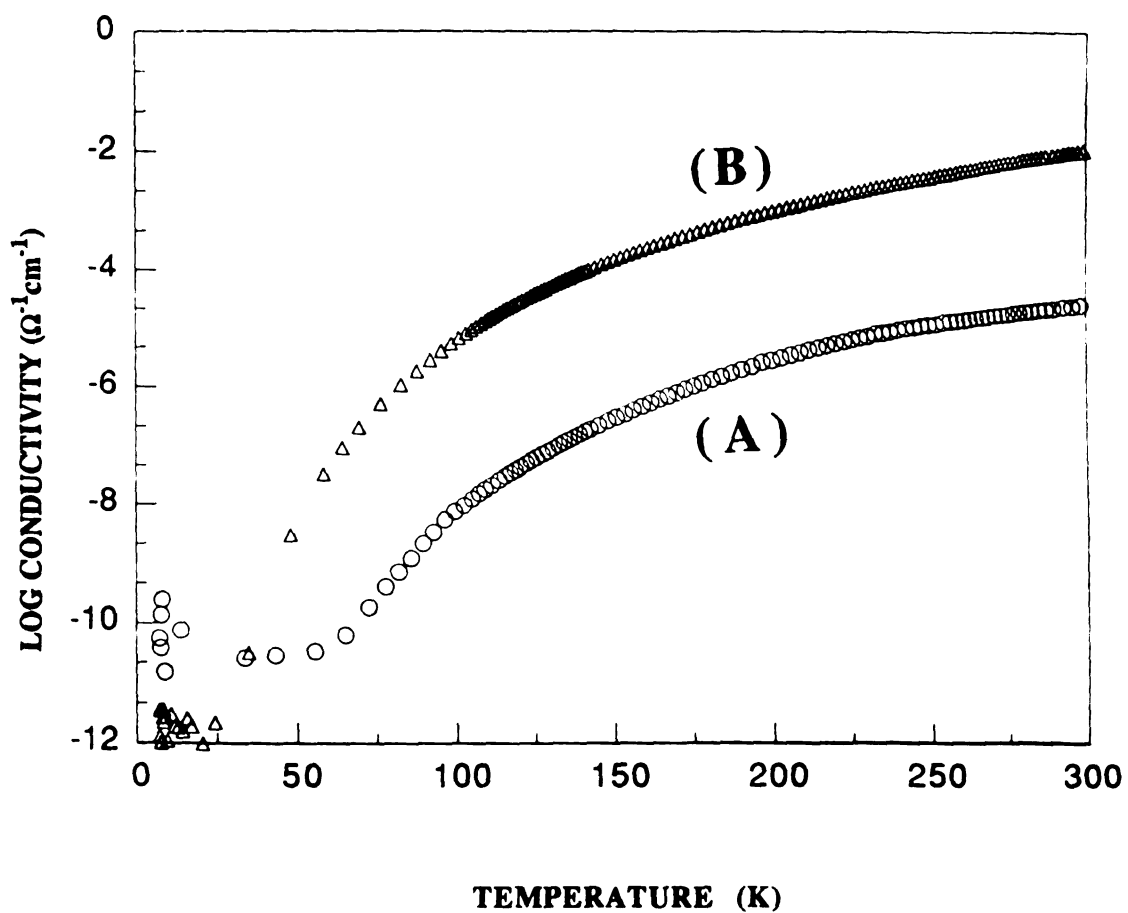
Figure 5.19. Four-probe variable temperature electrical conductivity data of pressed pellets of polyaniline extracted from (A) α - $(PANI)_{0.17}FeOCl$ (B) "β" - $(PANI)_{0.17}FeOCl$.

function of temperature. TP measurements are typically far less susceptible to artifacts arising from the resistive domain boundaries in the material because they are essentially zero-current measurements. The reason for this is because temperature drops across such boundaries are much less significant than voltage drops. Figure 5.20. shows typical TP data of α-(I) and "β" phase as a function of temperature. Accurate measurements at low temperatures were hindered by the very large sample resistivities. The room temperature TP of α-(I) is slightly positive (close to zero) and increases steadily with decreasing temperature, reaching the value of 100~400 μV/K at 150 K. The single crystal of α-$(PANI)_x FeOCl$ shows the same behavior. This behavior is characteristic of a p-type semiconductor, similar to that observed for (ferrocenium)$_{0.50}$FeOCl [27], but different from (Ppy)$_{0.34}$FeOCl [12] and (Pth)$_{0.24}$FeOCl [13] which show p-type metallic character. Since the emeraldine salt of polyaniline shows metal-like TP behavior [32], we can conclude that in α-$(PANI)_x FeOCl$, the reduced FeOCl framework dominates the charge transport properties. This can be explained by the formation of short polymer chains of polyaniline in the interlayer space which obstructs the chain to chain charge transport by introducing too many hopping barriers thus making charge transport through FeOCl layers more favorable.

Interestingly, the TP behavior of the "β" phase is dramatically different. The Seebeck coefficient is negative in this case indicating a conductivity change from p-type to n-type with typical value of around 0~2 μV/K , similar to the conducting form of polyaniline [29,30]. Unfortunately, there is little information available on the
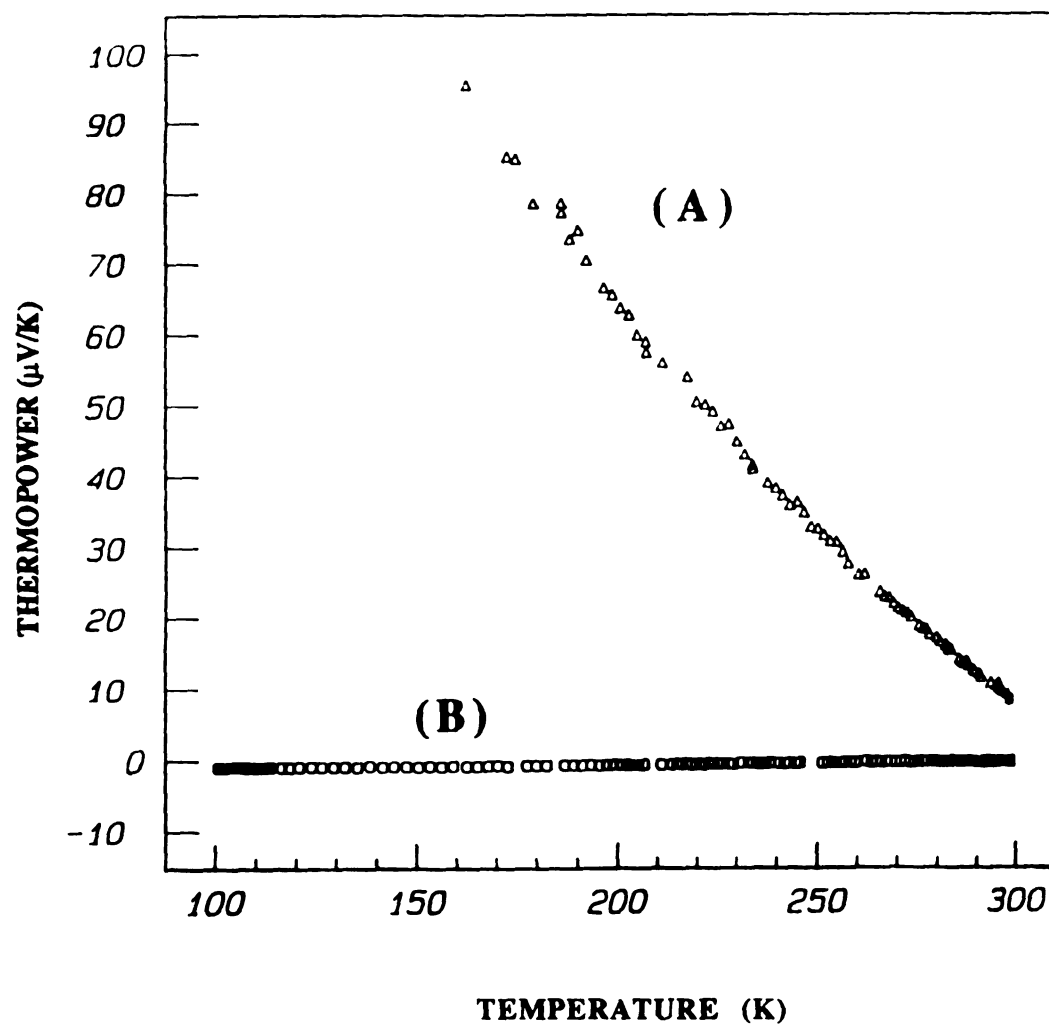
Figure 5.20. Variable temperature thermoelectric power data of (A) α-$(PANI)_{0.17}FeOCl$ (B) "β"-$(PANI)_{0.17}FeOCl$.

electrical properties of the yellow colored β-FeOOH. However, we expect the material to be an insulator. This is in agreement with our other experimental evidence that "β" phase is actually a mixture of PANI and β-FeOOH.

VI. Conclusions:

Conducting polyaniline (emeraldine salt) was formed inside FeOCl by an *in-situ* oxidative polymerization/ intercalation reaction between aniline and FeOCl. The rate of reaction under air is faster than under nitrogen because molecular oxygen acts as an electron and proton acceptor. The resulting crystalline compound, α-$(PANI)_x$FeOCl, consists of alternating monolayers of conducting polymer and inorganic framework FeOCl. The room temperature conductivity of α-$(PANI)_x$FeOCl is 10^{-2} $\Omega^{-1}cm^{-1}$ with typical p-type semiconductor behavior. The polyaniline chain-length inside the FeOCl layer continues to grow with time in the presence of ambient oxygen and moisture. At the same time hydrolysis of the FeOCl framework occurs to yield β-FeOOH. The conductivity of this intimate mixture is 10 times higher than α-$(PANI)_x$FeOCl and the thermopower is similar to the conducting polyaniline.

When single crystal FeOCl was used, polyaniline can be intercalated inside FeOCl without losing the crystallinity of the material. X-ray and electron diffraction studies show a superlattice formation in the product, confirming the regular arrangement of polyaniline chains in the FeOCl layers. Using crystalline host,

oriented conducting polymers can be obtained by *in-situ* oxidative polymerization/ intercalation reaction.

LIST OF REFERENCES

LIST OF REFERENCES

1. (a) Ito, T.; Shirakawa, H.; Ikeda, S. *J. Polym. Chem. Ed.* **1974**, <u>12</u>, 11. (b) Chiang, C. K.; MacDiarmid, A. G.; Park, Y. W; Shirakawa, H. *J. Am. Chem. Soc.* **1978**, <u>100</u>, 1013-1015.

2. Kanatzidis, M. G. *Chemical&Engineering News* "Special Report" **1990**, <u>68</u>, 36-54.

3. Letherby, H. *J. Chem. Soc.* **1862**, <u>15</u>, 161-163.

4. (a) MacDiarmid, A. G.; Epstein, A. J. *Faraday Disscuss Chem. Soc.* **1989**, <u>88</u>, 317-332. (b) Epstein, A. J.; Ginder, J. M.; Zuo, F.; Woo, H. S.; Tanner, B. D.; Richter, A. F.; Angelopoulos, M.; Huang, W. S.; MacDiarmid, A. G. *Synth. Met.* **1987**, <u>21</u>, 63-70.

5. See chapter 1.

6. (a) Tan, F. R.; Bard, A. J. *J. Electrochem. Soc.* **1986**, <u>133</u>, 301-304. (b) Penner, R. M.; Martin, C. R. *J. Electrochem. Soc.* **1986**, <u>133</u>, 310-315.

7. Jozefowicz, M. E.; Epstein, A. J.; Pouget, J. P.; Masters, J. G.; Sun, A. R. Y.; Tang, X.; MacDiarmid, A. G. Proc. ICSM 1906 (Tubingen, Sept. 1990) *Synth. Met.* **1991**, <u>41</u>, 723-726.

8. Baughman, R. H.; Wolf, J. F.; Eckhardt, H.; Shacklette, L. W. *Synth. Met.* **1988**, <u>25</u>, 121-137.

9. Inoue, H.; Yoneyama, H. *J. Electroanal. Chem.* **1987**, <u>233</u>, 291-294.

10. Brandt, P.; Fisher, R. D.; Martinez, E. S.; Calleja, R. D. *Angew. Chem. Int. Ed. Engl.* **1989**, <u>28</u>, 1265-1266.

11. (a) Enzel, P.; Bein, T. *J. Phys. Chem.* **1989**, 93, 6270-6272. (b) Bein, T.; Enzel, P. *Synth. Met.* **1989**, 29, E163-E168. (c) Enzel, P.; Bein, T. *J. Chem. Soc. Chem. Commun.* **1989**, 1326-1327. (d) Caspar, J. V.; Ramamurthy, V.; Corbin, D. R. *J. Am. Chem. Soc.* **1991**, 113, 600-610.

12. Lind, M. D. *Acta. Cryst.* **1970**, B20, 1058-1062.

13. (a) Kanatzidis, M. G.; Tonge, C. R.; Marks, T. J.; Marcy, H. O.; Kannewurf, C. R. *J. Am. Chem. Soc.* **1987**, 109, 3797-3799. (b) Kanatzidis, M. G.; Marcy, H. O.; McCarthy, W. J.; Kannewurf, C. R.; Marks, T. J. *Solid State Ionics* **1989**, 32/33, 594-608.

14. Kanatzidis, M. G.; Wu, C. G.; Marcy, H. O.; DeGroot, D. C.; Kannewurf, C. R. *Adv. Mater.* **1990**, 2, 364-366.

15. Kauzlarich, S. M.; Teo, B. K.; Averill, B. A. *Inorg. Chem.* **1986**, 25, 1209-1215.

16. Cao, Y.; Li, S.; Xue, Z.; Guo, D. *Synth. Met.* **1986**, 16, 305-315.

17. Maeda, Y.; Yamashita, M.; Ohshio, H.; Tsutsumi, N.; Takashima, Y. *Bull. Chem. Soc. Jpn.* **1982**, 55, 3138-3143.

18. See chapter 6.

19. (a) Wheland, R. C.; Gillson, J. L. *J. Am. Chem. Soc.* **1976**, 98, 3916-3925. (b) Palvadeau, P.; Coic, L.; Rouxel, J. *Mater. Res. Bull.* **1981**, 16, 1055-1065.

20. Bizette, H.; Adam, A. *C. R. Acad. Sci. Paris Ser.* B **1972**, 275, 911-913.

21. Halbert, T. R.; Johnston, D.C.; McCandish, L. E.; Thompson, L. J.; Scanion, J. C.; Dumesic, J. A. *Physica* B, **1980**, 99, 128-132.

22. McCall, R. P.; Ginder, J. M.; Leng, J. M.; Coplin, K. A.; Ye, H. J.; Epstein, A. J.; Asturias, G. E.; Manohar, S. K.; Masters, J. C.; Scherr, E. M.; Sun, Y.; MacDiarmid, A. G. *Synth. Met.* **1991**, 41-43, 1329-1332

23. Phillips, J. E.; Herber, R. H. *Inorg. Chem.* **1986**, 25, 3081-3088.

24. (a) Epstein, A. J.; Ginder, J. M.; Zuo, F.; Bigelow, R. W.; Woo, H. S.; Tanner, D. B.; Richter, A. F.; Huang, W. S.; MacDiarmid, A. G. *Synth. Met.* **1987**, 18, 303-309. (b) Ginder, J. M.; Richter, A. F.; MacDiarmid, A. G.; Epstein, A. J. *Solid State Commun.* **1987**, 63, 97-101.

25. Halbert, T. R.; Johnston, D. C.; McCaxdish, L. E.; Thompson, L. J.; Scanion, J. C.; Dumesic, J. A. *Physica* B, **1980**, 99, 128-132.

26. Averill, B. A.; Zauzlarich, S. M.; Antonio, M. R. *J. De Phys.* **1983**, C3-1373-C3-1376.

27. Villeneuve, G.; Dordor, P.; Palvadeau, P.; Venien, J. P. *Mater. Res. Bull.* **1982**, 17, 1407-1412.

28. Malhotra, B. D.; Kumar, N.; Chandra, S. *Prog. Polym. Sci.* **1986**, 12, 179.

29. (a) Park, Y. W.; Lee, Y. S.; Park, C. *Solid State Commun.* **1987**, 63, 1063-1066. (b) Zuo, F; Angelopoulos, M.; MacDiarmid, A. G.; Epstein, A. *J. Phys. Rev.* **1987**, B36, 3475-3478.

30. Nechtschein, M.; Santier, C.; Travers, J. P.; Chroboczek, J.; Alix, A.; Ripert, M. *Synth. Met.* **1987**, 18, 311-316.

31. Kauzlarich, S. M.; Ellena, J. F.; Ttupik, P. D.; Reiff, W. M.; Averill, B. A. *J. Am. Chem. Soc.* **1987**, 109, 4561-4570.

32. Bringley, J. F.; Averill, B. A. *J. Chem. Soc. Chem. Comm.* **1981**, 282-283.

33. Bringley, J. F.; Averill, B. A. *Mol. Cryst. Liq. Cryst.* **1988**, 170, 215-222.

34. Bringley, J. F.; Fabre, J. M.; Averill, B. A. *J. Am. Chem. Soc.* **1990**, 112, 4577-4579.

CHAPTER 6

A NEW ROUTE TO CHEMICAL POLYMERIZATION OF POLYFURAN

~ INTERCALATION OF TERFURAN IN FeOCl

ABSTRACT

Intercalation of polyfuran in FeOCl can be achieved by *in-situ* oxidative polymerization/ intercalation of terfuran and quaterfuran. Two products were isolated using different preparation procedures. In one, the organic monomer is refluxed with FeOCl in CH_3CN or MeOH, to produce r-$(PFu)_xFeOCl$. In the other, the reaction is carried out methanothermally at 100°C to produce m-$(PFu)_xFeOCl_y(OMe)_{1-y}$. The interlayer spacing of the two different products are 13.60Å and 15.62Å respectively. Although the two furan polymers formed inside both products are identical, the Cl atoms in FeOCl of the methanothermally prepared phase were partially replaced by methoxy groups. The physicochemical properties of the two products are very similar, except for their charge transport properties. The room temperature conductivity of r-$(PFu)_xFeOCl$ is in the range of 10^{-3} to 10^0 $\Omega^{-1}cm^{-1}$ while m-$(PFu)_xFeOCl_y(OMe)_{1-y}$ is in the range of 10^{-4} to 10^{-2} $\Omega^{-1}cm^{-1}$. The conductivity of both materials is independent of the polymer content and it is thermally activated. Variable temperature thermoelectric power of both phases reveal p-type semiconducting behavior. It is likely that in these materials the charge transport properties are dominated by the reduced FeOCl framework. Polyfuran extracted from $(PFu)_xFeOCl$ has smaller magnetic moment than bulk polyfuran with the same counterion, Cl^-, and it is essentially insulating.

I. Introduction:

The redox intercalation of conducting polymers, such as polypyrrole, polythiophene and polyaniline in layered hosts has been extensively studied. Our general goal is: to intercalate conducting polymers into structurally restricted hosts to obtain oriented polymers. These polymer derived composites may be characterized by crystallographic methods, as well as investigated a new class of materials with anisotropic electronic properties. To expand this interesting field of research, we investigated another conducting polymer, polyfuran [1]. In the literature, oligomers up to hexafuran have been known [2]. They are prepared, in low yields, from the couping of shorter chain oligomers or monomers and involve complicated organic synthesis [2]. There are no detailed studies of the structure and physicochemical properties of this polymer.

Similar to polypyrrole and polythiophene, polyfuran synthesis has been attempted by chemical [3] or electrochemical [1,4] polymerization of furan and its derivatives. However, due to the lower aromaticity of furan compared to pyrrole and thiophene, the conjugation of furan was easily destroyed during or after polymerization [4,5]. The resulting insulating polymer sometimes showed brown color with several structural defects, such as hydrogenation and ring opening. As a result studies on polyfuran have not been aggressively pursued. However, if oligomers of furan, such as bifuran, terfuran and tetrafuran, are used as starting materials, polymer with less structural defects may be obtained, due to two reasons: first, the oligomers have longer effective conjugation

length; second, their lower oxidation potentials compared to furan itself offer a relatively mild polymerization condition which may reduce the formation of structural defects in the polymer. Recently, we established a new route of synthesizing polyfuran by *in-situ* oxidative polymerization/ intercalation of terfuran and tetrafuran in FeOCl interlamellar space [6].

The redox intercalation of FeOCl with various organic molecules is well known [7] during which the organic species are oxidized and the FeOCl framework is reduced. The lower oxidative potential of terfuran and tetrafuran enable this redox intercalation reaction. This chapter describes in detail the redox intercalation of terfuran in FeOCl and the physicochemical properties of the resulting products. At the same time, due to the lack of available information in the literature for comparison, we also prepared bulk polyfuran by chemically ploymerizing terfuran with $FeCl_3$ in nitrogen atmosphere using acetonitrile as a solvent at room temperature (the dopant ion in this material is Cl^- or $FeCl_4^-$). Some physicochemical data of bulk polyfuran are used to compare with polyfuran extracted from $(PFu)_xFeOCl$.

II. Experimental Section:

Reagents: $FeCl_3$, Fe_2O_3, iso-propanol (i-PrOH), iso-butanol (i-BuOH) and 100% ethanol (EtOH) were purchased from commercial sources and were used without further purification. CH_3CN, MeOH and dimethylformamide (DMF) were dried over CaH_2 and distilled prior to use. Terfuran and quaterfuran were provided by M. Benz

and Professor LeGoff in the Department of Chemistry at Michigan State University.

Physicochemical Methods.

See chapter 2.

Synthesis of FeOCl.

See page 211.

Synthesis of Bulk Polyfuran, $(PFu)_x FeCl_4$.

In a nitrogen glove box, 0.2 g (1.0 mmol) of terfuran was dissolved in 30 ml CH_3CN. To this solution was added 30 ml 3.33 wt% of $FeCl_3$ acetonitrile solution. The mixture was stirred at room temperature for 9 hours. The black solid was isolated by filtration, washed with CH_3CN then ether and dried in vacuum. It was characterized by FTIR spectroscopy [8]. Elemental analysis: Calcd for $(C_4H_2O)(FeCl_4)_{0.063}$: C, 61,19%; H, 2.55%; Fe, 4.48%; Cl, 11.39%. Found: C, 58.54%; H, 3.14%; Fe, 4.32%; Cl, 11.36%.

Synthesis of Bulk Polyfuran, $(PFu)_x Cl$.

Under nitrogen, 0.3 g (1.5 mmol) of terfuran was dissolved in 50 ml CH_3CN. To this solution was then added 1.5 g (9.2 mmol) of $FeCl_3$. The mixture was stirred at room temperature for 9 hours. The black solid was isolated by filtration in air, washed with acetone and dried in vacuum. It was identified by FTIR spectroscopy.

Elemental analysis, Calcd for $(C_4H_2O)Cl_{0.23}$: C, 64.73%; H, 2.70%; Cl, 11.0%. Found: C, 49.49%; H, 3.22%; Cl, 8.59%; Fe, 1.52%. The trace amount of Fe could be the impurity comes from the oxidant, $FeCl_3$. Slightly changing the preparation procedure, polymers with different counterion were obtained.

Synthesis of Microcrystalline r-$(PFu)_{0.18}FeOCl$.

0.20 g (1.0 mmol) of terfuran was dissolved in 50 ml MeOH, and then 0.30 g (2.8 mmol) of FeOCl was added. The mixture was refluxed in air for 6 days. The black microcrystalline product was isolated by filtration, washed with acetone and dried in vacuum. Elemental analysis, Calcd for $(C_4H_2O)_{0.18}FeOCl$: C, 7.35%; H, 0.27%; Fe, 46.86%; Cl, 29.74%. Found: C, 7.45%; H, 0.98%; Fe, 46.38%; Cl, 29.44%.

Synthesis of r-$(PFu)_{0.28}FeOCl$ Using FeOCl Single Crystals.

0.24 g (1.2 mmol) of terfuran was dissolved in a mixed solvent of 60 ml CH_3CN/ 50 ml MeOH. To this solution, was added 0.28 g (2.61 mmol) of FeOCl single crystals. The mixture was allowed to stand in air at room temperature for 3 months. The shining black crystals were isolated by filtration, washed with acetone and dried in vacuum. Elemental analysis, Calcd for $(C_4H_2O)_{0.28}FeOCl$: C, 10.69%; H, 0.44%; Fe, 44.40%; Cl, 28.18%. Found: C, 10.49%; H, 1.27%; Fe, 44.11%; Cl, 28.0%.

Synthesis of m-(PFu)$_{0.47}$FeOCl$_{0.61}$(OMe)$_{0.39}$.

In a pyrex tube 0.30 g (2.8 mmol) of FeOCl and 0.40 g (2.0 mmol) of terfuran were mixed with 2.0 ml MeOH. The mixture was frozen with liquid nitrogen and it was flame-sealed under vacuum. The tube was sonicated for 4 minute and heated at 100°C for 6 days. The black shiny solid was isolated by filtration in air, washed with acetone and dried in vacuum. Elemental analysis: Calcd for (C$_4$H$_2$O)$_{0.47}$FeOCl$_{0.61}$(OMe)$_{0.39}$: C, 19.94%; H, 1.54%; Fe, 40.89%; Cl, 15.83%. Found: C, 20.02%; H, 1.71%; Fe, 37.60%; Cl, 14.53%. By varying the reagents ratios, under the same reaction conditions, different PFu/FeOCl stoichiometries can be obtained (the particle size of FeOCl sometimes also affect the PFu/FeOCl ratio of the product). Following is one example.

Synthesis of m-(PFu)$_{0.61}$FeOCl$_{0.49}$(OMe)$_{0.51}$.

In a pyrex tube 0.30 g (2.8 mmol) of FeOCl and 0.30 g (1.5 mmol) of terfuran were mixed with 1.5 ml MeOH. The mixture was frozen with liquid nitrogen and it was flame-sealed under vacuum. The tube was heated at 100°C for 6 days. The black shiny solid was isolated by filtration in air, washed with acetone and dried in vacuum Elemental analysis, Calcd for (C$_4$H$_2$O)$_{0.61}$FeOCl$_{0.49}$(OMe)$_{0.51}$: C, 24.36%; H, 1.89%; Fe, 38.44%; Cl, 12.44%. Found: C, 24.42%; H, 2.00%; Fe, 35.95%; Cl, 11.12%. Similar products can be obtained by using tetrafuran instead of terfuran under the same reaction

conditions. However, for the same mole ratio of reagents, the tetrafuran intercalated FeOCl needs longer time to go completion.

Extracting Polyfuran from r-(PFu)$_x$FeOCl and m-(PFu)$_x$FeOCl$_y$(OMe)$_{1-y}$.

0.3 g of r-(PFu)$_x$FeOCl (or m-(PFu)$_x$FeOCl$_y$(OMe)$_{1-y}$) was stirred with 100 ml 2M HCl(aq), at room temperature for 24 hours. The black residue was isolated by filtration, washed with water then acetone and dried in vacuum. It was characterized by FTIR spectroscopy. Elemental analysis, Calcd for (C$_4$H$_2$O)Cl$_{0.19}$: C, 65.99%; H, 2.75%; Cl, 9.26%. Found: C, 63.3%; H, 2.88%; Fe, 0.68%; Cl, 8.72%. The trace amount of Fe was also detected as impurity from decomposed FeOCl framework.

III. Results and Discussion:

A. Preparation and Characterization of Polyfuran.

The ideal oxidative polymerization of polyfuran is represented in equation 6.1, the furan rings are intact after polymerization.

$$\text{.......eq (6.1)}$$
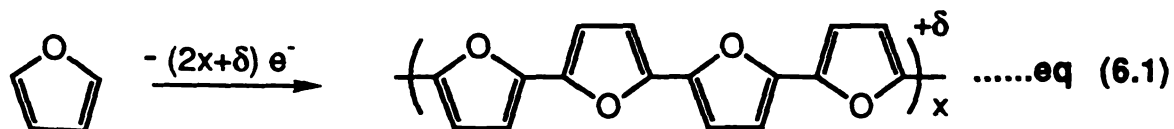
However, in the literature, the chemically polymerized polyfuran is not well characterized species [9], and it is thought to contain fragments such as -CH=CH-O-, -CH=(CH3)-O-, -C=O ...etc. In one case the furan ring was claimed to be totally absent [10]. The five-membered hetero-aromatic ring is relatively reactive due to its high oxidation potential and lower aromaticity. Taking advantage of the lower oxidation potential of terfuran and quaterfuran, we are able to prepare polyfuran with preservation of the furan ring. We prepared polyfuran by chemical polymerization of terfuran using $FeCl_3$ as an oxidant in nitrogen atmosphere as shown in equation 6.2.
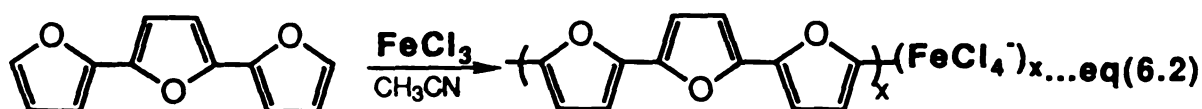
The resulting black powder preserves the structure of furan ring as evidenced in FTIR spectra (vide infra).

B. Intercalation of Polyfuran in FeOCl.

The insertion of polyfuran in FeOCl, the monomer furan and several linear oligomers of furan, such as bifuran, terfuran and tetrafuran were used. As expected, furan itself can not be intercalated in FeOCl within the experimental conditions because of its high oxidation potential. When bifuran was used, under the methanothermal reaction at 80°C for 10 days or 100°C for 7 days, the resulting brown solids showed an interlayer spacing of 9.6Å. The

FTIR spectra of this compound showed several vibration energies between 1600 cm^{-1} and 400 cm^{-1} which are different from bifuran and (PFu)$_x$FeCl$_4$ indicating significant structure degradation of the polymer backbone. Therefore, no further characterization was pursued for these brown products.

Both terfuran and tetrafuran were able to be intercalated in FeOCl by either reflux in CH$_3$CN or methanol or methanothermal synthesis at 80-100°C. When reactions were carried out in refluxing CH$_3$CN and methanol, the complete intercalation products, r-(PFu)$_x$FeOCl can be obtained, although sometimes parallel decomposition of the FeOCl framework was observed. Other alcohols, such as ethanol, i-PrOH and i-BuOH were also used as solvents, but no intercalation reaction was observed after refluxing FeOCl with terfuran for 5 days. In refluxing ethanol intercalation occurred in the beginning but the material decomposed before reaction went to completion. The reactions carried out in air are faster than those in nitrogen as observed in other conducting polymer intercalated V$_2$O$_5$ xerogel and FeOCl systems. The role of oxygen in this reaction was not investigated.

In general, during methanothermal synthesis, the terfuran (or quaterfuran)/FeOCl ratio should be larger than 0.25 in order to drive the reaction to completion. The reaction time is affected by the temperature, for example, at 80°C it takes 3 weeks for the reaction to go completion, while at 100°C it needs less than 1 week. However, the polymer content is independent of terfuran/FeOCl ratio and reaction temperature. The reaction rate of terfuran and tetrafuran in FeOCl is slower than that of pyrrole and 2,2'-bithiophene [11]

presumably due to the larger size and lower solubility of the furan oligomers in CH_3CN and MeOH. Similarly, the reaction rate of quaterfuran is slower than that of terfuran at the same reaction conditions. Nevertheless, regardless of using terfuran or quaterfuran as monomer, the resulting products have similar physicochemical properties. Some solvents such as CH_3CN, EtOH and DMF have also been used for the solvothermal reaction. Unfortunately, all afforded decomposition products (FeOCl decomposed to Fe_2O_3)

C. Infrared Spectroscopy and X-ray Diffraction Studies.

The evidence of forming polyfuran comes from the fourier transform infrared spectra. The r-$(PFu)_x$FeOCl and $(PFu)_x$FeCl$_4$ have comparable vibration peaks between 500 cm^{-1} and 1600 cm^{-1} as shows in Figure 6.1. Both spectra show some peaks between 1600 cm^{-1} and 1800 cm^{-1} which is due to the defects, such as ring opening, of the polymer backbones. Mostly probably they represent the formation of carbonyl groups as shown in equation 6.3.

$$\text{(structure)} \xrightarrow{\text{H}_2\text{O}} \text{(structure)} \qquad \dots\dots\dots\text{eq (6.3)}$$
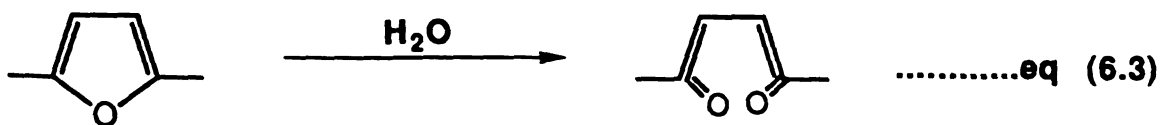
However, these defects are present in small concentrations than that in $(PFu)_x$FeCl$_4$, as judged by relative intensities of the peaks in 1600-1800 cm^{-1} region of the IR spectra. The polyfuran in $(PFu)_x$FeOCl can be extracted by decomposing the FeOCl framework with HCl aqueous

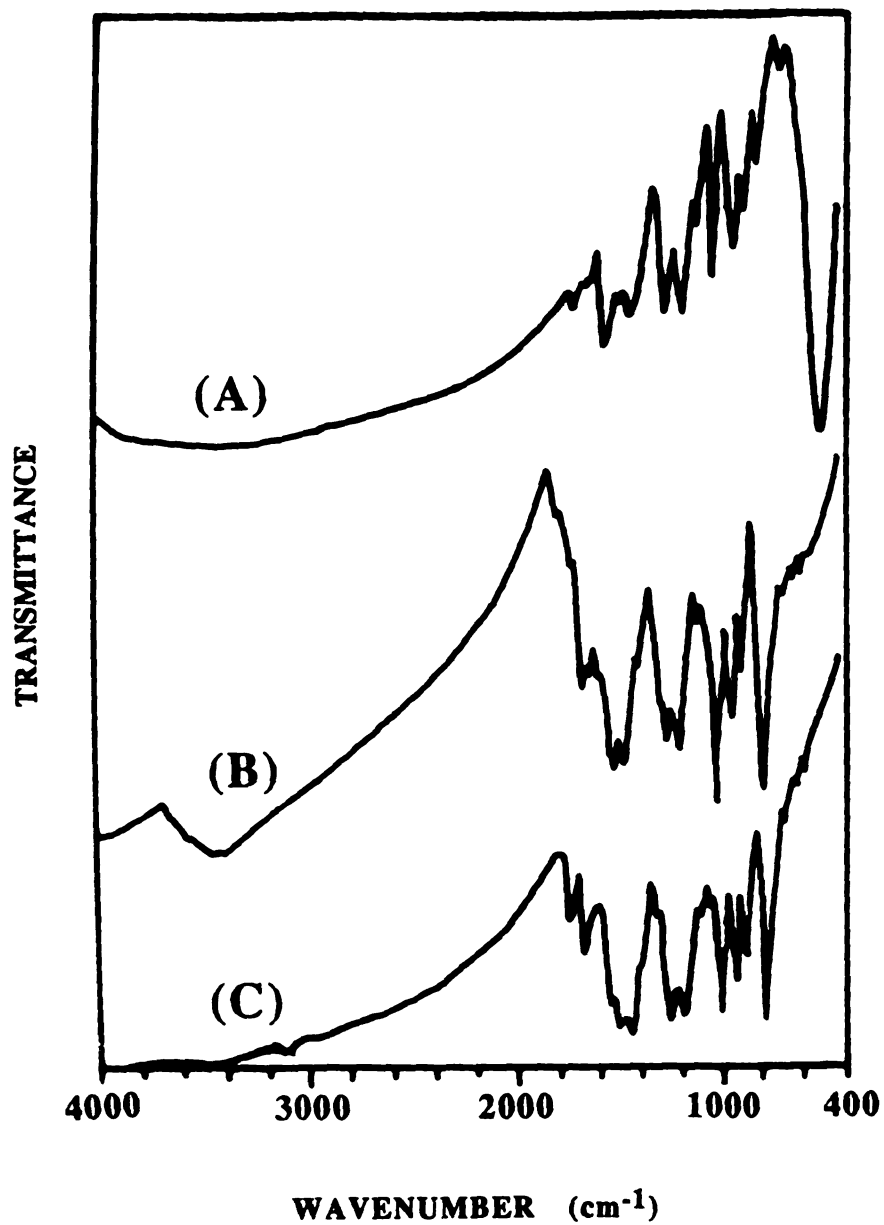Figure 6.1. FT-IR spectra (KBr pellets) of (A) r-(PFu)$_x$FeOCl (B) (PFu)$_x$FeCl$_4$ (C) Extracted polyfuran.

solution. The IR spectrum of extracted polyfuran shows more serious structural disruption (i.e. carbonyl formation) compared to that in FeOCl layers, although it has similar vibration energies to those of $(PFu)_x FeCl_4$ (see Figure 6.1).

The FTIR spectra of $m\text{-}(PFu)_x FeOCl_x(OMe)_{1-y}$ prepared from methanothermal synthesis show an extra peak at around 1040 cm^{-1} which is not observed in the samples prepared from refluxing MeOH or CH$_3$CN as shown in Figure 6.2. The intensity of this peak increases with reaction time and temperature. We attribute this absorption peak to methoxide groups which partially replaced the Cl atoms in FeOCl to form $FeOCl_y(OMe)_{1-y}$. For convenience, $(PFu)_x FeOCl$ prepared from refluxing MeOH or CH$_3$CN was called $r\text{-}(PFu)_x FeOCl$ and the samples prepared from methanothermal synthesis we called $m\text{-}(PFu)_x FeOCl_y(OMe)_{1-y}$. Polyfuran present in and extracted from $r\text{-}(PFu)_x FeOCl$ and $m\text{-}(PFu)_x FeOCl_y(OMe)_{1-y}$ have identical IR patterns. Table 6.1 lists some major vibration modes of $r\text{-}(PFu)_x FeOCl$, $m\text{-}(PFu)_x FeOCl_y(OMe)_{1-y}$, extracted polyfuran and $(PFu)_x Cl$.

Direct evidence of formation of intercalated compounds comes from X-ray powder diffraction studies as shown in Figure 6.3. Two different intercalated products have been obtained. When the reactions were carried out in refluxing CH$_3$CH or MeOH, the resulting black products have an interlayer spacing of 13.60Å. However, the interlayer spacing expansions vary by 0.5Å from batch to batch, depending on the particle size of FeOCl, the ratios of reagents, the solvent and reaction time. This may due to the imperfect orientation of polyfuran inside the host, which is also suggested by the broadness of XRD peaks. The 5.68Å interlayer spacing expansion of
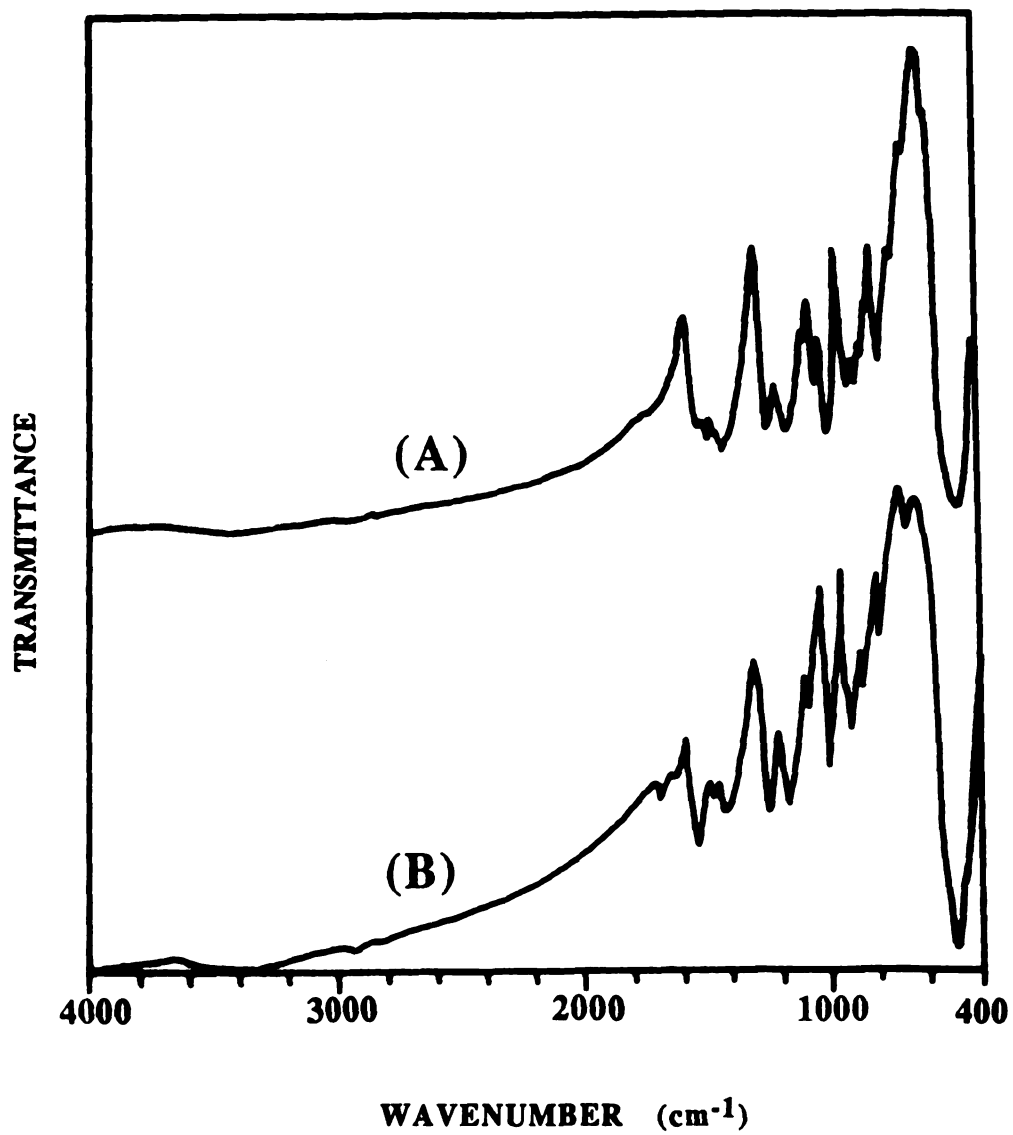
Figure 6.2. FT-IR spectra (KBr pellets) of (A) m-$(PFu)_xFeOCl_y(OMe)_{1-y}$ (B) r-$(PFu)_xFeOCl$.

Table 6.1. Major IR Vibration Modes of r-(PFu)xFeOCl, (PFu)xFeCl4 and Extracted Polyfuran.

r-(PFu)xFeOCl	(PFu)xFeCl4	Extracted polyfuran	Modes
m 1527 cm⁻¹	m 1527 cm⁻¹	m 1534 cm⁻¹	C=C str., C-H def
m 1492 cm⁻¹	m 1499 cm⁻¹	s 1492 cm⁻¹	ring def.
s 1436 cm⁻¹	s 1450 cm⁻¹	s 1429 cm⁻¹	C=C str., C-H def., C-O str.
s 1238 cm⁻¹	s 1238 cm⁻¹	s 1231 cm⁻¹	C-H def., ring def.
s 1175 cm⁻¹	s 1182 cm⁻¹	s 1175 cm⁻¹	C-H def., C-O str.
w 1084 cm⁻¹	w 1084 cm⁻¹	w 1084 cm⁻¹	C-H str., C-O str.
w 1048 cm⁻¹	w 1055 cm⁻¹	w 1049 cm⁻¹	C-O str., C-H str.
s 999 cm⁻¹	vs 1006 cm⁻¹	s 999 cm⁻¹	- - - -
m 929 cm⁻¹	s 939 cm⁻¹	s 922 cm⁻¹	ring def., C=C str.
s 879cm⁻¹	s 872cm⁻¹	s 879 cm⁻¹	ring def., C-O str.
w 823 cm⁻¹		vw 818 cm⁻¹	- - - -
s 781 cm⁻¹	vs 774 cm⁻¹	s 774 cm⁻¹	- - - -
w 731 cm⁻¹	w 682 cm⁻¹	w 682 cm⁻¹	- - - -
vs 464 cm⁻¹			Fe-O

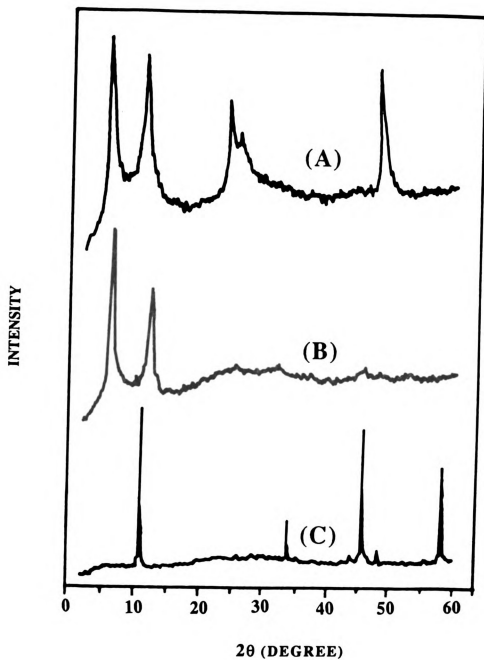*vs: very strong; s: strong; m: medium; w: weak; vw: very weak. **str.: streching; def.: deformation.

**Figure 6.3.** Reflection-mode X-ray powder diffraction patterns of (A) m-$(PFu)_{0.47}FeOCl_{0.61}(OMe)_{0.39}$ (B) r-$(PFu)_{0.27}FeOCl$ (C) FeOCl.

r-(PFu)$_x$FeOCl corresponds to intercalated monolayer of polyfuran inside the FeOCl layers with the five member rings roughly perpendicular to the FeOCl slabs as showed in Scheme 6.1. This arrangement is similar to its polypyrrole and polythiophene analogues [11].
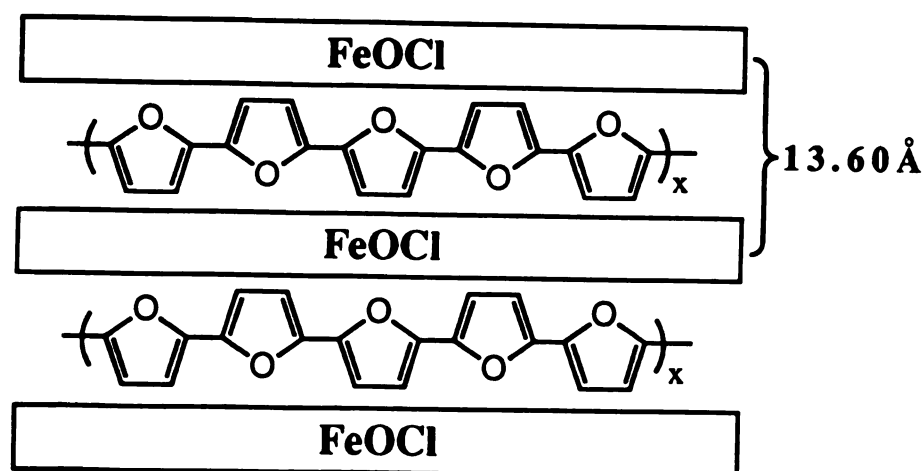
Scheme 1. Proposed arrangement of polyfuran chains in FeOCl layers.

The interlayer spacing of m-(PFu)$_x$FeOCl$_y$(OMe)$_{1-y}$ is significantly larger than r-(PFu)$_x$FeOCl, at 15.62Å (see Figure 6.3c). The higher expansion (7.7Å) of m-(PFu)$_x$FeOCl$_y$(OMe)$_{1-y}$ is due to the replacement of the Cl$^-$ groups in the FeOCl layers by the larger MeO$^-$ groups. FeO(OMe) is a known layered compound with interlayer spacing spacing of 9.91Å. This is larger than in FeOCl representing the larger size of MeO$^-$ groups. The replacement of Cl$^-$ by CH$_3$O$^-$ in this redox intercalation reaction was not expected, but it is not

surprising. It was observed in the reaction of (4-Ap)FeOCl (4-AP: 4-aminopyridine) with MeOH which gives FeO(OMe) [12]. Since terfuran in this case inserts (maybe also polymerize) in FeOCl layers, it expands the layer gallery and at the same time appears to act as a base helping the deprotonation of MeOH. The net layer expansion of m-$(PFu)_x FeOCl_y (OMe)_{1-y}$ due to the insertion of polyfuran is equal to 5.71Å (15.62-9.91Å) which is similar to r-$(PFu)_x FeOCl$ and corresponds to a monolayer of polyfuran with the five member ring roughly perpendicular to the host layers as showed in Scheme 6.2.
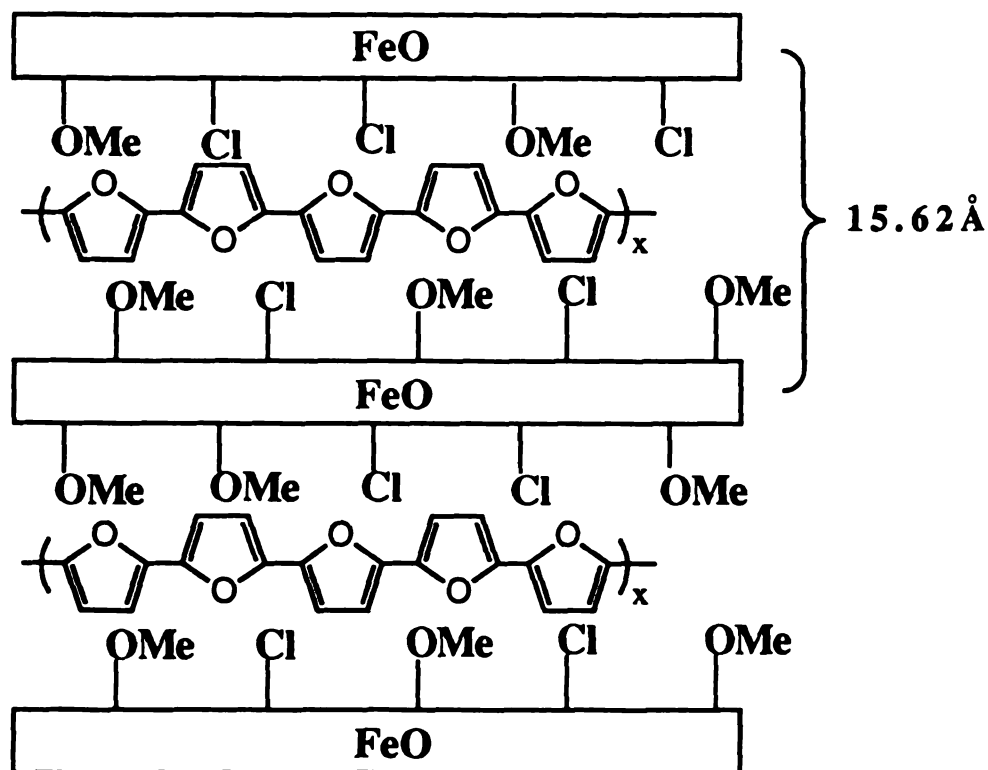
Scheme 6.2. Proposed structure of m-$(PFu)_x FeOCl_y (OMe)_{1-y}$

In general solvent trapping in the host layers is a common phenomenon [14] and it can be removed by heating at moderate temperature under vacuum. The present case is a rare example in which the solvent not only in co-intercalates but also reacts with the host framework. As observed by IR spectroscopy of the products during the intermediate stages of the reaction, the polyfuran formed first, followed by the incorporation of the methoxy group. The insertion of polyfuran opens up the FeOCl layers, so that the interlamellar space of FeOCl becomes accessible by MeOH molecules which under methanothermal conditions apparently have enough energy to nucleophilically replace Cl atoms in FeOCl. r-$(PFu)_x$FeOCl did not react with methanol at $110°C$ in sealed tube (in absence of terfuran) and neither did MeOH react with FeOCl under the same reaction conditions. Surprisingly, when terfuran and FeOCl were refluxed in methanol no ligand replacement was observed.

D. Scanning Electron Microscopy (SEM) and Selected Area Electron Diffraction (SAED).

The SEM micrographs of both r-$(PFu)_x$FeOCl and m-$(PFu)_x$FeOCl$_y$(OMe)$_{1-y}$ are shown in Figure 6.4. They reveal the crystalline and layered nature of these composites. Both single crystal and powder samples show smooth, clean surfaces and no impurity or amorphous phase. Selected area electron diffraction with the electron beam perpendicular to the slabs (ac plane) is shown in Figure 6.5. The diffraction spots can be indexed according to the original a and c axes of FeOCl lattice as expected from the
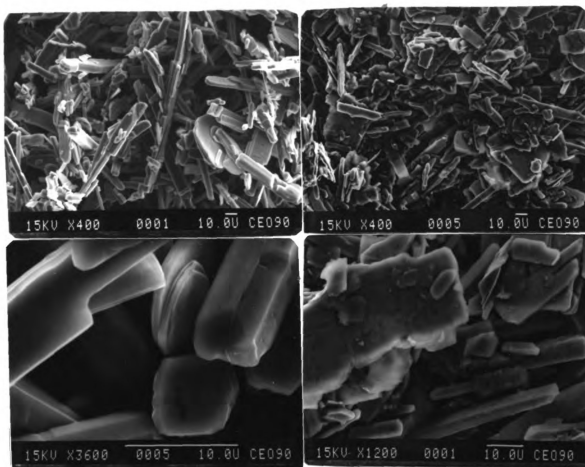
Figure 6.4. SEM micrographs of r-(PFu)$_x$FeOCl and
m-(PFu)$_x$FeOCl$_y$(OMe)$_{1-y}$
left: r-(PFu)$_x$FeOCl; right: m-(PFu)$_x$FeOCl$_y$(OMe)$_{1-y}$
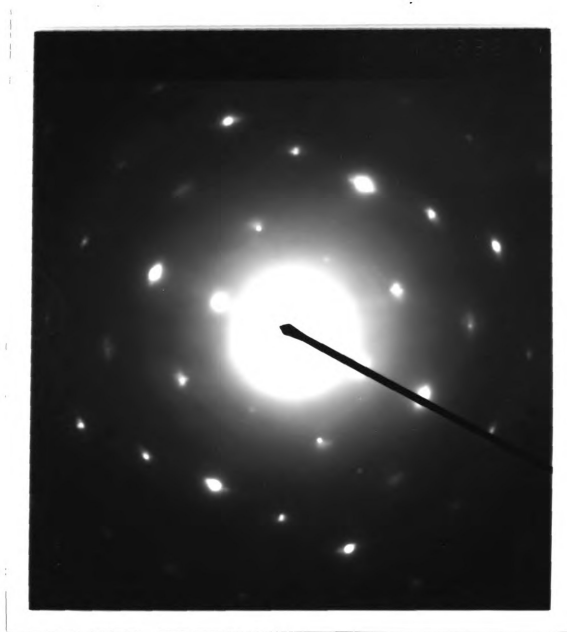
Figure 6.5.   Selected area electron diffraction (with electron beam perpendicular to the FeOCl layers) pattern of r-$(PFu)_x FeOCl$.

topotactic intercalation reaction. Similar observation were made in m-$(PFu)_x FeOCl_y(OMe)_{1-y}$, since the periodicity in the ac plane does not change significantly. This kind of intercalation can be regarded as pseudo-topotactic reaction and thus the similarity of the electron diffraction patterns between r and m-phase is expected.

E. Thermogravimetric Analysis (TGA) and Differential Scanning Calorimetry (DSC) Studies.

The thermal stabilities of both r-$(PFu)_x FeOCl$ and m-$(PFu)_x FeOCl_y(OMe)_{1-y}$ are lower than that of pristine FeOCl under oxygen or nitrogen flow. The TGA diagram of r-$(PFu)_x FeOCl$ shows a continued weight loss from room temperature to 400°C which is due to the decomposition of polymer and FeOCl framework. The weight stabilizes after 400°C as shown in Figure 6.6a. The wide range of decomposition temperature indicate that polyfuran chains inside the layers are inhomogeneous. m-$(PFu)_x FeOCl_y(OMe)_{1-y}$ is stable up to 300°C, see Figure 6.6b, fellow by two steps weight loss between 300°C and 550°C. This is due to the decomposition polymers and the FeOCl framework as seen in FeO(OMe) [12] and $M_x FeOCl$ [15] (M = K, Cs). Figure 6.7 shows the TGA diagrams of both extracted polyfuran and $(PFu)_x FeCl_4$. The polyfuran extracted from $(PFu)_x FeOCl$ has lower thermal stability than the chemically polymerized. This result is not surprising since the former is formed in structurally restricted host therefore it is expected to have shorter chain length. This tendency was also observed in polyaniline intercalated V_2O_5 and FeOCl, see

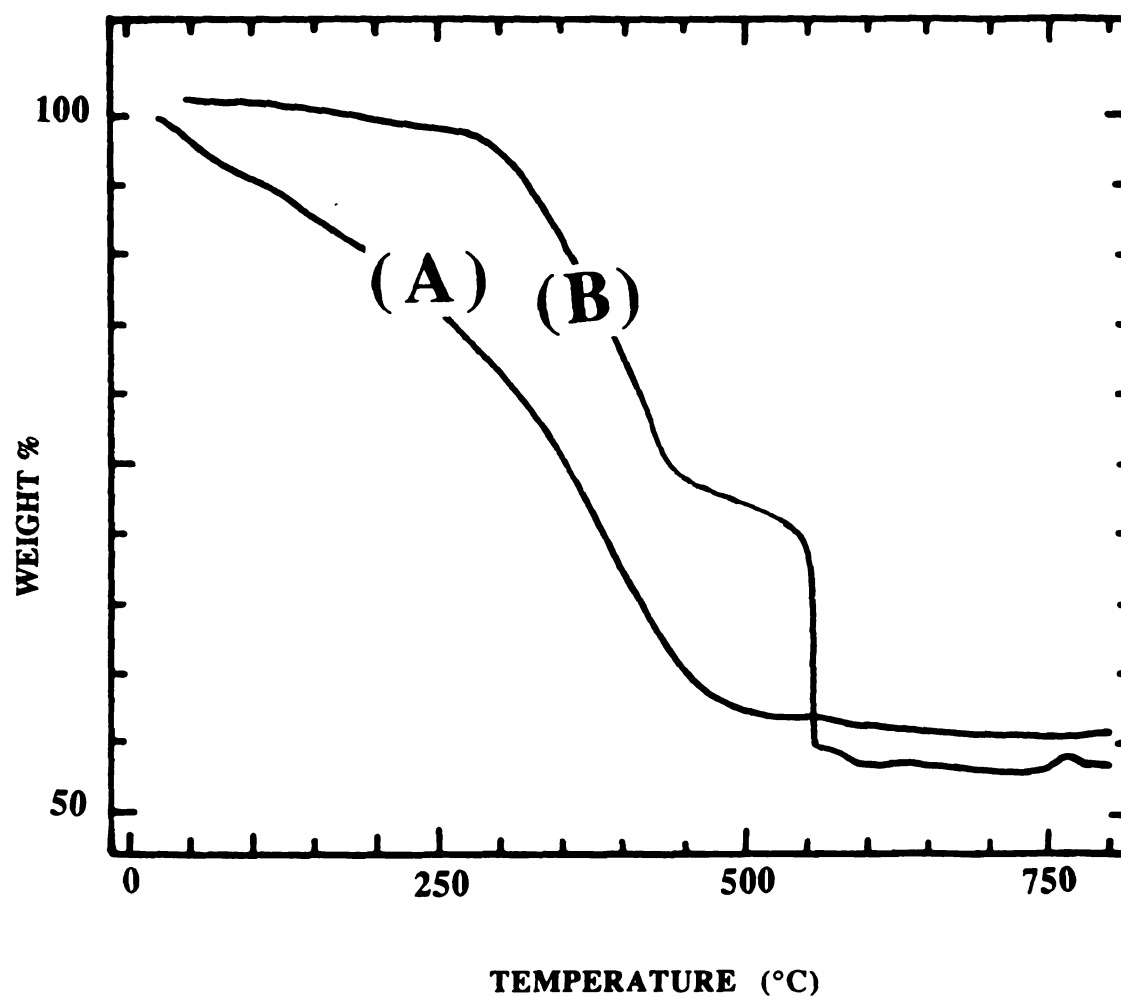**Figure 6.6.** TGA curves (under oxygen flow) of (A) r-$(PFu)_{0.27}FeOCl$ (B) m-$(PFu)_{0.54}FeOCl_{0.5}(OMe)_{0.5}$. (The heating rate was 5°C/min.)
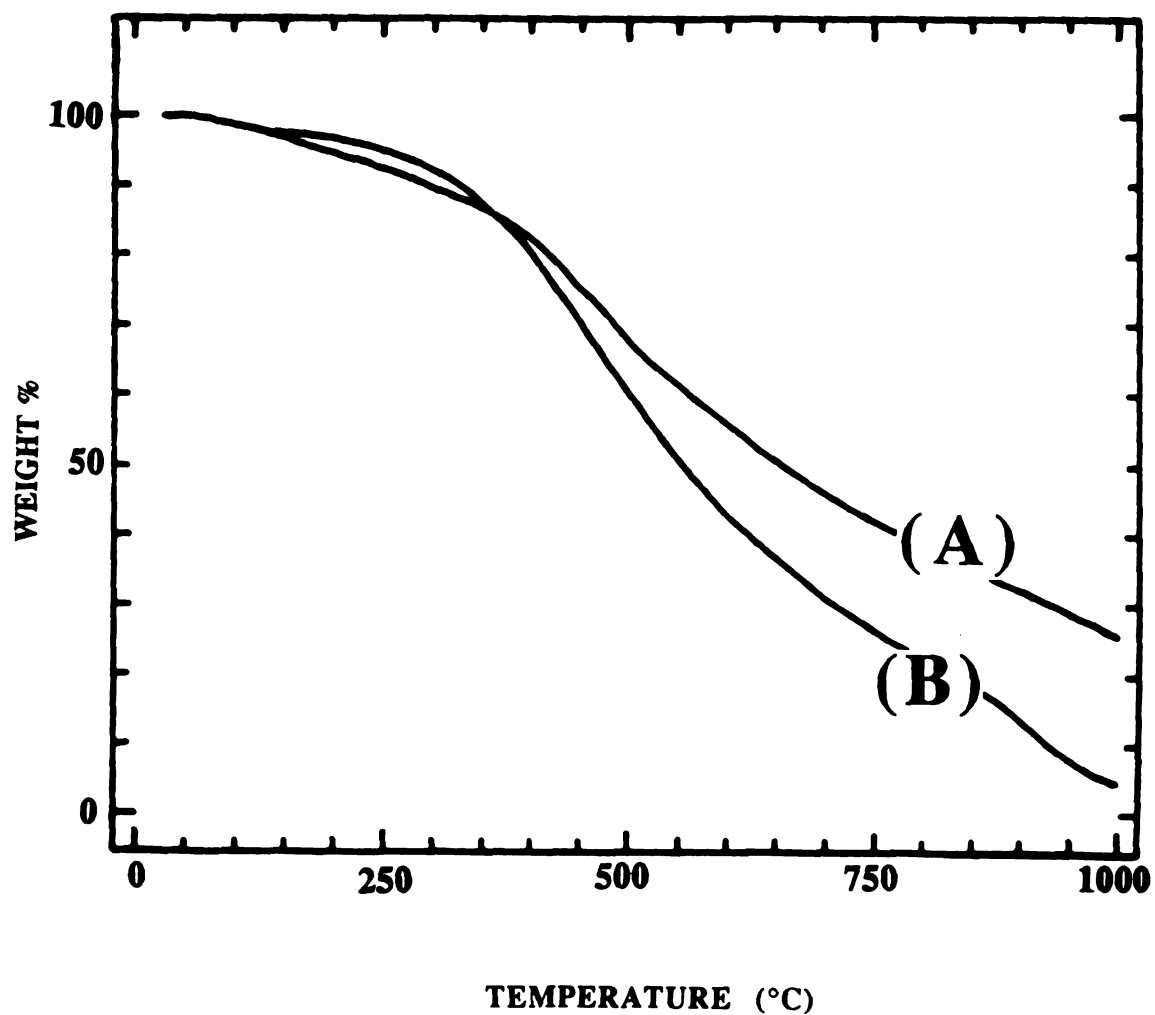
Figure 6.7. TGA curves (under nitrogen flow)of (A) $(PFu)_xFeCl_4$ (B) Extracted polyfuran. (The heating rate was 5°C/min.)

chapter 2&5. The chain length of polyfuran in these systems is still unknown at this moment.

The DSC diagrams of both r-(PFu)FeOCl and m-(PFu)$_x$FeOCl$_y$(OMe)$_{1-y}$ under nitrogen flow show an exothermic peak at 320°C and 280°C respectively. These peaks are due to the decomposition of FeOCl framework. In comparison with the pristine FeOCl which decomposed at around 460°C, the lower thermal stability of polyfuran/FeOCl composites was expected.

F. Electron Paramagnetic Resonance (EPR) Spectroscopy.

The EPR spectra of intercalated FeOCl compounds are broad and complicated, due to the antiferromagnetic nature of Fe atoms. As expected for intercalated compounds, the EPR of both r- and m- phases did not show any signal, due to the spin-spin interaction between polyfuran and Fe atoms through the intimate contact as shown in Figure 6.8a, 6.8b. The polyfuran extracted from (PFu)$_x$FeOCl showed a sharp signal at g value of 2.0023 with peak width (ΔH_{pp}) of 20 gauss which is similar to polyaniline. The EPR spectra of as prepared (PFu)$_x$FeCl$_4$ showed a broad peak (ΔH_{pp} = 600 gauss) at g equal to 2.0579 (see Figure 6.8c). However, when this polymer was stirred with 2 M HCl(aq) for 2 days, the acid treated (PFu)$_x$FeCl$_4$ showed a sharp signal, similar to (PFu)$_x$Cl and extracted polyfuran, at g equal to 2.0023 and the intensity of the broad peak decreased dramatically, see Figure 6.8d. This can be rationalized by the removal of the paramagnetic counter ion FeCl$_4^-$ in (PFu)$_x$FeCl$_4$
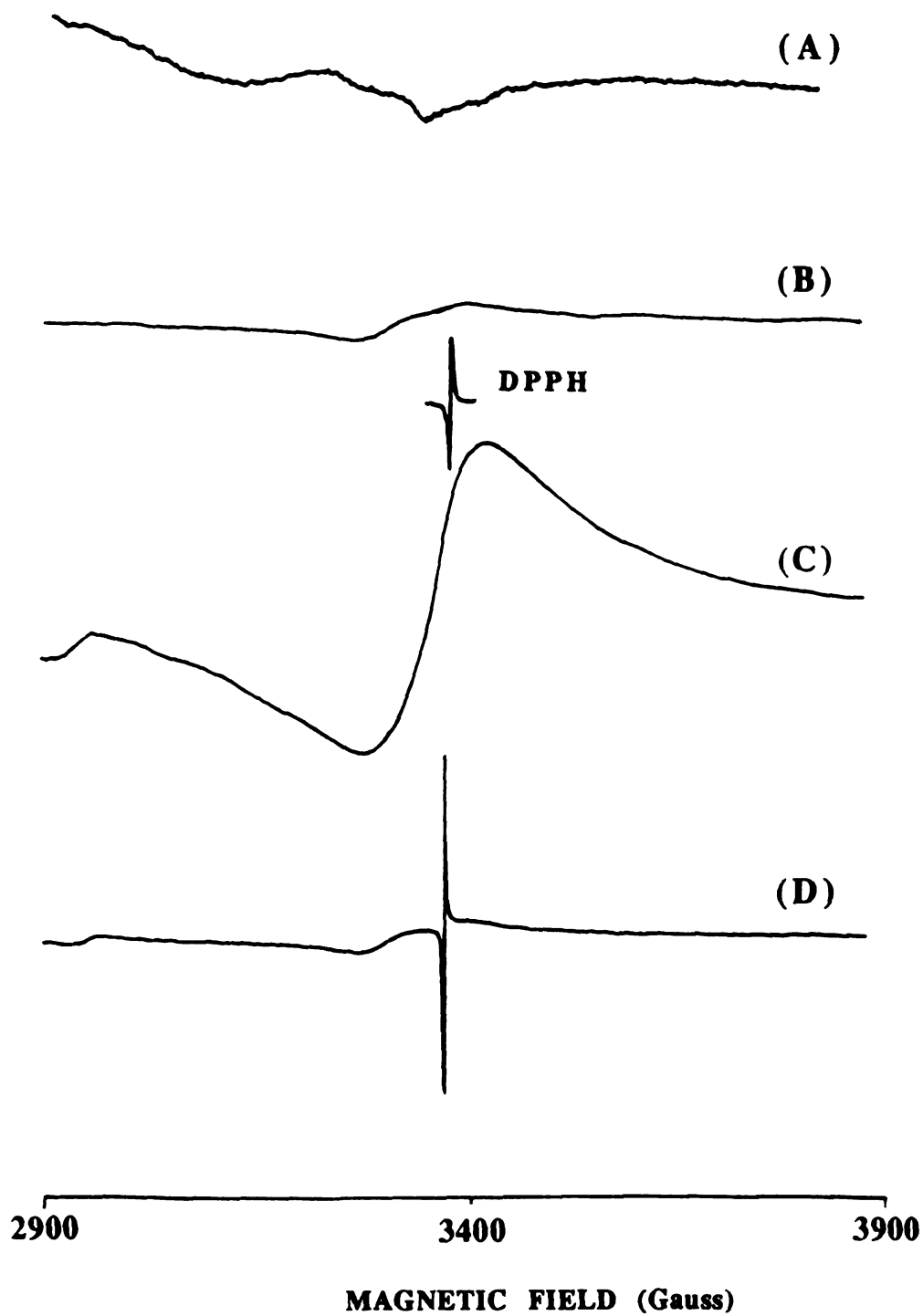
Figure 6.8. Room temperature EPR spectra of (A) r-$(PFu)_{0.27}FeOCl$ (B) m-$(PFu)_{0.51}FeOCl_{0.6}(OMe)_{0.4}$ (C) $(PFu)_xFeCl_4$ (D) $(PFu)_xCl$.

and exchange with the Cl^- ion. This was confirmed by EDS analysis. The as-prepared $(PFu)_xFeCl_4$ contains significant amount of Fe, However, extracted polyfuran and acid treated $(PFu)_xFeCl_4$ contain almost no Fe. Further studies on the physical and chemical properties of conducting polyfuran prepared from electrochemical or chemical polymerization are in progress.

G. Magnetic Susceptibility Studies.

The characteristic Curie-Weiss antiferromagnetic behavior of FeOCl was reported by Bizette and Adam [16]. A similar behavior was also observed in $(PANI)_xFeOCl$, see page 247. The magnetic susceptibilities of both $r-(PFu)_xFeOCl$ and $m-(PFu)_xFeOCl_y(OMe)_{1-y}$ are field independent at magnetic fields between 200 and 15000 gauss at 300 K. Therefore, all susceptibility data were recorded from 5 K to 300 K at constant magnetic field (5000 gauss). Typical variable temperature magnetic susceptibility of $r-(PFu)_xFeOCl$ and $m-(PFu)_xFeOCl_y(OMe)_{1-y}$ are shown in Figure 6.9. The magnetic behavior of $(PFu)_xFeOCl$ is similar to that of $(PANI)_xFeOCl$ implying that the short range magnetic order observed in FeOCl and $(PANI)_xFeOCl$ is also present in polyfuran/FeOCl. The room temperature effective spin-only magnetic moment, μ_{eff}, of $(PFu)_xFeOCl$ with various x are listed in Table 6.2. These values are well below 5.9 B.M., had the material been simply paramagnetic (high spin), due to the antiferromagnetic coupling between the Fe atoms. This also had been observed in pristine FeOCl and its intercalates [17]. We found no simple relationship between the
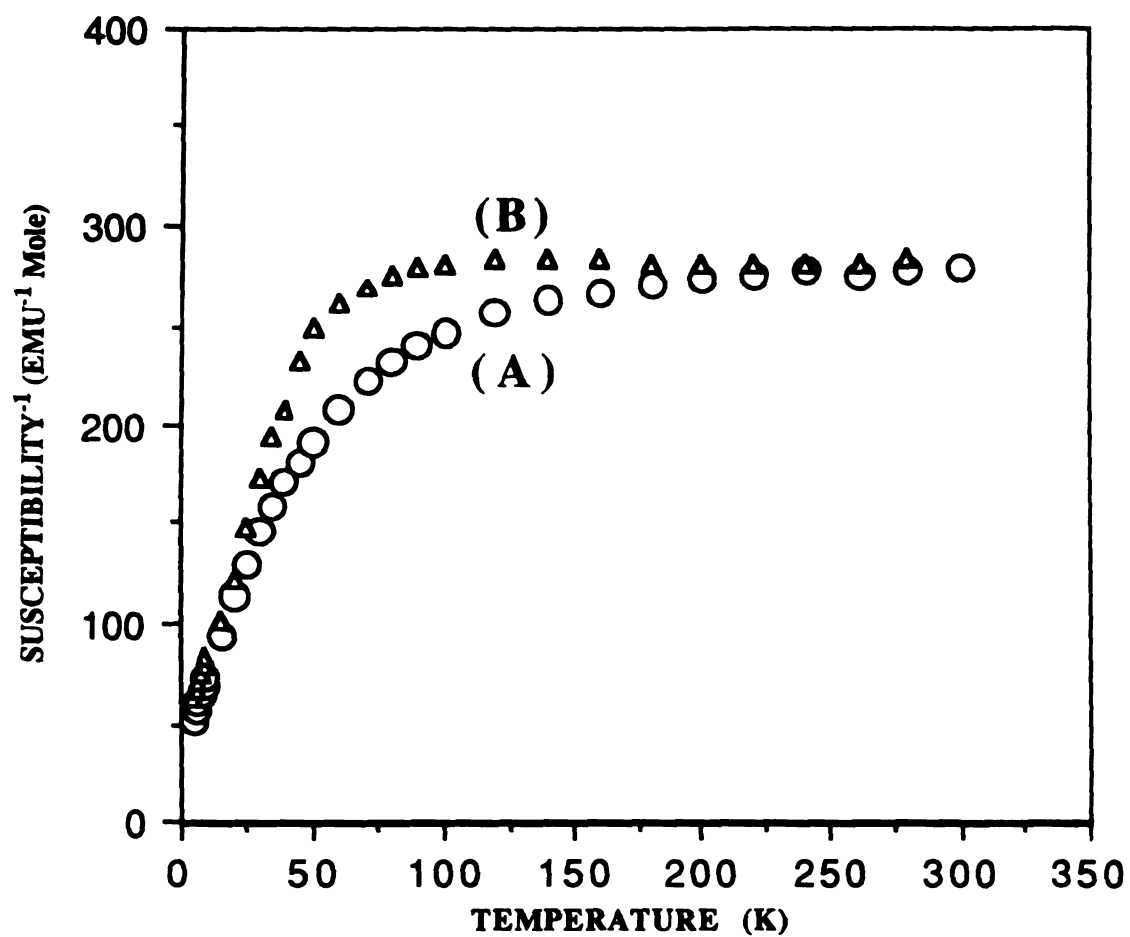
Figure 6.9. Variable temperature magnetic susceptibility data $(1/\chi_m)$ of (A) r-$(PFu)_{0.18}FeOCl$ (B) m-$(PFu)_{0.51}FeOCl_{0.6}(OMe)_{0.4}$

Table 6.2. Room Temperature Effective Spin-only Magnetic Moment (μ_{eff}) versus x of $(PFu)_x FeOCl$.

Compounds	$\mu_{eff}(B.M.)$
m-$(PFu)_{0.61}FeOCl_y(OMe)_{1-y}$	2.87
m-$(PFu)_{0.58}FeOCl_y(OMe)_{1-y}$	2.90
m-$(PFu)_{0.56}FeOCl_y(OMe)_{1-y}$	2.66
m-$(PFu)_{0.53}FeOCl_y(OMe)_{1-y}$	2.88
m-$(PFu)_{0.47}FeOCl_y(OMe)_{1-y}$	2.91
r-$(PFu)_{0.28}FeOCl$	3.39
r-$(PFu)_{0.27}FeOCl$	3.06
r-$(PFu)_{0.18}FeOCl$	2.93

magnetic moment and polymer content. Figure 6.10 shows the variable temperature μ_{eff} of r-$(PFu)_x$FeOCl and m-$(PFu)_x$FeOCl$_y$(OMe)$_{1-y}$. For both samples the μ_{eff} increases as temperature increases, further proving that antiferromagnetic coupling exists in these materials.

The magnetic properties of polyfuran in $(PFu)_x$FeOCl cannot be assessed due to the complicated magnetic behavior of the FeOCl layers. However, polyfuran can be extracted and studied separately by dissolving the FeOCl framework in HCl(aq). The magnetic susceptibility, χ, of both extracted and $(PFu)_x$FeCl$_4$ are similar to that of polyaniline which is paramagnetic. The χ increases with rising temperature as shown in Figure 6.11, slightly deviated from Curie-Weiss law. This probably is due to the contribution of Puli paramagnetic which is relatively small and only observed at high temperature when the normal paramagnetism is small. The room temperature effective spin-only magnetic moment, μ_{eff} of $(PFu)_x$Cl is equal to 0.74 BM and basically temperature independent, consistent with Curie-Weiss paramagnetic behavior, as shown in Figure 6.12. Polyfuran extracted from $(PFu)_x$FeOCl has room temperature μ_{eff} of 0.52 B.M. and also temperature independent within experiment error (see Figure 6.12b). Interestingly, the magnetic moment of $(PFu)_x$Cl is larger than extracted PFu. It had been suggested that the paramagnetism of conducting polyheterocycles may come from the defects of the polymer chain [18]. The smaller μ_{eff} of extracted polyfuran indicate that polyfuran extracted from $(PFu)_x$FeOCl have fewer paramagnetism and may have less structural defects.
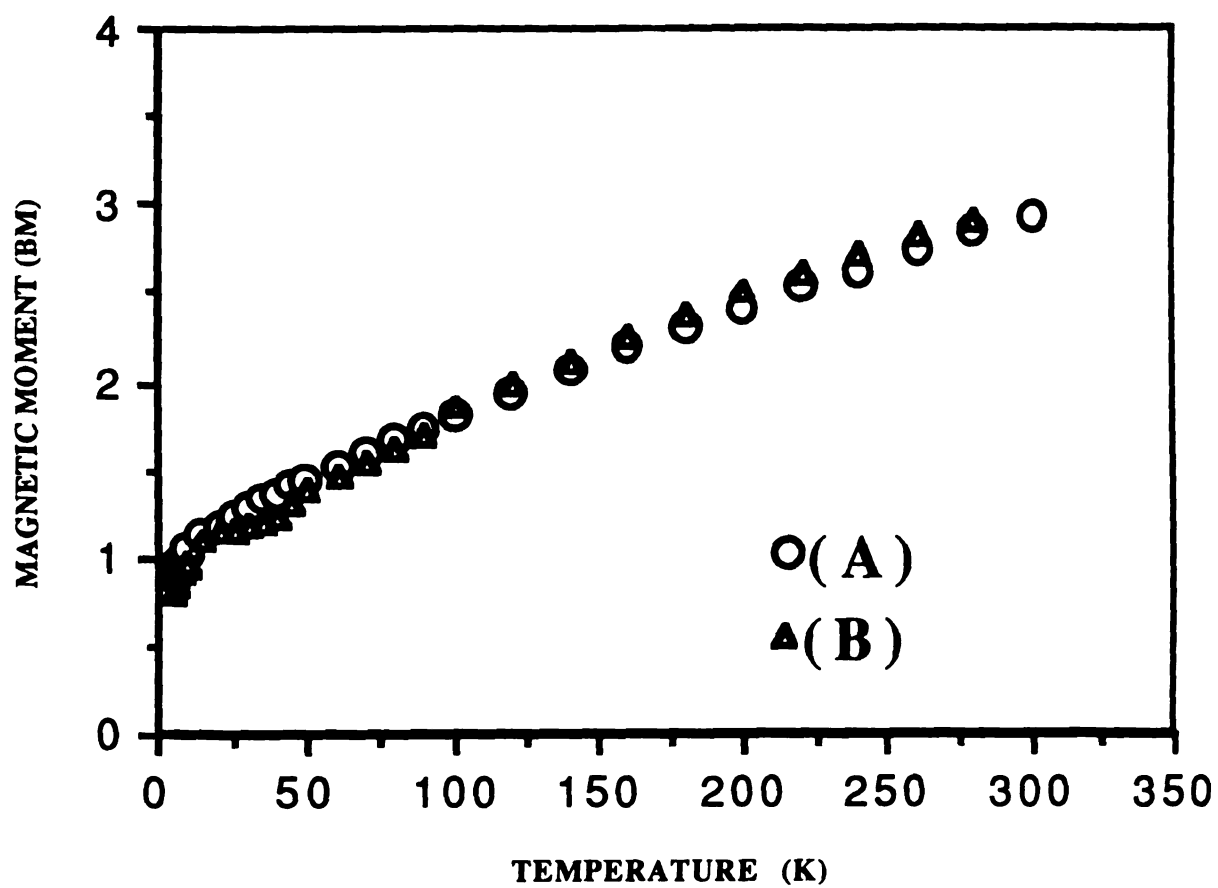
Figure 6.10   Variable temperature effective spin-
Only magnetic moment of (A) r-(PFu)$_x$FeOCl   (B) m-
(PFu)$_x$FeOCl$_y$ (OMe)$_{1-y}$.

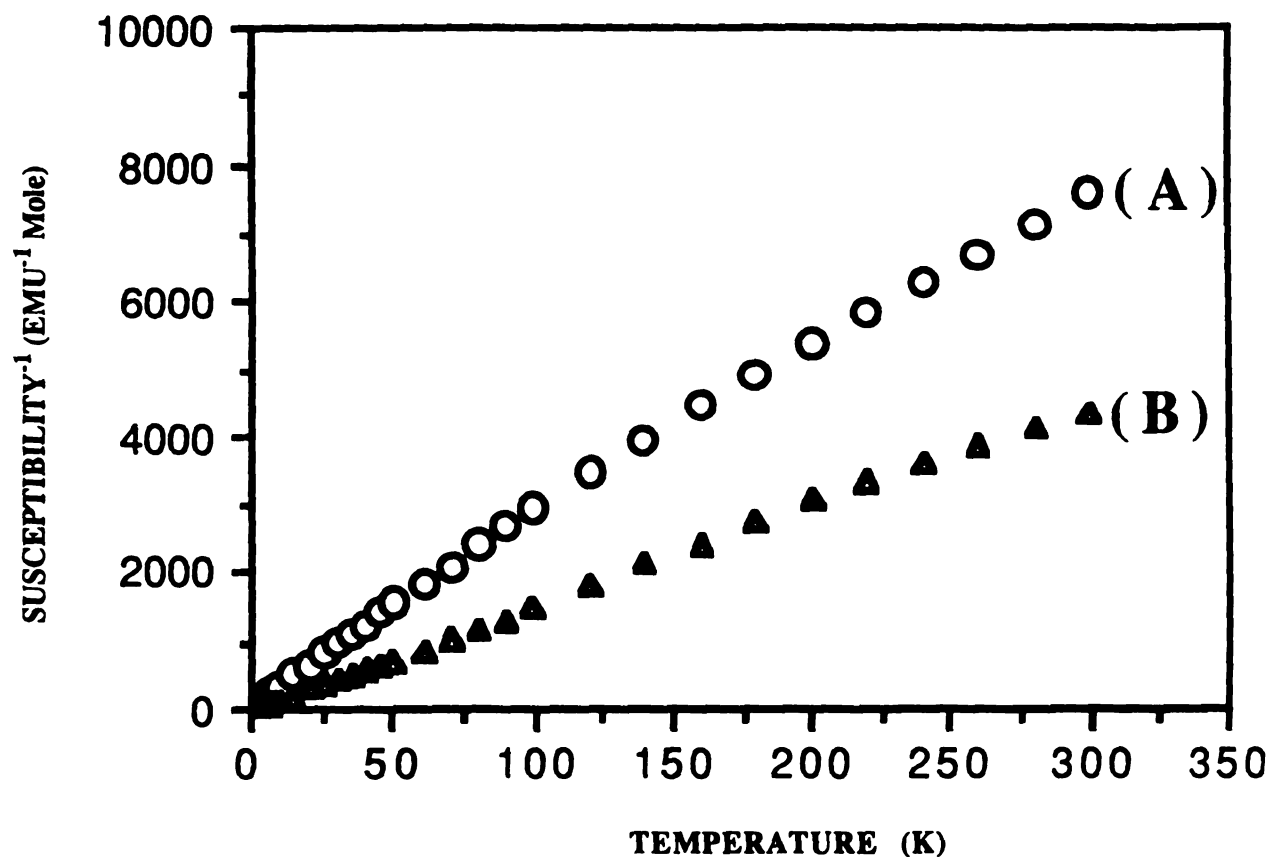**Figure 6.11.** Variable temperature magnetic susceptibility data $(1/\chi_m)$ of (A) $(PFu)_xCl$ (B) Extracted polyfuran.
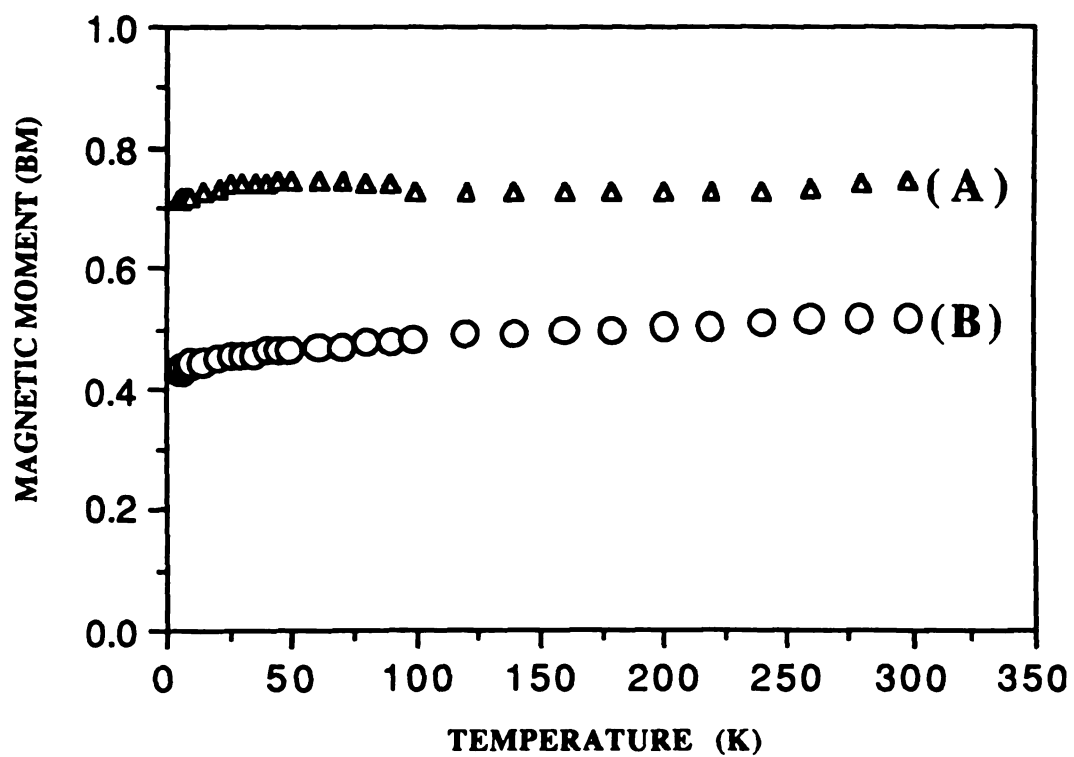
Figure 6.12. Variable temperature effective spin-only magnetic moment of (A) (PFu)ₓCl (B) Extracted polyfuran.

H. Charge Transport Properties.

Typical four-probe variable temperature electrical conductivity data on pressed pellets of r-(PFu)FeOCl and m-(PFu)$_x$FeOCl$_y$(OMe)$_{1-y}$ are shown in Figure 6.13. Both conductivities increase as temperature increases indicating thermally activated charge transport behavior which is dominated by the interparticle contact resistance. This is the common behavior of intercalated FeOCl compounds [11]. Generally, the conductivity of r-(PFu)$_x$FeOCl is higher than m-(PFu)$_x$FeOCl$_y$(OMe)$_{1-y}$. The conductivity of m-(PFu)$_x$FeOCl$_y$(OMe)$_{1-y}$ does not depend on x but relates to the intensity of the peak at 1050 cm^{-1} which comes from the MeO vibration of m-phase. The weaker the intensity, the higher conductivity. The room temperature conductivity of pressed pellet samples falls in the range of 10^{-4} ~10^0 Ω^{-1}cm^{-1} as lists in Table 6.3. Surprisingly, for r-(PFu)$_x$FeOCl the conductivity of single crystals is slightly lower than that of pressed pellet powder as shown in Figure 6.14. This may due to the poor crystallinity of the sample after intercalation as evidenced by the broad peaks in the X-ray diffraction pattern. Table 6.4 lists the room temperature conductivity of several intercalation compounds of FeOCl for comparison. The conductivity of r-(PFu)$_x$FeOCl is comparable to its polypyrrole and polythiophene analogs. The lower conductivity of m-(PFu)$_x$FeOCl$_y$(OMe)$_{1-y}$ may be due either to the present of shorter conjugated polymer segments inside the host or the chemical change of the FeOCl layers (i. e. formation of FeOCl$_y$(OMe)$_{1-y}$) or due to both.
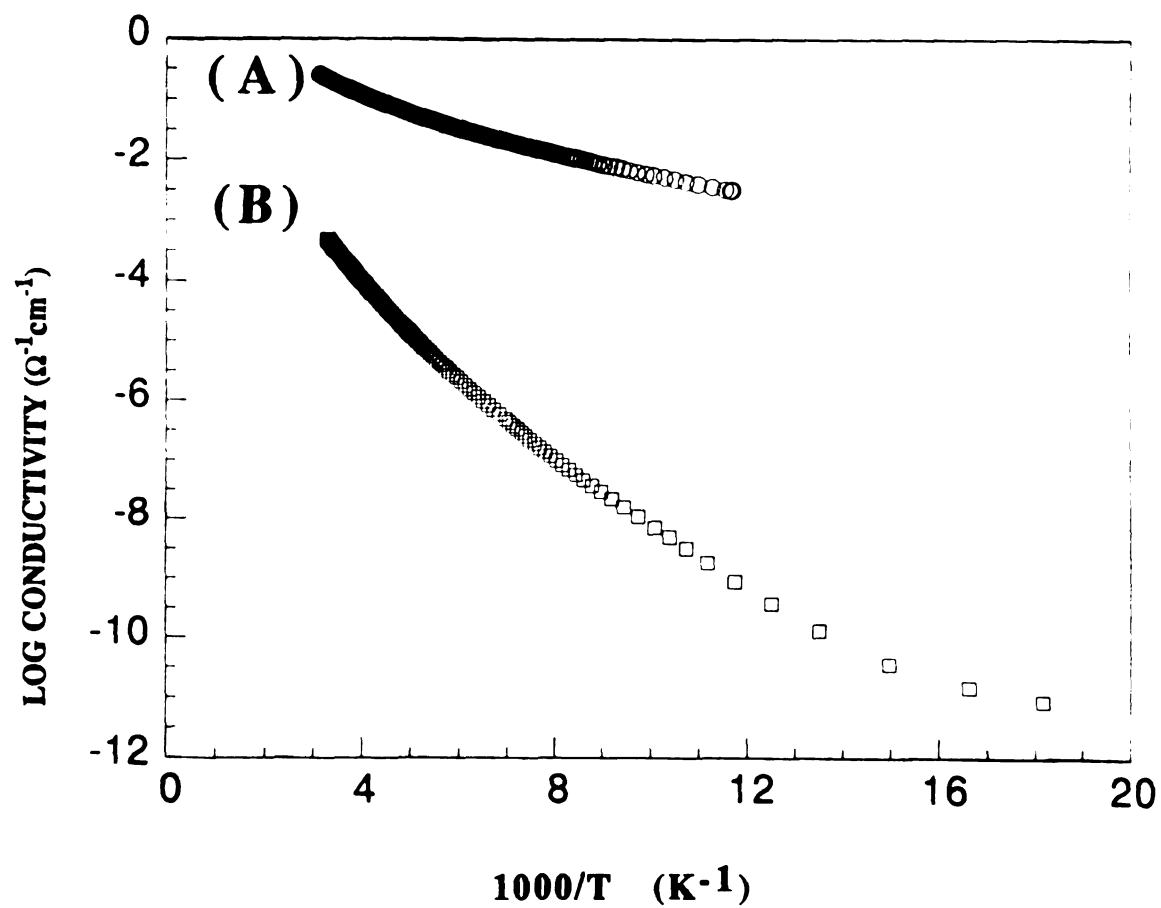
Figure 6.13. Four-probe variable temperature electrical conductivity data of pressed pellets of (A) r-$(PFu)_{0.27}FeOCl$ (B) m-$(PFu)_{0.51}FeOCl_{0.6}(OMe)_{0.4}$

Table 6.3. Room Temperature Electrical Conductivity (σ) versus x of r-(PFu)$_x$FeOCl and m-(PFu)$_x$FeOCl$_y$(OMe)$_{1-y}$.

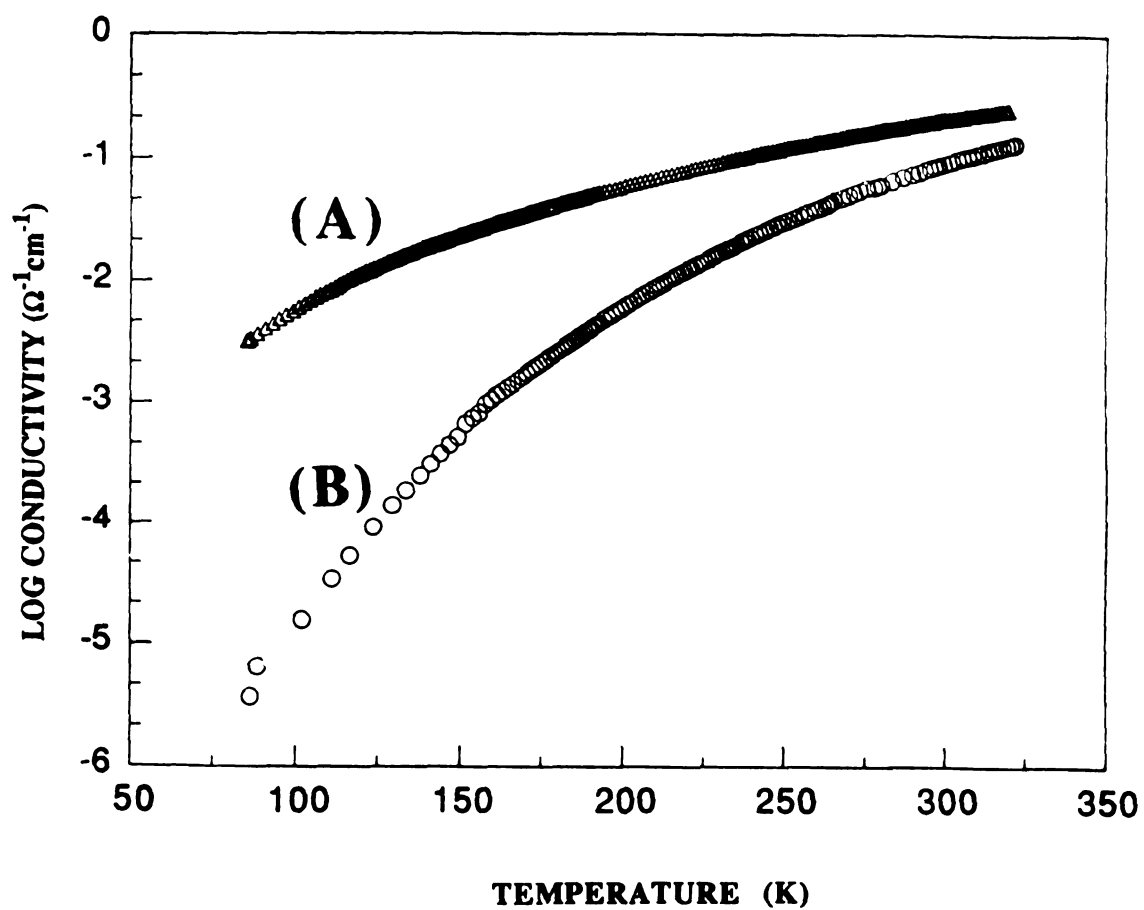| Compounds	$\sigma_{(R.T.)}(\Omega^{-1}cm^{-1})$
m-(PFu)$_{0.58}$FeOCl$_y$(OMe)$_{1-y}$	$10^{-5} \sim 10^{-4}$
m-(PFu)$_{0.56}$FeOCl$_y$(OMe)$_{1-y}$	$10^{-5} \sim 10^{-4}$
m-(PFu)$_{0.53}$FeOCl$_y$(OMe)$_{1-y}$	$10^{-3} \sim 10^{-2}$
m-(PFu)$_{0.47}$FeOCl$_y$(OMe)$_{1-y}$	$10^{-4} \sim 10^{-3}$
*r-(PFu)$_{0.28}$FeOCl	$10^{-1} \sim 10^0$
r-(PFu)$_{0.27}$FeOCl	$10^{-2} \sim 10^{-1}$
r-(PFu)$_{0.18}$FeOCl	$10^{-1} \sim 10^0$

* single crystal r-(PFu)$_x$FeOCl.

Figure 6.14. Four-probe variable temperature electrical conductivity data of r-(PFu)$_{0.27}$FeOCl in (A) Pressed pellet (B) Single crystal form.

Table 6.4. The Interlayer Spacing (d) and Room Temperature Electrical Conductivity (σ) of Several Intercalation Compounds of FeOCl.

Compounds	d (Å)	σ ($\Omega^{-1}cm^{-1}$)	Reference
$(TTF)_{0.10}FeOCl$	13.63	3.5×10^{-3}	15
$(TTT)_{0.14}FeOCl$	15.22	2.2×10^{-4}	15
$(TTN)_{0.50}FeOCl$	15.31	5.5×10^{-4}	15
$(TMTTF)_{0.08}FeOCl$	11.32	1.6×10^{-2}	18c
$(Ppy)_{0.34}FeOCl$	13.21	1.5×10^{-1}	12
$(Pth)_{0.28}FeOCl$	13.31	5.0	12
$(Ferrocene)_{0.17}FeOCl$	14.92	1.0×10^{-4}	20
$(Perylene)_{0.11}FeOCl$	16.769	2.3×10^{-2}	18b
$(TSF)_{0.12}FeOCl$	13.52	5.0×10^{-3}	18a
$(TMTSF)_{0.10}FeOCl$	13.82	5.4×10^{-4}	18a
$(ET)_{0.25}FeOCl$	22.18	2.6×10^{-1}	22
$(PANI)_{0.20-0.28}FeOCl$	13.92	$10^{-3} \sim 10^{-1}$	Chapter 5
$(PFu)_{0.18-0.28}FeOCl$	13.60	$10^{-2} \sim 10^{0}$	This work

The thermoelectric power of m-$(PFu)_x FeOCl_y(OMe)_{1-y}$ is unmeasurable due to very high contact resistance of the compound. Variable temperature thermoelectric power (TP) of r-(PFu)FeOCl in single crystals and pressed powders are shown in Figure 6.15. The TP of the single crystals is large, positive and increases with rising temperature, while the TP of pressed powder is smaller than that of single crystal as reveals the higher conductivity. It reaches the value of 45 μV/K at 230 K below which, the exact Seebeck coefficient cannot be obtained due to the high resistivity of the materials. However, both sets of thermoelectric power data exhibited typical p-type semiconductor behavior, similar to $(PANI)_x FeOCl$ and other intercalated FeOCl compounds. This is different from its polypyrrole and polythiophene analogs which show p-type metallic character [9]. The different charge transport properties between polyfuran/FeOCl and polypyrrole, polythiophene/FeOCl systems are hard to explain but it may reflect differences in the length of polymer chains and in the structural integrity of the polymer backbone in the interlamellar space of FeOCl. Therefore, the reduced FeOCl framework seems to be responsible for charge transport properties in the PFu/FeOCl system. This also explains why the conductivity of r- phase is higher than m-phase. Since the conductivity of $(PFu)_x FeOCl$ was dominated by FeOCl framework, the replacement of Cl by MeO may inhibit the charge transport by acting as disordered defects, thus decreasing the conductivity. The formation of the shorter conjugated segments of polyfuran in FeOCl may be due to two reasons: first $(PFu)_x FeOCl$ was prepared from larger molecular monomer (i.e. terfuran), the slow kinetic of large molecule will prohibit the extensive polymerization

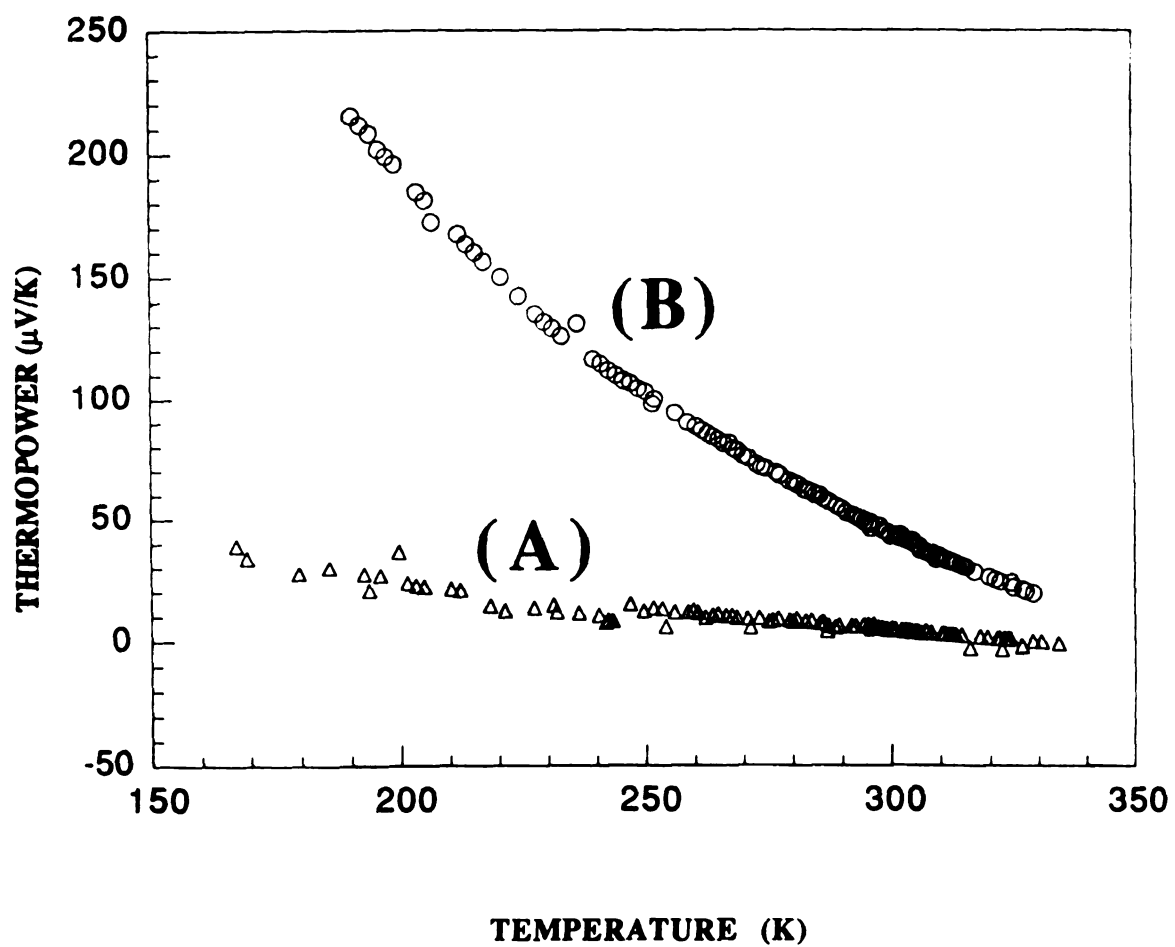**Figure 6.15.** Variable temperature thermoelectric power data of r-$(PFu)_{0.27}FeOCl$ in (A) Pressed pellet (B) Single crystal.

of monomers inside the FeOCl gallery; second, when the reaction were carried out in refluxing MeOH, the longer reaction time cause some structure defects on the polyfuran backbone (e.g. ring-opening) therefore reducing the conjugation length.

Unfortunately, polyfuran appears to be sensitive to acid, and the polyfuran extracted from both $r-(PFu)_x FeOCl$ and $m-(PFu)_x FeOCl_y(OMe)_{1-y}$ is essentially an insulator.

VI. Conclusions:

Polyfuran can be intercalated in FeOCl by *in-situ* oxidative polymerization/ intercalation of terfuran or tetrafuran in refluxing MeOH, CH_3CN or by methanothermal synthesis at 100°C. This polymer is of higher quality showing less ring-opening than what has been prepared in the literature. Two phases of $(PFu)_x FeOCl$ with different interlayer spacing were obtained depending on the reaction conditions. The compound prepared from methanothermal synthesis is a pure product, although it has lower conductivity and the reaction is not really topotactic. The Cl atoms in the FeOCl framework were partially replaced by (OMe) groups to form $FeOCl_y(OMe)_{1-y}$. $r-(PFu)_x FeOCl$ prepared from refluxing in MeOH and CH_3CN has room temperature conductivity up to $10^0 \ \Omega^{-1}cm^{-1}$ higher than m-phase. The p-type semiconductor behavior of both phases suggest that the charge transport properties are dominated by the reduced FeOCl framework. The redox intercalation of terfuran in FeOCl may offer a new avenue to synthesize better defined polyfuran through chemical polymerization method.

LIST OF REFERENCES

LIST OF REFERENCES

1. (a) Zotti, G.; Schiavon, G.; Comisso, N.; Berlin, A.; Pagani, G. *Synth. Met.* **1990**, 36, 337-351. (b) Tourillon, G.; Garnier, F. *J. Electroanal. Chem.* **1982**, 135, 173-178.

2. (a) Leung, W.-Y. Thesis Dissertation, Michigan State University **1988**. (b) Kauffmann, T.; Lexy, H. *Chem. Ber.* **1981**, 114, 3667-3673. (c) El-Hajj, T.; Martin, J.-C.; Descotes, G. *J. Heterocyclic Chem.* **1983**, 20, 233-235.

3. Kang, I. T.; Neoh, K. G. *Eur. Polym. J.* **1987**, 23, 719-922.

4. Cook, M. J.; Hatritzky, A. R.; Linda, P. *Adv. Hetercyclic Chem.* **1974**, 17, 293-307.

5. (a) Ohsawa, T.; Kaneto, K.; Yoshino, K. *Jpn. J. Appl. Phys.* **1984**, 23, L663-L665. (b) Armour, M.; Davies, A. G.; Upadhyay, J.; Wassermann, A. *J. Polym. Sci. A* **1967**, 5, 1527-1538.

6. Wu, C. G.; Marcy, H. O.; DeGroot, D. C.; Kannewurf, C. R.; Schindler, J. L.; Leang, W. Y.; Benz, M.; LeGoff, E.; Kanatzidis, M. G. *Synth. Met.* **1991**, 41/43, 693-698.

7. Coic, L.; Spiesser, M.; Palvadeau, P.; Rouxel, J. *Mat. Res. Bull.* **1981**, 16, 229-236.

8. Hernandez, V.; Lopez Navarrete, J. T.; Marcos, J. I. *Synth. Met.* **1991**, 41-43, 789-792.

9. (a) Yoshino, K.; Hayashi, S.; Sugimsto, R. *Jpn. J. Appl. Phys.* **1984**, 23, L899-L900. (b) Kresta, J.; Livingston, M. K. *Polym. Lett.* **1970**, 8, 795-803.

10. Ishigak, A.; Shono, T.; Hachihama, Y. *Kogyo Kagaku Zasshi* **1963**, 66, 119.

11. (a) Kanatzidis, M. G.; Tonge, C. R.; Marks, T. J.; Marcy, H. O.; Kannewurf, C. R. *J. Am. Chem. Soc.* **1987**, 109, 3797-3799. (b) Kanatzidis, M. G.; Marcy, H. O.; McCarthy, W. J.; Kannewurf, C. R.; Marks, T. J. *Solid State Ionics* **1989**, 32/33, 594-608.

12. Kikkawa, S.; Kanamaru, F.; Koizumi, M. *Inorg. Chem.* **1976**, 15, 2195-2197.

13. Son, S.; Kikkawa, S.; Kanamaru, F.; Koizumi, M. *Inorg. Chem.* **1980**, 19, 262-264.

14. Averill, B. A.; Kauzlarich, S. M.; Antonio, M. R. *J. De Phys.* **1983**, C3-1373-C3-1376.

15. Kanatzidis, M. G. et al work in progress.

16. Bizette, H.; Adam, A. *C. R. Acad. Sci. Paris Ser. B* **1972**, 275, 911-913.

17. (a) Antonio, M. R.; Averill, B. A. *Mol. Cryst. Liq. Cryst.* **1988**, 170, 215-222. (b) Bringley, J. F.; Averill, B. A. *J. Chem. Soc. Chem. Commu.* **1981**, 282-283. (c) Kauzlarich, S. M.; Ellena, J. F.; Stupik, P. D.; Reiff, W. M.; Averill, B. A. *J. Am. Chem. Soc.* **1987**, 109, 4561-4570.

18. (a) Bredas, J. L.; Street, G. B. *Acc. Chem. Res.* **1985**, 18, 309-315. (b) Patil, A. O.; Heeger, A. J.; Wudl, F. *Chem. Rev.* **1988**, 88, 183-200.

19. Villeneuve, G.; Dordor, P.; Palvadeau, P.; Venien, J. P. *Mat. Res. Bull.* **1982**, 17, 1407-1412.

20. Kanamaru, F.; Yamanaka, S.; Koizumi, M. *Chem. Lett.* **1974**, 373-376.

21. Bringley, J. F.; Fabre, J. M.; Averill, B. A. *J. Am. Chem. Soc.* **1990**, <u>112</u>, 4577-4579.

CONCLUDING REMARKS

The research of conducting polymers will still be active in this decade. Some issues, such as the structure, the properties and the new possible applications as well as discovery of new conducting polymers and their composites (or copolymers) still attract scientists. Approach of these issues needs intriguing ideas and correct directions. The *in-situ* oxidative polymerization/ intercalation of these polymers in layered hosts is a very recent development. It gives a promising solution to solve some remaining puzzles in conducting polymers. From the extensive study in our laboratory, three interesting discoveries have been made.

First: We were able to prepare organic polymer/inorganic composites with controllable charge transport properties ~ ranging from semiconductor to metal-like and with p-type carrier to n-type carrier. These rare and unique properties may offer some potential applications in electronic devices, such as p-n junction. Other applications may be discovered by cooperation of imaginative chemists and electrical engineers. This field of research can also be extended to other electrically active hosts to improve the physicochemical and mechanical properties of the resulting intercalation compounds.

Second: by using crystalline hosts, oriented polymer can be prepared. Even though we were not able, as yet, to solve the polyaniline structure inside $(PANI)_x FeOCl$, this discovery reveals an encouraging direction for further work. If we are able to find good crystalline hosts, conducting polymers may orient inside the hosts

and preserve the crystallinity of the entire system. The intercalation compound may enable us to characterize it by single crystal X-ray diffraction study.

Third: the results of intercalating polyfuran in FeOCl provide an alternative road to prepare a new polymer with more regular backbone by this special chemical polymerization/ intercalative method described in this thesis. Using this technique, we may obtain other known polymers with better structures.